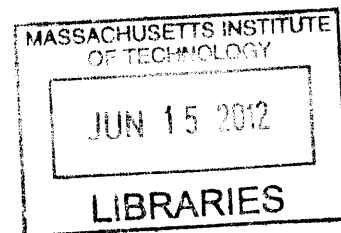


FUNCTIONALIZATION AND APPLICATIONS OF CARBON NANOTUBES

by

Jan M. Schnorr

Dipl. Chemiker (equivalent to M.Sc. in Chemistry)
J. W. Goethe Universität Frankfurt, Germany, 2006



ARCHIVES

SUBMITTED TO THE DEPARTMENT OF CHEMISTRY
IN PARTIAL FULFILMENT OF THE REQUIREMENTS FOR THE DEGREE OF

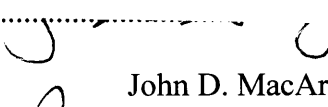
DOCTOR OF PHILOSOPHY IN CHEMISTRY

AT THE
MASSACHUSETTS INSTITUTE OF TECHNOLOGY
JUNE 2012

© 2012 Massachusetts Institute of Technology. All rights reserved.

Signature of Author 

Department of Chemistry
May 25, 2012

Certified by 

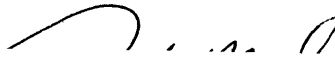
Timothy M. Swager
John D. MacArthur Professor of Chemistry
Thesis Supervisor

Accepted by 

Robert W. Field
Haslam and Dewey Professor of Chemistry
Chairman, Departmental Committee of Graduate Studies

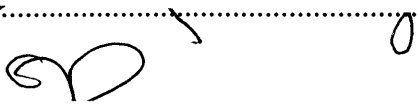
This doctoral thesis has been examined by a Committee of the Department of Chemistry as follows:

Professor Gregory C. Fu:



Chairman

Professor Timothy M. Swager:



Thesis Advisor

Professor Timothy F. Jamison:



Department of Chemistry

Dedicated to my family

FUNCTIONALIZATION AND APPLICATIONS OF CARBON NANOTUBES

by

Jan M. Schnorr

Submitted to the Department of Chemistry
on May 25, 2012 in Partial Fulfilment of the
Requirements for the Degree of Doctor of Philosophy in
Chemistry

ABSTRACT

Carbon nanotubes (CNTs) possess a unique set of electrical and mechanical properties and have been used in a variety of applications. In this thesis, we explore strategies to functionalize CNTs as well as applications which are enabled by functionalized CNTs.

Chapter 1 gives an overview of emerging applications of CNTs.

In Chapter 2, we describe a route that leads to highly water-soluble multi-walled CNTs (MWCNTs). The good solubility facilitates processing and manipulation of the CNTs. Furthermore, we explore the use of soluble MWCNTs as electrical interconnects in water. Using a Wacker type oxidation reaction, we demonstrate that this type of CNTs can have a positive effect on reactions that involve a metal to metal electron transfer.

In Chapter 3, we explore catalytic aziridination reactions to functionalize CNTs as well as [60]fullerene and graphite.

In Chapter 4, we use amine functionalized single-walled CNTs (SWCNTs) to attach receptors for gas sensing applications. We optimize the receptors and test the functionalized SWCNTs in an array sensor with regard to sensitivity, selectivity, stability and reproducibility.

In Chapter 5, we demonstrate a highly selective sensor for *N*-methylammonium salts based on SWCNTs that are functionalized with a cavitand.

In Chapter 6, we describe a sensor for the plant hormone ethylene. The sensor is based on SWCNTs that are non-covalently functionalized with a copper complex. The device shows good sensitivity and selectivity for ethylene and could be useful in the horticultural industries.

Thesis Supervisor: Timothy M. Swager

Title: John D. MacArthur Professor of Chemistry

Table of Contents

Title Page	1
Signature Page.....	2
Dedication	3
Abstract	4
Table of Contents	5
List of Abbreviations.....	7
List of Figures, Schemes, and Tables.....	8
Chapter 1	17
1.1. Introduction	18
1.2. CNT-based Electrodes	20
1.3. Supercapacitors	24
1.4. CNT-based Electronic Components.....	26
1.5. Catalysis	30
1.6. Filters and Membranes.....	33
1.7. Sensors	35
1.8. Biomedical Applications.....	41
1.9. Mechanical Applications.....	42
1.10. Challenges for Applications of CNTs	44
1.11. Conclusions	46
1.12. References	47
Chapter 2	57
2.1. Introduction	58
2.2. Results and Discussion.....	60
2.2.1. Solubilization of MWCNTs by Covalent Attachment of Sulfonate Groups.....	60
2.2.2. Sulfonate MWCNTs as Water Soluble Electrical Interconnects.....	64
2.3. Conclusions	68
2.4. Experimental Section	69
2.5. References	85
Chapter 3	87
3.1. Introduction	88
3.2. Results and Discussion.....	91
3.2.1. Evaluation of Different Aziridination Conditions on C ₆₀ and MWCNTs.....	91
3.2.2. Catalyzed aziridination of CNTs and graphite	97
3.3. Conclusions	101
3.4. Experimental Section	101
3.5. References	130

Chapter 4	132
4.1. Introduction	133
4.2. Results and Discussion.....	137
4.2.1. Functionalization of SWCNT with Thiourea and Squaramide Receptors	137
4.2.2. Sensor Fabrication and Evaluation.....	140
4.2.3. Optimization of Receptors	146
4.2.4. Sensor Array Measurements	149
4.3. Conclusions	157
4.4. Experimental Section	157
4.5. References	185
Chapter 5	187
5.1. Introduction	188
5.2. Results and Discussion.....	190
5.2.1. Functionalization of Carbon Nanotubes with Cavitands.....	190
5.2.2. Binding Studies	193
5.2.3. Amperometric Sensing Measurements.....	196
5.3. Conclusions	202
5.4. Experimental Section	202
5.5. References	216
Chapter 6	219
6.1. Introduction	220
6.2. Results and Discussion.....	223
6.2.1. Non-covalent SWCNT Functionalization and Sensor Fabrication	223
6.2.2. Ethylene Sensing: Sensitivity, Selectivity, and Stability	226
6.2.3. Monitoring of Fruit Ripening.....	233
6.3. Conclusions	235
6.4. Experimental Section	236
6.5. References	242
Curriculum Vitae.....	243
Acknowledgements	246

List of Abbreviations

ATR-IR	attenuated total reflectance infrared spectroscopy
CNT	carbon nanotube
Δ	heat
DMAD	dimethyl acetylenedicarboxylate
DMAP	4-dimethylaminopyridine
DMF	<i>N,N</i> -dimethyl formamide
DMSO	dimethyl sulfoxide
EtOH	ethanol
GC-MS	gas chromatography-mass spectrometry
HRMS	high-resolution mass spectrometry (exact mass)
$h\nu$	light
MeCN	acetonitrile
MeOH	methanol
m.p.	melting point
MWCNT	multi-walled carbon nanotube
NMR	nuclear magnetic resonance
r.t.	room temperature
SWCNT	single-walled carbon nanotube
TGA	thermogravimetric analysis
THF	tetrahydrofuran
UV-vis	ultraviolet-visible
wt	weight
XPS	X-ray photoelectron spectroscopy

List of Figures

Figure 1.1. Structural variety of CNTs. (a) Orientation of the carbon network in armchair (n, n) and zigzag ($n, 0$) CNTs. (b) Single, double and multi-walled CNTs.....	18
Figure 1.2. CNT-containing MnO ₂ nanotubes for use in lithium ion batteries. (a) SEM image and schematic representation of the coaxial structure. (b) Discharge capacity vs. cycle number for MnO ₂ /CNT coaxial nanotubes, MnO ₂ nanotubes and CNTs. Reprinted with permission from Ref 35. Copyright 2009 American Chemical Society.....	22
Figure 1.3. Fabrication of a high density SWCNT material by liquid-induced collapse of CNT forests. (a) SEM image of high density SWCNT (“solid”) and the surrounding SWCNT forest (b) Schematic diagram of the liquid-induced collapse process. Reprinted with permission from Ref 49. Copyright 2006 Nature Publishing Group.	25
Figure 1.4. Nanotube radio. (a) Schematic representation. Upon excitation by radio transmissions, the MWCNT tip resonates and emits electrons that are detected <i>via</i> the resulting current. (b) Transmission electron micrographs of the MWCNT radio off and on resonance. Reprinted with permission from Ref 79. Copyright 2007 American Chemical Society.....	30
Figure 1.5. Decrease in response time to DMMP from a CNT sensor coated with a strong hydrogen-bonding polycarbosilane (HC) (green curve) to one coated with a self-aligned monolayer (SAM) coating of hexafluoroisopropanol moieties (red curve). Reprinted with permission from Ref 14. Copyright 2005 American Association for the Advancement of Science.....	38
Figure 1.6. 1-Pyrenebutanoic acid succinimidyl ester is adsorbed onto the CNT surface providing a chemically reactive anchor for the immobilization of proteins. Reprinted with permission from Ref 15. Copyright 2001 American Chemical Society.....	40
Figure 1.7. Spinning of CNT yarns from MWCNT forests. (a and b) SEM images of the spinning process. Reprinted with permission from Ref 16. Copyright 2004 American Association for the Advancement of Science.....	43
Figure 2.1. Schematic representation of electron transfer facilitated by soluble MWCNT. A CNT-bound metal such as Pd(II) is reduced during the catalytic cycle and is subsequently regenerated via an electron transfer to an oxidant such as Cu(II) taking advantage of the conductivity of the soluble MWCNT.....	59
Figure 2.2. (a) UV-vis spectroscopy was used to determine the concentration of sulfMWCNT in water 24 h and 48 h after sonication as well as after subsequent centrifugation for 10 and 40 minutes (all samples were diluted 1:1000 directly before the measurement). (b) Optical micrograph of sulfMWCNTs in a water droplet, (c) propargyl MWCNTs, (d) pristine MWCNTs.	63
Figure 2.3. sulfMWCNTs in a biphasic H ₂ O/CH ₂ Cl ₂ system (a) before and (b) after shaking the vial showing the preference of the sulfMWCNTs for the aqueous phase, (c) free-standing film of sulfMWCNTs (thickness ca. 0.25 mm) obtained by drop-casting onto a glass surface from a suspension at 50 mg mL ⁻¹	64
Figure 2.4. (a) Schematic representation of the proposed mechanism of electron transfer facilitated by sulfMWCNT . The CNT-bound Pd(II) is reduced during the catalytic cycle and is subsequently	

regenerated via an electron transfer to Cu(II) taking advantage of the conductivity of the sulfMWCNT. (b) The addition of sulfMWCNTs leads to an increase in yield compared to the control without MWCNTs if metal sources with weakly coordinating counterions are used. (c) The addition of highly soluble sulfMWCNTs leads to an increase in yield which is more than twice as high as the yield-increasing effect of pristine SWCNTs and MWCNTs. Non-conductive sulfonated materials such as sulfSWCNTs lower the yield of 5. 66

Figure 2.5. TGA of propargyl SWCNTs (**1a**) and pristine SWCNTs..... 77

Figure 2.6. XPS spectra of propargyl SWCNTs (**1a**) and pristine SWCNTs..... 77

Figure 2.7. FT-IR spectra of propargyl SWCNTs (**1a**) and pristine SWCNTs..... 78

Figure 2.8. Raman spectra of propargyl SWCNTs (**1a**) and pristine SWCNTs..... 78

Figure 2.9. TGA of propargyl MWCNTs (**1b**) and pristine MWCNTs 79

Figure 2.10. XPS spectra of propargyl MWCNTs (**1b**) and pristine MWCNTs..... 79

Figure 2.11. FT-IR spectra of propargyl MWCNTs (**1b**) and pristine MWCNTs 80

Figure 2.12. Raman spectra of propargyl MWCNTs (**1b**) and pristine MWCNTs..... 80

Figure 2.13. TGA of sulfonate SWCNTs (**3a**) and pristine SWCNTs..... 81

Figure 2.14. XPS spectra of sulfonate SWCNTs (**3a**) and pristine SWCNTs..... 81

Figure 2.15. FT-IR spectra of sulfonate SWCNTs (**3a**) and pristine SWCNTs..... 82

Figure 2.16. Raman spectra of sulfonate SWCNTs (**3a**) and pristine SWCNTs..... 82

Figure 2.17. TGA of sulfonate MWCNTs (**3b**) and pristine MWCNTs 83

Figure 2.18. XPS spectra of sulfonate MWCNTs (**3b**) and pristine MWCNTs..... 83

Figure 2.19. FT-IR spectra of sulfonate MWCNTs (**3b**) and pristine MWCNTs..... 84

Figure 2.20. Raman spectra of sulfonate MWCNTs (**3b**) and pristine MWCNTs..... 84

Figure 3.1. XPS analysis of pristine MWCNTs, amine functionalized MWCNTs (Table 3.1, entry 7) and tosyl MWCNTs (Table 3.1, entry 1). Si 2p and Si 2s signals results from the utilized Si/SiO₂ substrate. The binding energy of Cu 2p has been labeled to show that no significant amount of copper is present in the products. 93

Figure 3.2. XPS analysis of *N*-tosylaziridine-functionalized SWCNTs and graphite..... 98

Figure 3.3. XPS analysis of aziridine-functionalized graphite using 4 equivalents PhINTs with 3% **17** (blue trace), 3% CuCl/2,6-lutidine (red trace), and 6% CuCl/2-6-lutidine (green trace)..... 99

Figure 3.4. Desired iodine reagents for CNT and graphite functionalization..... 100

Figure 3.5. XPS analysis of nosylaziridine-functionalized graphite using 4 equivalents PhINNs **18** with 6% CuCl/2,6-lutidine. 101

Figure 3.6. ¹H NMR Spectrum of **15** (CDCl₃) 114

Figure 3.7. ¹³C NMR Spectrum of **15** (CDCl₃) 114

Figure 3.8. ^1H NMR Spectrum of 2 (MeOD).....	115
Figure 3.9. ^1H NMR Spectrum of 12 (D_2O).....	115
Figure 3.10. ^{13}C NMR Spectrum of 12 (D_2O).....	116
Figure 3.11. ^1H NMR Spectrum of 14 (CDCl_3)	116
Figure 3.12. ^{13}C NMR Spectrum of 14 (CDCl_3)	117
Figure 3.13. ^1H NMR Spectrum of 18 ($\text{DMSO}-d_6$).....	117
Figure 3.14. ^{13}C NMR Spectrum of 18 ($\text{DMSO}-d_6$).....	118
Figure 3.15. ^1H NMR Spectrum of 16 (CDCl_3)	118
Figure 3.16. ^{13}C NMR Spectrum of 16 (CDCl_3)	119
Figure 3.17. XPS analysis of Table 3.1, Entry 1	119
Figure 3.18. XPS analysis of Table 3.1, Entry 2	120
Figure 3.19. XPS analysis of Table 3.1, Entry 3	120
Figure 3.20. XPS analysis of Table 3.1, Entry 4.....	121
Figure 3.21. XPS analysis of Table 3.1, Entry 5	121
Figure 3.22. XPS analysis of Table 3.1, Entry 6	122
Figure 3.23. XPS analysis of Table 3.1, Entry 7	122
Figure 3.24. XPS analysis of Table 3.3, Entry 1	123
Figure 3.25. XPS analysis of Table 3.3, Entry 2	123
Figure 3.26. XPS analysis of Table 3.3, Entry 3	124
Figure 3.27. XPS analysis of Table 3.3, Entry 4.....	124
Figure 3.28. XPS analysis of Table 3.3, Entry 5	125
Figure 3.29. XPS analysis of Table 3.3, Entry 6	125
Figure 3.30. XPS analysis of Table 3.3, Entry 7.....	126
Figure 3.31. XPS analysis of Table 3.3, Entry 8	126
Figure 3.32. XPS analysis of <i>N</i> -tosyl aziridine functionalized SWCNTs.....	127
Figure 3.33. XPS analysis of <i>N</i> -tosyl aziridine functionalized graphite, procedure 1	127
Figure 3.34. XPS analysis of <i>N</i> -tosyl aziridine functionalized graphite, procedure 2	128
Figure 3.35. XPS analysis of <i>N</i> -tosyl aziridine functionalized graphite, procedure 3	128
Figure 3.36. XPS analysis of <i>N</i> -tosyl aziridine functionalized graphite, procedure 4	129
Figure 3.37. XPS analysis of <i>N</i> -nosyl aziridine functionalized graphite	129
Figure 4.1. Common explosives TNT, PETN, RDX.....	133

Figure 4.2. Schematic representation of an amperometric CNT-based sensor	134
Figure 4.3. Sensing targets nitromethane (1) and cyclohexanone (2).	134
Figure 4.4. Thiourea (A) and Squaramide (B) based receptors attached to CNTs.....	136
Figure 4.5. XPS analysis of pristine SWCNTs (blue trace), NH ₂ -SWCNT (red trace), m-CF ₃ -Bn-TU-SWCNT (green trace), and m-CF ₃ -Bn-SQ-SWCNT (orange trace).	139
Figure 4.6. Fabrication of sensors.	140
Figure 4.7. Micrographs of SWCNT devices. (a) Optical micrograph; (b)-(f) scanning electron micrographs at different magnifications.	141
Figure 4.8. Glovebox for initial sensing measurements (a) photograph, (b) baseline drift over 7 h.....	142
Figure 4.9. Gas flow chamber for sensing measurements.	142
Figure 4.10. Baseline drift using a Teflon device enclosure. Photograph of (a) open and (b) closed enclosure; (c) baseline drift with enclosure connected to a nitrogen supply (blue trace) compared to baseline drift with glovebox depicted in Figure 4.8 (red trace).	143
Figure 4.11. Sensing responses of devices with different types of SWCNTs to 57 ppm 2, applied for 30 s starting at 50, 150, and 250 s.....	144
Figure 4.12. Sensing responses of devices fabricated using m-CF ₃ -Bn-TU-SWCNT. (a) response of three different devices exposed to 57 ppm cyclohexanone for 30 s every 100 s starting at 50 s as well as 283 ppm cyclohexanone for 30 s every 100 s starting at 600 s (device 1) or 550 s (devices 2 and 3); averages and errors are based on the four measurements at each concentration and across all devices; (b) response of device 2 after 16 days under ambient conditions upon exposure to 57 ppm cyclohexanone for 30 s every 100 s starting at 50 s as well as 283 ppm cyclohexanone for 30 s every 100 s starting at 550 s; (c) response of device 2 after 236 days under ambient conditions upon exposure to 57 ppm cyclohexanone for 30 s every 100 s starting at 50 s as well as 283 ppm cyclohexanone for 30 s every 100 s starting at 600 s; (d) overlay of sensing traces for freshly prepared device 2, device 2 after 16 days, and after 236 days under ambient conditions.	145
Figure 4.13. Model receptors for binding studies with substituted benzyl (14, 15) and phenyl groups (16, 17).	146
Figure 4.14. NMR binding study of 22 and cyclohexanone 2 in CDCl ₃	148
Figure 4.15. Devices for array measurements. (a) Schematic drawing and photograph of 14 devices on a glass slide; (b) photograph of glass slide with 14 devices contacted <i>via</i> an edge connector. Openings in the edge connector were covered with epoxy to provide a gas tight seal.	150
Figure 4.16. Sensing response of an array of SWCNT devices. Each line contains the overlaid response of two different devices of the same type of SWCNTs. Analytes and concentrations are listed in Table 4.3. Equilibration times when switching analytes or concentrations have been omitted for clarity. A 20 point floating average filter and baseline correction has been applied to the plotted data. (a) Overview of sensing response of all tested devices; (b) examples for reproducibility of consecutive measurements and across devices with the same type of SWCNTs.	153

Figure 4.17. Sensing response of an array of SWCNT devices. Averages and errors shown are based on 4 peaks and 2 devices for each type of analyte and SWCNT.....	154
Figure 4.18. Principal component analysis of the array sensing responses. First and second principal component shown.	156
Figure 4.19. Experimental setup for sensing measurements: A continuous gas flow is directed through the device chamber. The gas stream can be switched between nitrogen gas (“Zero” mode) or the nitrogen gas analyte mixture (“Span” mode), in which the gas stream runs through the flow chamber containing the analyte.	167
Figure 4.20. ¹ H NMR Spectrum of 3 (CDCl ₃)	169
Figure 4.21. ¹³ C NMR Spectrum of 3 (CDCl ₃)	169
Figure 4.22. ¹ H NMR Spectrum of 6 (CDCl ₃)	170
Figure 4.23. ¹³ C NMR Spectrum of 6 (CDCl ₃)	170
Figure 4.24. ¹ H NMR Spectrum of 8 (CDCl ₃)	171
Figure 4.25. ¹³ C NMR Spectrum of 8 (CDCl ₃)	171
Figure 4.26. ¹ H NMR Spectrum of 11 (CDCl ₃)	172
Figure 4.27. ¹³ C NMR Spectrum of 11 (CDCl ₃)	172
Figure 4.28. ¹ H NMR Spectrum of 12 (CDCl ₃)	173
Figure 4.29. ¹³ C NMR Spectrum of 12 (CDCl ₃)	173
Figure 4.30. ¹ H NMR Spectrum of 13 (CDCl ₃)	174
Figure 4.31. ¹³ C NMR Spectrum of 13 (CDCl ₃)	174
Figure 4.32. ¹ H NMR Spectrum of 14 (CDCl ₃)	175
Figure 4.33. ¹³ C NMR Spectrum of 14 (CDCl ₃)	175
Figure 4.34. ¹ H NMR Spectrum of 15 (CDCl ₃)	176
Figure 4.35. ¹³ C NMR Spectrum of 15 (CDCl ₃)	176
Figure 4.36. ¹ H NMR Spectrum of 16 (CDCl ₃)	177
Figure 4.37. ¹³ C NMR Spectrum of 16 (CDCl ₃)	177
Figure 4.38. ¹ H NMR Spectrum of 17 (CDCl ₃)	178
Figure 4.39. ¹³ C NMR Spectrum of 17 (CDCl ₃)	178
Figure 4.40. ¹ H NMR Spectrum of 21 (DMSO- <i>d</i> ₆).....	179
Figure 4.41. ¹³ C NMR Spectrum of 21 (DMSO- <i>d</i> ₆).....	179
Figure 4.42. ¹ H NMR Spectrum of 22 (DMSO- <i>d</i> ₆)	180
Figure 4.43. XPS analysis of NH ₂ -SWCNT.....	180
Figure 4.44. XPS analysis of Me-TU-SWCNT.....	181

Figure 4.45. XPS analysis of p-CF ₃ -Bn-TU-SWCNT.....	181
Figure 4.46. XPS analysis of m-CF ₃ -Bn-TU-SWCNT	182
Figure 4.47. XPS analysis of Me-SQ-SWCNT.....	182
Figure 4.48. XPS analysis of p-CF ₃ -Bn-SQ-SWCNT.....	183
Figure 4.49. XPS analysis of m-CF ₃ -Bn-SQ-SWCNT.....	183
Figure 4.50. XPS analysis of m-CF ₃ -Ph-TU-SWCNT.....	184
Figure 4.51. XPS analysis of Bis-U-SWCNT.....	184
Figure 4.52. XPS analysis of Bis-TU-SWCNT.....	185
Figure 5.1. Interaction of tetraphosphonate cavitaand Tiiii[C ₃ H ₇ , CH ₃ , Ph] with <i>N</i> -methylbutyl ammonium chloride in comparison to closely related compounds. Association constants are based on ref. 27 and have been obtained by isothermal titration calorimetry (ITC) in methanol.....	189
Figure 5.2. XPS spectrum of Tiiii@SWCNTs. Si and F in the spectra originate from the silicon substrate used. Cl signals were attributed to trace amounts of residual <i>o</i> -DCB.....	192
Figure 5.3. ³¹ P MAS NMR spectra of (a) pristine SWCNTs, (b) Tiiii, and (c) Tiiii@SWCNTs.....	193
Figure 5.4. XPS binding study with Tiiii@SWCNTs. (a) Reversible binding of guest 2 ; (b) XPS analysis of Tiiii@SWCNTs before exposure to 2 (blue), after exposure to 2 (red), and after subsequent washing with DBU (green). Si signals are due to the utilized Si substrate.	194
Figure 5.5. Host-guest binding studies using ³¹ P MAS NMR showing reversible binding of the host molecule. (a) Tiiii@SWCNTs, red trace; (b) after treatment with the guest, green trace; (c) after subsequent washing with DBU, blue trace.....	196
Figure 5.6. Liquid flow chamber for sensing measurements.	198
Figure 5.7. Setup for liquid flow sensing measurements. Using two 3-way valves, a liquid from one of two syringes could alternately be directed through the liquid flow chamber with the measurement device. Both syringes were connected to the same syringe pump ensuring the same flow rate for both liquids. .	198
Figure 5.8. Sensing of sarcosine with Tiiii@SWCNTs at (a) pH 7 and (b) pH 5, green arrows indicate exposure to analyte.....	199
Figure 5.9. Liquid flow sensing experiments with Tiiii@SWCNT-based devices at pH 5. a) Tiiii@SWCNTs and pristine SWCNTs show opposite responses upon exposure to a 1 mM solution of 4 b) Comparison of the current change upon exposure of Tiiii@SWCNTs and pristine SWCNTs devices to 4 (sarcosine ethyl ester hydrochloride), 5 (glycine ethyl ester hydrochloride) and 6 (tetraethylammonium chloride), error bars are based on three consecutive measurements c) Response of Tiiii@SWCNTs devices to different concentrations of 4 , error bars are based on three consecutive measurements d) Response of Tiiii@SWCNTs devices to alternating exposure to 4 and 5	201
Figure 5.10. ATR-FTIR Tiiii (blue trace) and Tiiii@SWCNTs (red trace).....	206
Figure 5.11. XPS spectrum of Tiiii@SWCNTs after treatment with guest 2	207

Figure 5.12. XPS spectrum of Tiiii@SWCNTs•2 after washing with DBU. Positions of Br signals are labeled for better comparison to Figure 5.11 .	208
Figure 5.13. XPS spectrum of pristine SWCNTs after treatment with 2 . Positions of Br and P signals are labeled for better comparison to Figure 5.11 .	208
Figure 5.14. SEM images of Tiiii@SWCNT film used in sensing measurements. a) 350x LEI b) 350x SEI c) 20,000x SEI d) 70,000x SEI	210
Figure 5.15. AFM images of Tiiii@SWCNT film used in sensing measurements	211
Figure 5.16. Sensing of 4 with Tiiii@SWCNTs at pH 5	212
Figure 5.17. Sensing of 5 with Tiiii@SWCNTs at pH 5	212
Figure 5.18. Sensing of 6 with Tiiii@SWCNTs at pH 5	212
Figure 5.19. Sensing of 4 with pristine SWCNTs at pH 5	212
Figure 5.20. Sensing of 5 with pristine SWCNTs at pH 5	213
Figure 5.21. Sensing of 6 with pristine SWCNTs at pH 5	213
Figure 5.22. Sensing of 4 with Tiiii@SWCNTs at pH 5 using device 1	214
Figure 5.23. Sensing of 4 with Tiiii@SWCNTs at pH 5 using device 2	214
Figure 5.24. Sensing of 4 with Tiiii@SWCNTs at pH 5 using device 3	214
Figure 5.25. Sensing of 4 with Tiiii@SWCNTs at pH 5 using device 4	214
Figure 5.26. Sensing of 4 with Tiiii@SWCNTs using different devices, error bars are based on three consecutive measurements with the same device.	215
Figure 5.27. Sensing of 4 with Tiiii@SWCNTs at pH 7 (using device 1)	215
Figure 6.1. Schematic representation of ethylene detection by an amperometric sensor: A network of SWCNTs containing copper complex 1 is deposited between two electrodes. Exposure to ethylene leads to formation of 2 resulting in a resistance change of the network.	222
Figure 6.2. FT-IR spectrum of 1-SWCNT .	223
Figure 6.3. Raman spectrum of 1-SWCNT in comparison to pristine SWCNTs	224
Figure 6.4. XPS measurements: (a) Survey scans of 1 , 2 , and 1-SWCNT and (b) high resolution scans of the Cu 2p region of 1 , 2 , and 1-SWCNT . Si and O signals are due to the utilized (partially oxidized) silicon substrate.	225
Figure 6.5. SEM images of 1-SWCNT devices: (a) 1-SWCNT drop-cast on glass at 3,300x magnification and (b) at 17,000x magnification	225
Figure 6.6. Experimental setup for sensing measurements: A continuous gas flow is directed through the device chamber. The gas stream can be switched between nitrogen gas (“Zero” mode) or the nitrogen gas analyte mixture (“Span” mode), in which the gas stream runs through the flow chamber containing the analyte (ethylene) or a piece of fruit.	226

Figure 6.7. Response of 1-SWCNT devices prepared from different types of SWCNTs to 20 ppm ethylene.	227
Figure 6.8. Relative response of 1-SWCNT devices to 0.5, 1, 2, 5, 20, and 50 ppm ethylene and of pristine SWCNT to 20 ppm ethylene (the inset shows the response of 1-SWCNT to 0.5, 1, and 2 ppm and of SWCNT to 20 ppm ethylene). Data plotted is the 5 s floating average of the measurement data.	228
Figure 6.9. (a) Average responses from three different 1-SWCNT devices each to different ethylene concentrations as well as the response of pristine SWCNT devices to 20 ppm ethylene; (b) average response vs. ethylene concentration for 1-SWCNT devices.	229
Figure 6.10. Responses of devices made from 1-SWCNT, 2-SWCNT, SWCNTs with 3, and 4-SWCNT to 20 ppm ethylene.	230
Figure 6.11. Response of 1-SWCNT devices and pristine SWCNTs to 50 ppm ethylene and various potential interferents. Concentrations are given in ppm.	231
Figure 6.12. SEM images of 1-PS-SWCNT devices with 5 wt% cross-linked polystyrene beads drop-cast on glass (a) at 3,300x magnification and (b) at 17,000x magnification.	232
Figure 6.13. Response of 1-SWCNT and 1-PS-SWCNT devices to 0.5, 1, and 2 ppm ethylene. (a) Current traces of 1-PS-SWCNT devices exposed to ethylene; 5 s floating average; (b) Comparison between 1-SWCNT and 1-PS-SWCNT devices.	232
Figure 6.14. Examples for analyte chambers containing (a) banana, (b) orange, and (c) apple.	233
Figure 6.15. Response of 1-SWCNT devices to different fruit compared to the response to 20 ppm ethylene. Responses are normalized to 100 g fruit.	234
Figure 6.16. Response of 1-SWCNT devices to different fruit during ripening relative to 20 ppm ethylene and normalized to 100 g fruit. Apple 1 was stored in a refrigerator between measurements while apple 2 was kept at room temperature.	235
Figure 6.17. Gas flow chamber for sensing measurements.	238

List of Schemes

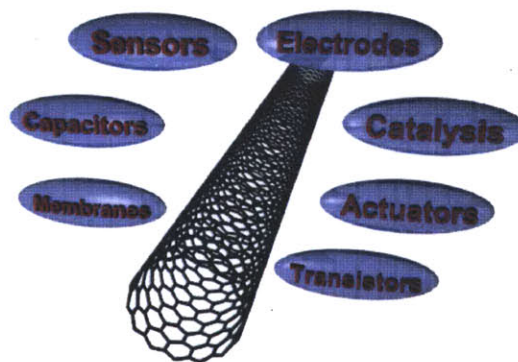
Scheme 2.1. Zwitterionic Approach toward CNT Functionalization	61
Scheme 2.2. Synthesis of sulfonate CNTs.....	61
Scheme 2.3. Wacker-type oxidation in the presence of sulfonated MWCNTs	65
Scheme 3.1. Examples of carbon nanotube functionalization reactions.....	88
Scheme 3.2. Examples for catalyzed aziridination reactions, utilizing PhINTs with Cu(acac) ₂ , ¹³ PhINTs with Cu(I) scorpionate 1 , ¹² in situ formed PhINTs with [Cu(CH ₃ CN) ₄]PF ₆ , ¹⁴ chloramine-T and CuCl, ¹⁵ and bromamine-T with Fe(TPP)Cl. ¹⁶	90
Scheme 3.3. Aziridination of C ₆₀ using Cu(I) scorpionate 6	95
Scheme 3.4. Aziridination of MWCNTs using PhINTs and Cu(I) complex 17	96
Scheme 4.1. Installation of amino groups on SWCNTs.	137
Scheme 4.2. Functionalization of SWCNTs with thiourea and squaramide receptors.	138
Scheme 4.3. Synthesis of receptors with two urea (21) or thiourea units (22).	147
Scheme 4.4. Synthesis of m-CF ₃ -Ph-TU-SWCNT, Bis-U-SWCNT, and Bis-TU-SWCNT.	149
Scheme 5.1. Synthesis of monoazide footed tetraphosphonate cavitand Tiiii[N ₃ , CH ₃ , Ph]	191
Scheme 5.2. SWCNT functionalization with Tiiii[N ₃ , CH ₃ , Ph]	191
Scheme 6.1. Poly(<i>p</i> -phenylene butadiynylene) P1 , copper scorpionate 1 and copper ethylene complex 2	221

List of Tables

Table 3.1. Evaluated conditions for MWCNT aziridination.	92
Table 3.2. Aziridination of C ₆₀	94
Table 3.3. Optimization of MWCNT functionalization conditions using BAT (12) and PhINTs (2).....	97
Table 4.1. Functional group densities for receptor-carrying SWCNTs.....	140
Table 4.2. Association constants for cyclohexanone and model receptors in CDCl ₃	147
Table 4.3. Analyte concentrations for array measurements.	152
Table 6.1. Pictures of fruit on different days of measurement.	240

CHAPTER 1

Emerging Applications of Carbon Nanotubes



Adapted and reprinted in part with permission from:

Schnorr, J. M.; Swager, T. M. "Emerging Applications of Carbon Nanotubes"

Chem. Mater. **2011**, *23*, 646-657

Copyright 2011 American Chemical Society

1.1. Introduction

Carbon nanotubes (CNTs) possess a unique set of electrical and mechanical properties which have been stimulating increasing interest in their applications.¹⁻⁵ Structurally, CNTs can be described as a sheet of graphene rolled into a tube. Depending on the orientation of the tube axis relative to the carbon network, different types of CNTs, described by the indices of their chiral vector, n and m , can be obtained. The CNTs that are formed by connection of the head and tail of the chiral vector are referred to by their respective indices (i.e. see the 14,0 and 8,8 structures in Figure 1). Armchair CNTs ($n = m$) usually show metallic conductivity while zigzag ($m = 0$) or chiral ($n \neq m$) CNTs are semiconducting (Figure 1.1a).

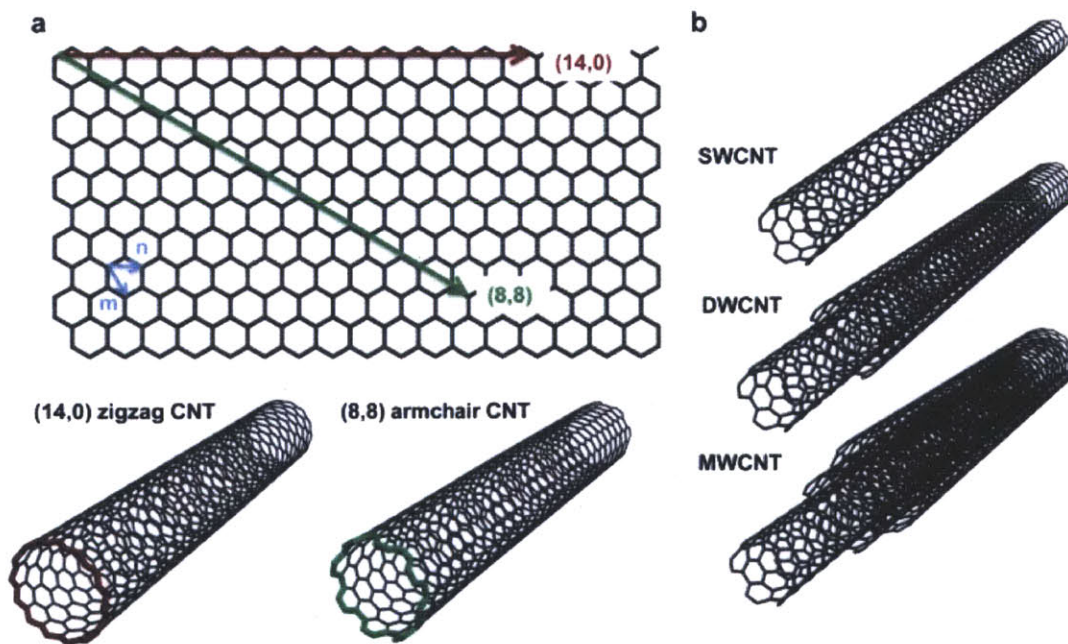


Figure 1.1. Structural variety of CNTs. (a) Orientation of the carbon network in armchair (n, n) and zigzag ($n, 0$) CNTs. (b) Single, double and multi-walled CNTs.

Additionally, CNTs can vary by the number of carbon-layers in their sidewalls. Single-walled CNTs (SWCNTs), double-walled CNTs (DWCNTs), and multi-walled CNTs (MWCNTs) have

been synthesized and are commercially available (Figure 1.1b).⁶⁻⁹ Indeed, this variety opens the field to many different applications. While semiconducting SWCNTs have, for example, been used in field-effect transistor (FET) based sensors¹⁰ metallic conducting MWCNTs have found their way into electrodes for electrocatalysis.¹¹

Even though CNTs are depicted as open-ended tubes for simplicity, their ends are usually capped by fullerene-type hemispheres. The higher curvature at these end groups compared to the sidewalls of the CNTs leads to a difference in chemical reactivity that can be exploited to selectively functionalize the ends of CNTs.¹² In addition to covalent functionalization, the properties of CNTs can be modified by deposition of metal or metal oxide particles¹³ or by the non-covalent attachment of polymers¹⁴ or small molecules.¹⁵ These different options add another level to the structural variety of CNTs and render them a highly customizable material.

In addition to their electrical properties, CNTs possess a very high strength which can be exploited in mechanical applications. Their high aspect ratio allows them to be fabricated into ropes analogous to spinning yarns from macroscopic fibers.¹⁶ Utilized in a different context this feature also enables the use of single CNTs as electrodes in nanoelectronic components.¹⁷ Finally, their high surface area to mass ratio has played a major role in CNT-based applications. This is a particularly important advantage in electrocatalytic processes wherein metal catalysts are immobilized on the surface of CNTs.¹⁸

This chapter provides an overview of a variety of applications that are based on the unique properties of pristine as well as functionalized CNTs. The intense research on CNT applications creates a dynamic situation with new discoveries being made constantly, hence it is impossible to

cover all published and noteworthy work. As a result, illustrative examples from the main areas of CNT-based applications are highlighted.

1.2. CNT-based Electrodes

Several properties of CNTs make them promising candidates for use as electrodes. Besides their good conductivity, they have a high surface per mass ratio. Furthermore, they can be used in a variety of shapes – as individual nanotube electrodes, as a layer on top of an existing electrode, or as a free standing electrode without any additional support.¹⁹ As discussed in the introduction, CNTs are known to interact with a variety of metal and metal oxide nanoparticles and can be covalently and non-covalently functionalized. Such modifications have been used to tune the properties of the CNT electrode to better suit the desired application.

Transparent Electrodes. Optically transparent electrodes (OTEs) are essential components of organic solar cells as well as organic light emitting diodes (OLEDs). Thin layers of CNTs, instead of the commonly used metal oxide conductive films like indium tin oxide, offer the advantage of more flexible electrodes and an alternative to rare metals such as indium. Depending on the desired application, CNT-OTEs must be processed into a thin film with strong (low resistivity) CNT-CNT junctions. Free standing thin films can be assembled by collecting dispersed CNTs on a filter^{20,21} or by solution casting of high quality dispersions followed by doping or extraction of polymer.²² These thin films can then be transferred onto the substrate. An alternative method involves direct spray-coating onto final substrates.^{23–25} The superior suitability of CNTs for flexible electrodes becomes particularly obvious when low bending radii are desired. OLEDs with CNT electrodes operate almost identically under bending, while the sheet resistance of ITO-based electrodes dramatically increases due to cracks in their surface.²⁴

An important aspect when utilizing CNTs as transparent electrodes is finding the proper balance between transparency and sheet resistance. While ITO is not well-suited for flexible OTEs, it offers a low sheet resistance at good transparencies compared to CNTs. Nevertheless, by optimizing these parameters, it is possible to assemble CNT-containing organic photovoltaic devices that come close to controls using ITO in terms of quantum efficiency and fill factor.²³ The film morphology of the CNT electrode is another important determinate of performance. When using CNT-OTEs in electroluminescent devices inhomogeneous films can limit the brightness and cause electric short circuits. Depositing CNTs onto substrates functionalized with amine groups suitable for interaction with the CNTs addresses this issue in part and leads to significantly better device performance,²¹ but it remains necessary to develop techniques that yield homogenous CNT films reproducibly. Another important contributor toward the performance of CNT-based electrodes is the effect of doping. The Stevenson group systematically studied the effect of different amounts of nitrogen doping on the density of states and the electrical conductivity of CNT electrodes.²⁶ It would be expected that an increasing nitrogen content with the resulting higher density of states results in higher conductivities of the CNT electrodes. In the presented study, this trend could however not be observed. The authors attribute this to differences in CNT length (and the resulting increased junction resistance for films of shorter CNTs) and morphology of the fabricated films. This underlines that CNT-based electrodes present a complex system and the careful control of a variety of factors is necessary on the way toward applications. Furthermore, the difference between mixtures of different types of SWCNTs (i. e. metallic and semiconducting) and purely metallic SWCNTs plays a role with regard to the stability of the sheet resistance of SWCNT thin films.²⁷ While the sheet resistance of a film consisting of a mixture of metallic and semiconducting SWCNTs dropped from

19.6 k Ω /sq to 0.99 k Ω /sq after air exposure and doping with H₂SO₄, a sample of 99 % metallic SWCNTs only showed a change from 1.03 k Ω /sq to 0.65 k Ω /sq after the same treatment.

Electrodes for Lithium Ion Batteries. Their high surface area and similarity to currently used graphite makes CNTs promising candidates for use in lithium ion batteries. Calculations suggest that SWCNT bundles can intercalate Li on the interior wall of the CNTs and in interstitial spaces up to a density of about one Li per two carbon atoms, which is significantly higher than graphite.²⁸ Furthermore, a theoretical study of the interaction between Li/Li⁺ and the CNT sidewall suggests that Li/Li⁺ transport is energetically favored along the interior walls of CNTs while the energy surface of lithium on the exterior wall suggests that the metal is localized above the centroid of the six membered rings.²⁹ Experimentally, the use of CNTs as electrodes for lithium batteries has been demonstrated by several laboratories.^{19,30–35} Examples include metal oxide modified CNTs that further improve the properties of the CNTs. Reddy *et al* demonstrate that the synthesis of CNTs inside MnO₂ nanotubes leads to a composite electrode material that is superior to both individual components in terms of the specific charge storage capacity (Figure 1.2).³⁵

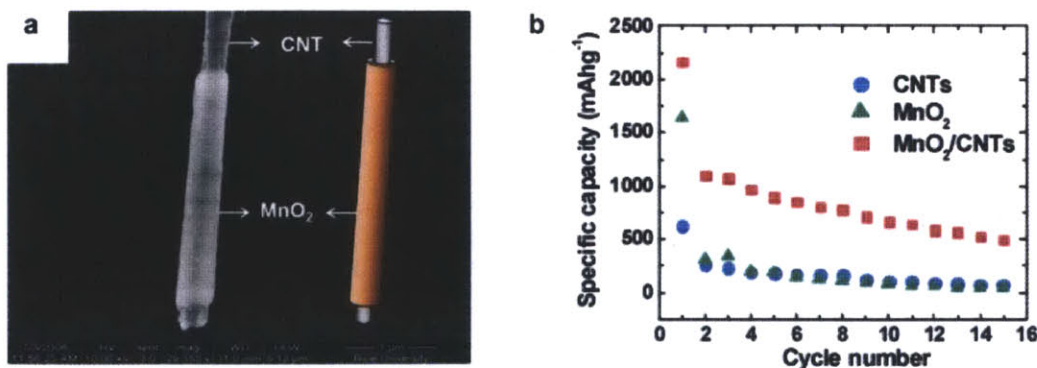


Figure 1.2. CNT-containing MnO₂ nanotubes for use in lithium ion batteries. (a) SEM image and schematic representation of the coaxial structure. (b) Discharge capacity vs. cycle number

for MnO₂/CNT coaxial nanotubes, MnO₂ nanotubes and CNTs. Reprinted with permission from Ref 35. Copyright 2009 American Chemical Society.

Other studies demonstrate a high rate of Li intercalation for TiO₂/CNT composites,³³ enhanced air stability and improved safety in dichalcogenide/CNT based Li⁺ batteries,³² and greater reversibility of Sb/CNT and SnSb_{0.5}/CNT based batteries compared to their CNT-free counterparts.³¹ CNTs in the form of aligned CNT arrays can be used as electrodes in battery applications without the need of an additional metal or metal oxide. However, achieving good electrical contacts between the aligned nanotubes has presented challenges. This can be overcome by using a conducting polymer such as PEDOT as a back contact.³⁰ The resulting electrode shows stable performance during a large number of cycles and is of considerably lower weight compared to conventional electrodes.

Another aspect that is important in the fabrication of batteries is the complexity of the electrode. Conventional electrodes usually consist of a metal substrate onto which a mixture of active material, binder, and electrical conductor is deposited. In contrast, CNTs can be fabricated into “buckypaper” electrodes by collection of surfactant-dispersed CNTs on a filter.¹⁹ Even though the discharge capacity of devices based on these electrodes is slightly lower than what can be obtained with conventional electrodes, the more facile fabrication is a clear advantage.

In addition to the illustrated examples, CNT-containing electrodes can be used in a variety of other applications. As will be discussed (*vide infra*), they can serve as components in sensors,^{12,36,37} fuel cells,^{38–42} dielectrophoretic trapping of DNA molecules,⁴³ and as superior electrodes in cyclic voltammetry for trace level detection.⁴⁴

1.3. Supercapacitors

Electrochemical double-layer capacitors (EDLCs), are considered a superior alternative to lithium batteries in applications that require high peak power for short periods of time. They store energy in the charged double layer that develops when a voltage is applied between electrodes that are immersed in an electrolyte. The capacitance of EDLCs scales with the active surface area of the electrode. In commercial EDLCs, carbon electrodes are rendered highly porous by thermal treatment to improve the surface area. In contrast, CNTs, offer intrinsically high surface areas and have thus been studied extensively as a material for EDLC applications. Extrapolation of experimental results has led Signorelli *et al* to suggest that CNT-based EDLCs can achieve approximately seven times higher energy densities than current activated carbon based devices.⁴⁵

Capacitors based on pristine CNTs. There are several ways to produce CNT-based supercapacitors. Pristine CNTs can be deposited onto a charge collector by electrophoretic deposition from a CNT suspension,⁴⁶ or they can be grown directly on a Ni support or a graphitic foil.^{47,48} Another method demonstrated by Futaba *et al* is the liquid-induced collapse of SWCNT forests to give a densified material (0.57 g cm^{-3} compared to 0.029 g cm^{-3} for as grown CNTs) that maintains a high Brunauer-Emmett-Teller (BET) surface area similar to the “as grown” CNTs (Figure 1.3).⁴⁹

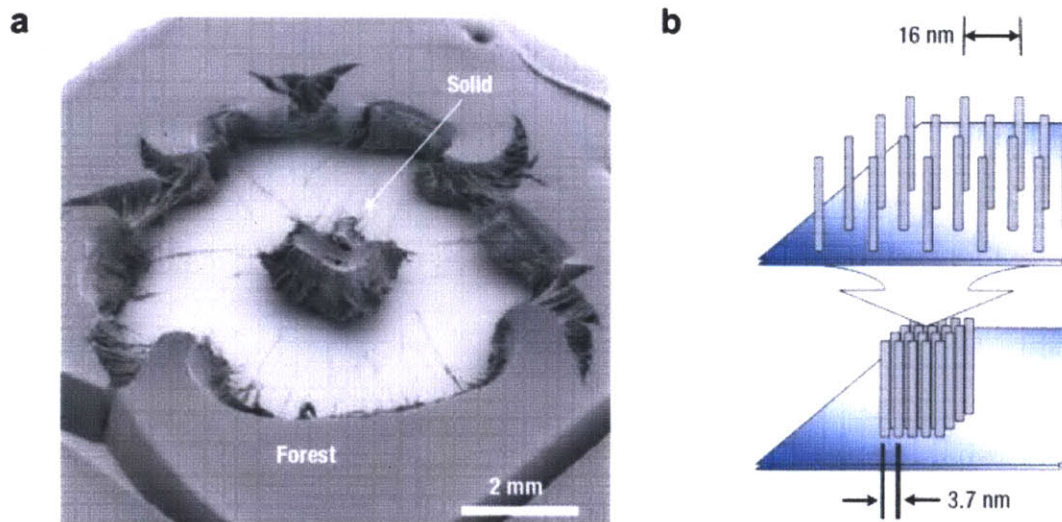


Figure 1.3. Fabrication of a high density SWCNT material by liquid-induced collapse of CNT forests. (a) SEM image of high density SWCNT (“solid”) and the surrounding SWCNT forest (b) Schematic diagram of the liquid-induced collapse process. Reprinted with permission from Ref 49. Copyright 2006 Nature Publishing Group.

In addition to these methods it is also possible to use binders such as poly(vinylidene chloride) for EDLCs.⁵⁰ Using this latter approach a specific capacitance of 180 F/g has been obtained.

Further improvement of the capacitance of an EDLC can be accomplished by the introduction of defect sites on the CNTs which add a redox pseudocapacitance to the double-layer capacitance. This can be achieved by plasma etching,⁵¹ argon irradiation,⁵² or by simply heating the CNTs in CO₂ or dry air.⁵³ Following this approach Lu *et al* were able to achieve energy densities of 148 Wh kg⁻¹ which is close to energy densities of Li ion batteries.⁵¹

Metal/CNT Capacitors. The combination of CNTs with metals or metal oxides is another route to improve the performance of EDLCs as a result of pseudocapacitance that originates from redox processes.^{54,55} The deposition of Ag nanoparticles has been shown to improve the specific capacitance of SWCNT based capacitors from 47 F g⁻¹ to 106 F g⁻¹.⁵⁴ In this context it is notable

that the capacitance increases with decreasing diameter of the utilized Ag nanoparticles in the observed range of 13 nm to 1 nm. An even larger increase in capacitance from 29.8 F g⁻¹ to 250.5 F g⁻¹ has been achieved when pristine MWCNTs were modified with MnO₂.⁵⁶

Polymer/CNT Composite Capacitors. Although the MnO₂-induced increase in capacitance discussed above is remarkable, only the fraction of the Mn moieties that are within a thin layer at the surface of the material are electrochemically active.⁵⁷ To achieve high loadings of electrochemically active MnO₂ in a supercapacitor, ternary composites of CNTs, polypyrrole (PPy), and MnO₂ have been investigated.⁵⁸ These composites exhibit high cyclability, retaining 88 % of the initial charge after 10,000 cycles. Sivakkumar *et al* attribute this performance to the CNTs ability to disperse high loads of MnO₂ in the conductive polymer. In those studies the ternary composite outperforms CNT/MnO₂ as well as PPy/MnO₂ composites in terms of specific capacitance.

The use of conducting polymers in CNT-based supercapacitors is not limited to devices that contain metal oxides. Composites of polyaniline (PANI) and SWCNTs have been shown to have superior performance compared to capacitors that use either material individually.⁵⁹ Khomenko *et al* demonstrated the use of two different types of conducting polymers, PPy and PANI, in a CNT-containing supercapacitor. Using PPy/MWCNT as the negative and PANI/MWCNT as the positive electrode they have achieved a capacitance of 320 F g⁻¹.⁶⁰

1.4. CNT-based Electronic Components

CNTs promise to be essential parts of many future electronic components such as nanowires, transistors, and switches. Assemblies of metallic as well as semiconducting CNTs can be used to

produce macroscopic devices, but methods are also being developed that allow for individual tubes to be used as nanoelectronic components.

Nanowires. The high aspect ratio and electronic transport capabilities of CNTs make them promising candidates for use in nanowires. These assertions are supported by both calculations and experimental results^{61,62} that demonstrate excellent performance even at temperatures up to 250 °C and high current densities of up to 10^9 to 10^{10} A cm⁻².⁶³ In nanowire performance, CNTs of typical dimensions (8.6 nm diameter and 2.6 μm in length) have been found to be comparable to the calculated properties of Au nanowires with the same dimensions.⁶⁴ In addition to individual CNTs, composites of CNTs and conducting polymers have many potential applications. Wang *et al* have demonstrated a template method wherein pyrrole is electropolymerized in the presence of CNTs to produce highly conductive nanowires.⁶⁵

Use of CNTs as Contacts in Organic Transistors. Aromatic organic molecules and conjugated polymers can interact with the surface of CNTs to give low contact resistance when CNTs are used as the electrodes in organic field effect transistors (organic FETs or OFETs).⁶⁶ The contact resistance of poly(3-hexylthiophene) (P3HT) thin-film FETs produced using spray-coated CNT array contacts was found to be similar to devices using Au bottom contacts. For pentacene-based transistors the CNT array contact resistance was found to be lower than that of the corresponding Au contacts.⁶⁶ In addition to deposition by spray-coating, CNT arrays can also be applied by spin-coating of CNTs that were previously dispersed in water by wrapping with poly(4-styrene sulfonate) (PSS). Pentacene FETs, so created, displayed field-effect mobilities that were four times higher than analogous FETs with Au bottom contacts.⁶⁷

In addition to this enhanced performance, pentacene-based FETs can be efficiently miniaturized when individual CNTs instead of CNT arrays are used as the source/drain electrodes. Qi *et al* recently demonstrated an FET in which pentacene bridges a sub-10 nm gap cut into a SWCNT.¹⁷ In an example published by Aguirre *et al*, individual CNTs proved to be well-suited contacts for charge injection into pentacene transistors, outperforming metal-based electrodes by an order of magnitude.⁶⁸

CNT-based Field Effect Transistors. While metallic conducting CNTs are a good material for the source/drain electrodes of OFETs, semiconducting SWCNTs themselves are an attractive active material for FETs. In addition to creating simplified structures for FETs, the use of SWCNTs has also led to the development of CNT-based sensors (*vide infra*).^{69,70} In an early example, Tans *et al* were able to fabricate a back-gated FET based on an individual semiconducting SWCNT that spanned the gap between two Pt electrodes on an Si/SiO₂ substrate.⁷¹ One challenge for early SWCNT FETs was the contact resistance at the interface between the CNTs and the metal electrodes, which limited the conductance in the “on” state. This problem was overcome by using Pd to contact the CNTs, as this material exhibits stronger interactions with the nanotubes. The resulting FETs have been shown to behave as ohmically contacted ballistic conductors when in the “on” state.⁷² In order to fabricate more complex devices it is necessary to employ methods to create arrays of individual CNT-based devices. Franklin *et al* demonstrated that arrays can be produced by catalytically growing SWCNTs between Mo contacts upon which catalyst particles had been deposited.⁷³ The yield of contacts that are bridged by individual SWCNTs was up to 30 % with a majority of the CNTs having the prerequisite semiconducting properties to produce high quality FETs.

Other uses of CNTs in electronic components. CNTs can be used as other active electronic components, including bistable molecular switches. Many examples of molecular switches have been demonstrated^{74,75} but in order to incorporate these switches into individually addressable electronic circuits, efficient contacts to discrete devices are necessary. CNTs are good candidates for this purpose because they provide good conductivity on the nanoscale and can also be attached covalently to molecular switching units. Recent theoretical studies suggest the feasibility of this concept for optically as well as nanomechanically induced switching mechanisms.⁷⁶⁻⁷⁸

A particularly interesting application of CNTs has been demonstrated by Jensen *et al.*,⁷⁹ wherein they describe a radio receiver based on a single MWCNT. In their setup, the MWCNT simultaneously acts as the antenna, tuner, amplifier, and demodulator – functions that are usually performed by individual components. The field emission from the tip of the MWCNTs in an electric field was monitored. When a radio signal, tuned to the resonance frequency of the MWCNTs, was broadcasted, the CNTs vibrate and the field emission changed as a function of the modulation of the radio signal (Figure 1.4). By connecting a sensitive speaker to this device, transmitted songs could be easily recognized by the human ear.

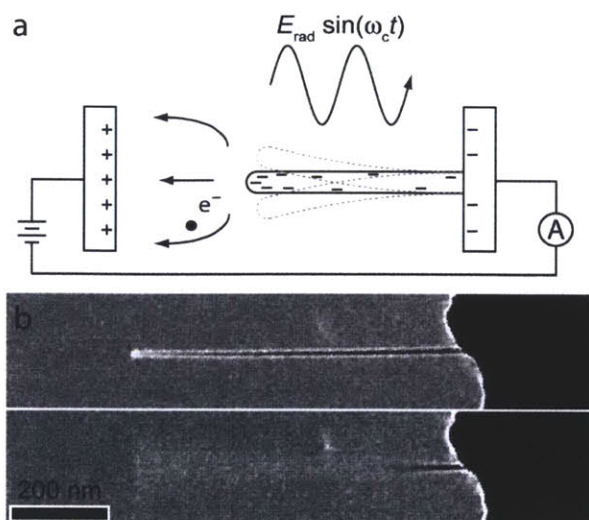


Figure 1.4. Nanotube radio. (a) Schematic representation. Upon excitation by radio transmissions, the MWCNT tip resonates and emits electrons that are detected *via* the resulting current. (b) Transmission electron micrographs of the MWCNT radio off and on resonance. Reprinted with permission from Ref 79. Copyright 2007 American Chemical Society.

1.5. Catalysis

Because of their conductivity, high surface area, and facile functionalization to give catalytically active sites, CNTs are promising candidates for catalysis. One important aspect that needs to be considered in this context is the purity of the CNTs. Commercial CNTs usually contain residual metal catalyst particles from the synthesis and typical washing procedures such as the use of nitric acid at elevated temperatures cannot always completely remove these impurities.⁸⁰ Purity is especially important in cases wherein electrocatalytic activity is attributed to pristine CNTs, because metal impurities can contribute toward the observed catalytic behavior.⁸¹

Fuel cells. In the interest of developing clean, sustainable, and mobile power sources, much attention has been focused on proton exchange membrane fuel cells (PEMFCs) in general, and direct methanol fuel cells (DMFCs) in particular.^{82–85} One limitation of these fuel cells is the high cost of the utilized Pt catalyst. By depositing catalyst nanoparticles on the surface of CNTs

with high active surface areas reduced amounts of Pt are needed to get high catalytic activity. Other carbon based materials such as high surface area carbon black can also be used for this purpose, but several studies demonstrate that MWCNT catalyst supports produce higher activities.^{82,83,86} There are multiple methods to synthesize Pt/MWCNT composites. CNTs are first oxidized by refluxing in HNO₃ or H₂SO₄/HNO₃ and subsequently mixed with a Pt nanoparticle precursor such as H₂PtCl₆. The latter salt is either reduced chemically with NaBH₄^{83,87} or reduced under thermal conditions using intermittent microwave irradiation to give MWCNT/Pt nanoparticle composites.⁸⁸ An alternative is the electrodeposition of the metal catalyst onto pristine CNTs.⁸⁶ Although the use of CNT/Pt composites reduces the required amount of the noble metal, it is still desirable to replace it with a more earth-abundant alternative. The use of covalent linkages has been demonstrated in MWCNT materials containing cobalt porphyrins and these materials have superior oxygen reduction performance as compared to other related systems.⁸⁹ More recently, another alternative has been demonstrated in which nickel bisdiphosphine units are covalently attached to MWCNTs via diazonium chemistry.⁸⁴ The active nickel center is a mimic of the active site of hydrogenase enzymes and also showed excellent catalytic activity and stability.

Organic Reaction Catalysis. Metal modified SWCNTs and MWCNTs have been reported to catalyze organic reactions. The aldehyde group in prenal (3-methyl-2-butenal) has been hydrogenated using a Pt/SWCNT system yielding the unsaturated alcohol prenol (3-methyl-2-butenol) in good selectivity relative to common side products 3-methyl-butyraldehyde and 3-methyl-butanol.⁹⁰ When compared to Al₂O₃ and SiO₂, CNTs display superior catalytic performance as supports for Pt or Pd catalysts in the hydrogenation of *o*-chloronitrobenzene to *o*-chloroaniline.⁹¹ Beyond the reduction of olefins and aldehydes, CNT-supported group 9 and 10

metal catalysts (Pt, Rh, PtPd and PdRh) have been investigated for the hydrogenation of aromatic molecules. In the hydrogenation of toluene and naphthalene, MWCNT supported PtPd exhibited particularly high initial turnover frequencies compared to SiO₂-Al₂O₃ or ZrPSi supported catalysts.¹⁸ The authors conclude that the low steric hindrance of metals adsorbed onto the external sidewall of the CNTs, as compared to the alternative supports, contributes to this effect. Furthermore, MWCNT-supported PdRh, Pt and Rh catalysts have been shown to hydrogenate benzene at room temperature, a process that is not possible with commercial carbon-based Pd and Rh catalysts.⁹² Beyond these examples, CNTs have been used as metal support for the oxidation of cellobiose⁹³ and in Suzuki coupling reactions.⁹⁴

Immobilization of Biomacromolecules. A prerequisite for the use of CNTs in biocatalysis is the successful immobilization of catalytically active biomacromolecules on the surface of the CNTs, ideally with an electrical interconnection that can lead to electrocatalytic activity. Enzymes such as horseradish peroxidase,⁹⁵ glucose oxidase,⁹⁶ or hydrogenase⁹⁷ have been successfully immobilized on CNT-modified electrodes and their electrocatalytic activity has been confirmed by cyclic voltammetry (CV). Several methods for the connection of CNTs and enzymes have been utilized. A facile way to immobilize enzymes is to drop-cast a suspension of CNTs onto an electrode and subsequently immerse this modified electrode in a solution of the enzyme.⁹⁷ The biocompatibility of the CNTs in this process is improved by covalently attaching poly(ethylene glycol) (PEG) chains.⁹⁸ This functionalization also increases the water solubility and thus facilitates the device fabrication. Alternatively, CNTs and enzymes can be deposited onto an electrode by successive spray-casting from the respective dispersions.⁹⁶ In addition to these non-covalent immobilization methods, it has been shown that covalently crosslinked networks of CNTs and enzymes can be formed and linked to Au electrodes using electropolymerizable

aniline moieties.⁹⁹ These resulting bioelectrocatalytic systems are able to oxidize glucose at a turnover rate of ca. 1025 s^{-1} thereby showing that the incorporation of the functionalization does not lead to degradation of the enzyme's activity.

1.6. Filters and Membranes

The interactions of the CNT surface with target molecules, in addition to the inherent porosity resulting from their tubular structure, renders them interesting materials for the formation of filters and membranes. For these applications, CNTs can be easily assembled onto a larger pore size supporting filter or networks of nanotubes can be created to produce all-CNT membranes.¹⁰⁰

Transport of Small Molecules Through CNTs. The internal diameter of CNTs varies depending on the conditions that are used to synthesize the CNTs, with typical diameters ranging from 1 nm for SWCNTs to several nanometers for MWCNTs. With diameters on the same order of magnitude as most single molecules, CNTs are well-suited as pores for molecular transport. Simulations have shown that water transport within the tubes is facile, which is at first glance remarkable considering that the non-polar surface of the CNTs does not interact well with polar water molecules.¹⁰¹ Water molecules inside the tubes are energetically stabilized by hydrogen bond interaction with their neighboring molecules. Subsequent theoretical investigations have built upon this and explored the possibility of using SWCNTs for water desalination.¹⁰² Although water can pass through armchair type SWCNTs with chiral vectors ranging between (5,5) and (8,8), the diffusion of sodium ions is energetically too high for the smaller (5,5) and (6,6) SWCNTs. This effect has been demonstrated experimentally in the direct contact membrane distillation (DCMD) of salt water utilizing self-supporting CNT membranes.¹⁰³ In these experiments 99% salt rejection could be achieved at flux rates of ca. $12 \text{ kg m}^{-2} \text{ h}^{-1}$.

Functionalization of the CNT end-groups, which are the entrances to the CNT pores, can also be used to influence the transport. In an early example, Hinds *et al* oxidized the end groups of the membrane-forming CNTs and subsequently covalently attached biotin to the terminal carboxylate groups which were then bound to streptavidin.¹⁰⁴ After streptavidin binding, the flux of $\text{Ru}(\text{NH}_3)_6^{3+}$ across the membrane was reduced by a factor of 15 showing the successful change of the transport through the pores. This approach has been extended to include functionalizing the end groups of CNTs with aliphatic groups of different chain lengths as well as anionically charged dye molecules.¹⁰⁵ The flux of cationic ruthenium trisbipyridine and methyl viologen was demonstrated to be significantly higher for the membranes that were functionalized with the anionic dye, as compared to those functionalized by nonpolar groups.

Although these examples are interesting for applications that require the permanent preference for the transport of a certain species, it is also desirable to have the ability to dynamically switch the transporting ability of membranes. This can be accomplished by modulating the water wettability of the CNTs in a membrane with external stimuli. Increasing the temperature of a CNT-membrane from 293 to 306 K, or exposing it to sonication, led to a significant increase in the diffusion of ionic compounds such as HCl, Na_2SO_4 or KCl, thereby demonstrating the feasibility of this concept.¹⁰⁶

Substrate-supported Filters Based on CNT Networks. CNT-based membranes are not only interesting candidates to discriminate between compounds that have a size on the Å scale, but can also be used to remove bacteria and viruses from water or to filter aerosols from air. A particular advantage of CNTs in this context is that the resulting filters can be easily cleaned by ultrasonication and autoclaving, which allows for repeated use with full filtering efficiency.¹⁰⁷ For these applications, the CNTs are typically deposited onto a membrane such as

polytetrafluoroethylene,¹⁰⁸ poly(vinylidene fluoride),¹⁰⁹ polyamide, or polypropylene for structural support.¹¹⁰ In these schemes SWCNTs as well as MWCNTs have been shown to exhibit excellent retention of bacteria and viruses. An additional benefit of this approach is that SWCNT-based filters exhibit high antimicrobial activity.¹⁰⁹

1.7. Sensors

CNTs are widely viewed as natural sensing elements that deliver a key nanowire architecture that had been previously identified as providing high sensitivity.¹¹¹ Several aspects of CNT properties that have been discussed earlier in the context of other applications can be exploited to create sensory responses. Specifically CNTs that are functionalized with molecular units imparting specificity can be used to make resistive or FET sensory devices. Electrical-based sensor schemes have the potential for facile integration into other electronic circuits, miniaturization, low power consumption, and low cost.

CNTs have been used in their pristine form to create sensory systems exploiting their high surface area and adsorptive properties. Alternatively, they can be functionalized with metal or metal oxide particles, coated with polymers, or covalently linked to DNA or enzymes to provide specificity.

Sensors based on pristine CNTs. Numerous examples of sensors employing pristine (unfunctionalized) SWCNTs have been reported. In these devices CNTs can interact directly with analytes *via* van der Waals or donor-acceptor interaction between the target molecule and the SWCNT sidewall. Additionally, sensitivity to specific classes of chemicals has been attributed to the presence of defect sites on the SWCNTs as well as residual metal catalyst that is left from the CNT fabrication process.

SWCNT-based sensors for reactive gases such NO_2 and NH_3 have been studied and in this case the respective oxidizing and reducing nature of the analytes allows for them to be distinguished with transistor type sensors using individual semiconducting SWCNTs.^{112,113} Under a gate voltage of + 4 V exposure to 200 ppm NO_2 resulted in an increase in conductivity by three orders of magnitude.¹¹³ Randomly grown networks of SWCNTs were used to create sensors for the nerve agent simulant dimethyl methylphosphonate (DMMP).¹¹² Sub-ppb levels of DMMP could be detected with minimal response to potentially interfering molecules, such as hydrocarbons or water. CNTs can also be fabricated into sensors by dispersion in a solvent such as DMF and subsequent drop-casting onto electrodes. A conductance-based sensor obtained in this fashion was able to detect NO_2 at a concentration of 44 ppb and nitrotoluene at 262 ppb.¹¹⁴

As a result of their fabrication and purification processes, CNTs contain defect sites and residual metal catalyst that can contribute to the sensing response. Purposely introducing defect sites by partial oxidation of CNTs increased their electrical response to various chemical vapors, presumably by creating stronger CNT-analyte interactions.¹¹⁵ As oxidative treatment is a common CNT purification method, this effect needs to be considered when utilizing “pristine” CNTs in a sensor. Iron oxide particles that are often present in unpurified CNT samples provide another source that can induce a sensing response that does not stem intrinsically from the carbon network. The Compton group investigated this effect by comparing the cyclic voltammetric response of a CNT-modified basal plane pyrolytic graphite (BPPG) electrode with an Fe (III) oxide modified BPPG electrode to H_2O_2 .³⁶ Based on their findings, they suggest that residual Fe_2O_3 particles on the CNT surface are the main cause for the response of CNT films to H_2O_2 .

Metal and Metal Oxide Particles. Beyond being a potential contaminant in CNT-based sensing devices, the aforementioned metal oxide particles can be introduced purposefully in order to create more pronounced or more specific sensing responses. A CuO/MWCNT modified electrode showed a significantly higher current response to glucose compared to a MWCNT electrode.¹³ Using a standard three electrode cell with the CuO/MWCNT electrode as the working electrode, this sensor was able to determine the glucose concentration in human blood serum samples. The response time was ca. 1 s and the sensor recovered almost completely after the measurement ($\geq 95\%$). In another example, an MWCNT-carrying glassy carbon electrode (GCE) was modified with a porous ZnO film.¹¹⁶ This sensor was used to detect hydroxylamine with a very low detection limit of 0.12 μM and also exhibited a quick sensing response of < 3 s, as well as complete recovery. In addition to metal oxides, metal nanoparticles have been used in CNT sensors. An electrode composed of MWCNTs, gold nanoparticles, and glucose oxidase was used as an amperometric biosensor for glucose achieving a detection limit of 20 μM .¹¹⁷

Coating with Polymers or Biomacromolecules. Polymers have been utilized to increase the sensitivity and selectivity of CNT-based sensors and Snow *et al* described a capacitive SWCNT sensor for a variety of chemical vapors.¹⁴ Coating the sensor with a thin layer of a strong hydrogen-bonding polycarbosilane (HC) increased the response to acetone ca. 100 fold, and a self-assembled monolayer (SAM) coating containing hexafluoroisopropanol moieties significantly decreased the response time for the nerve agent mimic DMMP (Figure 1.5).

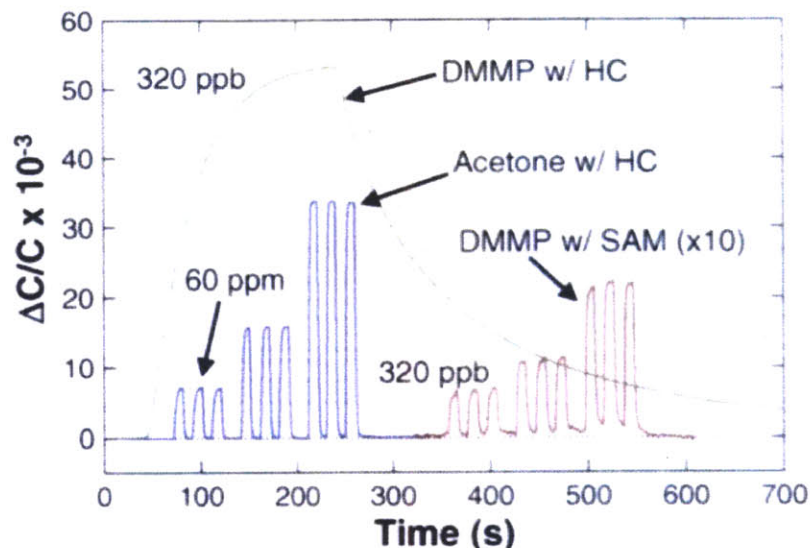


Figure 1.5. Decrease in response time to DMMP from a CNT sensor coated with a strong hydrogen-bonding polycarbosilane (HC) (green curve) to one coated with a self-aligned monolayer (SAM) coating of hexafluoroisopropanol moieties (red curve). Reprinted with permission from Ref 14. Copyright 2005 American Association for the Advancement of Science.

In another example, an SWCNT-based FET type sensor was coated with either the electron donating polymer polyethyleneimine (PEI) or the strongly acidic polymer Nafion.¹¹⁸ PEI lowered the detection limit for the oxidizing gas NO_2 from 10 – 50 ppb to 100 ppt as compared to an uncoated device. The PEI coated sensor did not react to NH_3 vapor (100 ppm in air), however Nafion coatings enabled NH_3 -detection while at the same time eliminating the response to NO_2 . Other recent examples of polymer enhanced selectivity include response to DMMP and xylene isomers by wrapping SWCNTs with functionalized polythiophenes.^{119,120} In the case of xylene detection, the latter method demonstrated the ability of sophisticated molecular recognition to create differential sensory responses based solely on the isomeric composition of an analyte.

Blending MWCNTs with functionalized poly(olefin sulfone)s (POSs), polymers that degrade upon exposure to radiation, led to devices which show a 5-fold increase in conductivity when

exposed to 5×10^3 rad of gamma radiation.¹²¹ The effects were optimized by creating polymers with affinities to the MWCNTs and heavy elements (bismuth) to create enhanced gamma ray absorption. The increased conduction stems from spontaneous depolymerization and the resulting increased interconnections of the conductive MWCNTs to create conductive pathways between electrodes.

DNA or other biomacromolecules can also be used to improve the performance of CNT-based sensors. Drop-casting a solution of single-stranded DNA (ss-DNA) onto an SWCNT FET sensor increased its response to several vapors including methanol, trimethylamine, and DMMP.¹⁰ Furthermore, ss-DNA-modified SWCNTs can be used to electrochemically detect the hybridization with a target ss-DNA strand.¹²² The polysaccharide chitosan was used to wrap MWCNTs and provided functional groups for the attachment of glucose dehydrogenase to create a glucose sensor.¹²³ Enzymes can also be incorporated in sensors by drop-casting directly onto an SWCNT electrode and subsequent coating with a nafion layer.¹²⁴ Another fabrication method for creating a biocomposite electrode is the mixing of tyrosinase, epoxy resin, and MWCNTs and subsequent curing at 40 °C for one week.¹²⁵ Using this electrode, catechol could be detected at a detection limit of 0.01 mM, a value about half of that obtainable with an analogous graphite sensor.

Non-covalent Attachment of Small Molecules. The non-covalent interactions of small molecules with the SWCNT surface have been used to provide functionality to increase sensor selectivity. An early approach involved sensors created by depositing hematoxylin onto an MWCNT-modified GCE.³⁷ Utilizing differential pulse voltammetry (DPV), the resulting electrode could be used to detect adrenaline with good sensitivity and selectivity over adrenalin, ascorbic acid, and uric acid.

As a result of the strong interaction with the π network of the CNT surface and pyrene, this group has been widely used for the non-covalent attachment of functional groups to CNTs. Chen *et al* exploited this by incubating CNTs in a solution of 1-pyrenebutanoic acid succinimidyl ester to create a precursor to biological functionalization. Subsequently, they immobilized various proteins on the CNT by reaction of the succinimidyl ester with amine groups (Figure 1.6).¹⁵

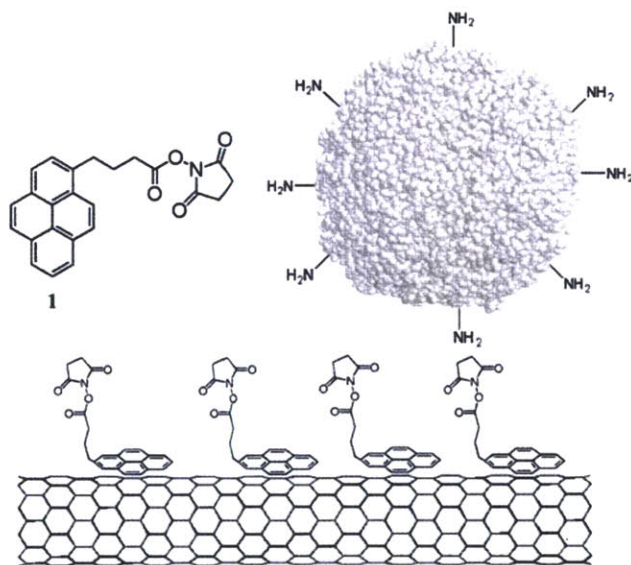


Figure 1.6. 1-Pyrenebutanoic acid succinimidyl ester is adsorbed onto the CNT surface providing a chemically reactive anchor for the immobilization of proteins. Reprinted with permission from Ref 15. Copyright 2001 American Chemical Society.

This method has further been utilized to incorporate glucose oxidase into an SWCNT sensor.¹²⁶ The same pyrene linker was reacted with a functionalized aniline to bind hexafluoroisopropanol (HFIP) to SWCNTs.¹²⁷ FET-type sensors based on these modified SWCNTs showed a very low detection limit of 50 ppb for the nerve agent mimic DMMP, as well as good selectivity over other chemical vapors such as ethanol, water, toluene, or hexane.

Chemical Modification. Another possibility for the connection of sensing units onto CNTs is to use covalent attachment of functional groups. Due to its simplicity, the oxidation of CNTs to yield carboxylic acid groups has been the dominant method for this purpose. The carboxylic acid groups can be used to attach oligonucleotides via carbodiimide chemistry.^{12,128} By combining electrodes obtained in this fashion with $\text{Ru}(\text{bpy})_3^{2+}$ mediated guanine oxidation, Li *et al* achieved detection limits of only a few attomoles in a DNA sensor.¹² The same strategy can also be used to attach the enzyme glucose oxidase for the detection of glucose.¹²⁹ Although less common, other covalent functionalization methods have been employed in order to fabricate CNT based sensors. SWCNTs have been covalently functionalized by phenyl boronic acid moieties for glucose sensing by both wrapping with poly(aminophenylboronic acid) or the covalent attachment of phenyl boronic acid using diazonium chemistry.⁶⁹

1.8. Biomedical Applications

With the development of covalent¹³⁰ and non-covalent¹³¹ methods to achieve water soluble CNTs as well as procedures to attach biomolecules to CNTs,¹⁰ the development of biomedical applications of CNTs became possible.¹³² An interesting field in this context is the use of CNTs for bioelectronic applications. The Kotov group demonstrated that it is possible to grow neuronal cells on an SWCNT-based IBI film and subsequently excite the cells by passing a current through the CNT network.¹³³ While a synthetic polymer (poly(acrylic acid)) was used for the anionic layers in this example, it is also possible to fabricate multilayer films using poly(styrene sulfonate) wrapped SWCNTs and laminin, a component of the human extracellular matrix.¹³⁴ Neural networks could be grown and electrically excited on this substrate. The interfacing of CNTs and neural cells can be an important step toward the development of bioelectronic components such as neural prosthetic devices. Nevertheless, other challenges have to be

overcome on the way to real world applications. One such challenge is the formation of CNT-based nerve mimics that contain a sufficiently high density of separately addressable conductive channels. One way to achieve this is by repeatedly drawing and bundling CNT-filled glass fibers.¹³⁵ Starting from a single channel with a diameter of 150 μm after the first draw, a bundle of 19600 channels with an individual channel diameter of 0.39 μm was obtained after three drawing and bundling cycles. The process also improves the CNT alignment inside the channels resulting in an increased conductivity after each drawing step. The conductivity is however still low (1.21×10^{-4} S/m) compared to other CNT-based electronic components and it would be desirable to increase this value.

Another field of research in the context of CNT-based biomedical applications is the use of CNTs for therapeutic applications. Several examples have been reported such as the CNT-assisted delivery of platinum anticancer drugs¹³⁶ or as molecular transporters for human T cells.¹³⁷ Even though the cytotoxicity of the CNTs was tested and shown to be low in both studies, the toxicity of CNTs remains a complex question and might limit their use in biomedical applications.¹³⁸

1.9. Mechanical Applications

As a result of their covalent carbon networks, CNTs are exceptionally strong materials and exhibit Young's moduli on the order of 1 TPa for SWCNTs and low defect density MWCNTs grown by arc-discharge.^{139,140}

High Strength Applications. CNTs strongly interact with each other *via* van der Waals forces and unless specially treated after their synthesis, they form bundles. Separating these bundles can be a challenge when individual CNTs are desired. In high strength applications, however, these

bundles or ropes allow for the realization of the CNT mechanical properties on a macroscopic scale. By manipulating ropes consisting of tens to hundreds of SWCNTs with an atomic force microscope tip (AFM tip), the tensile strength of these bundles has been determined to be on the order of 45 GPa.¹⁴¹ The synthesis of CNTs can be optimized to achieve ropes of macroscopic dimensions. Zhu *et al* fabricated SWCNT strands with lengths up to several centimeters by catalytic pyrolysis of n-hexane.¹⁴² These strands showed metallic conductance above 90 K and a Young's modulus of 49 to 77 GPa. By spinning MWCNTs from nanotube forests while introducing twist, CNT equivalents of cotton or wool yarns could be obtained (Figure 1.7).¹⁶

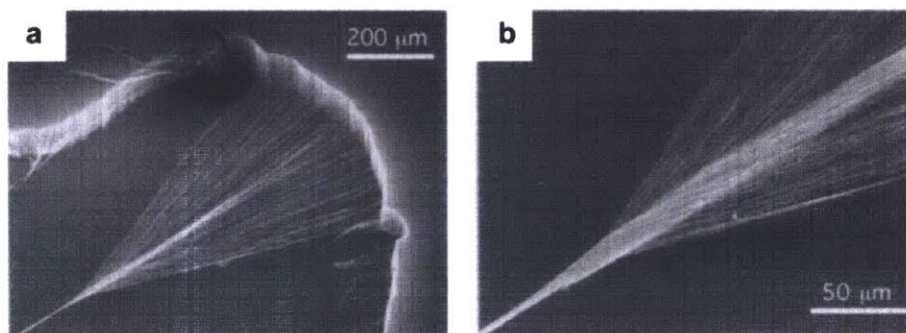


Figure 1.7. Spinning of CNT yarns from MWCNT forests. (a and b) SEM images of the spinning process. Reprinted with permission from Ref 16. Copyright 2004 American Association for the Advancement of Science.

The MWCNT yarns have a density of ca. 0.8 g cm^{-3} and a tensile strength of 460 MPa when combined into two-ply yarns. Yarns fabricated by this procedure have been assembled into sheets that were several centimeters wide and one meter long.¹⁴³ These hydrophobic sheets could support water droplets with a mass that was approximately 50,000 higher than the mass of the area of the MWCNT sheet they contacted.

CNT-containing Actuators. CNTs in pristine form or in combination with polymers have been fabricated into electromechanical actuators. In these actuators, a voltage is applied to CNTs immersed in an electrolyte and the charge injected into the CNTs is compensated by the formation of a double-layer. At low charge injection, this results in expansion of the material for electron injection and contraction for hole injection. In an early example, Baughman *et al* demonstrated this effect using sheets of SWCNTs that were immersed in NaCl solutions as well as other electrolytes.¹⁴⁴ Higher strain rates and amplitudes could be achieved by using resistance compensation.¹⁴⁵ Based on the same principle, a ply actuator has been demonstrated by forming a layered material of CNTs and an epoxy film.¹⁴⁶ CNTs can also be used in Nafion-based actuators wherein an applied voltage causes swelling, because the induced charge is compensated by uptake of ions from a surrounding electrolyte. Landi *et al* demonstrated that Nafion composites with high purity SWCNTs showed actuation with CNT contents as low as 0.5% w/w, which is an indication of the high conductivity and large aspect ratio of the CNTs.¹⁴⁷

1.10. Challenges for Applications of CNTs

CNTs are good candidates for a variety of applications. Nevertheless, there are several challenges associated with their synthesis, purification, processing and fabrication into devices. CNTs are usually synthesized by either chemical vapor deposition (CVD),¹⁴⁸ laser ablation¹⁴⁹ or arc discharge.³ While the use of a metal catalyst in these processes can be avoided in some cases such as the arc discharge production of MWCNTs, it is required in most synthetic processes. As a result, residual metal particles are a common impurity in CNT samples. If not removed properly, these impurities can significantly change the behavior of a CNT-based device as illustrated by the Compton group and described previously.³⁶ In addition to metal particles, as synthesized CNTs commonly contain amorphous carbon, fullerenes and carbon nanoparticles.¹⁵⁰

Several purification procedures have been suggested such as the gas¹⁵¹ and liquid phase¹⁵² as well as electrochemical oxidation¹⁵³ of impurities and high purities of over 99 % (with respect to metal content) have been achieved. It has to be noted, however, that some of these methods significantly alter the properties of the CNTs. The treatment with H₂SO₄/HNO₃ for example is known to cut long CNTs into smaller fragments introducing carboxylic acid groups at their ends.¹⁵⁴ While this can be desirable for the subsequent attachment of functional groups it can be a disadvantage when defect-free CNTs with high aspect ratios are required in electronic applications. Physical methods such as filtration,¹⁵⁵ centrifugation¹⁵⁶ or high temperature annealing¹⁵⁷ can avoid CNT shortening and oxidation, but they are less effective in removing impurities compared to oxidative methods and in some cases require dispersible CNT samples. Therefore, the combination of chemical and physical methods has been attempted. Li *et al.* reported a procedure in which SWCNT bundles were purified by washing with benzene and HCl as well as ultrasonic and freezing treatment.¹⁵⁸ A purity of 95 % was achieved while no damage to the SWCNT bundles was observed by SEM and Raman measurements.

Despite these advances the purification of CNTs remains challenging. It is therefore desirable to develop CNT synthesis conditions that result in low amounts of impurities. Hata *et al.* have been able to synthesize SWCNT forests with a carbon purity of over 99.98 %.¹⁵⁹ They observed that water activates the metal catalyst in ethylene CVD. By optimizing the water and ethylene level during the reaction, they were able to increase the SWCNT product to catalyst ratio by two orders of magnitude compared to the high-pressure carbon monoxide (HiPCO) process which led to the observed very high purities. Optimizing the CNT synthesis conditions can lead to other advantages such as the formation of CNTs with narrow diameter distribution¹⁶⁰ or the preferred synthesis of metallic SWCNTs (up to 91 %).¹⁶¹

Besides synthesis and purification, the processing of CNTs is a key challenge on the way to applications. The major limiting factor in this context is the low solubility of CNTs.¹⁶² Several attempts have been made in order to overcome this limitation including the noncovalent attachment of solubilizing units^{131,163} as well as the oxidation of defect sites¹⁶⁴ or sidewall functionalization using azomethine ylides¹³⁰ or diazonium chemistry.¹⁶⁵ While pristine CNTs are essentially insoluble especially in polar solvents such as water, aqueous solubilities of up to 20 mg/mL have been reported using the mentioned methods. This has enabled the use of solution processing techniques such as drop-casting, spin-casting or spraying which facilitates the fabrication of CNT-based devices and opens the field for new applications. Nevertheless, it has to be noted that many of the reported high CNT solubilities rely on high-density covalent sidewall-functionalization. When SWCNTs are used, this functionalization results in a drastically reduced conductivity and is therefore not a viable option for many electronic applications. The development of novel methods that facilitate the processing of CNTs while having little impact on their electrical properties or providing the option to restore the conductivity in a subsequent step would therefore be desirable.

1.11. Conclusions

Many applications of pristine and modified SWCNTs and MWCNTs have emerged since their discovery about 20 years ago. The broad scope of these applications suggests that a multitude of CNT-based technologies will result of their unique properties of high electrical conductivity, mechanical strength, high aspect ratio, and nanoscale diameter. Many methods have been developed to modify carbon nanotubes including the deposition of metal nanoparticles or metal oxides, the non-covalent attachment of polymers, biomacromolecules and small aromatic compounds as well as various methods for the covalent functionalization. Additionally, various

ways to fabricate CNT-based devices such as drop-casting, spin-casting, spraying, or deposition onto a filter support have been developed. A combination of these functionalization and fabrication methods has made it possible to use CNTs in electrodes, capacitors and other electronic components, sensors, filters and membranes, and in catalysis, biomedical and mechanical applications. A prerequisite for further progress will be an increased availability of high-quality CNTs combined with newly developed modification and fabrication methods that overcome challenges that are currently limiting some applications of CNTs. Amazing progress has been made in all areas of CNT applications in the recent past and based on the amount of research that is being done on CNTs as well as the scientific community's fascination, significant further progress can be expected to create dramatic technological advances.

1.12. References

- (1) Mintmire, J. W.; Dunlap, B. I.; White, C. T. *Phys. Rev. Lett.* **1992**, *68*, 631.
- (2) Saito, R.; Fujita, M.; Dresselhaus, G.; Dresselhaus, M. S. *Phys. Rev. B.* **1992**, *46*, 1804.
- (3) Iijima, S. *Nature.* **1991**, *354*, 56.
- (4) Falvo, M. R.; Clary, G. J.; Taylor II, R. M.; Chi, V.; Brooks Jr, F. P.; Washburn, S.; Superfine, R. *Nature.* **1997**, *389*, 582.
- (5) Iijima, S.; Ichihashi, T. *Nature.* **1993**, *363*, 603.
- (6) Ajayan, P. M. *Chem. Rev.* **1999**, *99*, 1787.
- (7) Ebbesen, T. W.; Ajayan, P. M. *Nature.* **1992**, *358*, 220.
- (8) Hutchison, J. L.; Kiselev, N. A.; Krinichnaya, E. P.; Krestinin, A. V.; Loutfy, R. O.; Morawsky, A. P.; Muradyan, V. E.; Obraztsova, E. D.; Sloan, J.; Terekhov, S. V.; Zakharov, D. N. *Carbon.* **2001**, *39*, 761.
- (9) Flahaut, E.; Bacsá, R.; Peigney, A.; Laurent, C. *Chem. Commun.* **2003**, 1442.
- (10) Staii, C.; Johnson, A. T.; Chen, M.; Gelperin, A. *Nano Lett.* **2005**, *5*, 1774.

- (11) Banks, C. E.; Davies, T. J.; Wildgoose, G. G.; Compton, R. G. *Chem. Commun.* **2005**, 829.
- (12) Li, J.; Ng, H. T.; Cassell, A.; Fan, W.; Chen, H.; Ye, Q.; Koehne, J.; Han, J.; Meyyappan, M. *Nano Lett.* **2003**, 3, 597.
- (13) Jiang, L.-C.; Zhang, W.-D. *Biosens. Bioelectron.* **2010**, 25, 1402.
- (14) Snow, E. S.; Perkins, F. K.; Houser, E. J.; Badescu, S. C.; Reinecke, T. L. *Science.* **2005**, 307, 1942.
- (15) Chen, R. J.; Zhang, Y.; Wang, D.; Dai, H. *J. Am. Chem. Soc.* **2001**, 123, 3838.
- (16) Zhang, M.; Atkinson, K. R.; Baughman, R. H. *Science.* **2004**, 306, 1358.
- (17) Qi, P.; Javey, A.; Rolandi, M.; Wang, Q.; Yenilmez, E.; Dai, H. *J. Am. Chem. Soc.* **2004**, 126, 11774.
- (18) Pawelec, B.; Parola, V. La; Navarro, R. M.; Murcia-Mascaros, S.; Fierro, J. L. G. *Carbon.* **2006**, 44, 84.
- (19) Ng, S. H.; Wang, J.; Guo, Z. P.; Chen, J.; Wang, G. X.; Liu, H. K. *Electrochim. Acta.* **2005**, 51, 23.
- (20) Chien, Y.-M.; Lefèvre, F.; Shih, I.; Izquierdo, R. *Nanotechnology.* **2010**, 21, 134020.
- (21) Kim, M. J.; Shin, D. W.; Kim, J.-Y.; Park, S. H.; Han, I. T.; Yoo, J. B. *Carbon.* **2009**, 47, 3461.
- (22) Gu, H.; Swager, T. M. *Adv. Mater.* **2008**, 20, 4433.
- (23) Feng, Y.; Ju, X.; Feng, W.; Zhang, H.; Cheng, Y.; Liu, J.; Fujii, A.; Ozaki, M.; Yoshino, K. *Appl. Phys. Lett.* **2009**, 94, 123302.
- (24) Hu, L.; Li, J.; Liu, J.; Grüner, G.; Marks, T. *Nanotechnology.* **2010**, 21, 155202.
- (25) Vasilyeva, S. V.; Unur, E.; Walczak, R. M.; Donoghue, E. P.; Rinzler, A. G.; Reynolds, J. R. *ACS Appl. Mater. Interfaces.* **2009**, 1, 2288.
- (26) Wiggins-Camacho, J. D.; Stevenson, K. J. *J. Phys. Chem. C.* **2009**, 113, 19082.
- (27) Miyata, Y.; Yanagi, K.; Maniwa, Y.; Kataura, H. *J. Phys. Chem. C.* **2008**, 112, 3591.
- (28) Zhao, J.; Buldum, A.; Han, J.; Ping, L. *J. Phys. Rev. Lett.* **2000**, 85, 1706.
- (29) Udomvech, A.; Kerdcharoen, T.; Osotchan, T. *Chem. Phys. Lett.* **2005**, 406, 161.

- (30) Chen, J.; Liu, Y.; Minett, A. I.; Lynam, C.; Wang, J.; Wallace, G. G. *Chem. Mater.* **2007**, *19*, 3595.
- (31) Chen, W. X.; Lee, J. Y.; Liu, Z. *Carbon.* **2003**, *41*, 959.
- (32) Dominko, R.; Arčon, D.; Mrzel, A.; Zorko, A.; Cevc, P.; Venturini, P.; Gaberscek, M.; Remskar, M.; Mihailovic, D. *Adv. Mater.* **2002**, *14*, 1531.
- (33) Moriguchi, I.; Hidaka, R.; Yamada, H.; Kudo, T.; Murakami, H.; Nakashima, N. *Adv. Mater.* **2006**, *18*, 69.
- (34) Morris, R. S.; Dixon, B. G.; Gennett, T.; Raffaele, R.; Heben, M. J. *J. Power Sources.* **2004**, *138*, 277.
- (35) Reddy, A. L. M.; Shaijumon, M. M.; Gowda, S. R.; Ajayan, P. M. *Nano Lett.* **2009**, *9*, 1002.
- (36) Sljukić, B.; Banks, C. E.; Compton, R. G. *Nano Lett.* **2006**, *6*, 1556.
- (37) Zare, H. R.; Nasirizadeh, N. *Sensor Actuator. B.* **2010**, *143*, 666.
- (38) Somani, S. P.; Somani, P. R.; Sato, A.; Umeno, M. *Diam. Relat. Mater.* **2009**, *18*, 497.
- (39) Tang, Z.; Chua, D. H. C. *J. Electrochem. Soc.* **2010**, *157*, B868.
- (40) Tang, Z.; Ng, H. Y.; Lin, J.; Wee, A. T. S.; Chua, D. H. C. *J. Electrochem. Soc.* **2010**, *157*, B245.
- (41) Yang, J.; Liu, D.-J. *Carbon.* **2007**, *45*, 2845.
- (42) Yun, Y. S.; Bak, H.; Jin, H.-J. *Synth. Met.* **2010**, *160*, 561.
- (43) Tuukkanen, S.; Toppari, J. J.; Kuzyk, A.; Hirviniemi, L.; Hytönen, V. P.; Ihalainen, T.; Törmä, P. *Nano Lett.* **2006**, *6*, 1339.
- (44) Bertoncello, P.; Edgeworth, J. P.; Macpherson, J. V.; Unwin, P. R. *J. Am. Chem. Soc.* **2007**, *129*, 10982.
- (45) Signorelli, R.; Ku, D. C.; Kassakian, J. G.; Schindall, J. E. *Proc. IEEE.* **2009**, *97*, 1837.
- (46) Du, C.; Pan, N. *J. Power Sources.* **2006**, *160*, 1487.
- (47) Yoon, B.-J.; Jeong, S.-H.; Lee, K.-H.; Kim, H. S.; Park, C. G.; Han, J. H. *Chem. Phys. Lett.* **2004**, *388*, 170.

- (48) Chen, J. H.; Li, W. Z.; Wang, D. Z.; Yang, S. X.; Wen, J. G.; Ren, Z. F. *Carbon*. **2002**, *40*, 1193.
- (49) Futaba, D. N.; Hata, K.; Yamada, T.; Hiraoka, T.; Hayamizu, Y.; Kakudate, Y.; Tanaike, O.; Hatori, H.; Yumura, M.; Iijima, S. *Nat. Mater.* **2006**, *5*, 987.
- (50) An, K. H.; Kim, W. S.; Park, Y. S.; Choi, Y. C.; Lee, S. M.; Chung, D. C.; Bae, D. J.; Lim, S. C.; Lee, Y. H. *Adv. Mater.* **2001**, *13*, 497.
- (51) Lu, W.; Qu, L.; Henry, K.; Dai, L. *J. Power Sources*. **2009**, *189*, 1270.
- (52) Hoefler, M.; Bandaru, P. R. *Appl. Phys. Lett.* **2009**, *95*, 183108.
- (53) Yamada, Y.; Kimizuka, O.; Machida, K.; Suematsu, S.; Tamamitsu, K.; Saeki, S.; Yamada, Y.; Yoshizawa, N.; Tanaike, O.; Yamashita, J.; Don, F.; Hata, K.; Hatori, H. *Energ. Fuel*. **2010**, *24*, 3373.
- (54) Wee, G.; Mak, W. F.; Phonthammachai, N.; Kiebele, A.; Reddy, M. V.; Chowdari, B. V. R.; Gruner, G.; Srinivasan, M.; Mhaisalkar, S. G. *J. Electrochem. Soc.* **2010**, *157*, A179.
- (55) Zhang, W.-D.; Chen, J. *Pure Appl. Chem.* **2009**, *81*, 2317.
- (56) Xie, X.; Gao, L. *Carbon*. **2007**, *45*, 2365.
- (57) Toupin, M.; Brousse, T.; Bélanger, D. *Chem. Mater.* **2004**, *16*, 3184.
- (58) Sivakkumar, S. R.; Ko, J. M.; Kim, D. Y.; Kim, B. C.; Wallace, G. G. *Electrochim. Acta*. **2007**, *52*, 7377.
- (59) Zhou, Y.-k.; He, B.-l.; Zhou, W.-j.; Huang, J.; Li, X.-h.; Wu, B.; Li, H.-l. *Electrochim. Acta*. **2004**, *49*, 257.
- (60) Khomenko, V.; Frackowiak, E.; Béguin, F. *Electrochim. Acta*. **2005**, *50*, 2499.
- (61) Tans, S. J.; Devoret, M. H.; Dai, H.; Thess, A.; Smalley, R. E.; Geerligs, L. J.; Dekker, C. *Nature*. **1997**, 386, 474.
- (62) White, C. T.; Todorov, T. N. *Nature*. **1998**, *393*, 240.
- (63) Wei, B. Q.; Vajtai, R.; Ajayan, P. M. *Appl. Phys. Lett.* **2001**, *79*, 1172.
- (64) Kreupl, F.; Graham, A. P.; Duesberg, G. S.; Steinhögl, W.; Liebau, M.; Unger, E.; Hönlein, W. *Microelectron. Eng.* **2002**, *64*, 399.
- (65) Wang, J.; Dai, J.; Yarlagadda, T. *Langmuir*. **2005**, *21*, 9.

- (66) Southard, A.; Sangwan, V.; Cheng, J.; Williams, E. D.; Fuhrer, M. S. *Org. Electron.* **2009**, *10*, 1556.
- (67) Hong, K.; Nam, S.; Yang, C.; Kim, S. H.; Chung, D. S.; Yun, W. M.; Park, C. E. *Org. Electron.* **2009**, *10*, 363.
- (68) Aguirre, C. M.; Ternon, C.; Paillet, M.; Desjardins, P.; Martel, R. *Nano Lett.* **2009**, *9*, 1457.
- (69) Vlandas, A.; Kurkina, T.; Ahmad, A.; Kern, K.; Balasubramanian, K. *Anal. Chem.* **2010**, *82*, 6090.
- (70) Goldoni, A.; Petaccia, L.; Lizzit, S.; Larciprete, R. *J. Phys.-Condens. Mat.* **2010**, *22*, 013001.
- (71) Tans, S. J.; Verschueren, A. R. M.; Dekker, C. *Nature.* **1998**, *393*, 49.
- (72) Javey, A.; Guo, J.; Wang, Q.; Lundstrom, M.; Dai, H. *Nature.* **2003**, *424*, 654.
- (73) Franklin, N. R.; Wang, Q.; Tomblor, T. W.; Javey, A.; Shim, M.; Dai, H. *Appl. Phys. Lett.* **2002**, *81*, 913.
- (74) Collier, C. P.; Mattersteig, G.; Wong, E. W.; Luo, Y.; Beverly, K.; Sampaio, J.; Raymo, F. M.; Stoddart, J. F.; Heath, J. R. *Science.* **2000**, *289*, 1172.
- (75) Dulić, D.; Der Molen, S. J. van; Kudernac, T.; Jonkman, H. T.; Jong, J. J. D. de; Bowden, T. N.; Esch, J. van; Feringa, B. L.; Wees, B. J. van *Phys. Rev. Lett.* **2003**, *91*, 1.
- (76) Li, X.-F.; Wang, L.; Chen, K.-Q.; Luo, Y. *Appl. Phys. Lett.* **2009**, *95*, 232118.
- (77) Zhao, P.; Fang, C. F.; Wang, Y. M.; Zhai, Y. X.; Liu, D. S. *Physica E.* **2009**, *41*, 474.
- (78) Zhao, P.; Wang, P.; Zhang, Z.; Fang, C.; Wang, Y.; Zhai, Y.; Liu, D. *Solid State Commun.* **2009**, *149*, 928.
- (79) Jensen, K.; Weldon, J.; Garcia, H.; Zettl, A. *Nano Lett.* **2007**, *7*, 3508.
- (80) Pumera, M. *Carbon.* **2007**, 6453.
- (81) Banks, C. E.; Crossley, A.; Salter, C.; Wilkins, S. J.; Compton, R. G. *Angew. Chem. Int. Edit.* **2006**, *45*, 2533.
- (82) Li, W.; Liang, C.; Zhou, W.; Qiu, J.; Zhou, Z.; Sun, G.; Xin, Q. *J. Phys. Chem. B.* **2003**, *107*, 6292.

- (83) Prabhuram, J.; Zhao, T. S.; Tang, Z. K.; Chen, R.; Liang, Z. X. *J. Phys. Chem. B.* **2006**, *110*, 5245.
- (84) Goff, A. Le; Artero, V.; Joussetme, B.; Tran, P. D.; Guillet, N.; Métayé, R.; Fihri, A.; Palacin, S.; Fontecave, M. *Science.* **2009**, *326*, 1384.
- (85) Wang, C.; Waje, M.; Wang, X.; Tang, J. M.; Haddon, R. C.; Yan, Y. *Nano Lett.* **2004**, *4*, 345.
- (86) Tang, H.; Chen, J. H.; Huang, Z. P.; Wang, D. Z.; Ren, Z. F.; Nie, L. H.; Kuang, Y. F.; Yao, S. Z. *Carbon.* **2004**, *42*, 191.
- (87) Golikand, A. N.; Lohrasbi, E.; Maragheh, M. G.; Asgari, M. *J. Appl. Electrochem.* **2009**, *39*, 2421.
- (88) Tian, Z. Q.; Jiang, S. P.; Liang, Y. M.; Shen, P. K. *J. Phys. Chem. B.* **2006**, *110*, 5343.
- (89) Zhang, W.; Shaikh, A. U.; Tsui, E. Y.; Swager, T. M. *Chem. Mater.* **2009**, *21*, 3234.
- (90) Lordi, V.; Yao, N.; Wei, J. *Chem. Mater.* **2001**, *13*, 733.
- (91) Jiang, L.; Gu, H.; Xu, X.; Yan, X. *J. Mol. Catal. A-Chem.* **2009**, *310*, 144.
- (92) Yoon, B.; Pan, H.-B.; Wai, C. M. *J. Phys. Chem. C.* **2009**, 1520.
- (93) Tan, X.; Deng, W.; Liu, M.; Zhang, Q.; Wang, Y. *Chem. Commun.* **2009**, 7179.
- (94) Sullivan, J. A.; Flanagan, K. A.; Hain, H. *Catal. Today.* **2009**, *145*, 108.
- (95) Chen, H.; Dong, S. *Biosens. Bioelectron.* **2007**, *22*, 1811.
- (96) Zhao, H.-Z.; Sun, J.-J.; Song, J.; Yang, Q.-Z. *Carbon.* **2010**, *48*, 1508.
- (97) Luo, X.; Brugna, M.; Tron-Infossi, P.; Giudici-Ortoni, M. T.; Lojou, É. *J. Biol. Inorg. Chem.* **2009**, *14*, 1275.
- (98) Wen, Y.; Wu, H.; Chen, S.; Lu, Y.; Shen, H.; Jia, N. *Electrochim. Acta.* **2009**, *54*, 7078.
- (99) Baravik, I.; Tel-Vered, R.; Ovits, O.; Willner, I. *Langmuir.* **2009**, *25*, 13978.
- (100) López-Lorente, A. I.; Simonet, B. M.; Valcárcel, M. *Anal. Chem.* **2010**, *82*, 5399.
- (101) Hummer, G.; Rasaiah, J. C.; Noworyta, J. P. *Nature.* **2001**, *414*, 188.
- (102) Corry, B. *J. Phys. Chem. B.* **2008**, *112*, 1427.

- (103) Dumée, L. F.; Sears, K.; Schütz, J.; Finn, N.; Huynh, C.; Hawkins, S.; Duke, M.; Gray, S. *J. Membrane Sci.* **2010**, *351*, 36.
- (104) Hinds, B. J.; Chopra, N.; Rantell, T.; Andrews, R.; Gavalas, V.; Bachas, L. G. *Science*. **2004**, *303*, 62.
- (105) Majumder, M.; Chopra, N.; Hinds, B. J. *J. Am. Chem. Soc.* **2005**, *127*, 9062.
- (106) Yu, M.; Funke, H. H.; Falconer, J. L.; Noble, R. D. *J. Am. Chem. Soc.* **2010**, *132*, 8285.
- (107) Srivastava, A.; Srivastava, O. N.; Talapatra, S.; Vajtai, R.; Ajayan, P. M. *Nat. Mater.* **2004**, *3*, 610.
- (108) Brady-Estévez, A. S.; Nguyen, T. H.; Gutierrez, L.; Elimelech, M. *Water Res.* **2010**, *44*, 3773.
- (109) Brady-Estévez, A. S.; Kang, S.; Elimelech, M. *Small*. **2008**, *4*, 481.
- (110) Guan, T.; Yao, M. *J. Aerosol. Sci.* **2010**, *41*, 611.
- (111) Swager, T. M. *Accounts Chem. Res.* **1998**, *31*, 201.
- (112) Novak, J. P.; Snow, E. S.; Houser, E. J.; Park, D.; Stepnowski, J. L.; McGill, R. A. *Appl. Phys. Lett.* **2003**, *83*, 4026.
- (113) Kong, J.; Franklin, N. R.; Zhou, C.; Chapline, M. G.; Peng, S.; Cho, K.; Dai, H. *Science*. **2000**, *287*, 622.
- (114) Li, J.; Lu, Y.; Ye, Q.; Cinke, M.; Han, J.; Meyyappan, M. *Nano Lett.* **2003**, *3*, 929.
- (115) Robinson, J. A.; Snow, E. S.; Badescu, S. C.; Reinecke, T. L.; Perkins, F. K. *Nano Lett.* **2006**, *6*, 1747.
- (116) Zhang, C.; Wang, G.; Liu, M.; Feng, Y.; Zhang, Z.; Fang, B. *Electrochim. Acta.* **2010**, *55*, 2835.
- (117) Rakhi, R. B.; Sethupathi, K.; Ramaprabhu, S. *J. Phys. Chem. B.* **2009**, *113*, 3190.
- (118) Qi, P.; Vermesh, O.; Grecu, M.; Javey, A.; Wang, Q.; Dai, H.; Peng, S.; Cho, K. *J. Nano Lett.* **2003**, *3*, 347.
- (119) Wang, F.; Yang, Y.; Swager, T. M. *Angew. Chem. Int. Ed.* **2008**, *47*, 8394.
- (120) Wang, F.; Gu, H.; Swager, T. M. *J. Am. Chem. Soc.* **2008**, *130*, 5392.
- (121) Lobez, J. M.; Swager, T. M. *Angew. Chem. Int. Edit.* **2010**, *49*, 95.

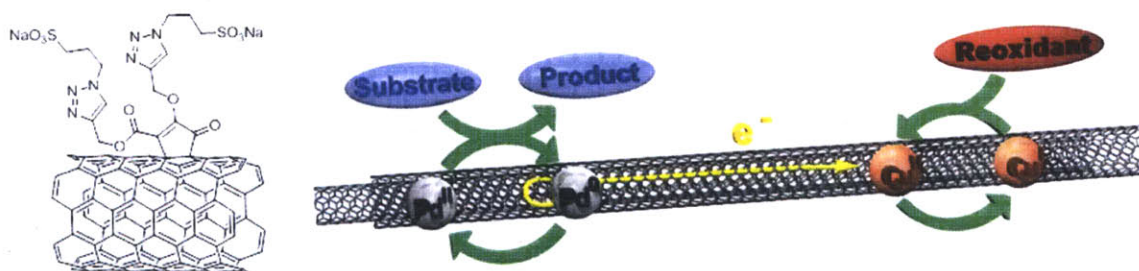
- (122) Zhang, X.; Jiao, K.; Liu, S.; Hu, Y. *Anal. Chem.* **2009**, *81*, 6006.
- (123) Zhang, M.; Smith, A.; Gorski, W. *Anal. Chem.* **2004**, *76*, 5045.
- (124) Pham, X.-H.; Bui, M.-P. N.; Li, C. A.; Han, K. N.; Kim, J. H.; Won, H.; Seong, G. H. *Anal. Chim. Acta.* **2010**, *671*, 36.
- (125) Pérez López, B.; Merkoçi, A. *Analyst.* **2009**, *134*, 60.
- (126) Besteman, K.; Lee, J.-O.; Wiertz, F. G. M.; Heering, H. A.; Dekker, C. *Nano Lett.* **2003**, *3*, 727.
- (127) Kong, L.; Wang, J.; Luo, T.; Meng, F.; Chen, X.; Li, M.; Liu, J. *Analyst.* **2010**, *135*, 368.
- (128) Cai, H.; Cao, X.; Jiang, Y.; He, P.; Fang, Y. *Anal. Bioanal. Chem.* **2003**, *375*, 287.
- (129) Lin, Y.; Lu, F.; Tu, Y.; Ren, Z. *Nano Lett.* **2004**, *4*, 191.
- (130) Georgakilas, V.; Tagmatarchis, N.; Pantarotto, D.; Bianco, A.; Briand, J.-P.; Prato, M. *Chem. Commun.* **2002**, 3050.
- (131) Star, A.; Steuerman, D. W.; Heath, J. R.; Stoddart, J. F. *Angew. Chem. Int. Edit.* **2002**, *41*, 2508.
- (132) Yang, W.; Thordarson, P.; Gooding, J. J.; Ringer, S. P.; Braet, F. *Nanotechnology.* **2007**, *18*, 412001.
- (133) Gheith, M. K.; Pappas, T. C.; Liopo, A. V.; Sinani, V. A.; Shim, B. S.; Motamedi, M.; Wicksted, J. P.; Kotov, N. A. *Adv. Mater.* **2006**, *18*, 2975.
- (134) Kam, N. W. S.; Jan, E.; Kotov, N. A. *Nano Lett.* **2009**, *9*, 273.
- (135) Hendricks, T. R.; Ivanov, I. N.; Schaeffer, D. A.; Menchhofer, P. A.; Simpson, J. T. *Nanotechnology.* **2010**, *21*, 115301.
- (136) Feazell, R. P.; Nakayama-Ratchford, N.; Dai, H.; Lippard, S. J. *J. Am. Chem. Soc.* **2007**, *129*, 8438.
- (137) Liu, Z.; Winters, M.; Holodniy, M.; Dai, H. *Angew. Chem. Int. Edit.* **2007**, *46*, 2023.
- (138) Poland, C. A.; Duffin, R.; Kinloch, I.; Maynard, A.; Wallace, W. A. H.; Seaton, A.; Stone, V.; Brown, S.; Macnee, W.; Donaldson, K. *Nat. Nanotechnol.* **2008**, *3*, 423.
- (139) Salvétat, J.-P.; Bonard, J.-M.; Thomson, N. H.; Kulik, A. J.; Forró, L.; Benoit, W.; Zuppiroli, L. *Appl. Phys. A-Mater.* **1999**, *69*, 255.

- (140) Ruoff, R. S.; Lorents, D. C. *Carbon*. **1995**, *33*, 925.
- (141) Walters, D. A.; Ericson, L. M.; Casavant, M. J.; Liu, J.; Colbert, D. T.; Smith, K. A.; Smalley, R. E. *Appl. Phys. Lett.* **1999**, *74*, 3803.
- (142) Zhu, H. W.; Xu, C. L.; Wu, D. H.; Wei, B. Q.; Vajtai, R.; Ajayan, P. M. *Science*. **2002**, *296*, 884.
- (143) Zhang, M.; Fang, S.; Zakhidov, A. A.; Lee, S. B.; Aliev, A. E.; Williams, C. D.; Atkinson, K. R.; Baughman, R. H. *Science*. **2005**, *309*, 1215.
- (144) Baughman, R. H.; Cui, C.; Zakhidov, A. A.; Iqbal, Z.; Barisci, J. N.; Spinks, G. M.; Wallace, G. G.; Mazzoldi, A.; Rossi, D. De; Rinzler, A. G.; Jaschinski, O.; Roth, S.; Kertesz, M. *Science*. **1999**, *284*, 1340.
- (145) Barisci, J. N.; Spinks, G. M.; Wallace, G. G.; Madden, J. D.; Baughman, R. H. *Smart Mater. Struct.* **2003**, *12*, 549.
- (146) Yun, Y.-H.; Shanov, V.; Schulz, M. J.; Narasimhadevara, S.; Subramaniam, S.; Hurd, D.; Boerio, F. J. *Smart Mater. Struct.* **2005**, *14*, 1526.
- (147) Landi, B. J.; Raffaele, R. P.; Heben, M. J.; Alleman, J. L.; VanDerveer, W.; Gennett, T. *Nano Lett.* **2002**, *2*, 1329.
- (148) Cheng, H. M.; Li, F.; Su, G.; Pan, H. Y.; He, L. L.; Sun, X.; Dresselhaus, M. S. *Appl. Phys. Lett.* **1998**, *72*, 3282.
- (149) Thess, A.; Lee, R.; Nikolaev, P.; Dai, H.; Petit, P.; Robert, J.; Xu, C.; Lee, Y. H.; Kim, S. G.; Rinzler, A. G.; Colbert, D. T.; Scuseria, G. E.; Tomanek, D.; Fischer, J. E.; Smalley, R. E. *Science*. **1996**, *273*, 483.
- (150) Hou, P.; Liu, C.; Cheng, H. *Carbon*. **2008**, *46*, 2003.
- (151) Chiang, I. W.; Brinson, B. E.; Huang, A. Y.; Willis, P. A.; Bronikowski, M. J.; Margrave, J. L.; Smalley, R. E.; Hauge, R. H. *J. Phys. Chem. B*. **2001**, *105*, 8297.
- (152) Li, Y.; Zhang, X.; Luo, J.; Huang, W.; Cheng, J.; Luo, Z.; Li, T.; Liu, F.; Xu, G.; Ke, X.; Li, L.; Geise, H. J. *Nanotechnology*. **2004**, *15*, 1645-1649.
- (153) Fang, H.-T.; Liu, C.-G.; Liu, C.; Li, F.; Liu, M.; Cheng, H.-M. *Chem. Mater.* **2004**, *16*, 5744.
- (154) Liu, J.; Rinzler, A.; Dai, H.; Hafner, J.; Bradley, R.; Boul, P.; Lu, a; Iverson, T.; Shelimov, K.; Huffman, C.; Rodriguez-Macias, F.; Shon, Y.; Lee, T.; Colbert, D.; Smalley, R. *Science*. **1998**, *280*, 1253-6.

- (155) Shelimov, K. B.; Esenaliev, R. O.; Rinzler, A. G.; Huffman, C. B.; Smalley, R. E. *Chem. Phys. Lett.* **1998**, 282, 429.
- (156) Hu, H.; Yu, A.; Kim, E.; Zhao, B.; Itkis, M. E.; Bekyarova, E.; Haddon, R. C. *J. Phys. Chem. B.* **2005**, 109, 11520.
- (157) Lambert, J. M.; Ajayan, P. M.; Bernier, P.; Planeix, J. M.; Brotons, V.; Coq, B.; Castaing, J. *Chem. Phys. Lett.* **1994**, 226, 364.
- (158) Li, F.; Cheng, H. M.; Xing, Y. T.; Tan, P. H.; Su, G. *Carbon.* **2000**, 38, 2041.
- (159) Hata, K.; Futaba, D. N.; Mizuno, K.; Namai, T.; Yumura, M.; Iijima, S. *Science.* **2010**, 306, 1362.
- (160) Dervishi, E.; Li, Z.; Watanabe, F.; Xu, Y.; Saini, V.; Biris, A. R.; Biris, A. S. *J. Mater. Chem.* **2009**, 19, 3004.
- (161) Harutyunyan, A. R.; Chen, G.; Paronyan, T. M.; Pigos, E. M.; Kuznetsov, O. a; Hewaparakrama, K.; Kim, S. M.; Zakharov, D.; Stach, E. a; Sumanasekera, G. U. *Science.* **2009**, 326, 116-20.
- (162) Tasis, D.; Tagmatarchis, N.; Georgakilas, V.; Prato, M. *Chem. Eur. J.* **2003**, 9, 4000.
- (163) Backes, C.; Schmidt, C. D.; Hauke, F.; Böttcher, C.; Hirsch, A. *J. Am. Chem. Soc.* **2009**, 131, 2172.
- (164) Asuri, P.; Karajanagi, S. S.; Sellitto, E.; Kim, D.-Y.; Kane, R. S.; Dordick, J. S. *Biotechnol. Bioeng.* **2006**, 95, 804.
- (165) Li, H.; Cheng, F.; Duft, A. M.; Adronov, A. *J. Am. Chem. Soc.* **2005**, 127, 14518.

CHAPTER 2

Water Soluble Multi-Walled Carbon Nanotubes



Adapted and reprinted in part from:

Schnorr, J. M.; Swager, T. M. “Wiring-up catalytically active metals in solution with sulfonated carbon nanotubes”

J. Mater. Chem. **2011**, *21*, 4768-4770

Reproduced by permission of The Royal Society of Chemistry

2.1. Introduction

As described in chapter 1, carbon nanotubes (CNTs) possess unique mechanical and electrical properties which have led to intense research and enabled a variety of applications.¹⁻³ Despite intense investigations and some progress, the low stability of CNT dispersions in a variety of solvents and, in particular, in water remains a challenge which complicates processing, manipulation, analysis, and ultimately, limits the scope of their applications.⁴ Several approaches to improve the solubility of CNTs in water have been explored including the non-covalent attachment of solubilizing molecules,⁵⁻⁹ functionalization by oxidation of defect sites to carboxylates^{10,11} (with concomitant amide or ester formation¹²⁻¹⁵), as well as sidewall functionalization by reaction with azomethine ylides¹⁶ or diazonium chemistry.¹⁷ Each approach has particular advantages. Non-covalent functionalization of CNTs typically only requires mixing and sonication of CNTs with the solubilizing agent and thus has the advantage of being easy to execute, especially in the case of commercially available solubilizing agents. Covalent functionalization on the other hand can lead to higher functional group densities on the CNT surface compared to non-covalent approaches and as a result very high solubilities especially when ionic groups are attached to the CNTs.¹⁶ Furthermore, covalent attachment avoids potential phase separation of the solubilizing agent and the CNTs and can, therefore, offer a longer shelf-life of the soluble CNTs. Water solubilities obtained by the described methods range from below 1.0 mg mL^{-1} up to 20 mg mL^{-1} .

It has to be noted in this context that in contrast to determining the solubility of small organic molecules or inorganic salts there is no common standard for the determination of CNT solubilities. The high absorption coefficient of CNTs in the visible range makes it difficult to distinguish a suspension from a solution by optical methods without prior dilution. Furthermore,

reported CNT solubilities usually do not represent the formation of a solution with a negative free energy change of mixing but rather maximum concentrations that form stable dispersions for an extended amount of time and/or under centrifugation conditions.¹⁸ Even though the exact conditions vary, in many cases a mixture of solubilized CNTs and water is centrifuged to remove undispersed aggregates. Subsequently, a sample of the supernatant is diluted to reach an optical density compatible with UV-vis spectroscopy directly followed by an absorption measurement to determine the concentration. Alternatively, the concentration is determined after letting aggregates settle for a certain amount of time without centrifugation. For the work described in this chapter, we have chosen the first method, because it gives more conservative estimates and because it is more widely used.

Despite of previous progress in solubilizing CNTs, we anticipated that a further improved solubility of CNTs would not only simplify manipulation and handling of CNTs, but could also lead to new applications. One such application enabled by soluble CNTs is their use as electronic interconnects in an aqueous system (Figure 2.1).

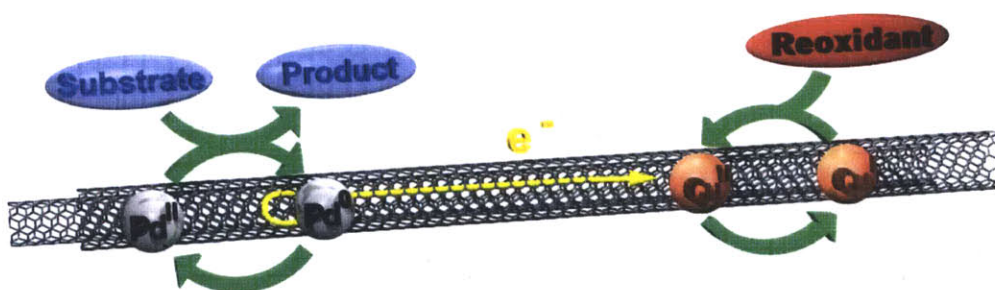


Figure 2.1. Schematic representation of electron transfer facilitated by soluble MWCNT. A CNT-bound metal such as Pd(II) is reduced during the catalytic cycle and is subsequently regenerated via an electron transfer to an oxidant such as Cu(II) taking advantage of the conductivity of the soluble MWCNT.

Such a system can potentially accelerate electron transfer processes between metal centers in small molecule catalysis, as well as between proteins in biocatalysis, and can lead to more efficient processes. This chapter describes a method for the covalent functionalization of multi-walled CNTs (MWCNTs) that introduces a high density of sulfonate groups on the CNT surface. The very high solubility of these sulfonate MWCNTs (sulfMWCNTs) in polar solvents (up to 31 mg mL⁻¹ in water) led us to investigate their use as an additive to improve electron transfer processes in a Wacker type oxidation reaction.

2.2. Results and Discussion

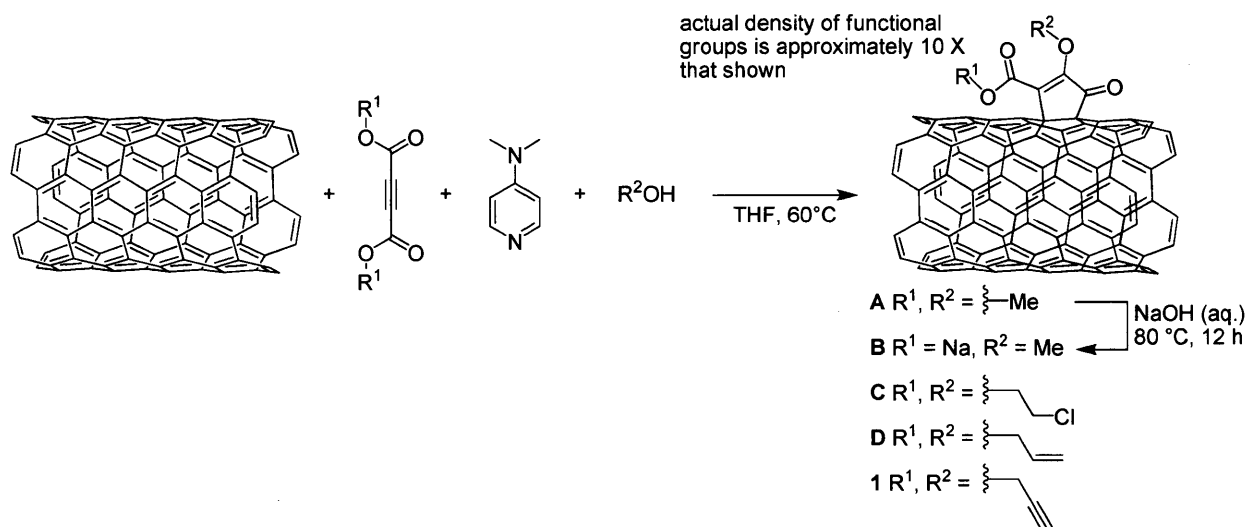
2.2.1. Solubilization of MWCNTs by Covalent Attachment of Sulfonate Groups

In order to enable applications, such as the use of soluble CNTs as electrical interconnects in a polar environment, several criteria have to be met. Firstly, a sufficient solubility has to be achieved by installing a high density of functional, ideally ionic, groups on the surface of CNTs. Secondly, the solubilizing groups should be compact enough to allow access to the surface of CNTs and allow electron transfers to and from the CNTs. Thirdly, the CNT itself has to be sufficiently conductive.

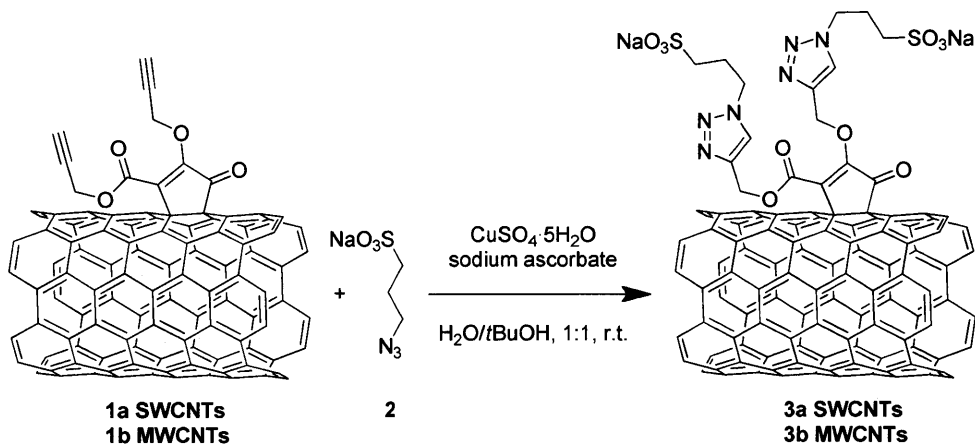
We envisioned that these criteria could be met by following a two-step protocol to covalently functionalize CNTs with sulfonate groups. As covalent functionalization partially disrupts the conjugation on the CNT surface, and thus lowers the conductivity, we chose MWCNTs for this project. These materials offer the advantage that their surface can be functionalized to provide the necessary solubility while the inner CNT layers remain unfunctionalized and, therefore, conductive. In the first step, we utilized a method outlined in Scheme 2.1 to install acetylene moieties on the surface of MWCNTs. This route, previously developed in our laboratory¹⁹, leads

to high functional group densities and exhibits a good functional group tolerance compatible with terminal acetylenes.^{20,21} In the second step, the acetylene-functionalized MWCNTs were reacted with sodium 3-azidopropane-1-sulfonate in a copper catalyzed 1,3-dipolar cycloaddition reaction yielding sulfMWCNTs (**3**, Scheme 2.2).

Scheme 2.1. Zwitterionic Approach toward CNT Functionalization



Scheme 2.2. Synthesis of sulfonate CNTs



Although azides, such as 3-azidopropane-1-sulfonate, are known to react directly with CNTs at elevated temperature,²² the utilized two-step approach allowed us to install two sulfonate moieties per functional group on the CNT offering higher sulfonate densities.

To establish the generality of the functionalization process and test the role of the electronic properties of CNTs in our study, we also covalently functionalized single-walled CNTs (SWCNTs) with sulfonate groups. Fourier-transform infrared (FT-IR) spectroscopic analysis indicated the presence of acetylene units in **1a** and subsequent formation of 1,2,3-triazole groups, as well as the introduction of sulfonates in **3a**. The functional group density was determined by X-ray photoelectron spectroscopy (XPS) to be one triazole sulfonate group per 17 SWCNT-carbon atoms (based on the ratio of C1s to S2p signal). Thermogravimetric analysis (TGA) provided a slightly lower estimate of one triazole sulfonate per 20 SWCNT-carbons. After confirming high degrees of SWCNT functionalization, we extended this method to the synthesis of sulfMWCNTs **3b**. Successful functionalization was confirmed by FT-IR, TGA and XPS at densities of 1 sulfonate group per 43 carbon atoms of the MWCNT.

To quantify the water solubility of **3b** for comparison to other methods, the compound was sonicated for 1 h in milliQ water at a concentration of 65 mg mL⁻¹. Aggregates were allowed to settle for 24 h, and the concentration of sulfMWCNT in supernatant was determined to be 63 mg/mL using UV-vis spectroscopy with a previously determined extinction coefficient (see Experimental Section). After an additional 24 h, the concentration of sulfMWCNT in solution further decreased to 52 mg/mL. To complete the precipitation of aggregates, the mixture of dissolved and aggregated sulfMWCNTs was then centrifuged for 10 minutes at 5,000 rpm resulting in a sulfMWCNT concentration of 31 mg/mL in the supernatant. Centrifugation for an additional 30 min did not further reduce the concentration, suggesting that the precipitation of

aggregates was complete and the measured concentration represents the amount of dissolved sulfMWCNTs (Figure 2.2a). We attribute the obtained high CNT concentration to the large dissociation constant of the sodium from the sulfonate groups as well as the high density of these moieties on the surface of the CNTs. It should be noted that based on this data, 48h without centrifugation are not sufficient for complete precipitation of CNT aggregates further underlining that care has to be taken when comparing reported CNT solubilities in the literature that are based on different protocols (e.g., with and without centrifugation).

The good solubility of sulfMWCNTs could further be confirmed qualitatively by comparing optical micrographs of droplets of **3b** (20 mg mL^{-1}) with droplets containing pristine and propargyl MWCNTs (Figure 2.2b-d).

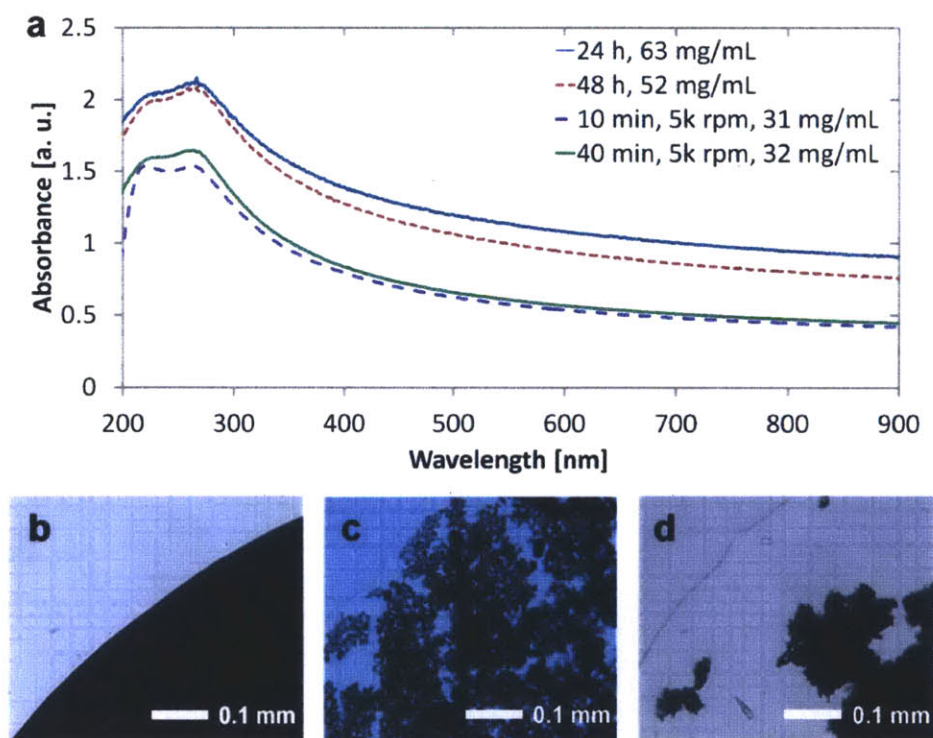


Figure 2.2. (a) UV-vis spectroscopy was used to determine the concentration of sulfMWCNT in water 24 h and 48 h after sonication as well as after subsequent centrifugation for 10 and 40

minutes (all samples were diluted 1:1000 directly before the measurement). (b) Optical micrograph of sulfMWCNTs in a water droplet, (c) propargyl MWCNTs, (d) pristine MWCNTs.

While pristine MWCNTs and propargyl functionalized MWCNTs both show strong aggregation, the sulfMWCNT sample appears homogenous at the utilized magnification. Furthermore, in a biphasic solvent system of water and dichloromethane, the sulfMWCNTs clearly prefer the aqueous phase (Figure 2.3a-b). Free-standing films obtained by drop-casting concentrated aqueous suspensions of sulfMWCNTs (50 mg mL^{-1}) on the surface of glass show a smooth surface on both sides appearing “shiny” on a photograph (Figure 2.3c) suggesting a small amount or the absence of CNT aggregates whose presence would lead to a visibly higher surface roughness.

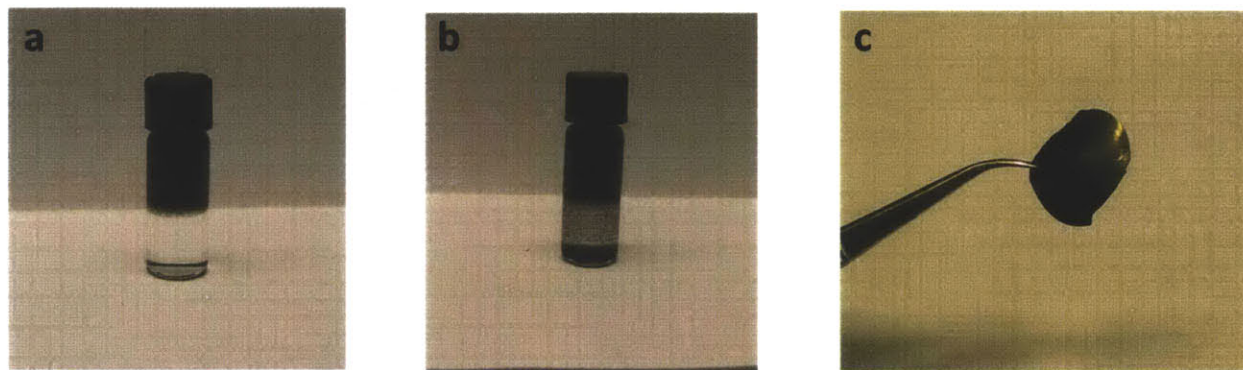


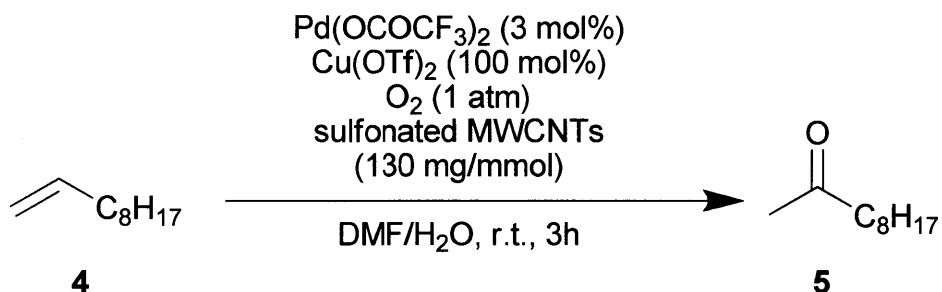
Figure 2.3. sulfMWCNTs in a biphasic $\text{H}_2\text{O}/\text{CH}_2\text{Cl}_2$ system (a) before and (b) after shaking the vial showing the preference of the sulfMWCNTs for the aqueous phase, (c) free-standing film of sulfMWCNTs (thickness ca. 0.25 mm) obtained by drop-casting onto a glass surface from a suspension at 50 mg mL^{-1} .

2.2.2. Sulfonate MWCNTs as Water Soluble Electrical Interconnects

After confirming the high solubility of sulfMWCNTs in water, we investigated the possibility of using the functionalized CNTs to connect metal ions in solution. In this context, the sulfonate

and 1,2,3-triazole groups that were introduced on the CNT surface could potentially act as metal binding sites in addition to providing water solubility. As a model demonstration system we examined the Wacker oxidation of 1-decene to 2-decanone (Scheme 2.3).²³

Scheme 2.3. Wacker-type oxidation in the presence of sulfonated MWCNTs



Mechanistically, during the Wacker reaction, the palladium(II) catalyst is first reduced to palladium(0) and then regenerated by oxidative electron transfer to copper(II).²⁴ Provided that the sulfMWCNTs can provide an electrical connection between the two metals, the addition of sulfMWCNTs should lead to an observable rate enhancement (Figure 2.4a).

According to the literature,²³ as well as in our hands, the Wacker oxidation of 1-decene to 2-decanone, in the absence of MWCNTs as additives, goes to completion within 24 h. To successfully observe meaningful rate enhancements in this transformation both, the catalyst loading as well as the reaction time, were reduced compared to the literature procedure (3 mol% vs. 10 mol% Pd, 3 h instead of 24 h). The yield after 3 h *versus* biphenyl as an internal standard was determined by gas chromatography (GC) and used as an indicator for the influence of the sulfMWCNTs on the reaction rates.

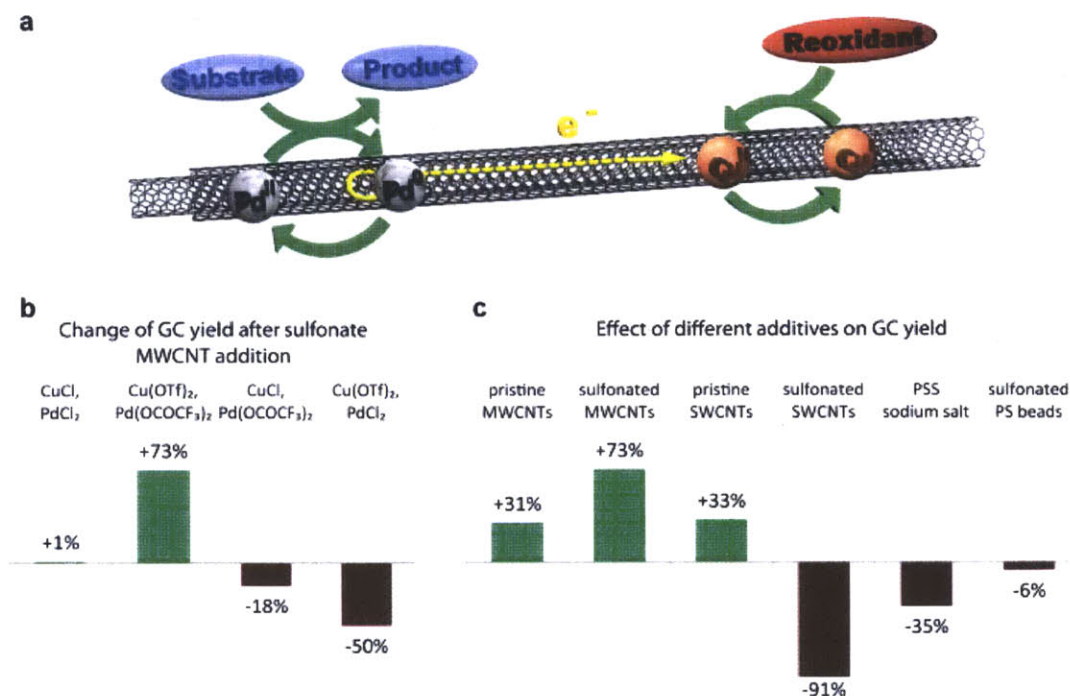


Figure 2.4. (a) Schematic representation of the proposed mechanism of electron transfer facilitated by sulfMWCNT. The CNT-bound Pd(II) is reduced during the catalytic cycle and is subsequently regenerated via an electron transfer to Cu(II) taking advantage of the conductivity of the sulfMWCNT. (b) The addition of sulfMWCNTs leads to an increase in yield compared to the control without MWCNTs if metal sources with weakly coordinating counterions are used. (c) The addition of highly soluble sulfMWCNTs leads to an increase in yield which is more than twice as high as the yield-increasing effect of pristine SWCNTs and MWCNTs. Non-conductive sulfonated materials such as sulfSWCNTs lower the yield of 5. Reaction conditions see Scheme 2.3 and Experimental Section.

In initial studies using PdCl₂ and *in situ* oxidized CuCl as the metal sources, the addition of sulfMWCNTs did not have an appreciable effect on the yield after 3 h, suggesting negligible metal-CNT interactions. This prompted us to investigate metal sources with less coordinating counterions to favor metal-CNT association. Repeating the reaction with palladium bistrifluoroacetate and copper triflate reduced the yield of the CNT-free control reaction. In the

CNT free reactions, 41 % yield were obtained using PdCl₂ and CuCl while the yield using Pd(OCOCF₃)₂ and Cu(OTf)₂ was 16 %.

However, under these conditions, the addition of sulfMWCNTs resulted in a 73% increase in yield after 3 h compared to a CNT free control reaction (the yield increased from 16 % to 29 %).

When only one of the metal chlorides was replaced by the more soluble metal source, a decrease in yield was observed which suggests that only one metal interacted well with the CNT. As a result, the CNT-facilitated electron transfer could not take place and sequestration of one of the metals caused the negative effect on the yield (Figure 2.4b).

To further explore which role the conductivity, solubility, and surface functionalization of the sulfMWCNTs played for the observed effect on the Wacker-type oxidation, we investigated pristine MWCNTs and SWCNTs as conductive, but less soluble alternatives to sulfMWCNTs. Both additives resulted in an improved yield (+31% for MWCNTs and +31% for SWCNTs) compared to CNT-free controls (Figure 2.4c). Nevertheless, this improvement was significantly lower than the effect of sulfMWCNTs even though both types of pristine CNTs showed a higher conductivity (3.9 S cm⁻¹ for pristine MWCNTs, 21.8 S cm⁻¹ for SWCNTs compared to 2.8 S cm⁻¹ for sulfMWCNTs in thin film measurements).

To gain further insight into the role of the conductivity of the additives, soluble but significantly less conductive sulfSWCNTs (0.6 S cm⁻¹ in thin film) were used instead of sulfMWCNTs. The lower conductivity of sulfSWCNTs compared to their MWCNT counterparts stems from the absence of conductive inner layers to compensate for the loss of conductivity in the outer CNT layer after covalent functionalization. This stronger effect of covalent functionalization on SWCNTs compared to MWCNTs is even more obvious when comparing the sulfCNTs to their

pristine CNT starting material. In the case of MWCNTs, the functionalization procedure reduces the conductivity by 28%, while the SWCNT's conductivity is lowered by as much as 97% as a result of the covalent attachment of sulfonate groups in the described fashion. When using sulfSWCNTs as an additive, the yield was decreased by 91%. This finding further supports the idea that binding of the catalytically active metal ions to a conductive CNT is needed to facilitate electron transfer. If the inner conductive CNTs are not present as in the case of sulfSWCNTs, sequestration of the metal ions has a negative effect on the yield.

In further control experiments we examined the effect of sodium poly(styrene sulfonate) as well as sulfonated polystyrene spheres. Similar to sulfSWCNTs the addition of these non-conductive sulfonated materials resulted in a reduction in the reaction yield confirming that the positive effect of the sulfMWCNTs is based primarily on their conductivity and not on the type or density of surface functionalization (Figure 2.4c).

2.3. Conclusions

In summary, SWCNTs and MWCNTs have been functionalized with a high density of sulfonate groups of 1 group for every 17 and 43 CNT carbon atoms, respectively. The obtained sulfMWCNTs exhibited a water solubility of 31 mg per mL, which is ca. 50% higher than solubilities obtained with previous methods. Furthermore, the addition of sulfMWCNTs to a Wacker type oxidation reaction led to an increase in yield compared to controls without CNTs. SulfMWCNTs performed significantly better than conductive but less soluble pristine CNTs as well as soluble but less conductive sulfonated materials such as sulfSWCNTs which suggests that modified CNTs that combine solubility and conductivity can be used to provide an electrical connection between catalytically active metals in solution.

2.4. Experimental Section

Materials

SWCNTs were received from SouthWest NanoTechnologies (CG-100, >90% carbon content, lot # CG100-000-0012) and used without further purification. MWCNTs were obtained from Aldrich (>95% purity, for small-scale reactions) and Bayer Group (Baytubes[®]C 150 P, >95% purity, for large-scale reactions) and used as received. All solvents were of spectroscopic grade unless otherwise noted. Sodium 3-azidopropane-1-sulfonate²⁵ and dipropargyl acetylenedicarboxylate²¹ were synthesized following reported procedures. All other chemicals were of reagent grade and used as received.

General Methods and Instrumentation

Fourier transform infrared (FT-IR) spectroscopy was performed on a Perkin-Elmer model 2000 FT-IR spectrophotometer using the Spectrum v. 2.00 software package. Raman spectra were measured on a Horiba LabRAM HR Raman Spectrometer using the excitation wavelength of 785 nm for SWCNTs and 532 nm for MWCNTs. The spectra in the UV-Vis range were obtained using an Agilent 8453 UV-visible spectrophotometer. TGA analyses were performed with a TGA Q50 apparatus (TA instruments). Experiments were carried out under nitrogen. Samples were heated at 15 °C/min from 50 °C to 900 °C. The thickness of thin films was measured using a Dektak 6M stylus profiler by Veeco and their conductivities were measured utilizing a Signatone four point probe with a 1.27 mm spacing connected to a Keithley 2400 source meter. XPS spectra were recorded on a Kratos AXIS Ultra X-ray Photoelectron Spectrometer. Gas chromatography (GC) was performed on an Agilent Technologies 7890A GC system. Optical

micrographs were recorded using a Leica DMRXP optical microscope with an attached Sony DXC-970MD camera. All synthetic manipulations were carried out under an argon atmosphere using standard Schlenk techniques unless otherwise noted.

Synthesis

Synthesis of propargyl SWCNTs 1a. A suspension of SWCNTs (240 mg, 20 mmol of carbon) in 1,4-dioxane (240 mL) was sonicated for 3 h. The mixture was heated to 60 °C and a solution of dipropargyl acetylenedicarboxylate (11.2 g, 59 mmol) in 1,4-dioxane (30 mL) and a solution of 4-dimethylaminopyridine (8.4 g, 69 mmol) in CHCl₃ (30 mL) were added simultaneously via syringe pump over 36 h. Subsequently, propargyl alcohol (9 mL, 8.7 g, 156 mmol) was added and the mixture was stirred at 60 °C for another 3 h. The reaction mixture was then cooled to room temperature and centrifuged at 3500 rpm for 20 min. The supernatant was discarded and the residue was extracted in a Soxhlet apparatus with *N,N*-dimethylformamide (DMF) at reduced pressure for 3 days. Afterwards, the obtained black solid was washed by dispersing, centrifuging and decanting using acetone, water, ethanol and hexanes as solvents upon which it was dried at high vacuum overnight. The sample was analyzed by TGA (Figure 2.5), XPS (Figure 2.6), FT-IR (Figure 2.7) and Raman spectroscopy (Figure 2.8).

Synthesis of propargyl MWCNTs 1b. A suspension of MWCNTs (1.2 g, 100 mmol of carbon) in 1,4-dioxane (1.2 L) was sonicated for 3 h using an ultrasonic probe. The mixture was heated to 60 °C and a solution of dipropargyl acetylenedicarboxylate (57 g, 300 mmol) in 1,4-dioxane (75 mL) and a solution of 4-dimethylaminopyridine (42.7 g, 350 mmol) in CHCl₃ (150 mL) were added simultaneously via syringe pump over 36 h. Subsequently, propargyl alcohol (45 mL, 43.7 g, 780 mmol) was added and the mixture was stirred at 60 °C for 3 more hours. The reaction

mixture was then cooled to room temperature and centrifuged at 3500 rpm for 20 min. The supernatant was discarded and the residue was washed in a Soxhlet apparatus with DMF at reduced pressure for 2 days. Afterwards, the obtained black solid was washed by dispersing, centrifuging and decanting using DMF, *N*-methyl-2-pyrrolidone (NMP), dichloromethane (DCM) and hexane as solvents upon which it was dried at high vacuum overnight. The sample was analyzed by TGA (Figure 2.9), XPS (Figure 2.10), FT-IR (Figure 2.11) and Raman spectroscopy (Figure 2.12).

Synthesis of sulfonate SWCNTs 3a. A suspension of propargyl SWCNTs (**1a**, 150 mg) in water/*tert*-butanol (1:1, 15 mL) was sonicated for 15 minutes. Sodium 3-azidopropane-1-sulfonate (**2**, 735 mg, 3.9 mmol), sodium ascorbate (78 mg, 0.39 mmol) and copper(II) sulfate pentahydrate (10 mg, 0.04 mmol) were added and the mixture was sonicated for 50 more minutes. After stirring at room temperature for 4 days, the reaction mixture was centrifuged and the supernatant was discarded. The black residue was transferred into an ultrafiltration cell equipped with a polycarbonate membrane (Millipore, Isopore membrane, 50 nm pore size) and washed with water until the filtrate was clear. The resulting black solid was washed by dispersing, centrifuging and decanting using ethanol and hexane as solvents before it was dried at high vacuum overnight. The sample was analyzed by TGA (Figure 2.13), XPS (Figure 2.14), FT-IR (Figure 2.15) and Raman spectroscopy (Figure 2.16).

Synthesis of sulfonate MWCNTs 3b. Propargyl MWCNTs (**1b**, 1 g) were suspended in a 1:1 mixture of water and *tert*-butanol (100 mL) by sonication for 10 min. Subsequently, sodium 3-azidopropane-1-sulfonate (**2**, 4.9 g, 26 mmol), sodium ascorbate (520 mg, 2.6 mmol) and copper(II) sulfate pentahydrate (65 mg, 0.26 mmol) were added and the mixture was sonicated for 50 more minutes. The mixture was stirred at room temperature for 12 days and sonicated for

2 h every 2 days during this period. Afterward, the reaction mixture was centrifuged, the supernatant was discarded and the residue was transferred into an ultrafiltration cell equipped with a polycarbonate membrane (Millipore, Isopore membrane, 50 nm pore size). It was washed with water until the filtrate was clear upon which it was dried at high vacuum overnight. The sample was analyzed by TGA (Figure 2.17), XPS (Figure 2.18), FT-IR (Figure 2.19) and Raman spectroscopy (Figure 2.20).

Determination of the mass extinction coefficient of sulfonate MWCNTs (3b). Sulfonate MWCNTs (**3b**, 8 mg), were dissolved in MilliQ water (8 mL) by sonication for 5 min. Subsequently, the solution was diluted with MilliQ water to obtain concentrations of 0.1, 0.05, 0.025, 0.01 and 0.005 mg/mL. The UV-vis spectra of these solutions were measured and the mass extinction coefficient was determined using the Beer-Lambert law with the absorbance at 650 nm yielding a mass extinction coefficient of $1.65 \times 10^3 \text{ mL m}^{-1} \text{ g}^{-1}$.

Measurement of sulfonate MWCNT (3b) solubility. Sulfonate MWCNTs (**3b**, 130 mg) were added to MilliQ water (2 mL) and sonicated for 1 h. Aggregates were allowed to settle for 24 h upon which a sample was taken from the supernatant, diluted 1:1000 with MilliQ water and its UV-vis spectrum was immediately measured. Another sample was taken, diluted and analyzed by UV-vis spectroscopy after allowing aggregates to settle for 24 more hours. Subsequently, the mixture was centrifuged for 10 min at 5000 rpm, another sample from the supernatant was taken and treated similarly. The last sample was taken from the supernatant after centrifugation for 30 more minutes at 5000 rpm. It was diluted and the UV-vis absorption spectrum was recorded. The concentration of **3b** in all samples was determined using the absorption at 650 nm and the experimentally obtained mass extinction coefficient of $1.65 \times 10^3 \text{ mL m}^{-1} \text{ g}^{-1}$ (Figure 2.2a).

General procedure for the Wacker-type oxidation of 1-decene (4) to 2-decanone (5).

Palladium bistrifluoroacetate (1.5 mg, 4.5 μmol) and copper(II) triflate (53.5 mg, 0.148 mmol) were dissolved in a 7:1 mixture of DMF and water (0.5 mL) containing biphenyl (11.5 mg, 0.0746 mmol) as an internal standard. Sulfonate MWCNTs (**3b**, 20 mg) were added and the mixture was sonicated for 1 min. The reaction tube was purged with oxygen, sealed and an oxygen-filled balloon was attached. 1-Decene (28 μL , 21 mg, 0.15 mmol) was added via syringe. The mixture was stirred at room temperature for 3 h upon which it was filtered through glass wool. Brine (1 mL) was added and the mixture was extracted with diethyl ether (2 x 1 mL). The organic phase was run through a short silica plug and then analyzed by gas chromatography (GC) to determine the yield of 2-decanone vs. the internal standard. GC-yield vs. biphenyl: 29 % (in the presence of 20 mg of **3b**), 16 % (without addition of **3b**).

Wacker-type oxidation of 1-decene (4) to 2-decanone (5) using PdCl₂ and CuCl as the catalysts.

The reaction was performed analogous to the general procedure using PdCl₂ (0.80 mg, 4.5 μmol) and CuCl (14.6 mg, 0.147 mmol; oxidized prior to the addition of 1-decene by stirring for 1 h in an oxygen atmosphere) as the catalysts. GC-yield vs. biphenyl: 41 % (in the presence of 20 mg of **3b**), 41 % (without addition of **3b**).

Wacker-type oxidation of 1-decene (4) to 2-decanone (5) using palladium bistrifluoroacetate and CuCl as the catalysts.

The reaction was performed analogous to the general procedure using palladium bistrifluoroacetate (1.5 mg, 4.5 μmol) and CuCl (14.6 mg, 0.147 mmol; oxidized prior to the addition of 1-decene by stirring for 1 h in an oxygen atmosphere) as the catalysts. GC-yield vs. biphenyl: 34 % (in the presence of 20 mg of **3b**), 42 % (without addition of **3b**).

Wacker-type oxidation of 1-decene (4) to 2-decanone (5) using PdCl₂ and copper(II) triflate as the catalysts. The reaction was performed analogous to the general procedure using PdCl₂ (0.80 mg, 4.5 μmol) and copper(II) triflate (53.5 mg, 0.148 mmol) as the catalysts. GC-yield vs. biphenyl: 5 % (in the presence of 20 mg of **3b**), 10 % (without addition of **3b**).

Wacker-type oxidation of 1-decene (4) to 2-decanone (5) using palladium bistrifluoroacetate and copper(II) triflate as the catalysts in the presence of pristine SWCNTs. The reaction was performed analogous to the general procedure using palladium bistrifluoroacetate (1.5 mg, 4.5 μmol) and copper(II) triflate (53.5 mg, 0.148 mmol) as the catalysts and pristine SWCNTs (20 mg) as an additive instead of **3b**. GC-yield vs. biphenyl: 21 %.

Wacker-type oxidation of 1-decene (4) to 2-decanone (5) using palladium bistrifluoroacetate and copper(II) triflate as the catalysts in the presence of pristine MWCNTs. The reaction was performed analogous to the general procedure using palladium bistrifluoroacetate (1.5 mg, 4.5 μmol) and copper(II) triflate (53.5 mg, 0.148 mmol) as the catalysts and pristine MWCNTs (20 mg) as an additive instead of **3b**. GC-yield vs. biphenyl: 21 %.

Wacker-type oxidation of 1-decene (4) to 2-decanone (5) using palladium bistrifluoroacetate and copper(II) triflate as the catalysts in the presence of sulfonate SWCNTs (3a). The reaction was performed analogous to the general procedure using palladium bistrifluoroacetate (1.5 mg, 4.5 μmol) and copper(II) triflate (53.5 mg, 0.148 mmol) as the catalysts and sulfonate SWCNTs (**3a**, 20 mg) as an additive instead of **3b**. GC-yield vs. biphenyl: 1 %.

Wacker-type oxidation of 1-decene (4) to 2-decanone (5) using palladium bistrifluoroacetate and copper(II) triflate as the catalysts in the presence of sodium polystyrene sulfonate. The reaction was performed analogous to the general procedure using palladium bistrifluoroacetate (1.5 mg, 4.5 μmol) and copper(II) triflate (53.5 mg, 0.148 mmol) as the catalysts and sodium polystyrene sulfonate (20 mg) as an additive instead of **3b**. GC-yield vs. biphenyl: 10 %.

Wacker-type oxidation of 1-decene (4) to 2-decanone (5) using palladium bistrifluoroacetate and copper(II) triflate as the catalysts in the presence of sulfonated polystyrene beads. The reaction was performed analogous to the general procedure using palladium bistrifluoroacetate (1.5 mg, 4.5 μmol) and copper(II) triflate (53.5 mg, 0.148 mmol) as the catalysts and sulfonate polystyrene beads (Amberlyst 15, 20 mg) as an additive instead of **3b**. GC-yield vs. biphenyl: 14 %.

Determination of the influence of sulfonate MWCNTs on the 2-decanone to biphenyl ratio.

In six sealable test tubes, Palladium bistrifluoroacetate (1.5 mg, 4.5 μmol) and copper(II) triflate (53.5 mg, 0.148 mmol) were dissolved in a 7:1 mixture of DMF and water (0.5 mL) containing biphenyl (11.5 mg, 0.0746 mmol) as an internal standard. 2-decanone (15 μL , 0.079 mmol) was added via pipette. To three test tubes, sulfonate MWCNTs (20 mg) were added and all test tubes were sonicated for 1 min. The reaction tubes were purged with oxygen, sealed and an oxygen-filled balloon was attached. All mixtures were stirred at room temperature for 4 h, before brine (1 mL) was added. The mixtures were extracted with diethyl ether (2 x 1 mL) and the organic phases were run through a short silica plug. Subsequently the ratio of 2-decanone to biphenyl was determined via GC. Ratio 2-decanone to biphenyl: 1.14 ± 0.02 (without sulfonate MWCNTs), 1.12 ± 0.05 (with sulfonate MWCNTs).

General procedure for the determination of conductivities of pristine and sulfonate SWCNTs and MWCNTs. A CNT sample was sonicated in water (sulfonate CNTs) or DMF (pristine CNTs) for 1 min. Subsequently, 20 μL of the suspension were drop-cast onto a glass slide and air-dried to create a thin film. Using a four point probe setup, the electric potential was measured at a current of 2 μA at three different positions for each film. Subsequently, the thickness of the film was measured using a profilometer and the conductivity was calculated using equation 1

$$\sigma = I / (V \cdot t \cdot CF) \text{ (for } t/s < 0.4) \text{ (1)}$$

where I is the current, V is the voltage, t is the sample thickness, CF is the sheet resistance correction factor,²⁶ and s is the four point probe spacing.

Conductivity of pristine SWCNTs The conductivity of a drop-cast film of pristine SWCNTs was determined to be 21.8 S cm^{-1} (average of five films and three measurements each).

Conductivity of pristine MWCNTs The conductivity of a drop-cast film of pristine MWCNTs was determined to be 3.9 S cm^{-1} (average of five films and three measurements each).

Conductivity of sulfSWCNTs (3a) The conductivity of a drop-cast film of sulfSWCNTs was determined to be 0.6 S cm^{-1} (average of five films and three measurements each).

Conductivity of sulfMWCNTs (3b) The conductivity of a drop-cast film of pristine SWCNTs was determined to be 2.8 S cm^{-1} (average of five films and three measurements each).

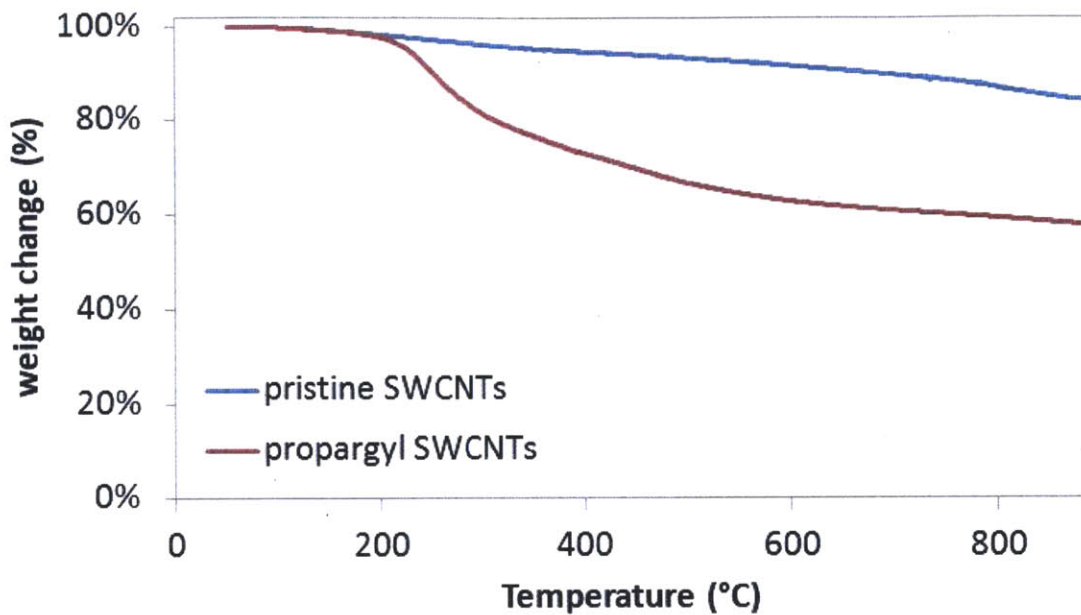


Figure 2.5. TGA of propargyl SWCNTs (**1a**) and pristine SWCNTs

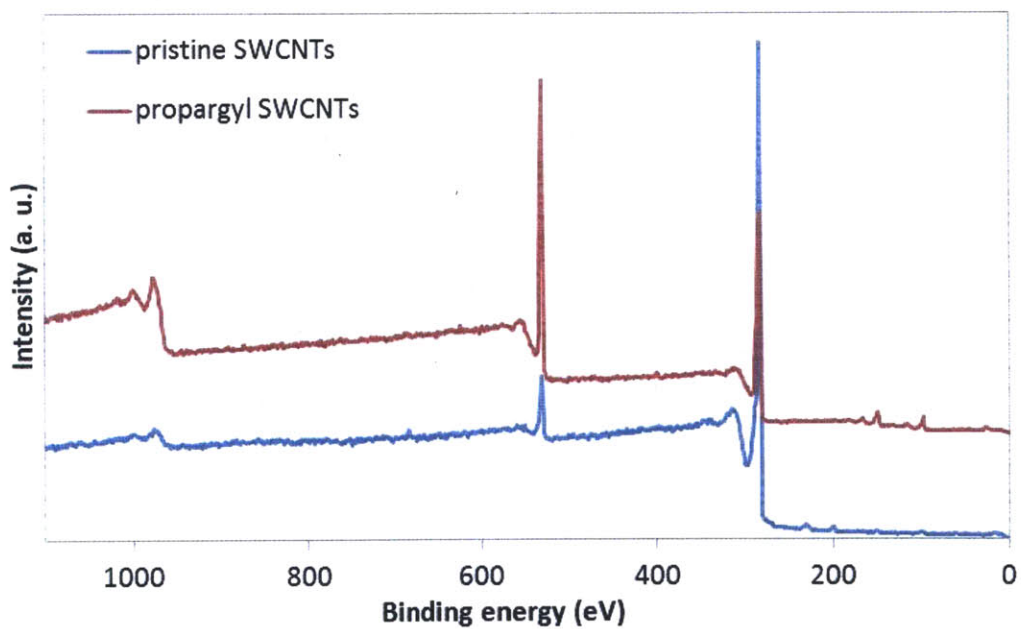


Figure 2.6. XPS spectra of propargyl SWCNTs (**1a**) and pristine SWCNTs

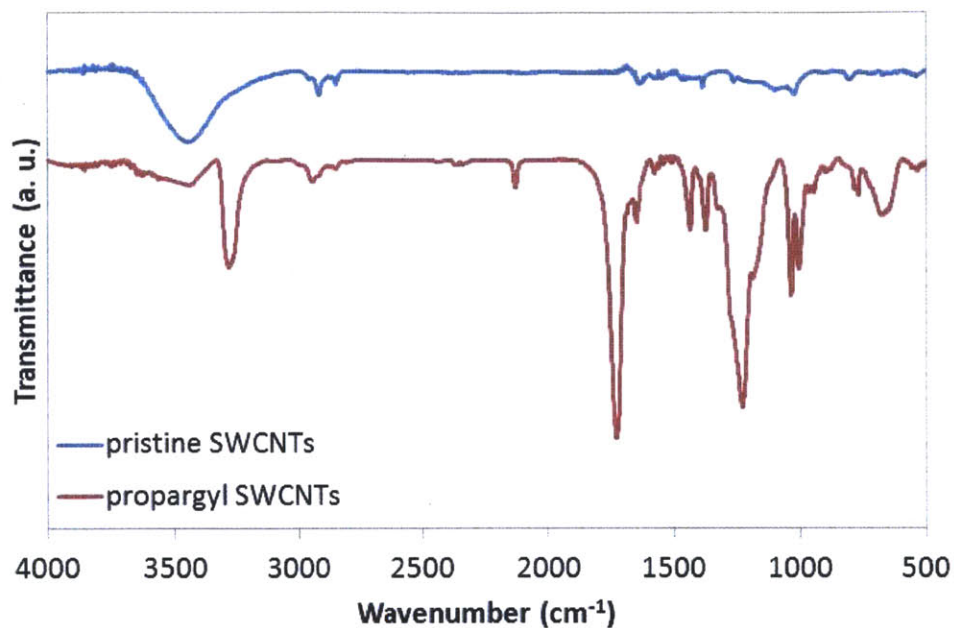


Figure 2.7. FT-IR spectra of propargyl SWCNTs (**1a**) and pristine SWCNTs

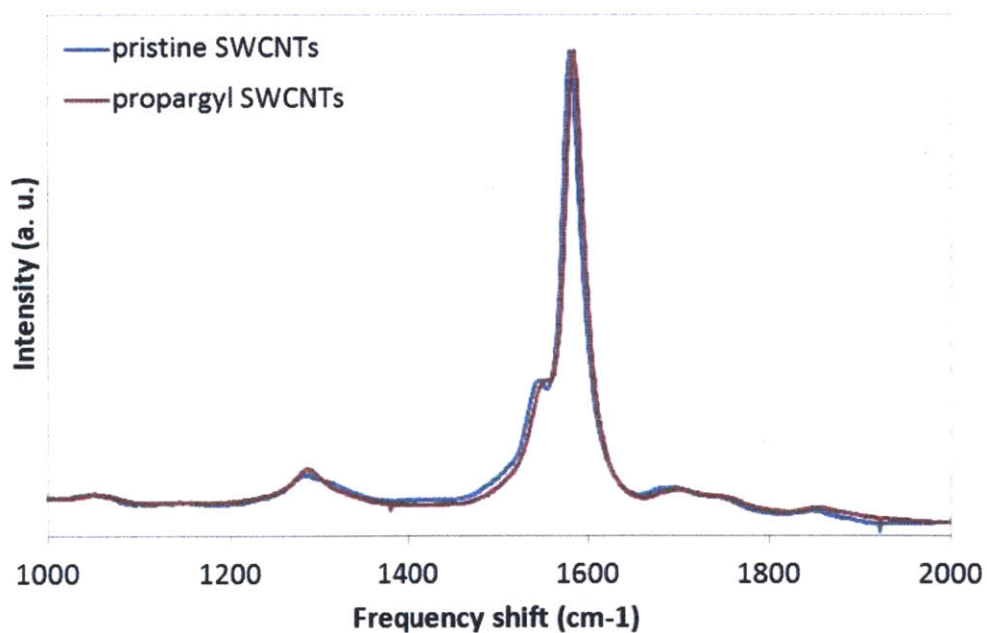


Figure 2.8. Raman spectra of propargyl SWCNTs (**1a**) and pristine SWCNTs

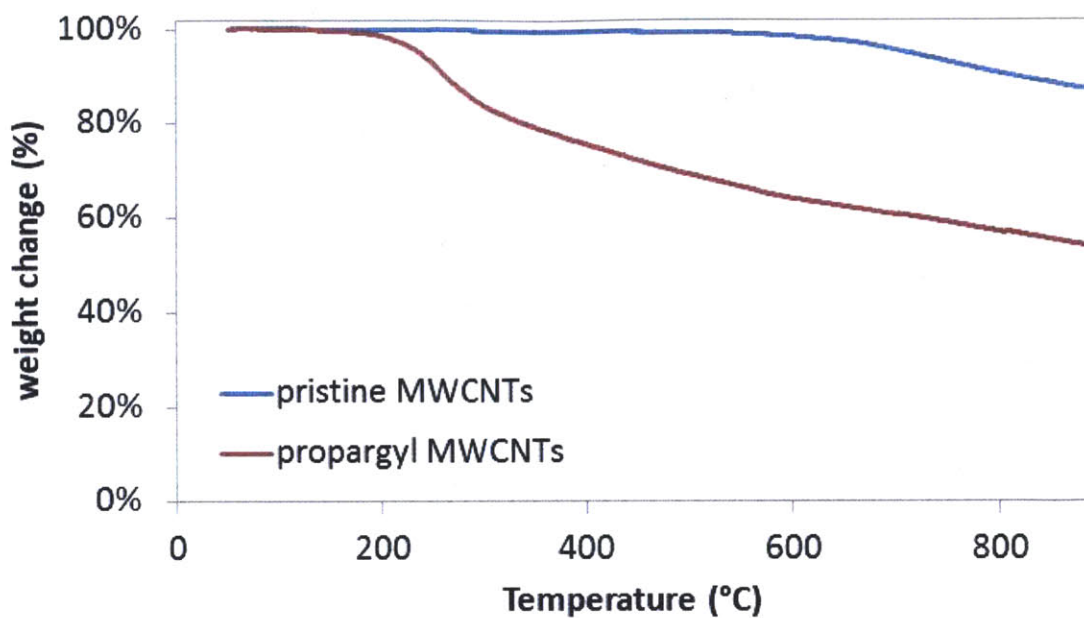


Figure 2.9. TGA of propargyl MWCNTs (**1b**) and pristine MWCNTs

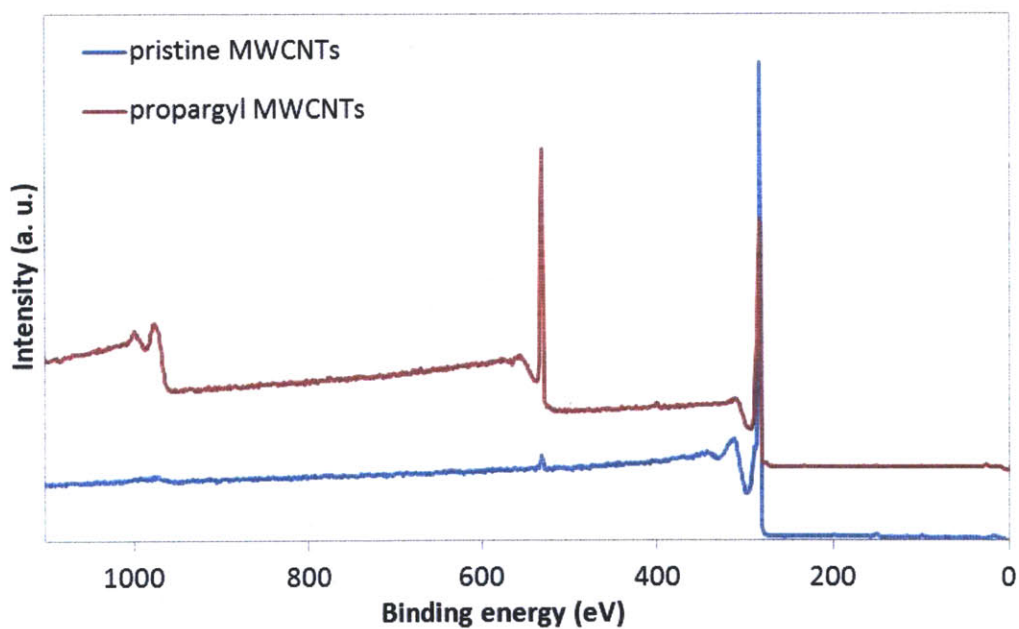


Figure 2.10. XPS spectra of propargyl MWCNTs (**1b**) and pristine MWCNTs

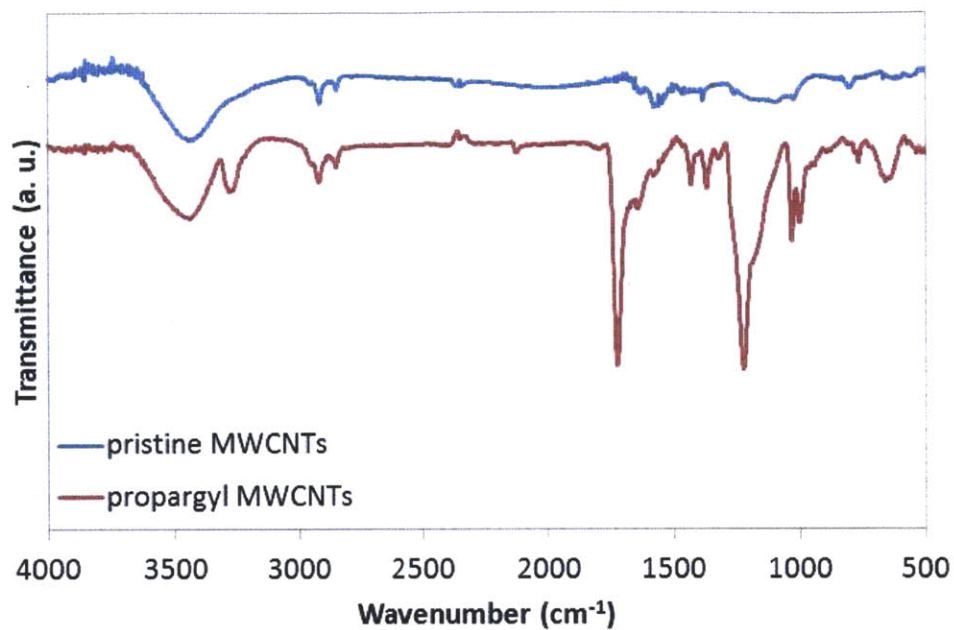


Figure 2.11. FT-IR spectra of propargyl MWCNTs (**1b**) and pristine MWCNTs

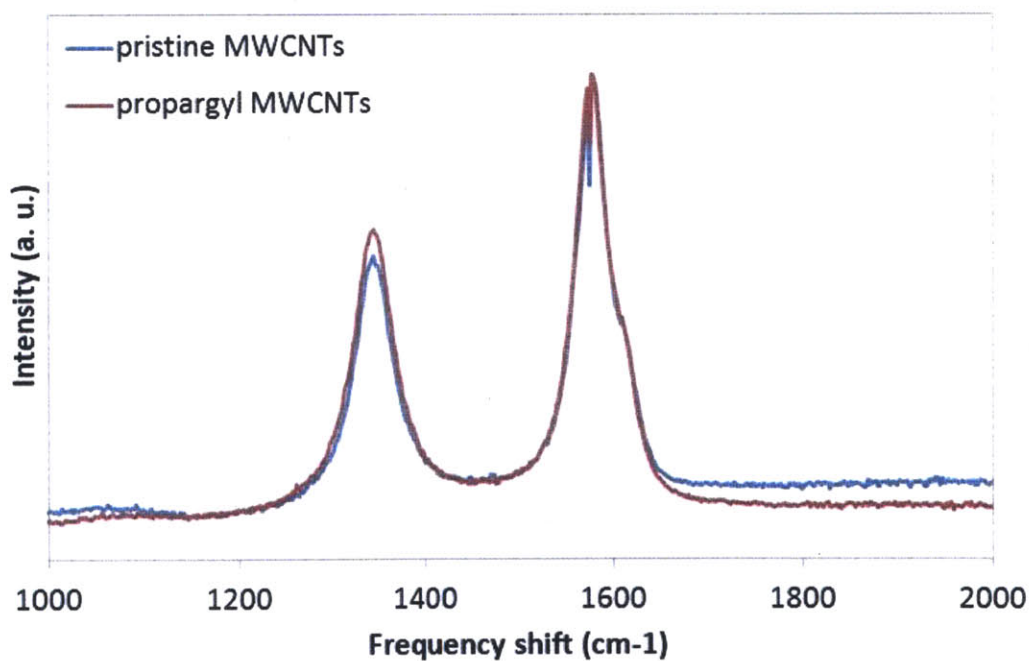


Figure 2.12. Raman spectra of propargyl MWCNTs (**1b**) and pristine MWCNTs

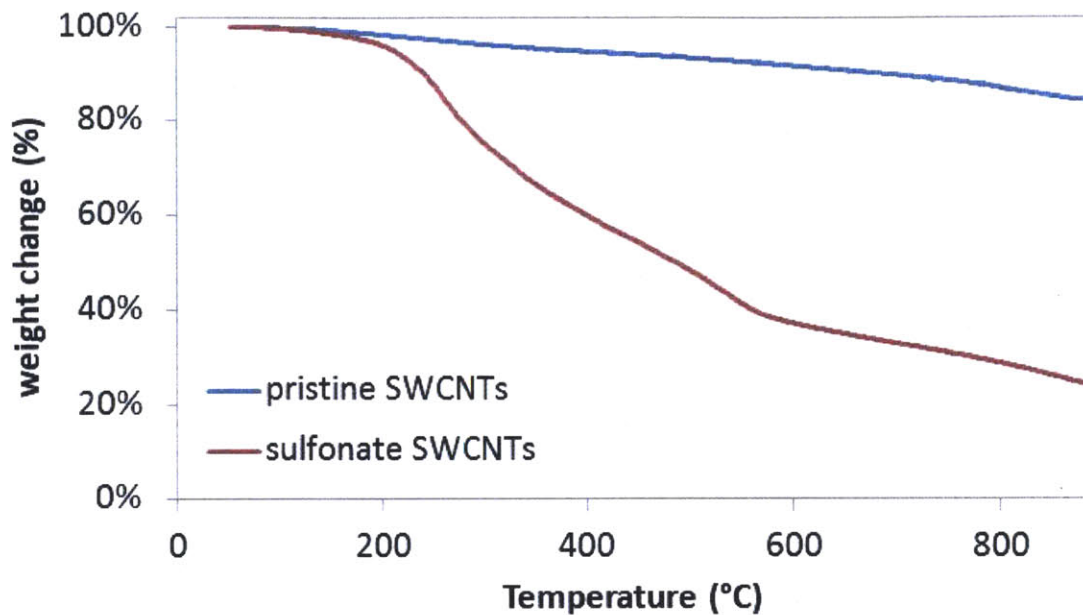


Figure 2.13. TGA of sulfonate SWCNTs (3a) and pristine SWCNTs

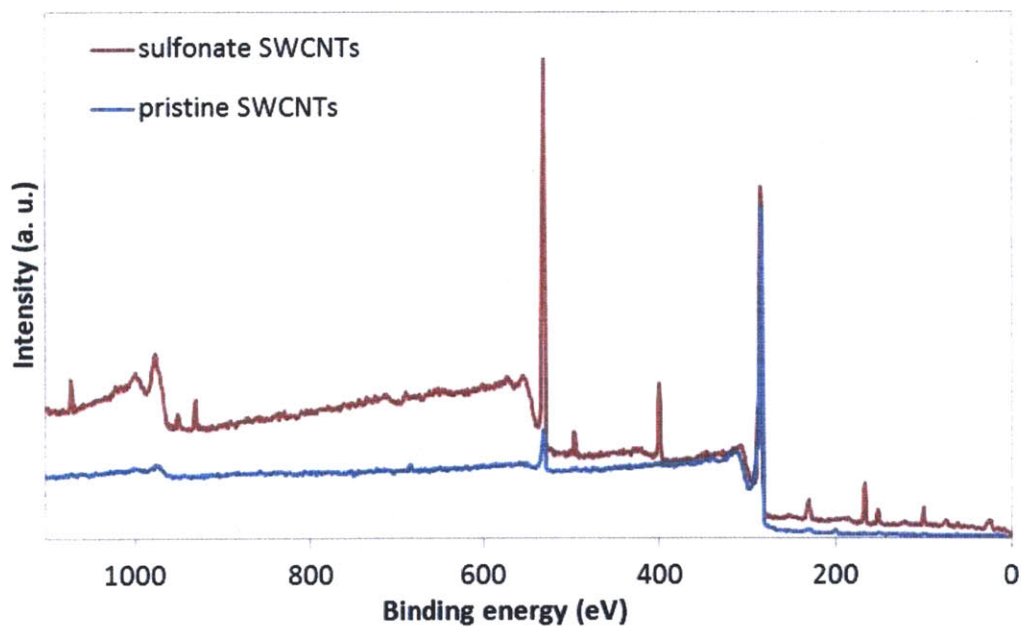


Figure 2.14. XPS spectra of sulfonate SWCNTs (3a) and pristine SWCNTs

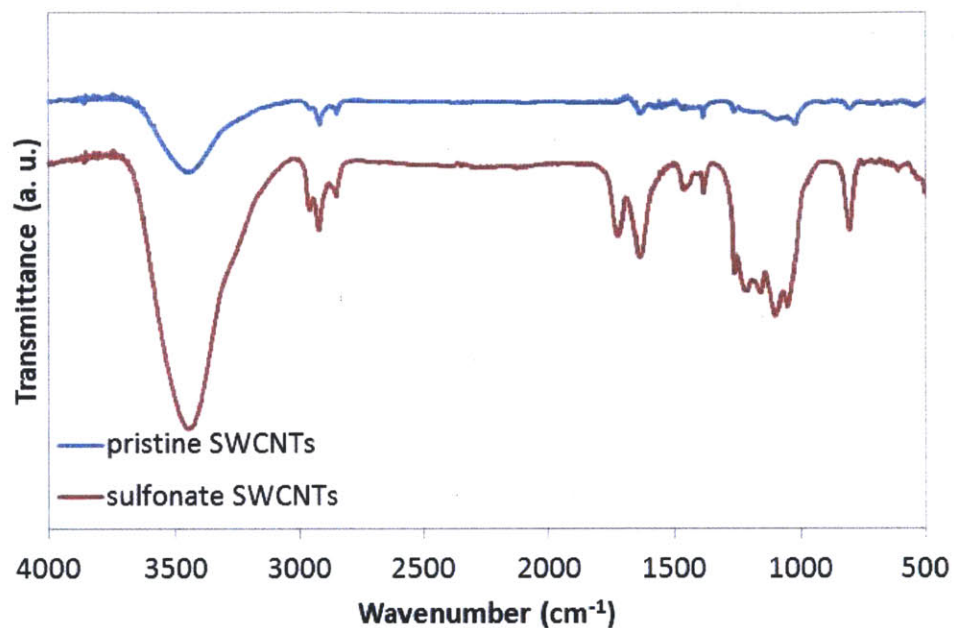


Figure 2.15. FT-IR spectra of sulfonate SWCNTs (**3a**) and pristine SWCNTs

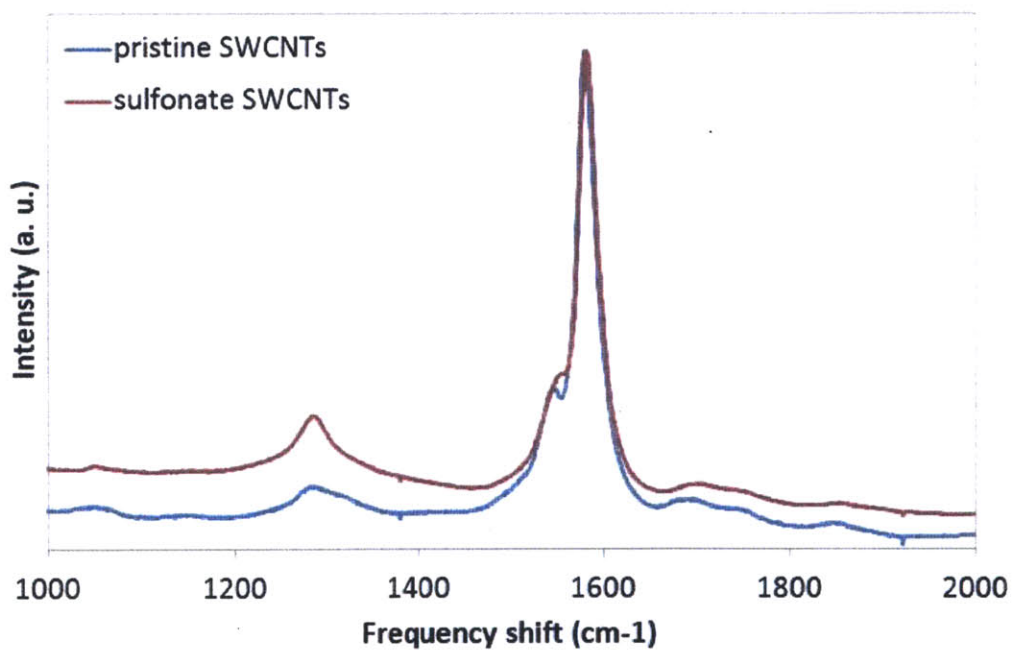


Figure 2.16. Raman spectra of sulfonate SWCNTs (**3a**) and pristine SWCNTs

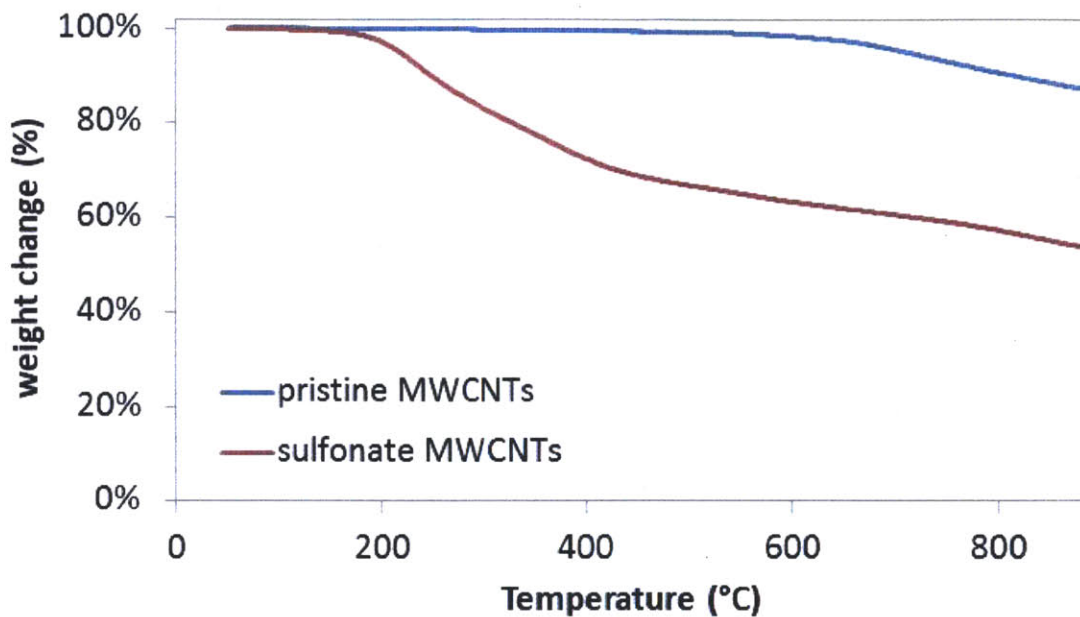


Figure 2.17. TGA of sulfonate MWCNTs (**3b**) and pristine MWCNTs

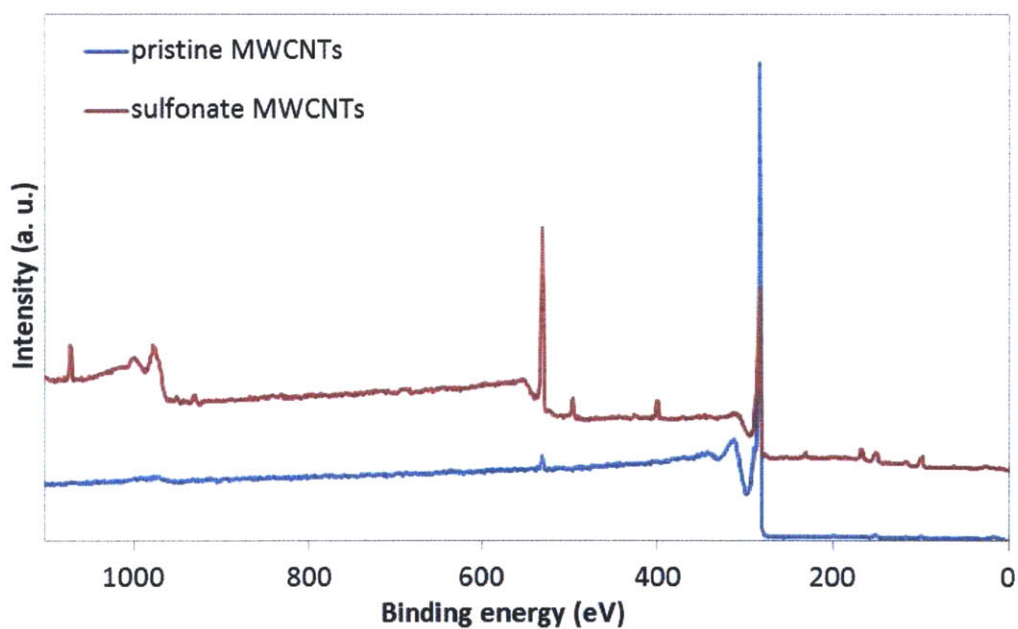


Figure 2.18. XPS spectra of sulfonate MWCNTs (**3b**) and pristine MWCNTs

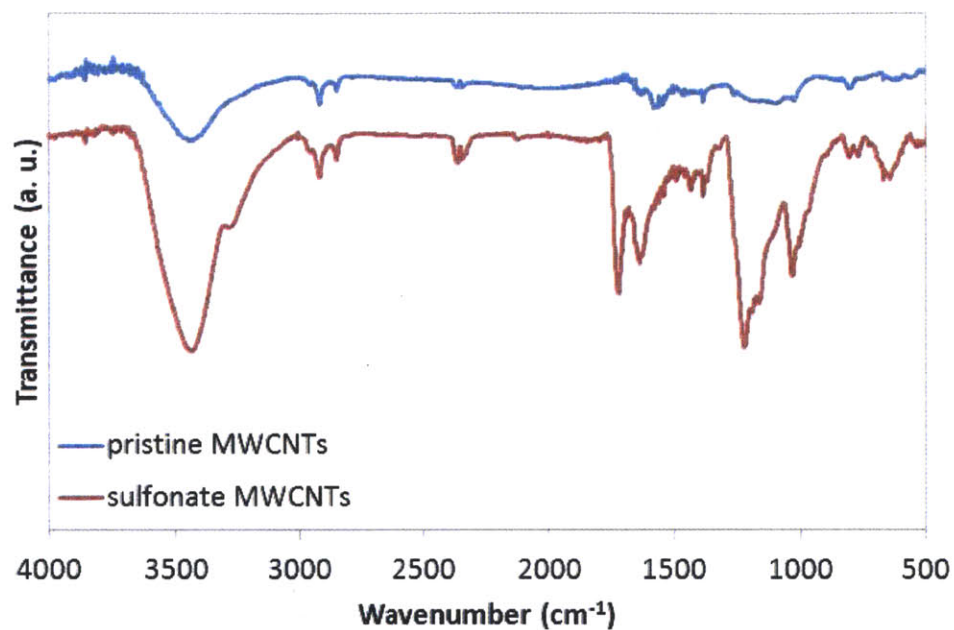


Figure 2.19. FT-IR spectra of sulfonate MWCNTs (**3b**) and pristine MWCNTs

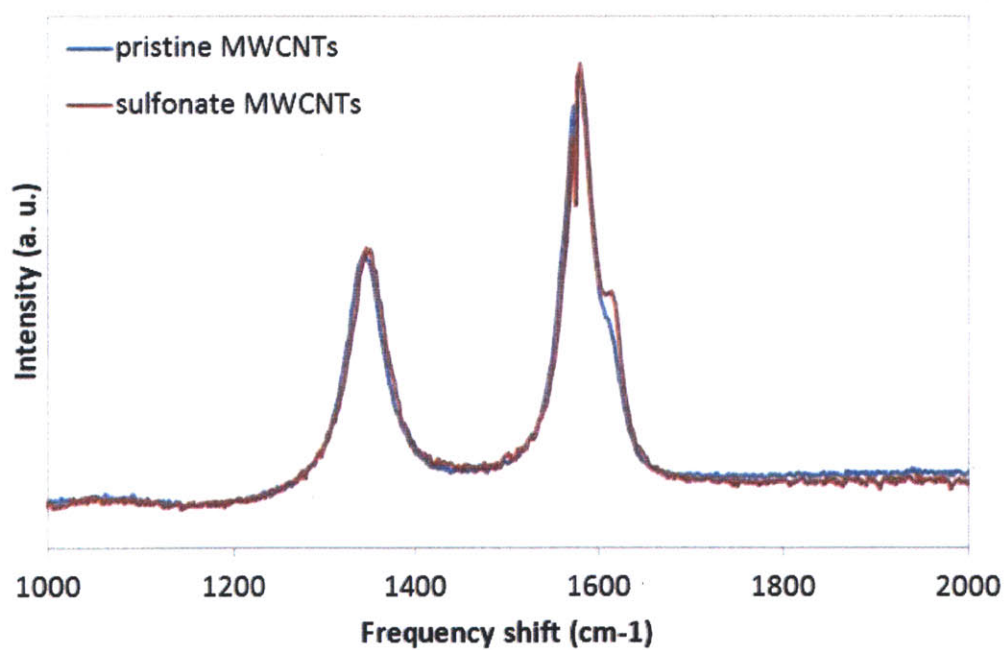


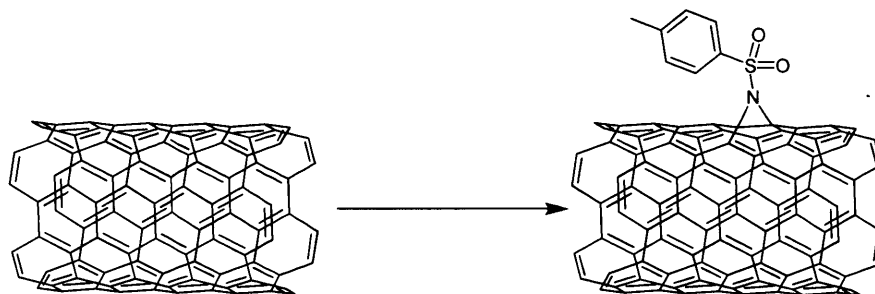
Figure 2.20. Raman spectra of sulfonate MWCNTs (**3b**) and pristine MWCNTs

2.5. References

- (1) Falvo, M. R.; Clary, G. J.; Taylor II, R. M.; Chi, V.; Brooks Jr, F. P.; Washburn, S.; Superfine, R. *Nature*. **1997**, *389*, 582.
- (2) Schnorr, J. M.; Swager, T. M. *Chem. Mater.* **2011**, *23*, 646.
- (3) Iijima, S. *Nature*. **1991**, *354*, 56.
- (4) Tasis, D.; Tagmatarchis, N.; Bianco, A.; Prato, M. *Chem. Rev.* **2006**, *106*, 1105-36.
- (5) Backes, C.; Schmidt, C. D.; Hauke, F.; Böttcher, C.; Hirsch, A. *J. Am. Chem. Soc.* **2009**, *131*, 2172.
- (6) Nakashima, N.; Fujigaya, T. *Chem. Lett.* **2007**, *36*, 692-697.
- (7) Star, A.; Steuerman, D. W.; Heath, J. R.; Stoddart, J. F. *Angew. Chem. Int. Edit.* **2002**, *41*, 2508.
- (8) Hu, C.; Chen, Z.; Shen, A.; Shen, X.; Li, J.; Hu, S. *Carbon*. **2006**, *44*, 428.
- (9) Duque, J. G.; Parra-Vasquez, A. N. G.; Behabtu, N.; Green, M. J.; Higginbotham, A. L.; Price, B. K.; Leonard, A. D.; Schmidt, H. K.; Lounis, B.; Tour, J. M.; Doorn, S. K.; Cognet, L.; Pasquali, M. *ACS nano*. **2010**, *4*, 3063.
- (10) Asuri, P.; Karajanagi, S. S.; Sellitto, E.; Kim, D.-Y.; Kane, R. S.; Dordick, J. S. *Biotechnol. Bioeng.* **2006**, *95*, 804.
- (11) Kakade, B. A.; Pillai, V. K. *Appl. Surf. Sci.* **2008**, *254*, 4936.
- (12) D'Este, M.; Nardi, M. De; Menna, E. *Eur. J. Org. Chem.* **2006**, 2517.
- (13) Li, B.; Shi, Z.; Lian, Y.; Gu, Z. *Chem. Lett.* **2001**, *30*, 598.
- (14) Sun, Y.-ping; Huang, W.; Lin, Y.; Fu, K.; Kitaygorodskiy, A.; Riddle, L. A.; Yu, Y. J.; Carroll, D. L. *Chem. Mater.* **2001**, *13*, 2864.
- (15) Zhao, B.; Hu, H.; Yu, A.; Perea, D.; Haddon, R. C. *J. Am. Chem. Soc.* **2005**, *127*, 8197.
- (16) Georgakilas, V.; Tagmatarchis, N.; Pantarotto, D.; Bianco, A.; Briand, J.-P.; Prato, M. *Chem. Commun.* **2002**, 3050.
- (17) Li, H.; Cheng, F.; Duft, A. M.; Adronov, A. *J. Am. Chem. Soc.* **2005**, *127*, 14518.

- (18) Fagan, J. A.; Bauer, B. J.; Hobbie, E. K.; Becker, M. L.; Hight Walker, A. R.; Simpson, J. R.; Chun, J.; Obrzut, J.; Bajpai, V.; Phelan, F. R.; Simien, D.; Huh, J. Y.; Migler, K. B. *Adv. Mater.* **2011**, *23*, 338.
- (19) Zhang, W.; Swager, T. M. *J. Am. Chem. Soc.* **2007**, *129*, 7714.
- (20) Peng, X.; Wong, S. S. *Adv. Mater.* **2009**, *21*, 625.
- (21) Zhang, W.; Sprafke, J. K.; Ma, M.; Tsui, E. Y.; Sydlik, S. A.; Rutledge, G. C.; Swager, T. M. *J. Am. Chem. Soc.* **2009**, *131*, 8446.
- (22) Gao, C.; He, H.; Zhou, L.; Zheng, X.; Zhang, Y. *Chem. Mater.* **2009**, *21*, 360.
- (23) Tsuji, J.; Nagashima, H.; Nemoto, H. *Org. Synth.* **1984**, *62*, 9.
- (24) Tsuji, J. *Synthesis.* **1984**, 369.
- (25) Kong, X.; Migneault, D.; Valade, I.; Wu, X.; Gervais, F. *WO 2004/113275.* **2004**.
- (26) Swartzendruber, L. J. *National Bureau of Standards.* **1964**, Technical Note 199.

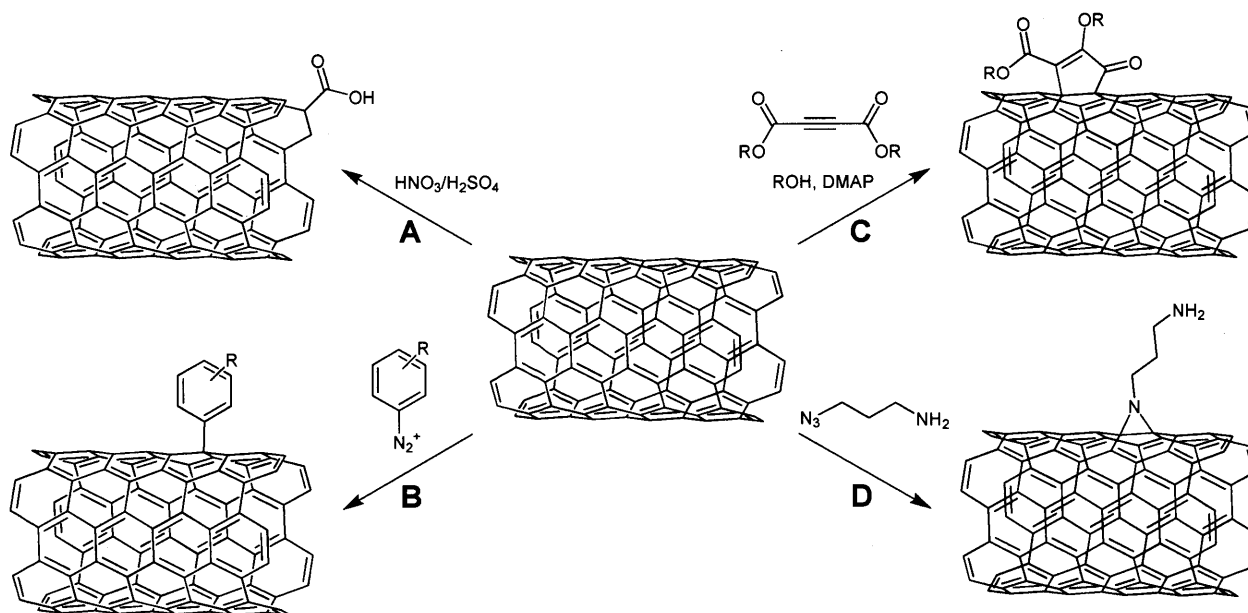
CHAPTER 3
**Copper-Catalyzed Aziridination of Fullerene,
Carbon Nanotubes, and Graphite**



3.1. Introduction

Since their discovery in 1991,¹ a variety of reactions have been developed to functionalize carbon nanotubes (CNTs).^{2,3} A few notable methods include the oxidation of carbon nanotubes with mixtures of sulfuric acid and nitric acid (in some cases followed by amide formation),^{4,5} functionalization *via* diazonium chemistry,⁶ the zwitterionic approach described in chapter 2,^{7,8} and thermal aziridination with azides (Scheme 3.1).⁹

Scheme 3.1. Examples of carbon nanotube functionalization reactions.



Each of these methods have particular strengths and weaknesses. While the oxidation with nitric acid (Scheme 3.1A) does not require air or moisture free conditions and is thus relatively easy to conduct, it generates defect sites on the surface of the CNTs affecting their electronic and mechanical properties. However, functionalization preferentially occurs on the end groups of the CNTs and if this oxidation is performed in conjunction with an approach developed by our group to shield defect sites on the surface of the nanotubes, selective functionalization of the tips of the CNTs can be achieved.⁴ Diazonium salts show good reactivity toward CNT surfaces, but as the

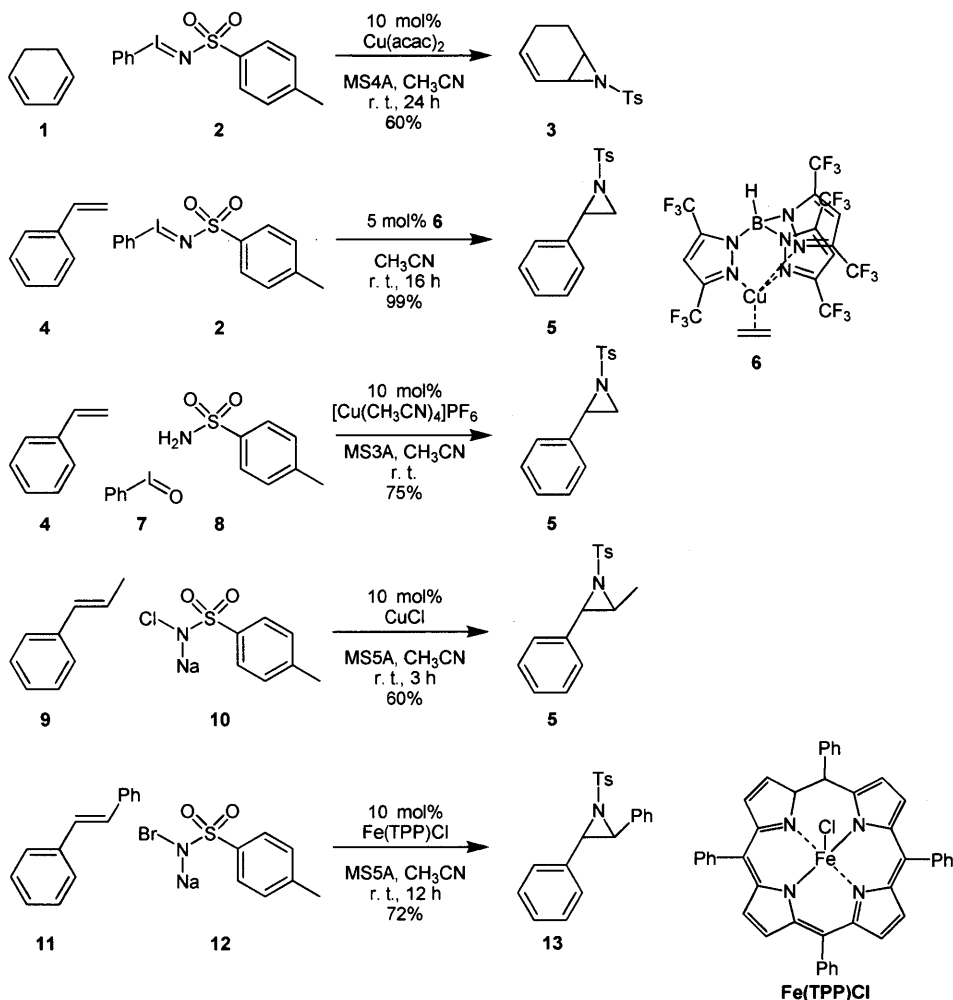
installed functional group typically reacts with diazonium salts as well, this method can lead to branched groups on the surface (Scheme 3.1B). The reaction of CNTs with acetylene dicarboxylic acid esters (Scheme 3.1C) avoids this problem and furthermore shows a very good functional group tolerance,⁸ but it is complicated by oligomerization of the esters under the requisite basic reaction conditions – even when the reagent concentration is kept low by utilizing syringe pump addition.¹⁰ As a large excess of reagent is used in the reaction (typically 3 equivalents per CNT carbon atom), the formed side-product greatly hinders the workup of the functionalized CNTs.

Installing aziridines on the surface of CNTs *via* thermal reaction with azides (Scheme 3.1D) typically requires a similarly large excess of reagent (ca. 3 equivalents per CNT carbon atom), but the side-products and/or excess reagent are easier to separate from the functionalized CNT product, which can be a significant practical advantage. Using this method, gram quantities of multi-walled CNTs (MWCNTs) can be easily functionalized with a variety of groups including hydroxyls, amines, bromines, and carboxylates.⁹ A challenging aspect of this chemistry, however, is the large amount of potentially explosive azides involved in the reaction. The described installation of hydroxyl groups for example requires 20 g of 2-azido-ethanol per gram of MWCNTs.

We were curious if a more reagent-efficient approach could be developed for the functionalization of CNTs by taking advantage of the variety of catalyzed nitrene transfer reactions reported for small molecules.¹¹ In this context, different reagents have been used as nitrene sources such as PhINTs (**2**),¹²⁻¹⁴ chloramine-T (**10**, CAT),¹⁵ or bromamine-T (**12**, BAT) (Scheme 3.2).¹⁶ In addition to finding suitable conditions for the installation of aziridines on

CNTs, we were interested in testing if the developed method could also be used to modify C_{60} or the less reactive graphite.

Scheme 3.2. Examples for catalyzed aziridination reactions, utilizing PhINTs with $Cu(acac)_2$,¹³ PhINTs with Cu(I) scorpionate **1**,¹² in situ formed PhINTs with $[Cu(CH_3CN)_4]PF_6$,¹⁴ chloramine-T and CuCl,¹⁵ and bromamine-T with $Fe(TPP)Cl$.¹⁶



At the onset of this project, aziridination reactions on nano-carbon materials were primarily done thermally^{9,17,18} and attempts at catalyzed aziridination of C_{60} were sparse and only provided low yields (< 10%).¹⁹ Additionally, this reaction had not been extended to CNTs or graphite. During the course of the project, Itami and coworkers reported an improved procedure for the

functionalization of C₆₀ using PhINTs in combination with a Cu(I)Cl/2,6-lutidine system, however, in their study functionalization of CNTs or graphite was not attempted.²⁰ Initially, we investigated the aziridination of MWCNTs. CNTs pose additional challenges in terms of characterization and workup compared to C₆₀ as the functionalization product cannot be analyzed by mass spectrometry or standard NMR techniques and chromatographic techniques are not possible for purification. Nevertheless, this approach ensured that the initial leads for reaction conditions would be compatible with CNTs. Afterward, we further optimized the conditions using C₆₀ before transferring the most promising conditions back to the functionalization of SWCNTs, MWCNTs as well as graphite.

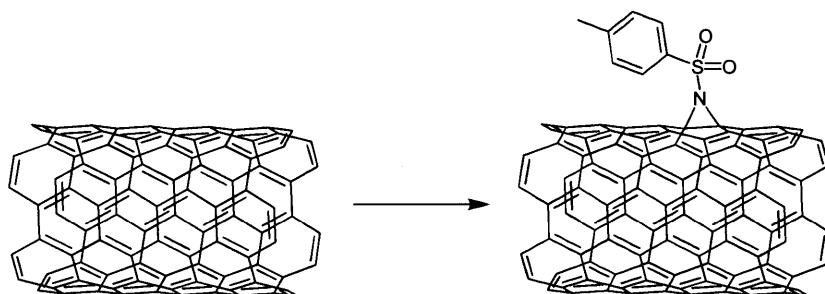
3.2. Results and Discussion

3.2.1. Evaluation of Different Aziridination Conditions on C₆₀ and MWCNTs

Initially, aziridination conditions that were closely related to reactions on small molecules were investigated with MWCNTs. These included the use of [Cu(CH₃CN)₄]PF₆ as a catalyst with previously prepared as well as *in situ* formed PhINTs (**2**),¹⁴ chloramine-T (**10**) and CuCl,¹⁵ as well as bromamine-T (**12**) with Fe(TPP)Cl.¹⁶ Furthermore, thermal and photochemical aziridination with 4-methylbenzenesulfonyl azide (**14**) was attempted.²¹ The thermal aziridination of MWCNTs with 3-azidopropan-1-amine (**15**) was performed for comparison.⁹ As techniques such as gas chromatography-mass spectrometry (GC-MS) or nuclear magnetic resonance spectroscopy (NMR) were not suitable for determining the success of the reaction, X-ray photoelectron spectroscopy (XPS) was chosen to analyze the product of the reaction. Pristine MWCNTs do not contain nitrogen (neither in the actual CNTs nor as a common impurity) and the ratio of nitrogen to carbon based on the N 1s and C 1s signals could be used to determine the density of installed functional groups.

No nitrogen signal was observed for the thermally performed reaction (Table 3.1, Entry 5) with **14** and only low incorporation of nitrogen was achieved photochemically with **14** (Table 3.1, Entry 4). In the latter case, the high absorbance of the MWCNTs in the UV-vis range was likely the cause for the poor functionalization.

Table 3.1. Evaluated conditions for MWCNT aziridination.



Entry	Reagent(s) ^a	Catalyst	N/C ratio ^b
1	PhINTs (2)	[Cu(CH ₃ CN) ₄]PF ₆	1.7%
2	PhIO (7) + H ₂ NTs (8)	[Cu(CH ₃ CN) ₄]PF ₆	0.4% ^c
3	Chloramine-T (10)	CuI	0.9%
4	N ₃ Ts ^d (14)		0.5%
5	N ₃ Ts ^e (14)		0% ^f
6	Bromamine-T (12) ^g	Fe(TPP)Cl	1.3%
7	N ₃ (CH ₂) ₃ NH ₂ ^h (15)		2.1% funct. group density

^aStandard conditions: 9 mg MWCNT, 0.2 eq. reagent per carbon, CH₃CN, rt, 25 h. ^bBy XPS analysis of the product. ^cThe product also contained 2.9 % iodine as insoluble PhIO could not be completely removed. ^d500 W Hg lamp, rt, 1h. ^eCH₃CN, reflux, 19 h. ^fNo nitrogen peak could be observed by XPS. ^gCH₃CN, rt, 19 h. ^h2.4 equiv per CNT carbon atom, NMP, 160 °C, 2 d, yielding propylamine functionalized MWCNTs.

Among the other investigated conditions (Table 3.1, Entries 1-3 and 6) the highest incorporation of nitrogen into the sample was obtained by using PhINTs with $[\text{Cu}(\text{CH}_3\text{CN})_4]\text{PF}_6$. Besides the incorporated nitrogen atoms, XPS analysis further confirmed the presence of oxygen (O 1s) and sulfur (S 2s and S 2p) (Figure 3.1).

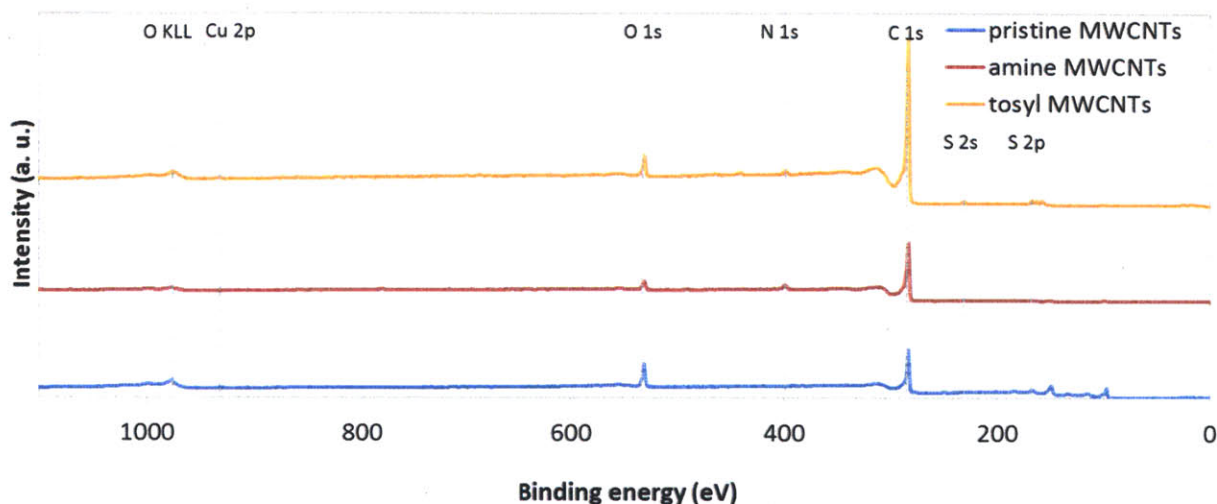
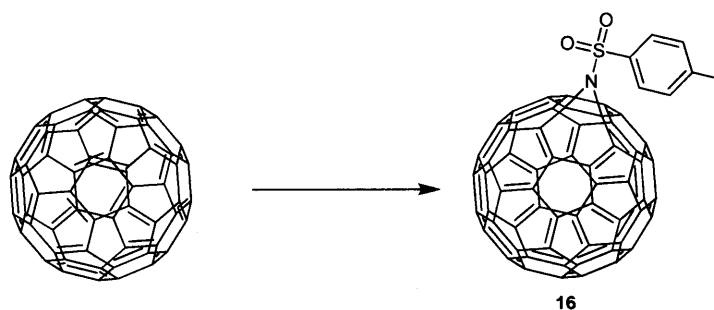


Figure 3.1. XPS analysis of pristine MWCNTs, amine functionalized MWCNTs (Table 3.1, entry 7) and tosyl MWCNTs (Table 3.1, entry 1). Si 2p and Si 2s signals results from the utilized Si/SiO₂ substrate. The binding energy of Cu 2p has been labeled to show that no significant amount of copper is present in the products.

Based on these results, we decided to investigate the copper-catalyzed aziridination using PhINTs as well as the reaction with **12** and Fe(TPP)Cl on C₆₀ leading to *N*-tosyl[1,2]aziridino[60]fullerene **16**. In contrast to reactions on CNTs, the crude products of C₆₀ reactions can be purified and analyzed by standard chemical techniques (chromatography, NMR etc.). Initial attempts with PhINTs as the nitrene source and different Cu(I) and Cu(II) salts as catalysts in acetonitrile did not show any product formation by thin layer chromatography (TLC), presumably due to the poor solubility of fullerene in this solvent. Therefore, 1,2-dichlorobenzene was used as a solvent for further experiments. In addition to being well suited for tests with C₆₀,

1,2-dichlorobenzene is also commonly used for reaction with CNTs. While some product formation was observed in 1,2-dichlorobenzene, only 3% yield could be obtained (Table 3.2). Therefore, bromamine-T was further investigated as the nitrene source instead of PhINTs.

Table 3.2. Aziridination of C₆₀



Entry	Reagent ^a	Catalyst	Yield
1	PhINTs (2)	Cu(CF ₃ SO ₃) ₂	3%
2	BAT (12)	Fe(TPP)Cl	- ^b
3	BAT ^c	Fe(TPP)Cl	29%
4	BAT ^{c,d}	Fe(TPP)Cl	32% ^e
5	BAT ^{c,d}	Fe(TPP)Cl	30% ^f
6	BAT ^{c,d}	Fe(TPP)Cl	29% ^g
7	BAT ^{c,d}	[Cu(CH ₃ CN) ₄]PF ₆	25%
8	BAT ^{c,d}	Cu(OTf) ₂	13%
9	BAT ^{c,d}	Cu(acac) ₂	25%
10	BAT ^{c,d}	none	17%

^aStandard conditions: 20 mg C₆₀, 1 eq. reagent, 10 mol% catalyst, 1,2-dichlorobenzene, rt, 18 h.

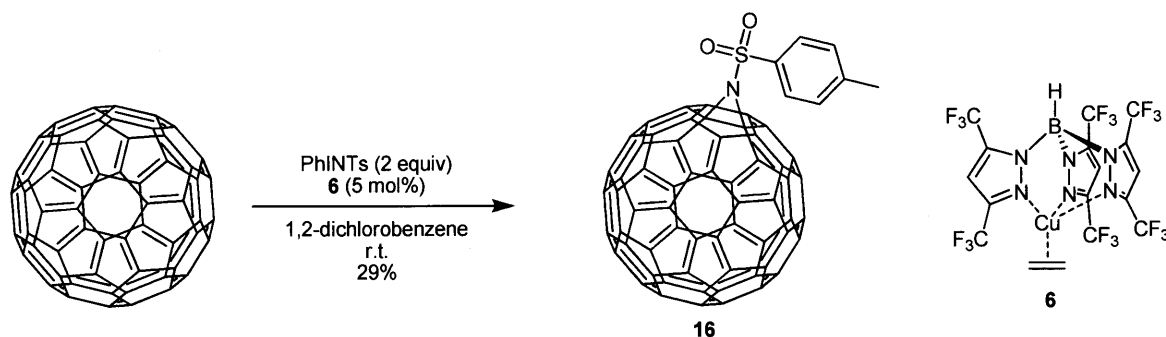
^bNo conversion by TLC. ^cA solution of BAT in 0.5 mL DMF was added over 30 min. ^d2 eq. of BAT were used. ^eReaction performed at 40 °C. ^f60 °C. ^g80 °C.

Slow addition of BAT led to a yield of 29% (Table 3.2, Entry 3) of the desired aziridinofullerene as determined by $^1\text{H-NMR}$ spectroscopy, a superior yield than previously reported for metal-catalyzed versions of this transformation.¹⁹

Further optimization revealed that varying the temperature only had a small effect on the yield and the best results were obtained at room temperature and 40 °C (Table 3.2, Entries 3-6). The use of different copper catalysts also resulted in lower yields (Table 3.2, Entries 7-9). Subsequently, the reaction was run in the absence of a metal catalyst and the product could be isolated in 17 % yield (Table 3.2, Entry 10). These data suggest that the reaction follows an ionic pathway as previously reported for chloramine-T at least in the catalyst-free case.²²

In addition to the commercially available catalysts screened (Table 3.2), a Cu(I) scorpionate complex was tested (Scheme 3.3). This complex previously displayed good activity in aziridination reactions of small molecules.¹²

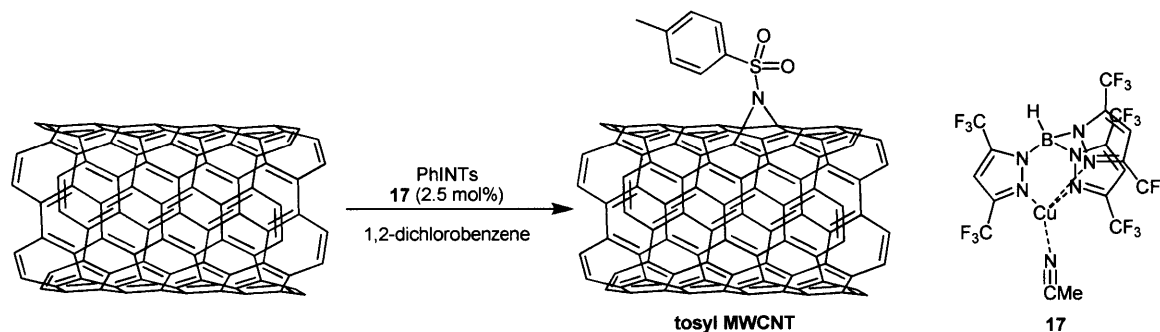
Scheme 3.3. Aziridination of C_{60} using Cu(I) scorpionate **6**.



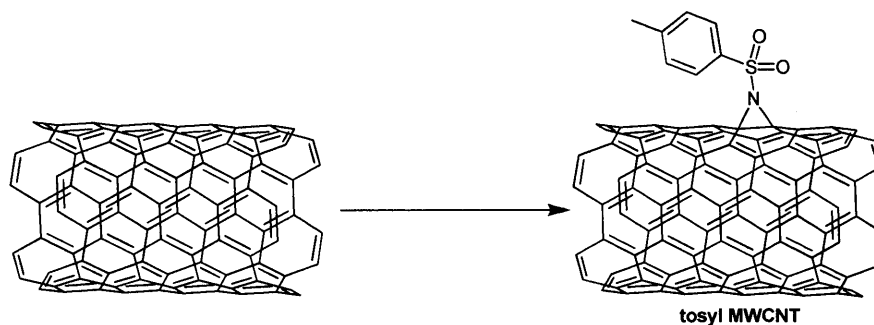
Upon subjecting C_{60} to Cu(I) scorpionate (**6**) and PhINTs, 29% of desired product **16** was isolated. However, unlike with the other catalysts employed, 27% of higher adducts were observed. This result underlined the efficiency of the reaction and rendered it promising for the functionalization of the more challenging nano-carbons CNT and graphite.

After investigating conditions for catalytic aziridinations on C₆₀, we tested the two most promising reagent/catalyst combinations, BAT in combination with Fe(TPP)Cl as well as PhINTs with Cu(I) catalyst **6**, with MWCNTs. Additionally, the acetonitrile complex of the Cu(I) scorpionate (**17**) was evaluated as it could be prepared more easily than its ethylene counterpart (Scheme 3.4).²³

Scheme 3.4. Aziridination of MWCNTs using PhINTs and Cu(I) complex **17**.



The modified MWCNTs were evaluated by XPS to determine their relative functional group densities (Table 3.3). At room temperature, the Cu(I) catalyst systems performed best among the tested conditions, leading to N/C ratios of 2.2% and 1.9%, respectively (Table 3.3, Entries 5-6). Increasing the reaction temperature to 60 °C or 80 °C led to a further increase of the functional group density (Table 3.3, Entries 7-8). XPS analysis showed a N/C ratio of 6.9% and 7.5%, respectively, corresponding to a functional group density of up to 1 group per 13-14 carbon atoms on the MWCNT surface. This density is significantly higher than the density obtained with the reference reaction (thermal aziridination with **15**) which only led to functional group densities of ca. 1 per 50 carbons on the MWCNT surface. Furthermore, the catalyzed reaction only required the use of 1 equivalent of reagent per CNT carbon atom while the thermal aziridination required over two equivalents of reagent.

Table 3.3. Optimization of MWCNT functionalization conditions using BAT (**12**) and PhINTs (**2**).

Entry	Reagent(s) ^a	Catalyst	N/C ratio ^b
1	BAT (12) ^c	Fe(TPP)Cl ^c	0.8%
2	BAT ^c	Fe(TPP)Cl ^d	0.6%
3	BAT ^d	Fe(TPP)Cl ^d	1.4%
4	BAT ^c	none	0.7%
5	PhINTs (2) ^c	6	2.2%
6	PhINTs ^{f,g}	17	1.9%
7	PhINTs ^{f,h}	17	6.9%
8	PhINTs ^{f,i}	17	7.5%

^aStandard conditions: 18 mg MWCNT, 0.4 eq. BAT per CNT carbon atom, DMF, r.t., 14 h. ^bBy XPS analysis of the product. ^cAddition of a solution in DMF over 10 h via syringe pump. ^dImmediate addition of a solution in DMF. ^e10 mg MWCNTs, 1 eq. PhINTs per CNT carbon atom, 1,2-dichlorobenzene, r.t. 7 d. ^f10 mg MWCNTs, 1 eq. PhINTs per CNT carbon atom, 1,2-dichlorobenzene, 13 d. ^g r.t. ^h60 °C. ⁱ80 °C

3.2.2. Catalyzed aziridination of CNTs and graphite

After confirming successful functionalization of MWCNTs using **17** and PhINTs, we transitioned to SWCNT and graphite modification. The reaction was performed for 5 days at 80

°C using 1 equivalent of reagent per carbon atom of the CNTs or graphite and 2.5% catalyst (relative to reagent). Based on N 1s and C 1s signals in XPS, functional group densities of 1 per 22 carbons and 1 per 20 carbons were obtained for SWCNTs and graphite, respectively (Figure 3.2).

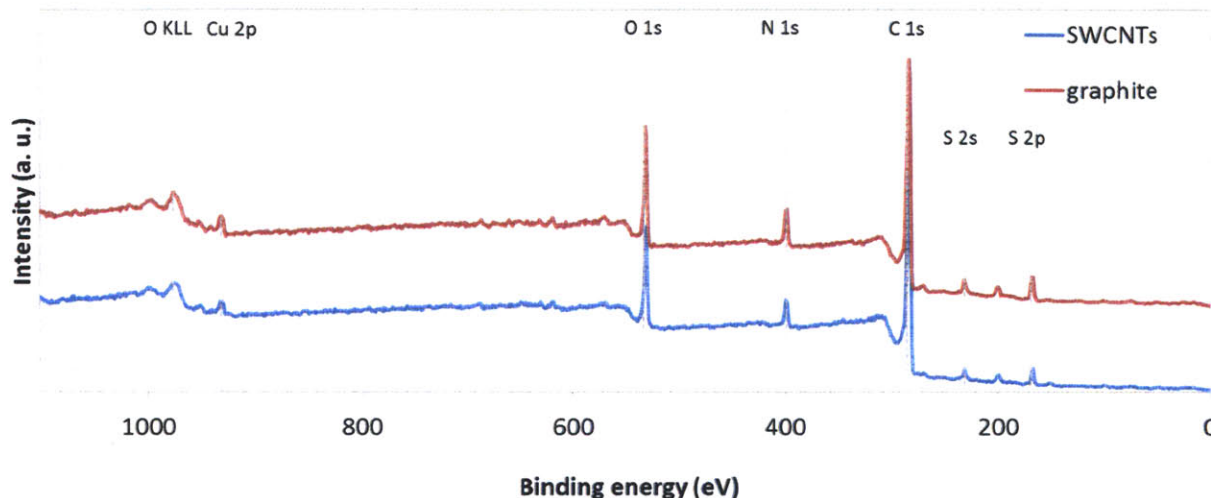


Figure 3.2. XPS analysis of *N*-tosylaziridine-functionalized SWCNTs and graphite.

With these initial results, we looked to optimize the reaction conditions for decreased catalyst loadings. Large amounts of catalyst are common for CNT and graphite functionalization reactions as they are calculated relative to the reagent. In our case, 2.5 % catalyst loading corresponds to 150 wt% of **17** relative to graphite or CNTs. Unfortunately, we found that reducing the catalyst loading to 1% for the reaction on graphite, resulted in a lower functional group density of 1 per 40 graphite carbons. This effect could not be compensated by using a higher amount of reagent (4 equivalents). In this case a functional group density of 1 per 40 graphite carbons was achieved as well suggesting the catalyst loading dictates the degree of functionalization.

With a limited supply of catalyst **17**, we returned to the commercially available CuCl/2,6-lutidine catalyst system.²⁰ Using 3% catalyst loading and 4 equivalents of **2** per graphite carbon atom, a functional group density of 1 per 30 C was achieved (based on S 2p vs. C 1s by XPS). By comparison, these same conditions with the Cu(I) scorpionate complex **17** yielded 1 functional group per 12 graphite carbons, further demonstrating the already established superiority of this reaction. However, these high degrees of functionalization could be achieved with the CuCl/2,6-lutidine system if a 6% catalyst loading was employed (functional group density of over 1 per 10 graphite carbons, Figure 3.3).

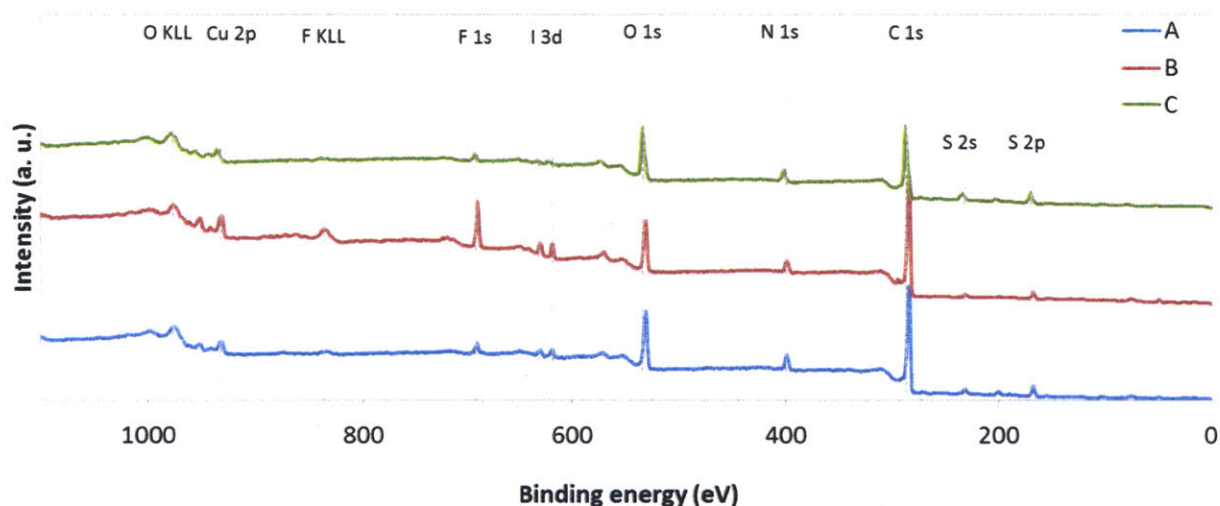


Figure 3.3. XPS analysis of aziridine-functionalized graphite using 4 equivalents PhINTs with 3% **17** (blue trace), 3% CuCl/2,6-lutidine (red trace), and 6% CuCl/2,6-lutidine (green trace).

To broaden the scope of the reaction, the synthesis of other iodine reagents to be used instead of PhINTs was pursued (Figure 3.4). Among these was [*N*-(2-nitrophenylsulfonyl)imino]phenyliodine **18** as the nosyl group could potentially be cleaved after aziridination leading to the NH-carrying species. Furthermore, iodine reagents that carried

reactive groups such as amines or substituents that could affect the polarity of the product such as sulfonates or long alkyl chains were of interest.

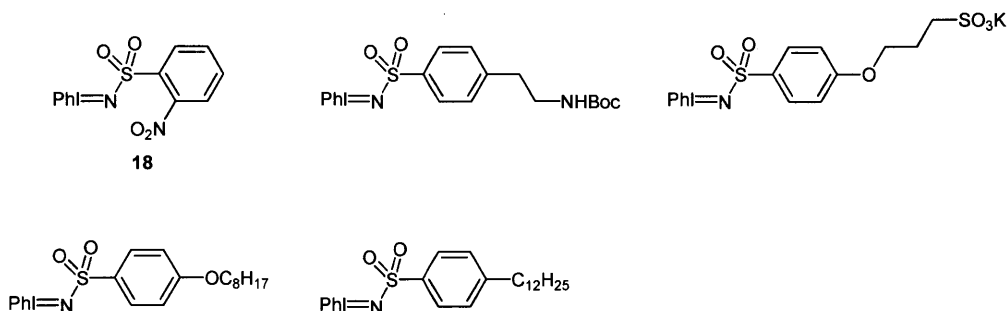


Figure 3.4. Desired iodine reagents for CNT and graphite functionalization.

Of these derivatives, only **18** could be obtained in sufficient quantity and purity. Although iodines are regularly used for the aziridination of small molecules, their preparation is described as difficult to reproduce with conflicting reports in the literature.²⁴

Using the previously optimized conditions (4 equiv of reagent, 6% CuCl/2,6-lutidine, 80 °C) aziridination of graphite with **18** was performed. XPS characterization (S 2p vs C 1s) of the resulting graphite revealed that the obtained functional group density was only 1 per 150 graphite carbon atoms (Figure 3.5).

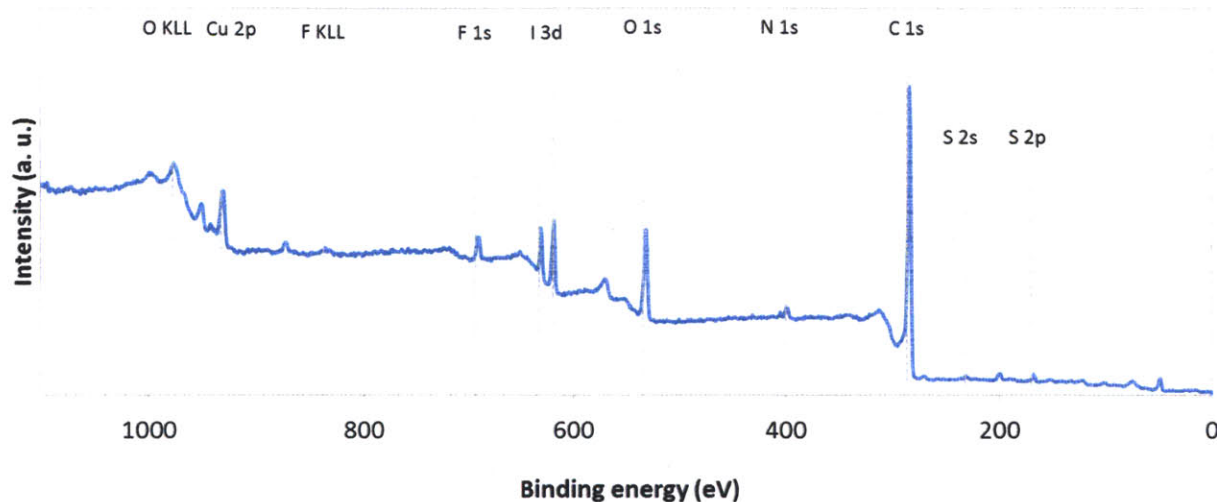


Figure 3.5. XPS analysis of nosylaziridine-functionalized graphite using 4 equivalents PhINNs **18** with 6% CuCl/2,6-lutidine.

3.3. Conclusions

In summary, C₆₀, SWCNTs, MWCNTs, and graphite were functionalized using optimized conditions with Cu(I) scorpionate **17** as the catalyst and the aziridination reagent PhINTs (**2**). Very good yields could be obtained on C₆₀ and high functional group densities were achieved on CNTs and graphite. Utilizing different iodine reagents to access a wider range of products, however, proved to be difficult due to the challenging synthetic access to the required iodine reagents.

3.4. Experimental Section

Materials: SWCNTs were received from SouthWest NanoTechnologies (CG-100, >90% carbon content, lot # CG100-000-0012) and used without further purification. MWCNTs were obtained from Aldrich (>95% purity, for small-scale reactions) and Bayer Group (Baytubes[®]C 150 P, >95% purity, for large-scale reactions) and used as received. Graphite was received from Alfa

Aesar. Cu(I) scorpionates **6** and **17** were prepared by Birgit Esser following literature procedures.^{12,23} All other chemicals were of reagent grade and used as received.

General Methods and Instrumentation: Fourier transform infrared (FT-IR) spectroscopy was performed on a Perkin-Elmer model 2000 FT-IR spectrophotometer using the Spectrum v. 2.00 software package. XPS spectra were recorded on a Kratos AXIS Ultra X-ray Photoelectron Spectrometer. All synthetic manipulations were carried out under an argon atmosphere using standard Schlenk techniques unless otherwise noted.

3-azidopropan-1-amine 15. **15** was synthesized following a literature procedure.⁹ Note: Molecules with a high density of azide groups are potentially explosive and particular caution has thus to be used, especially when isolating azides.^{25,26} Before synthesizing the compound on the described scale the molecule was prepared on small scale and the explosive hazard has been evaluated (shock, heat). 65.6 g (0.30 mol) 3-bromopropylamine hydrobromide were dissolved in 200 mL H₂O and added to 39.0 g (2 equiv) sodium azide in 160 mL H₂O. The mixture was refluxed for 15 h and subsequently cooled in an ice bath. Afterward, it was poured into 400 mL diethyl ether containing 24 g NaOH (2 equiv). The organic phase was separated and the aqueous phase was extracted twice with 100 mL Et₂O. The combined organic phases were dried over MgSO₄, filtered and stored in solution. A small aliquot was concentrated for characterization by NMR. The concentration in solution was determined by ¹H-NMR to be 0.3 M using toluene as an internal standard. Yield: 470 mL of 0.3 M solution (47%). ¹H-NMR (CDCl₃, 400 MHz): δ = 3.33 (t, 2H, *J* = 6.6 Hz); 2.76 (t, 2H, *J* = 7.0 Hz); 1.68 (quin, 2H, *J* = 6.8 Hz); 1.17 (s, broad, 2H). ¹³C-NMR (CDCl₃, 100 MHz): δ = 49.2, 39.4, 32.6.

PhINTs 2. PhINTs was synthesized following a literature procedure.²⁷ $\text{PhI}(\text{OAc})_2$ (32.0 g, 100 mmol) was added to a clear solution of H_2NTs (17.1 g, 1 equiv) and KOH (14 g, 2.5 equiv) in 400 mL MeOH at 0 °C. The mixture was stirred for 3 h at room temperature and then poured into 600 mL H_2O . Water was added until no further precipitation was observed. Subsequently, the solid was collected by filtration. It was washed with water and diethyl ether and dried under vacuum overnight. 24.10 g (65 mmol, 65%) of a yellow solid were obtained. $^1\text{H-NMR}$ (MeOD, 400 MHz): $\delta = 8.52$ (dd, 2H, $J = 8.4, 2.4$ Hz); 7.80 (d, 2H, $J = 8.4$ Hz); 7.60-7.58 (m, 3H); 7.37 (d, 2H, $J = 8.0$ Hz); 2.43 (s, 3H).

PhI=O 7. PhI=O was synthesized following a literature procedure.¹⁴ 45 mL of an aqueous 3 N NaOH solution were added to $\text{PhI}(\text{OAc})_2$ (8.05 g, 25 mmol) over the course of 10 min. The yellow suspension was stirred at room temperature for 90 minutes. 40 mL H_2O were added and the mixture was stirred vigorously for an additional hour. A solid precipitated, was collected by filtration and washed with water and CHCl_3 . It was suspended in acetone and subsequently concentrated *in vacuo*. 2.66 g (12.1 mmol, 48%) of a pale yellow solid were obtained. mp 215 °C (decomp., lit: 209-210 °C). The product was not soluble enough to obtain an NMR spectrum.

Bromamine-T 12. Bromamine-T was synthesized following a literature procedure.²⁸ 5.00 g Chloramine-T trihydrate (17.8 mmol) were dissolved in 100 mL H_2O . 1.0 mL Br_2 (19 mmol) were added slowly *via* syringe upon which a yellow precipitate forms. The suspension was stirred at room temperature for 1 hour. The solid was collected by filtration and 5.53 g of a yellow intermediate were obtained after drying. 80 mL of 4 N aqueous NaOH solution were added to the intermediate. After 1 h, the suspension was cooled to 0 °C and then stored in a refrigerator overnight. The solid was collected by filtration and washed with ice water and dried. 3.53 g (13.0 mmol, 85%) of a yellow solid were obtained. $^1\text{H-NMR}$ (D_2O , 400 MHz): $\delta = 7.66$

(d, 2H, $J = 8.0$ Hz); 7.35 (d, 2H, $J = 8.0$ Hz); 2.36 (s, 3H). ^{13}C -NMR (D_2O , 100 MHz): $\delta = 143.3$, 137.3, 129.6, 127.1, 20.6.

4-methylbenzenesulfonyl azide 14. **14** was synthesized following a literature procedure.²⁹ 3.53 g 4-methylbenzenesulfonyl chloride (18.5 mmol) were dissolved in 8 mL acetone. 1.2 g (1 equiv) NaN_3 in 5 mL H_2O were slowly added via syringe. The mixture was stirred at room temperature for 6 days after which 50 mL saturated aqueous Na_2CO_3 solution and 50 mL ethyl acetate were added. The phases were separated and the aqueous phase was extracted with ethyl acetate. The combined organic phases were dried over MgSO_4 , filtered and concentrated. The crude product was purified via column chromatography (hexanes/ethyl acetate 4:1). 3.00 g of a colorless oil were obtained (15.2 mmol, 82%). ^1H -NMR (CDCl_3 , 400 MHz): $\delta = 7.81$ (d, 2H, $J = 8.4$ Hz); 7.37 (d, 2H, $J = 8.8$ Hz); 2.45 (s, 3H). ^{13}C -NMR (CDCl_3 , 100 MHz): $\delta = 146.4$, 135.6, 130.5, 127.7, 21.9.

[*N*-(2-nitrophenylsulfonyl)imino]phenyliodinane 18. **18** was synthesized following a literature procedure.³⁰ Iodobenzene diacetate (19.3 g, 60 mmol) was added to a suspension of KOH (8.4 g, 2.5 equiv) and 2-nitrobenzenesulfonamide (12.1 g, 1 equiv) in 240 mL MeOH while the temperature was kept at 5-10 °C. The mixture was stirred for 4 h at room temperature after which the mixture was poured into 400 mL ice water. The formed precipitate was collected by filtration and washed with water. The solid was dried *in vacuo* overnight. 17.1 g (42 mmol, 70%) of pale yellow solid were obtained. ^1H -NMR ($\text{DMSO-}d_6$, 400 MHz): $\delta = 7.78$ (d, 2H, $J = 7.2$ Hz); 7.67 (d, 1H, $J = 7.6$ Hz); 7.58 (d, 1H, $J = 7.6$ Hz); 7.50 (t, 1H, $J = 7.6$ Hz); 7.46-7.38 (m, 2H); 7.29 (t, 2H, $J = 8.0$ Hz). ^{13}C -NMR ($\text{DMSO-}d_6$, 100 MHz): $\delta = 195.5$, 181.5, 147.2, 136.8, 133.6, 131.6, 131.1, 130.8, 130.3, 129.4, 122.9, 117.2.

N-tosyl aziridine functionalized MWCNTs general procedure (Table 3.1). 9.0 mg MWCNTs (0.75 mmol carbon), 0.2 equivalents aziridination reagent and 10 mol% catalyst were added to a flame dried Schlenk flask. 2.5 mL acetonitrile were added and the mixture was sonicated for 120 min (bath sonicator). Afterward, the suspension was stirred for 25 h at r.t. The CNTs were collected by centrifugation and washed by repeated redispersion and centrifugation with acetonitrile, CH₂Cl₂, hexanes, water and methanol before being dried *in vacuo*.

N-tosyl aziridine functionalized MWCNTs (Table 3.1, Entry 1). 56 mg (0.15 mmol) **2** and 5.6 mg (0.1 equiv) [Cu(CH₃CN)₄]PF₆ were used. N/C ratio by XPS (based on N 1s vs. C 1s): 1.7%.

N-tosyl aziridine functionalized MWCNTs (Table 3.1, Entry 2). 34.2 mg (0.20 mmol) **8**, 33.0 mg (0.15 mmol) **7** and 5.6 mg (0.1 equiv) [Cu(CH₃CN)₄]PF₆ were used. N/C ratio by XPS (based on N 1s vs. C 1s): 0.4%.

N-tosyl aziridine functionalized MWCNTs (Table 3.1, Entry 3). 34.1 mg (0.15 mmol) **10**, obtained from chloramine-T trihydrate by drying at 90 °C *in vacuo* for 4 h, and 2.9 mg (0.1 equiv) CuI were used. N/C ratio by XPS (based on N 1s vs. C 1s): 0.9%.

N-tosyl aziridine functionalized MWCNTs (Table 3.1, Entry 4). 29.6 mg (0.15 mmol) **14**, 9 mg MWCNTs and 2.5 mL acetonitrile were added to a flame dried Schlenk flask. The mixture was sonicated for 30 min and subsequently irradiated for 55 min with a 500 W Hg lamp using an OD 0.5 filter. The workup was similar to the general procedure. N/C ratio by XPS (based on N 1s vs. C 1s): 0.5%.

N-tosyl aziridine functionalized MWCNTs (Table 3.1, Entry 5). 29.6 mg (0.15 mmol) **14**, 9 mg MWCNTs and 2.5 mL acetonitrile were added to a flame dried Schlenk flask. The mixture

was sonicated for 30 min and then refluxed for 19 h followed by workup similar to the general procedure. No N 1s peak was observed by XPS.

N-tosyl aziridine functionalized MWCNTs (Table 3.1, Entry 6). The general procedure was followed using 40.8 mg (0.15 mmol) **12** and 5.3 mg (0.05 equiv) Fe(TPP)Cl. N/C ratio by XPS (based on N 1s vs. C 1s): 1.3%.

Amino functionalized MWCNTs (Table 3.1, Entry 7). 100 mg MWCNTs (8.3 mmol carbon) were added to a flame dried Schlenk flask. 5 mL NMP were added and the mixture was sonicated for 80 min. Afterward, 2 g . 3-azidopropan-1-amine **15** were added and the reaction was stirred at 160 °C for 2 d. The suspension was cooled to r.t. and the solid was collected by centrifugation. The crude product was washed by repeated redispersion and centrifugation with acetone, water, methanol and hexanes. N/C ratio by XPS (based on N 1s vs. C 1s): 4.2% (functional group density: 2.1%).

N-tosyl[1,2]aziridino[60]fullerene 16; optimized procedure. C₆₀ (100 mg, 139 μmol), **2** (103 mg, 2 equiv), and Cu(I) complex **17** (5 mg, 5 mol%) were added to a flame-dried Schlenk flask under Argon. 10 mL *ortho*-dichlorobenzene was added and the mixture was sonicated for 40 min. After stirring at room temperature for 2 days, the solvent was distilled off at reduced pressure and 50 °C. Subsequently, the remaining solid was purified by flash silica gel chromatography (hexanes/toluene, 2:1) affording 33.7 mg (37.9 μmol, 27%) of a dark brown solid. ¹H-NMR (CDCl₃, 400 MHz): δ = 8.23 (d, 2H, *J* = 8.4 Hz); 7.51 (d, 2H, *J* = 8.0 Hz); 2.52 (s, 3H. ¹³C-NMR (CDCl₃, 100 MHz): δ = 146.1, 145.6, 145.4, 145.3, 145.3, 144.8, 144.4, 144.2, 144.1, 143.4, 143.4, 143.3, 143.0, 142.4, 142.1, 141.6, 141.1, 135.6, 130.4, 128.7, 77.4, 22.1.

***N*-tosyl[1,2]aziridino[60]fullerene 16 general procedure (Table 3.2).** 20 mg (28 μmol) C_{60} , 28 μmol aziridination reagent and 2.8 μmol catalyst and 1.5 mL 1,2-dichlorobenzene were added to a flame dried Schlenk flask. The mixture was sonicated for 15 min and then stirred at r.t. for 18 h. The solvent was evaporated *in vacuo* and the product was purified by flash silica gel chromatography (hexanes/toluene 1:1).

***N*-tosyl[1,2]aziridino[60]fullerene 16 (Table 3.2, Entry 1).** 10.4 mg (28 μmol) **2** and 1 mg (2.8 μmol) $\text{Cu}(\text{OTf})_2$ were used. Yield: 1 mg (3%)

***N*-tosyl[1,2]aziridino[60]fullerene 16 (Table 3.2, Entry 2).** 7.5 mg (28 μmol) **12** and 1 mg (2.8 μmol) $\text{Fe}(\text{TPP})\text{Cl}$ were used. No product was observed by TLC.

***N*-tosyl[1,2]aziridino[60]fullerene 16 (Table 3.2, Entry 3).** 7.5 mg (28 μmol) **12** and 1 mg (2.8 μmol) $\text{Fe}(\text{TPP})\text{Cl}$ were used. **12** was added via syringe as a solution in 0.5 mL DMF over 30 min. Yield: 7.2 mg (29%)

***N*-tosyl[1,2]aziridino[60]fullerene 16 (Table 3.2, Entry 4).** 15 mg (56 μmol) **12** and 1 mg (2.8 μmol) $\text{Fe}(\text{TPP})\text{Cl}$ were used. **12** was added via syringe as a solution in 0.5 mL DMF over 30 min and the reaction was conducted at 40 $^{\circ}\text{C}$. Yield: 8.0 mg (32 %)

***N*-tosyl[1,2]aziridino[60]fullerene 16 (Table 3.2, Entry 5).** 15 mg (56 μmol) **12** and 1 mg (2.8 μmol) $\text{Fe}(\text{TPP})\text{Cl}$ were used. **12** was added via syringe as a solution in 0.5 mL DMF over 30 min and the reaction was conducted at 60 $^{\circ}\text{C}$. Yield: 7.5 mg (30 %)

***N*-tosyl[1,2]aziridino[60]fullerene 16 (Table 3.2, Entry 6).** 15 mg (56 μmol) **12** and 1 mg (2.8 μmol) $\text{Fe}(\text{TPP})\text{Cl}$ were used. **12** was added via syringe as a solution in 0.5 mL DMF over 30 min and the reaction was conducted at 80 $^{\circ}\text{C}$. Yield: 7.1 mg (29 %)

***N*-tosyl[1,2]aziridino[60]fullerene 16 (Table 3.2, Entry 7).** 15 mg (56 μmol) **12** and 1 mg (2.8 μmol) $[\text{Cu}(\text{CH}_3\text{CN})_4]\text{PF}_6$ were used. **12** was added via syringe as a solution in 0.5 mL DMF over 30 min. Yield: 6.2 mg (25 %)

***N*-tosyl[1,2]aziridino[60]fullerene 16 (Table 3.2, Entry 8).** 15 mg (56 μmol) **12** and 1 mg (2.8 μmol) $\text{Cu}(\text{OTf})_2$ were used. **12** was added via syringe as a solution in 0.5 mL DMF over 30 min. Yield: 3.2 mg (13 %)

***N*-tosyl[1,2]aziridino[60]fullerene 16 (Table 3.2, Entry 9).** 15 mg (56 μmol) **12** and 0.7 mg (2.8 μmol) $\text{Cu}(\text{acac})_2$ were used. **12** was added via syringe as a solution in 0.5 mL DMF over 30 min. Yield: 6.2 mg (25 %)

***N*-tosyl[1,2]aziridino[60]fullerene 16 (Table 3.2, Entry 10).** 15 mg (56 μmol) **12** were used without additional catalyst. **12** was added via syringe as a solution in 0.5 mL DMF over 30 min. Yield: 4.1 mg (17 %)

***N*-tosyl[1,2]aziridino[60]fullerene 16 using Cu(I) scorpionate 6.** 20 mg (28 μmol) C_{60} were sonicated in 1,2-dichlorobenzene for 15 min upon which 21 mg (56 μmol) **2** and 1 mg (2.8 μmol) **6** were added as solids. The solution was stirred at r.t. for 20 h. The workup was similar to the general procedure for **16**. Yield: 7.2 mg (8.1 μmol , 29 %)

***N*-tosyl aziridine functionalized MWCNTs (Table 3.3, Entry 1).** 18 mg MWCNTs (1.5 mmol carbon) and 11 mL DMF were added to a flame dried Schlenk flask and the mixture was sonicated for 60 min (bath sonicator). Afterward, 163 mg (0.6 mmol) **12** in 5.4 mL DMF and 21.2 mg (0.03 mmol) $\text{Fe}(\text{TPP})\text{Cl}$ in 4 mL DMF were added via syringe pump over 10 h. After 4 additional hours, the CNTs were collected by centrifugation and washed by repeated redispersion

and centrifugation using DMF followed by drying *in vacuo*. N/C ratio by XPS (based on N 1s vs. C 1s): 0.8%.

N-tosyl aziridine functionalized MWCNTs (Table 3.3, Entry 2). 18 mg MWCNTs (1.5 mmol carbon) and 11 mL DMF were added to a flame dried Schlenk flask and the mixture was sonicated for 60 min (bath sonicator). 21.2 mg (0.03 mmol) Fe(TPP)Cl in 4 mL DMF after which 163 mg (0.6 mmol) **12** in 5.4 mL DMF were added via syringe pump over 10 h. After 4 additional hours, the CNTs were collected by centrifugation and washed by repeated redispersion and centrifugation using DMF followed by drying *in vacuo*. N/C ratio by XPS (based on N 1s vs. C 1s): 0.6%.

N-tosyl aziridine functionalized MWCNTs (Table 3.3, Entry 3). 18 mg MWCNTs (1.5 mmol carbon) and 11 mL DMF were added to a flame dried Schlenk flask and the mixture was sonicated for 60 min (bath sonicator). 21.2 mg (0.03 mmol) Fe(TPP)Cl in 4 mL DMF and 163 mg (0.6 mmol) **12** in 5.4 mL DMF were added. The suspension was stirred for 14 h after which the CNTs were collected by centrifugation and washed by repeated redispersion and centrifugation using DMF followed by drying *in vacuo*. N/C ratio by XPS (based on N 1s vs. C 1s): 1.4%.

N-tosyl aziridine functionalized MWCNTs (Table 3.3, Entry 4). 18 mg MWCNTs (1.5 mmol carbon) and 11 mL DMF were added to a flame dried Schlenk flask and the mixture was sonicated for 60 min (bath sonicator). 21.2 mg (0.03 mmol) Fe(TPP)Cl in 4 mL DMF and 163 mg (0.6 mmol) **12** in 5.4 mL DMF were added. The suspension was stirred for 14 h after which the CNTs were collected by centrifugation and washed by repeated redispersion and

centrifugation using DMF followed by drying *in vacuo*. N/C ratio by XPS (based on N 1s vs. C 1s): 1.4%.

N-tosyl aziridine functionalized MWCNTs (Table 3.3, Entry 5). 10 mg MWCNTs (0.83 mmol carbon) and 10 mL 1,2-dichlorobenzene were added to a flame dried Schlenk flask and the mixture was sonicated for 90 min (bath sonicator). 300 mg (0.8 mmol) **2** and 14.6 mg (20 μ mol) **6** were added. The suspension was stirred for 7 d after which the CNTs were collected by centrifugation and washed by repeated redispersion and centrifugation using 1,2-dichlorobenzene, CH₂Cl₂, hexanes, and methanol followed by drying *in vacuo*. N/C ratio by XPS (based on N 1s vs. C 1s): 2.2%.

N-tosyl aziridine functionalized MWCNTs (Table 3.3, Entry 6). 10 mg MWCNTs (0.83 mmol carbon) and 10 mL 1,2-dichlorobenzene were added to a flame dried Schlenk flask and the mixture was sonicated for 2.5 h (bath sonicator). 300 mg (0.8 mmol) **2** and 14.7 mg (20 μ mol) **17** were added. The suspension was stirred at r.t. for 13 d after which the CNTs were collected by centrifugation and washed by repeated redispersion and centrifugation using 1,2-dichlorobenzene, CH₂Cl₂, ethanol, methanol, and hexanes followed by drying *in vacuo*. N/C ratio by XPS (based on N 1s vs. C 1s): 1.9%.

N-tosyl aziridine functionalized MWCNTs (Table 3.3, Entry 7). 10 mg MWCNTs (0.83 mmol carbon) and 10 mL 1,2-dichlorobenzene were added to a flame dried Schlenk flask and the mixture was sonicated for 2.5 h (bath sonicator). 300 mg (0.8 mmol) **2** and 14.7 mg (20 μ mol) **17** were added. The suspension was stirred at 60 °C for 13 d after which the CNTs were collected by centrifugation and washed by repeated redispersion and centrifugation using 1,2-

dichlorobenzene, CH₂Cl₂, methanol, and hexanes followed by drying *in vacuo*. N/C ratio by XPS (based on N 1s vs. C 1s): 6.9%.

N-tosyl aziridine functionalized MWCNTs (Table 3.3, Entry 8). 10 mg MWCNTs (0.83 mmol carbon) and 10 mL 1,2-dichlorobenzene were added to a flame dried Schlenk flask and the mixture was sonicated for 2.5 h (bath sonicator). 300 mg (0.8 mmol) **2** and 14.7 mg (20 μmol) **17** were added. The suspension was stirred at 80 °C for 13 d after which the CNTs were collected by centrifugation and washed by repeated redispersion and centrifugation using 1,2-dichlorobenzene, CH₂Cl₂, methanol, and hexanes followed by drying *in vacuo*. N/C ratio by XPS (based on N 1s vs. C 1s): 7.5%.

N-tosyl aziridine functionalized SWCNTs. 5 mg SWCNTs (0.4 mmol carbon) and 5 mL 1,2-dichlorobenzene were added to a flame dried Schlenk flask and the mixture was sonicated for 2 h (bath sonicator). 150 mg (0.4 mmol) **2** and 7.4 mg (10 μmol) **17** were added. The suspension was stirred at 80 °C for 5 d after which the CNTs were collected by centrifugation and washed by repeated redispersion and centrifugation using 1,2-dichlorobenzene, CH₂Cl₂, hexanes, ethanol, and methanol followed by drying *in vacuo*. N/C ratio by XPS (based on N 1s vs. C 1s): 4.5%.

N-tosyl aziridine functionalized graphite, procedure 1. 5 mg graphite (0.4 mmol carbon) and 5 mL 1,2-dichlorobenzene were added to a flame dried Schlenk flask and the mixture was sonicated for 2 h (bath sonicator). 150 mg (0.4 mmol) **2** and 7.4 mg (10 μmol) **17** were added. The suspension was stirred at 80 °C for 5 d after which the CNTs were collected by centrifugation and washed by repeated redispersion and centrifugation using 1,2-dichlorobenzene, CH₂Cl₂, hexanes, ethanol, and methanol followed by drying *in vacuo*. N/C ratio by XPS (based on N 1s vs. C 1s): 5%.

N-tosyl aziridine functionalized graphite, procedure 2. 25 mg graphite (2 mmol carbon), 3 g (8 mmol) **2** and 58 mg (80 μ mol) **17** were added to a flame dried Schlenk flask. 25 mL 1,2-dichlorobenzene were added and the mixture was sonicated for 5 min. The suspension was stirred at 80 °C for 4 d after which the graphite was collected by centrifugation and washed by repeated redispersion and centrifugation using acetone, water, methanol, and hexanes followed by drying *in vacuo*. N/C ratio by XPS (based on N 1s vs. C 1s): 8.3%.

N-tosyl aziridine functionalized graphite, procedure 3. 23.8 mg (0.06 mmol) CuCl and 51.4 mg (0.12 mmol) 2,6-lutidine were dissolved in 25 mL 1,2-dichlorobenzene and stirred at r.t. for 30 min. Subsequently, 25 mg graphite (2 mmol carbon) and 3 g (8 mmol) **2** were added and the mixture was sonicated for 15 min. The suspension was stirred at 80 °C for 5 d after which the graphite was collected by centrifugation and washed by repeated redispersion and centrifugation using acetone, methanol, CH₂Cl₂, and hexanes followed by drying *in vacuo*. N/C ratio by XPS (based on N 1s vs. C 1s): 3.3%.

N-tosyl aziridine functionalized graphite, procedure 4. 47.5 mg (0.12 mmol) CuCl and 102.9 mg (0.24 mmol) 2,6-lutidine were dissolved in 25 mL 1,2-dichlorobenzene and stirred at r.t. for 30 min. Subsequently, 25 mg graphite (2 mmol carbon) and 3 g (8 mmol) **2** were added and the mixture was sonicated for 15 min. The suspension was stirred at 80 °C for 5 d after which the graphite was collected by centrifugation and washed by repeated redispersion and centrifugation using acetone, methanol, CH₂Cl₂, and hexanes followed by drying *in vacuo*. N/C ratio by XPS (based on N 1s vs. C 1s): 16.7%.

N-nosyl aziridine functionalized graphite. 47.5 mg (0.12 mmol) CuCl and 102.9 mg (0.24 mmol) 2,6-lutidine were dissolved in 25 mL 1,2-dichlorobenzene and stirred at r.t. for 30 min.

Subsequently, 25 mg graphite (2 mmol carbon) and 3.2 g (8 mmol) **18** were added and the mixture was sonicated for 15 min. The suspension was stirred at 80 °C for 5 d after which the graphite was collected by centrifugation and washed by repeated redispersion and centrifugation using acetone, methanol, CH₂Cl₂, and hexanes followed by drying *in vacuo*. N/C ratio by XPS (based on N 1s vs. C 1s): 0.7%.

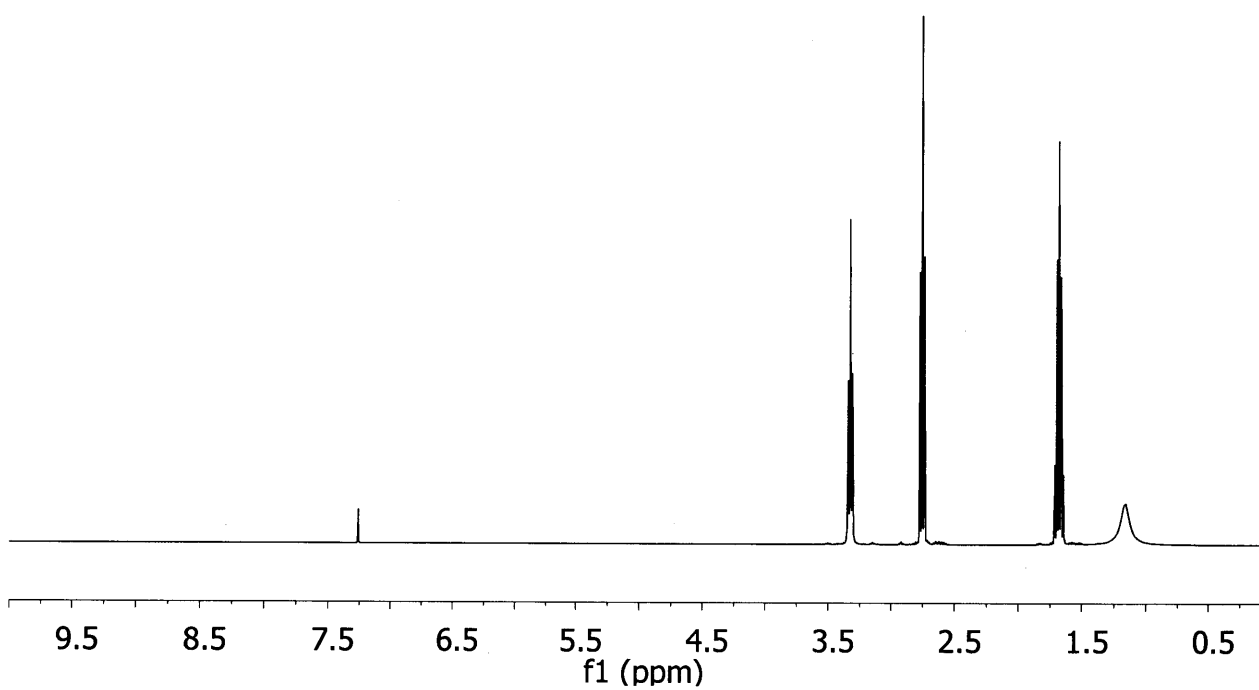


Figure 3.6. ^1H NMR Spectrum of **15** (CDCl_3)

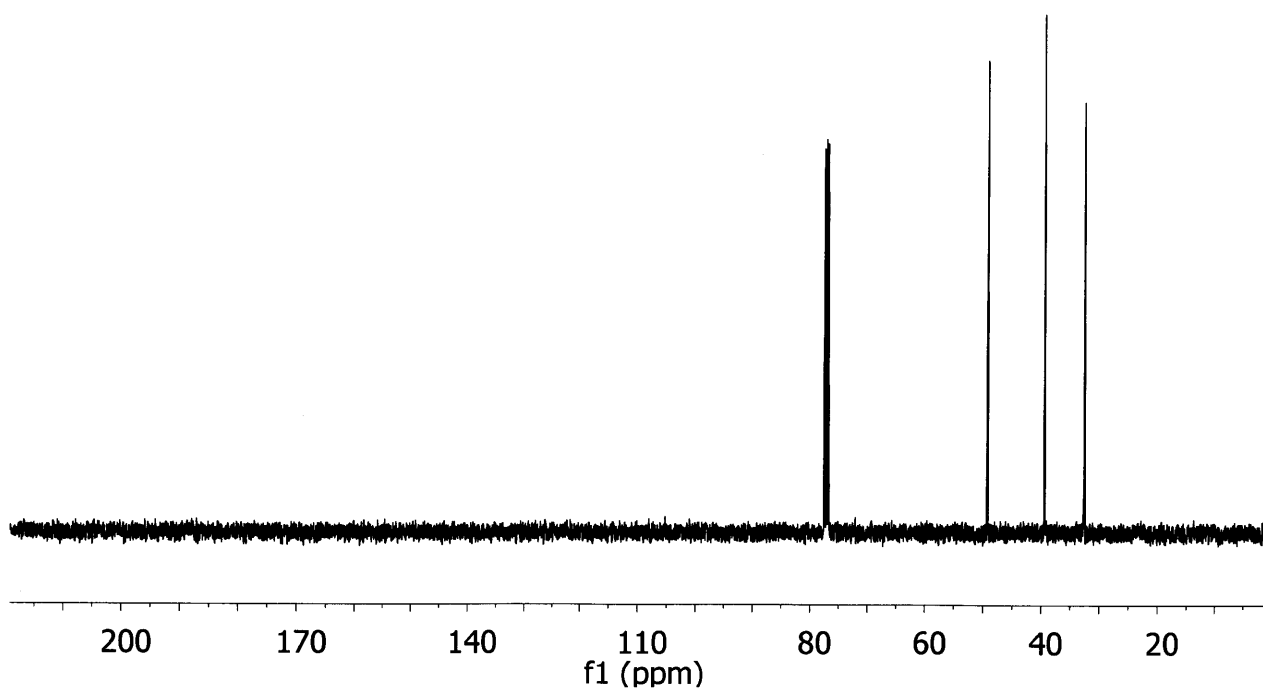


Figure 3.7. ^{13}C NMR Spectrum of **15** (CDCl_3)

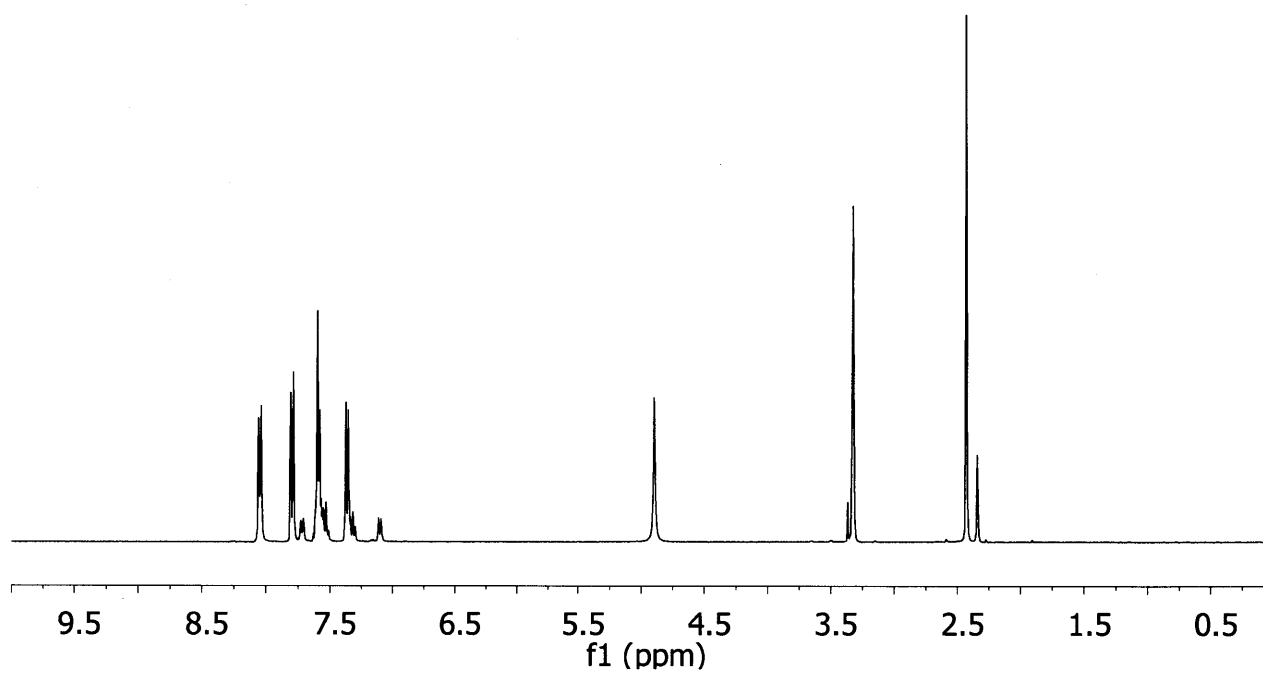


Figure 3.8. ¹H NMR Spectrum of **2** (MeOD)

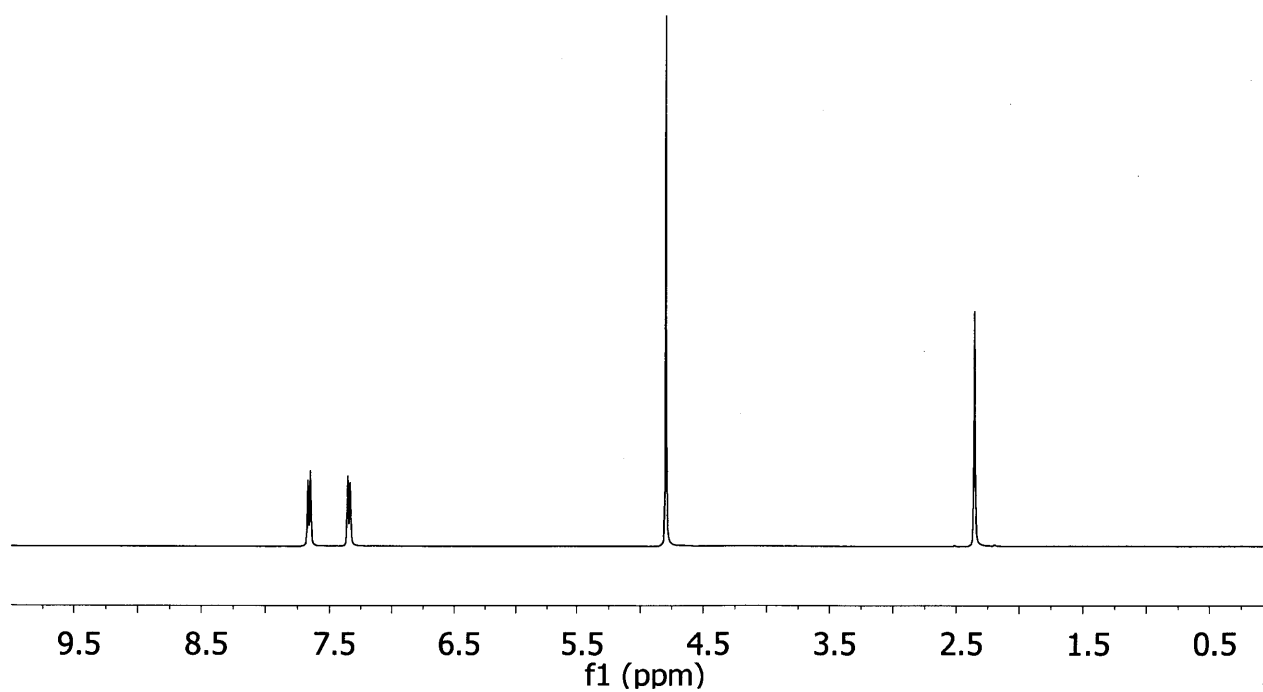


Figure 3.9. ¹H NMR Spectrum of **12** (D₂O)

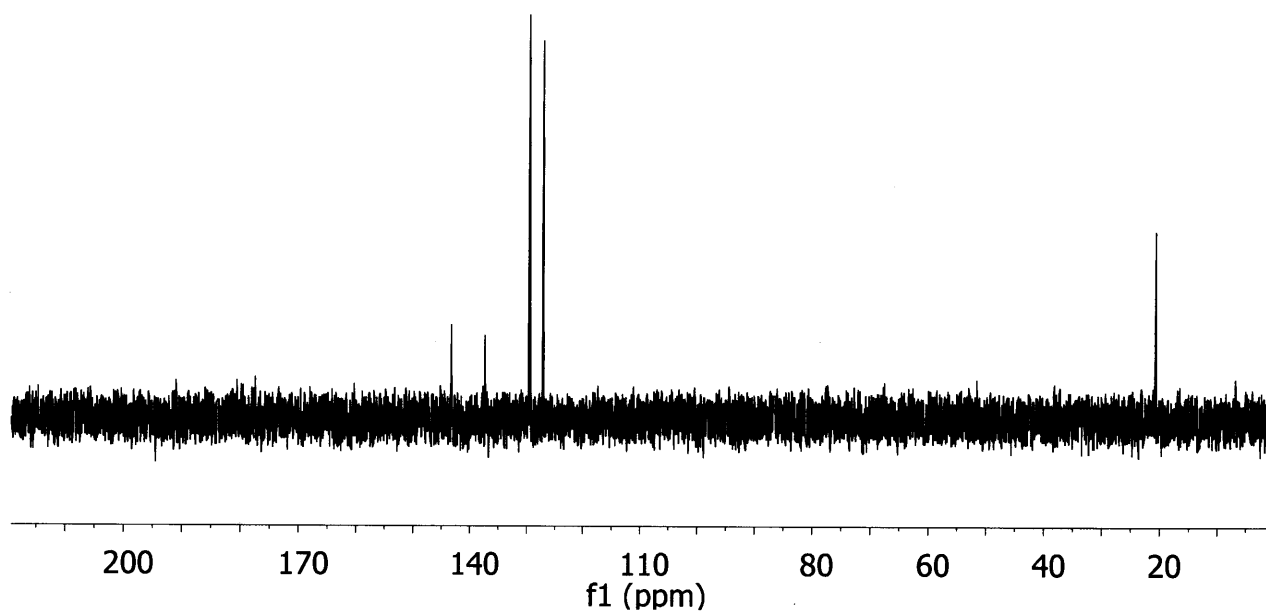


Figure 3.10. ^{13}C NMR Spectrum of **12** (D_2O)

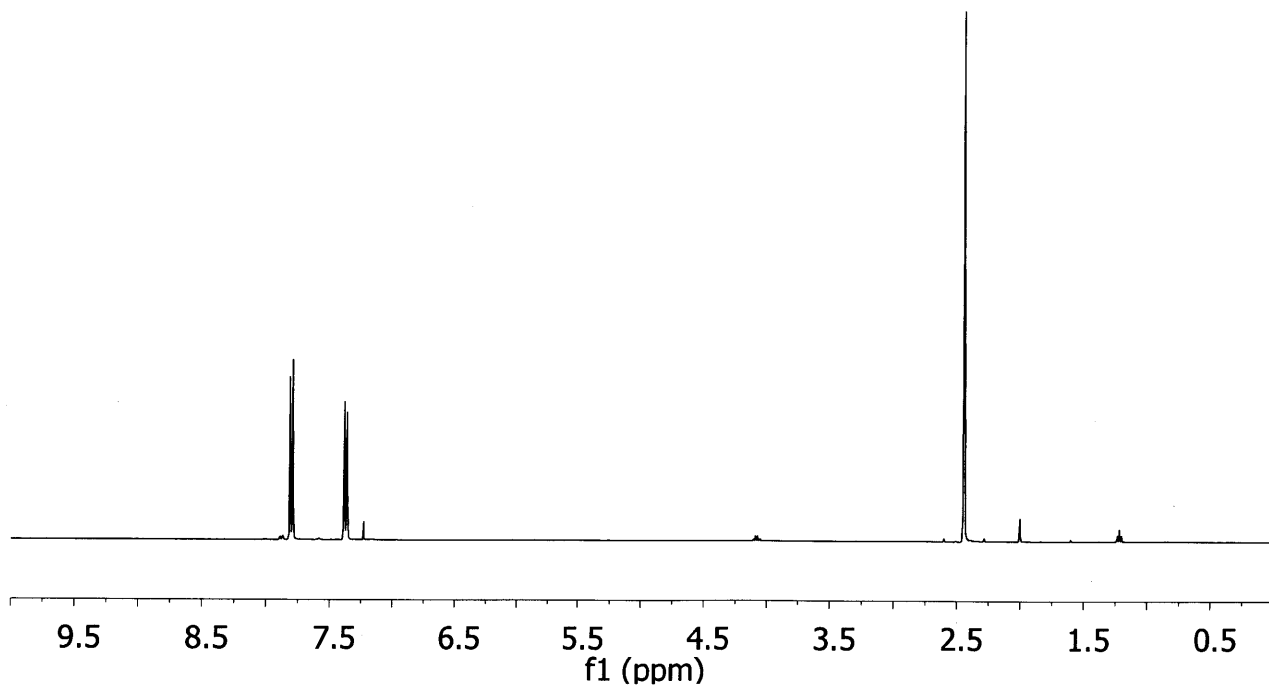


Figure 3.11. ^1H NMR Spectrum of **14** (CDCl_3)

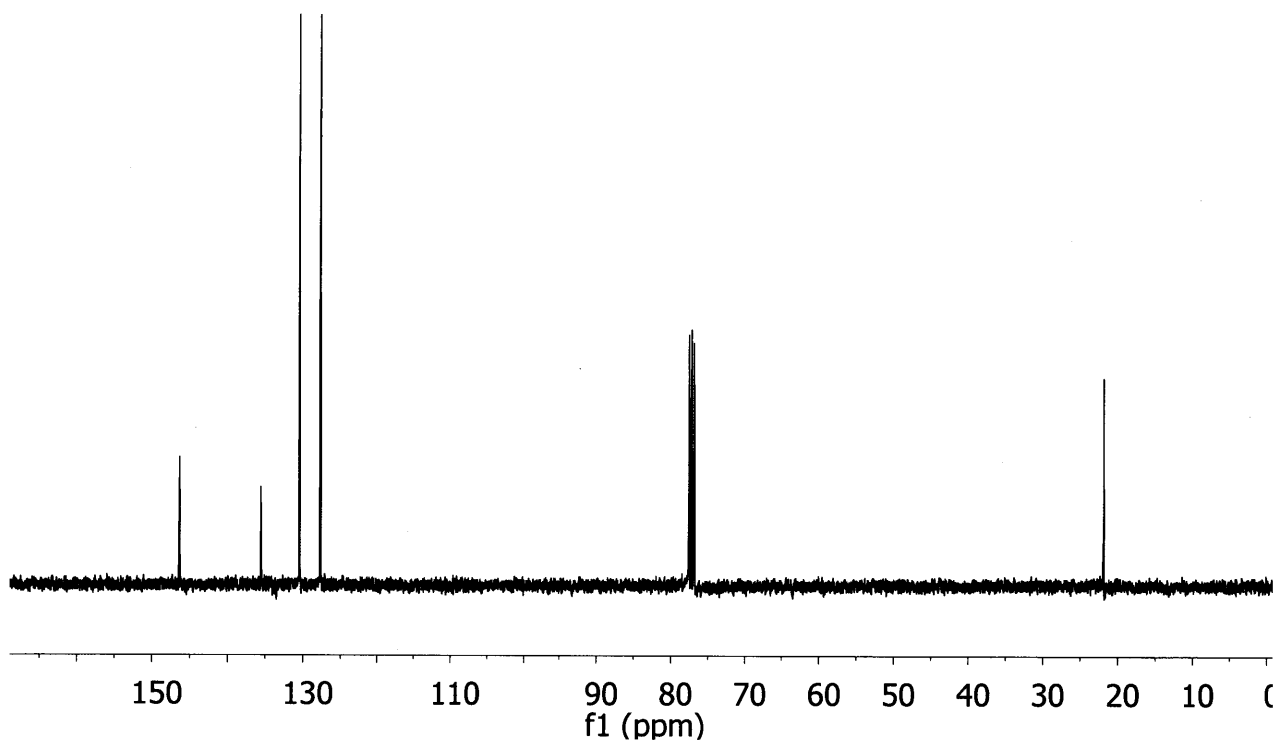


Figure 3.12. ^{13}C NMR Spectrum of **14** (CDCl_3)

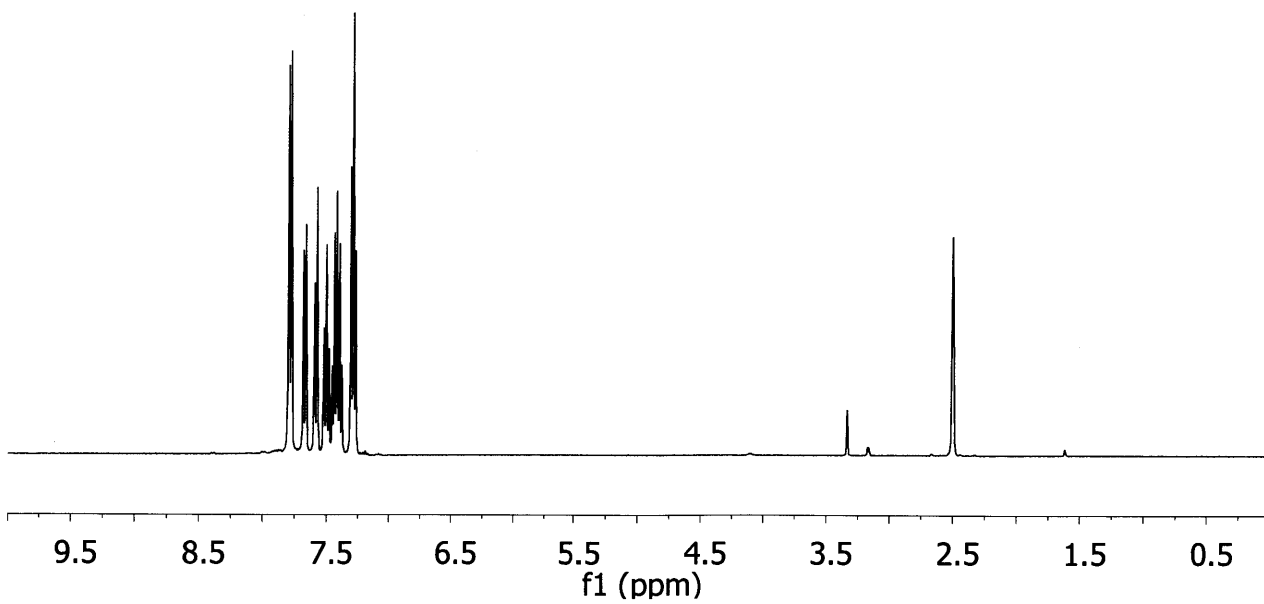


Figure 3.13. ^1H NMR Spectrum of **18** ($\text{DMSO}-d_6$)

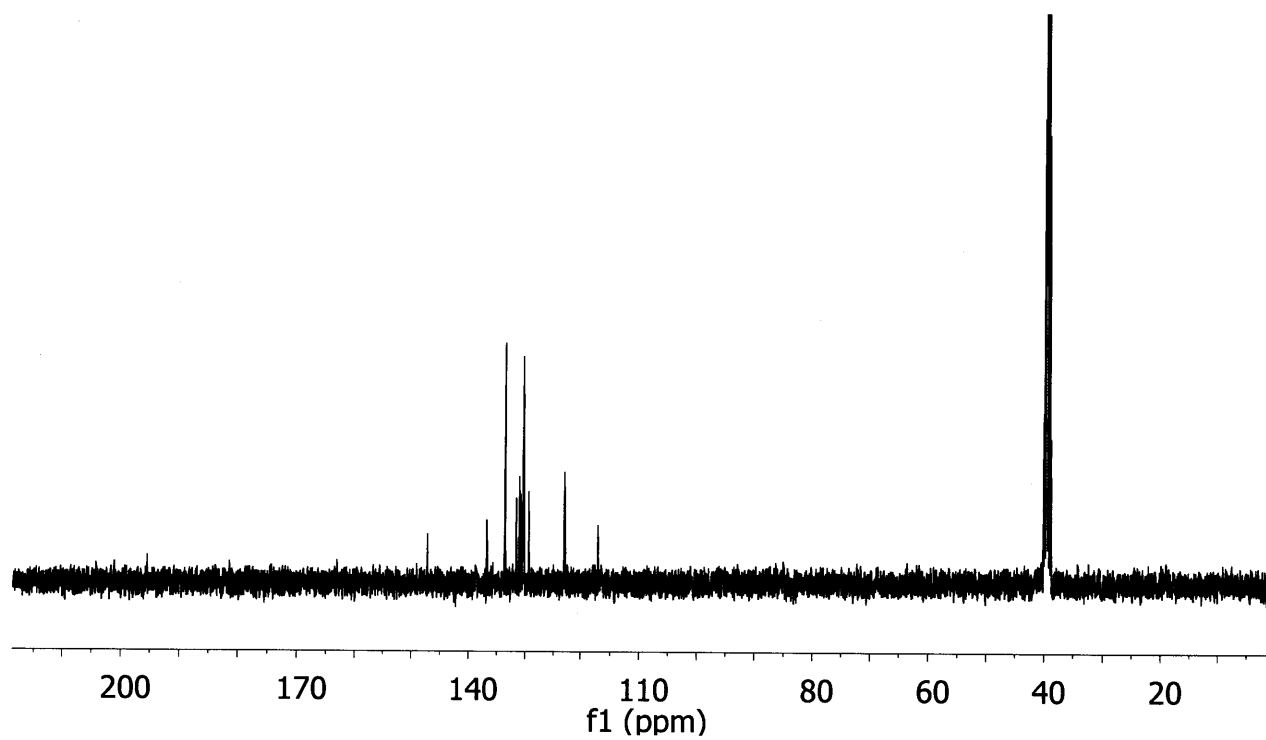


Figure 3.14. ^{13}C NMR Spectrum of **18** ($\text{DMSO-}d_6$)

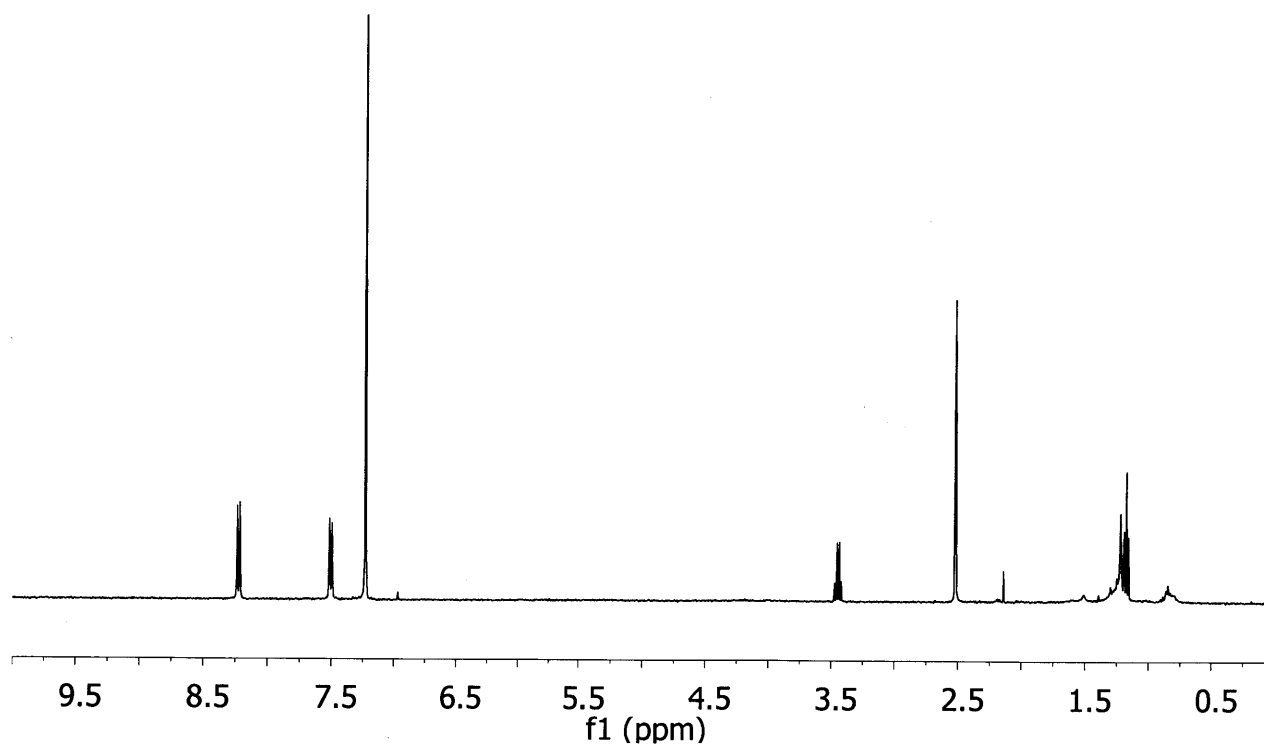


Figure 3.15. ^1H NMR Spectrum of **16** (CDCl_3)

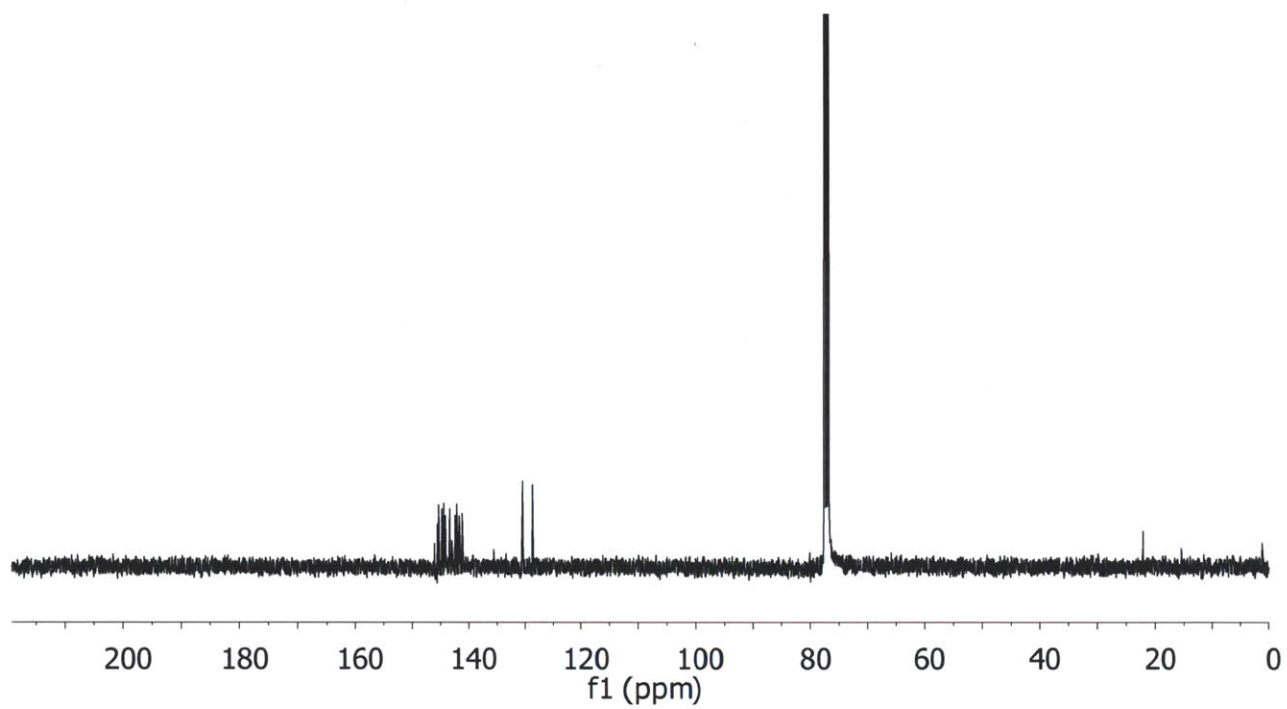


Figure 3.16. ^{13}C NMR Spectrum of **16** (CDCl_3)

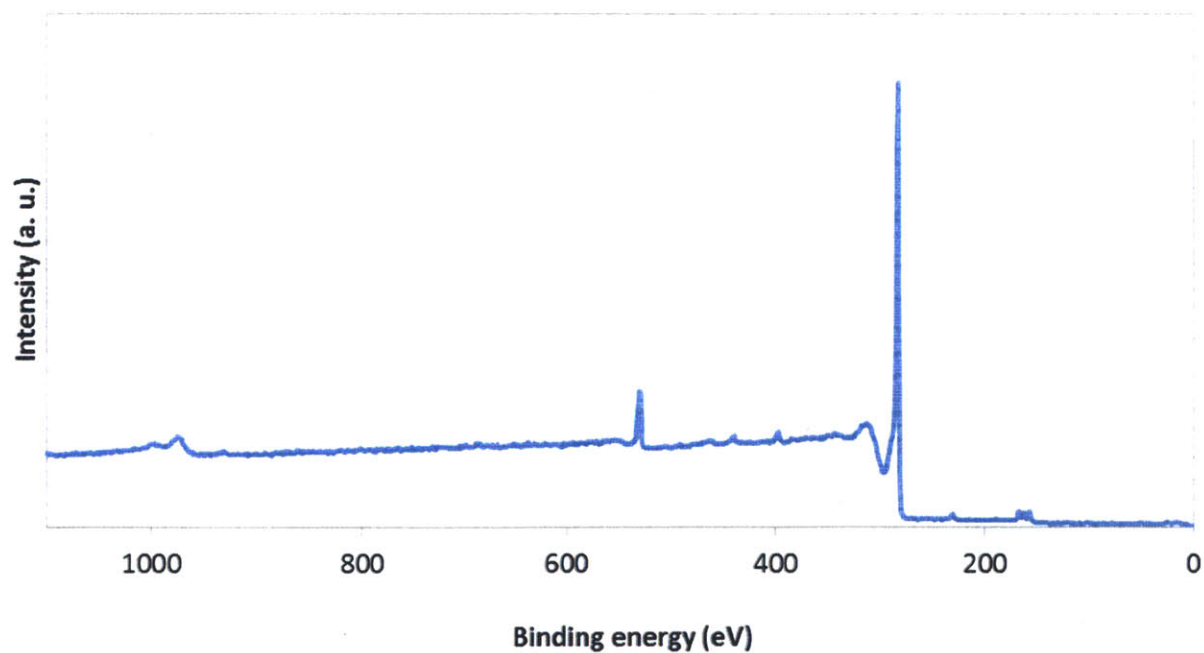


Figure 3.17. XPS analysis of Table 3.1, Entry 1

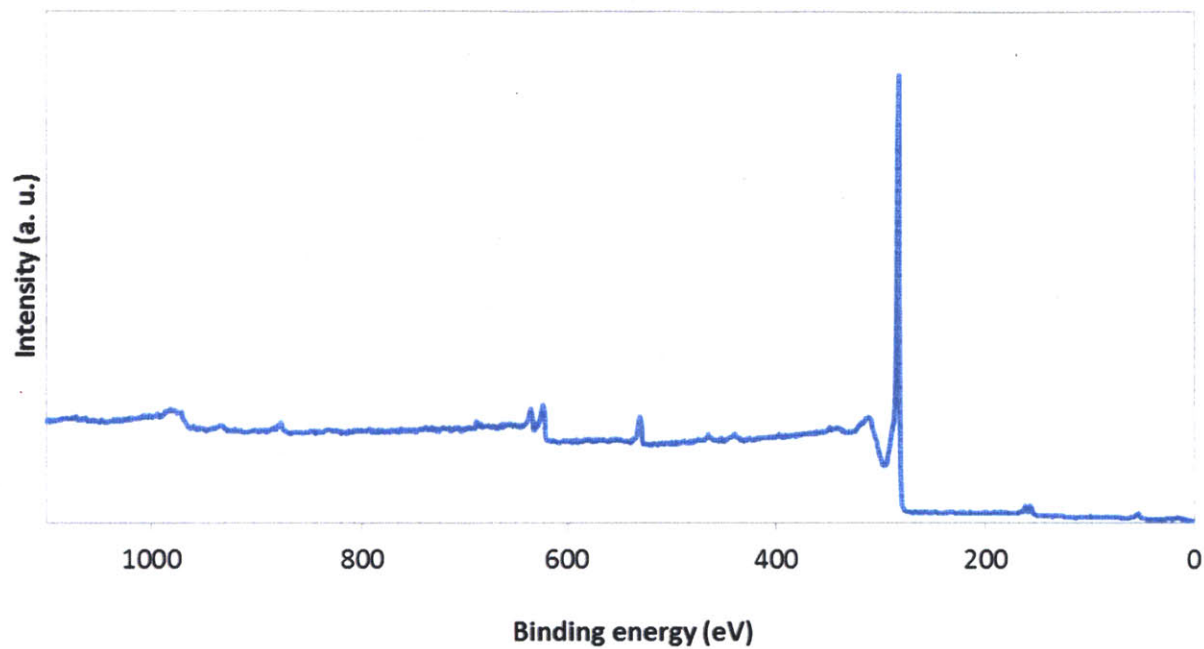


Figure 3.18. XPS analysis of Table 3.1, Entry 2

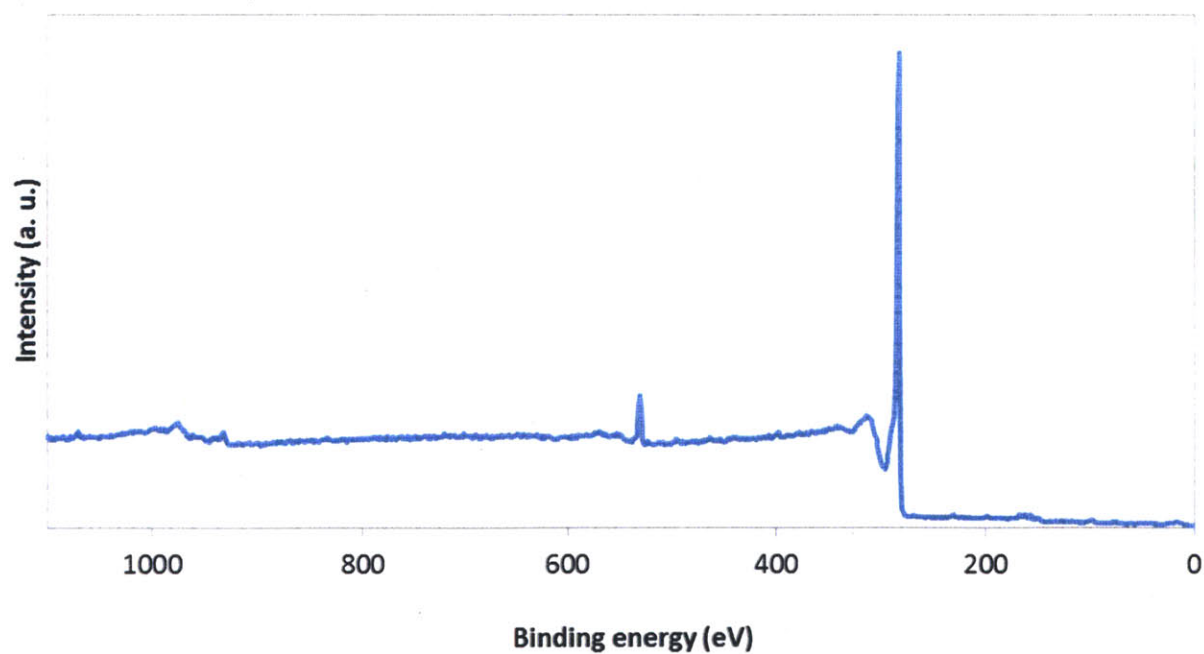


Figure 3.19. XPS analysis of Table 3.1, Entry 3

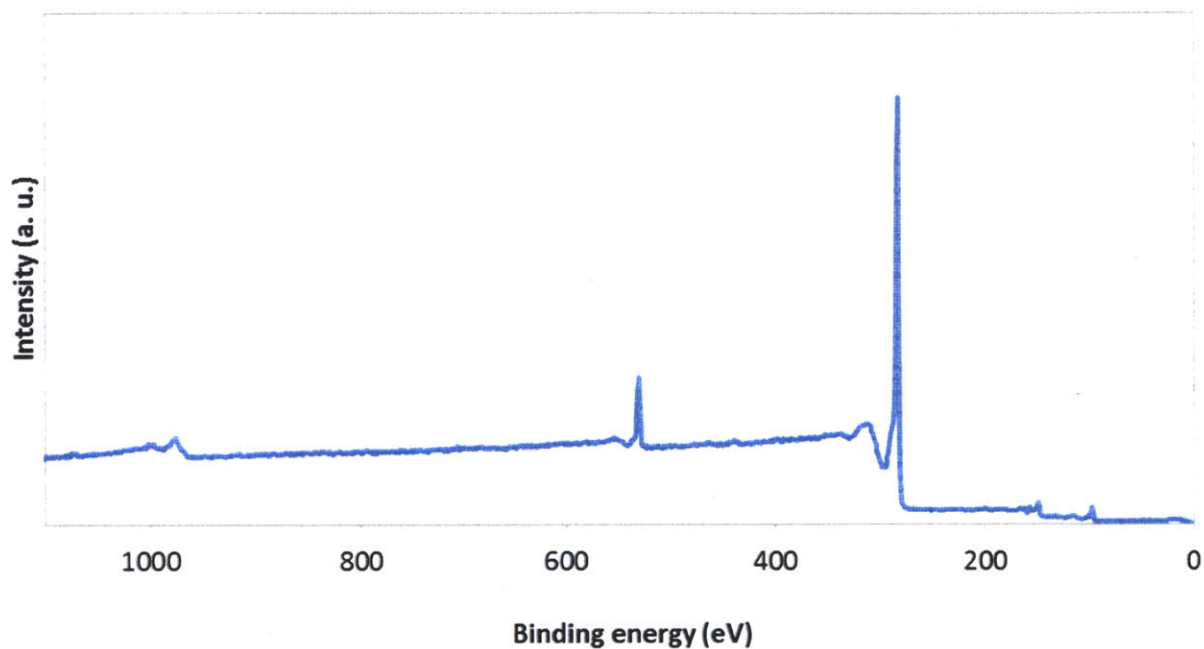


Figure 3.20. XPS analysis of Table 3.1, Entry 4

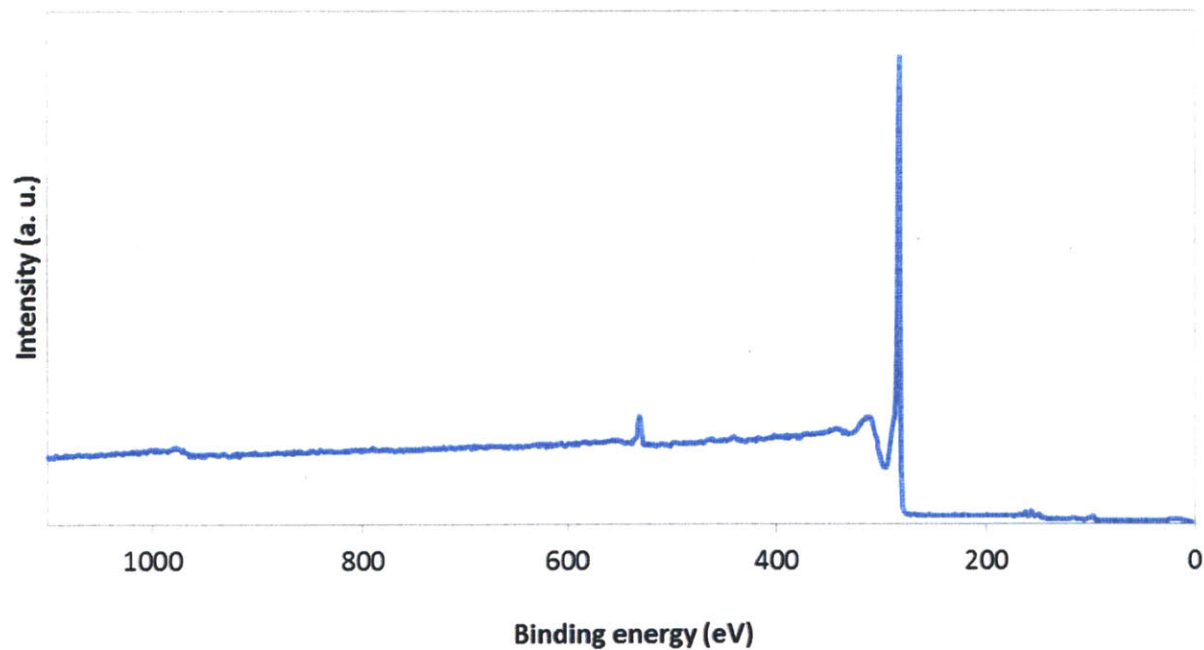


Figure 3.21. XPS analysis of Table 3.1, Entry 5

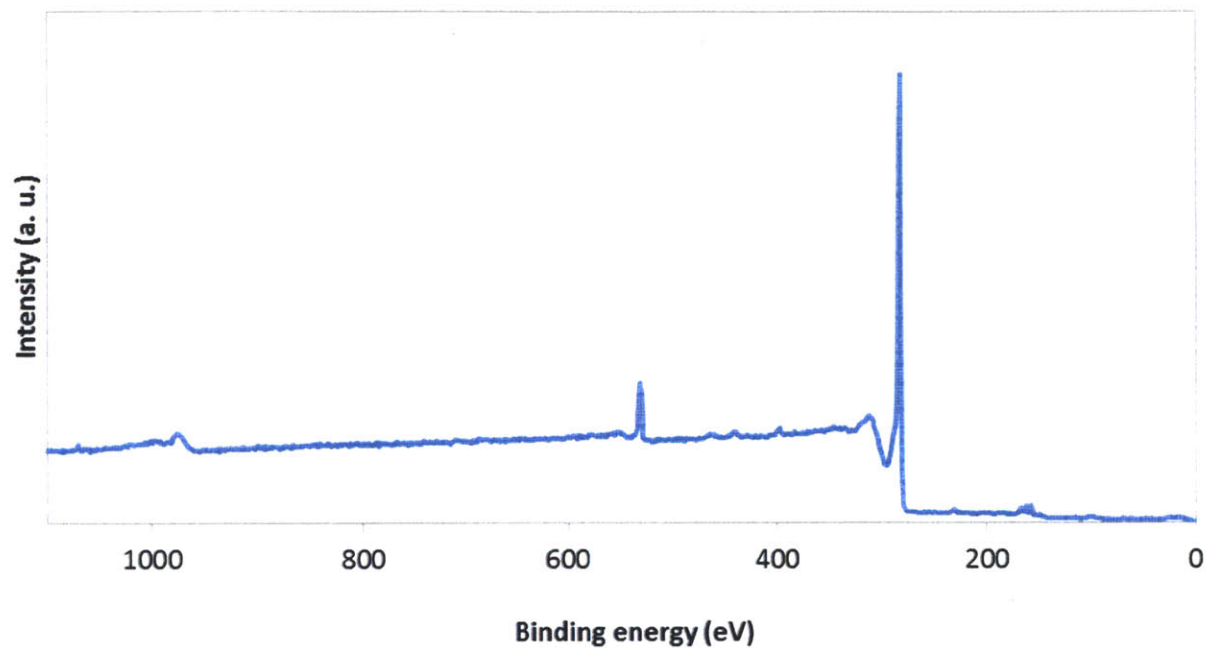


Figure 3.22. XPS analysis of Table 3.1, Entry 6

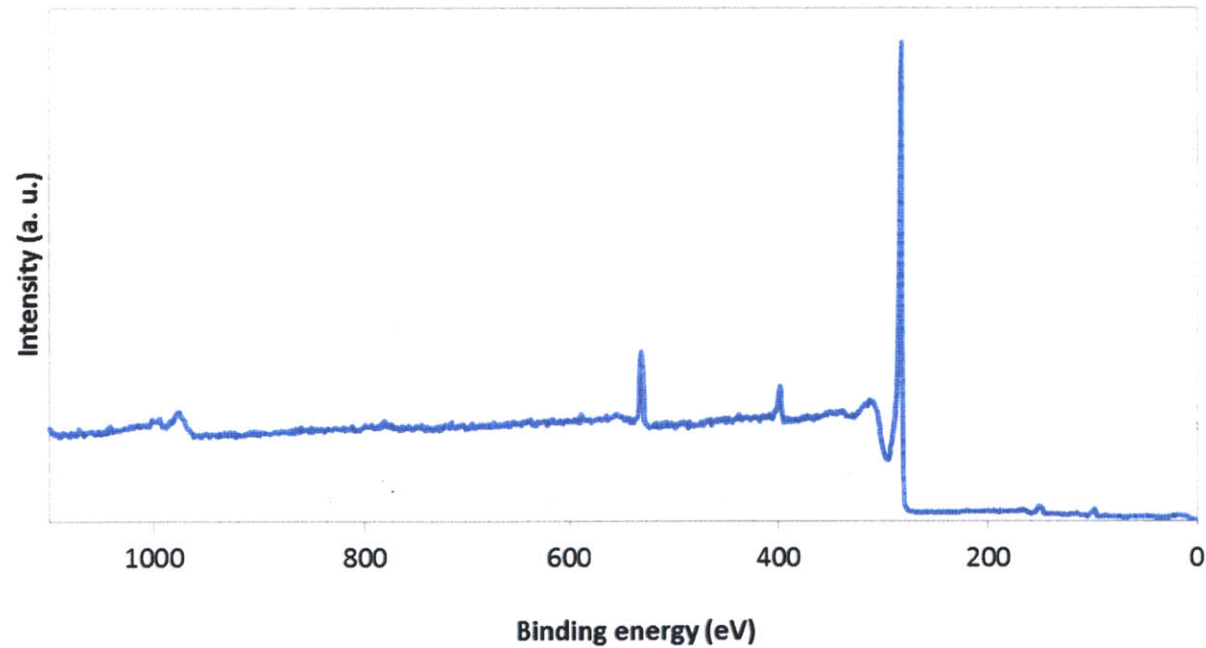


Figure 3.23. XPS analysis of Table 3.1, Entry 7

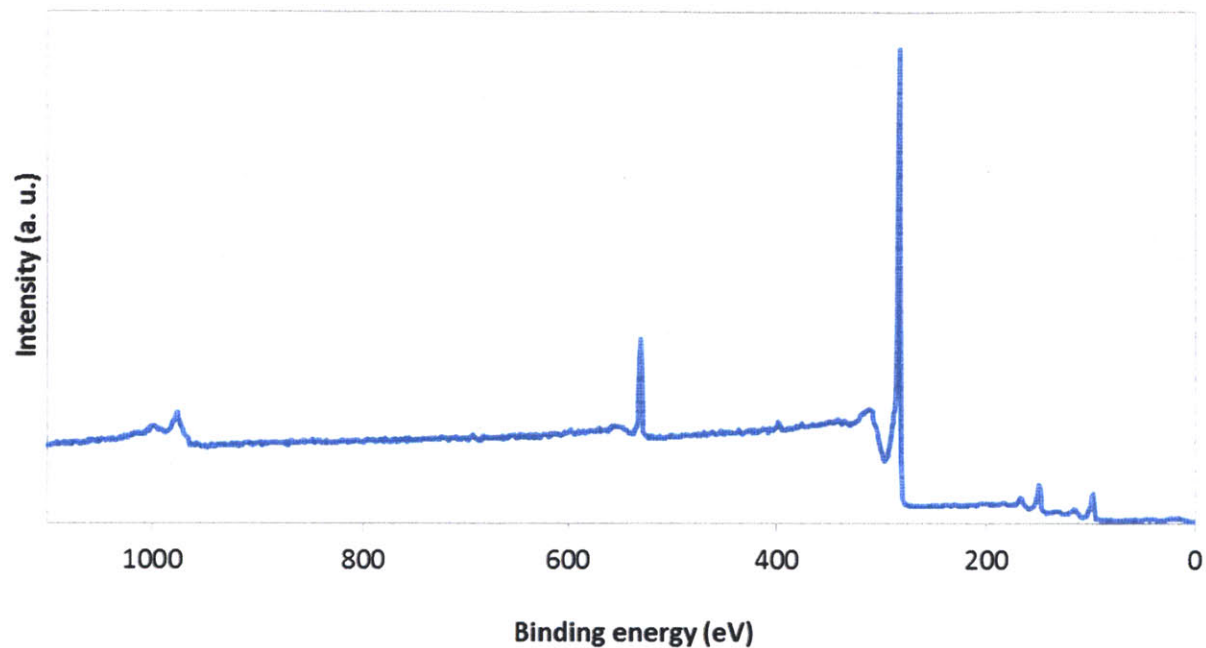


Figure 3.24. XPS analysis of Table 3.3, Entry 1

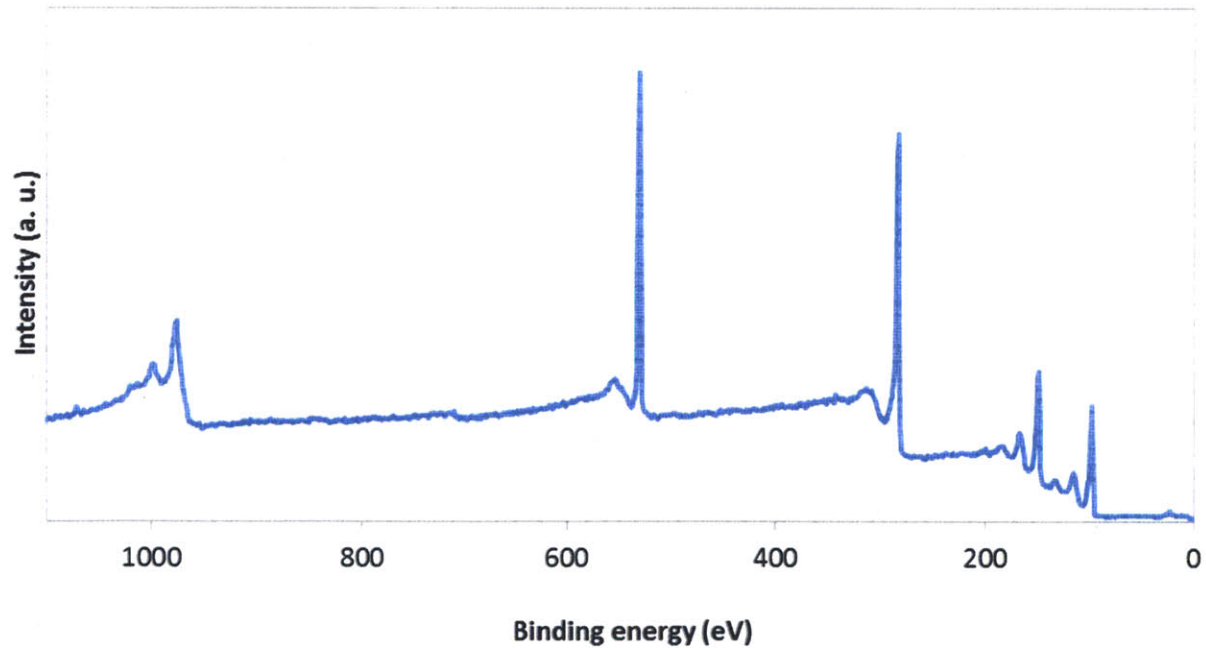


Figure 3.25. XPS analysis of Table 3.3, Entry 2

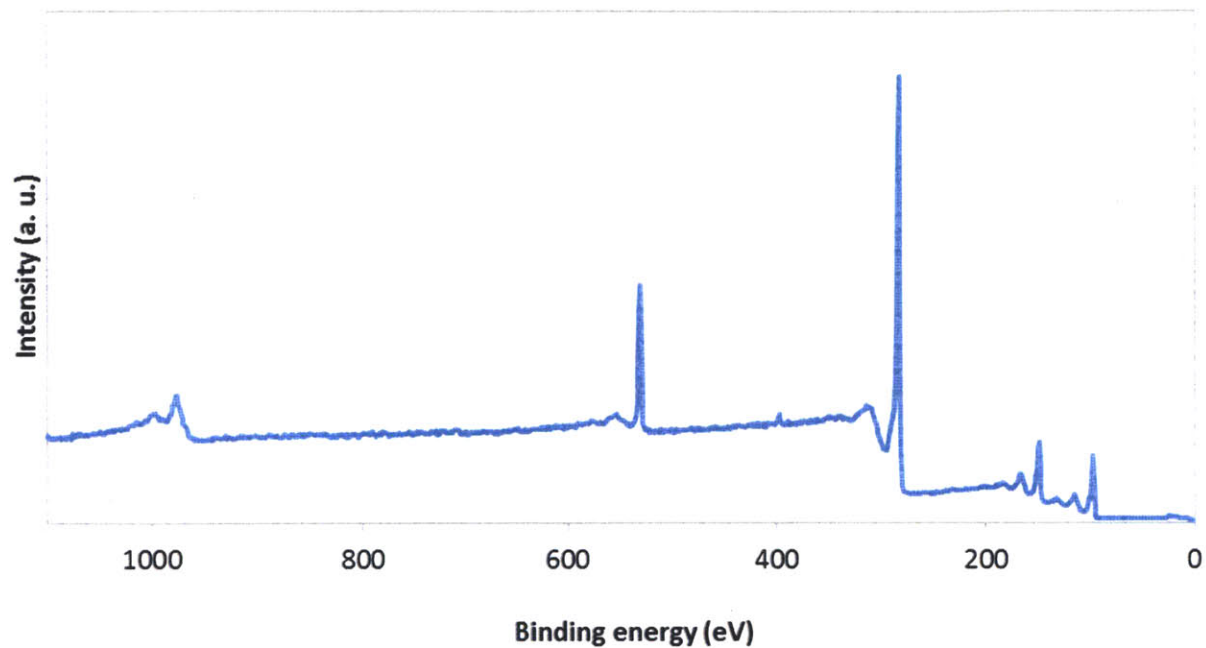


Figure 3.26. XPS analysis of Table 3.3, Entry 3

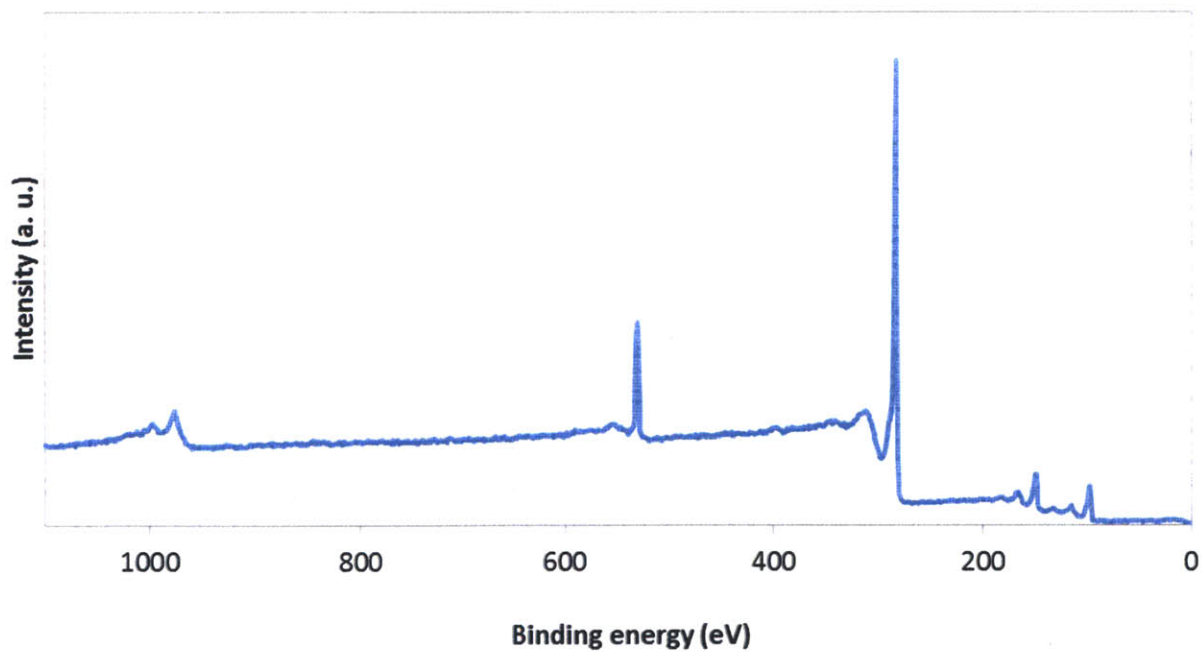


Figure 3.27. XPS analysis of Table 3.3, Entry 4

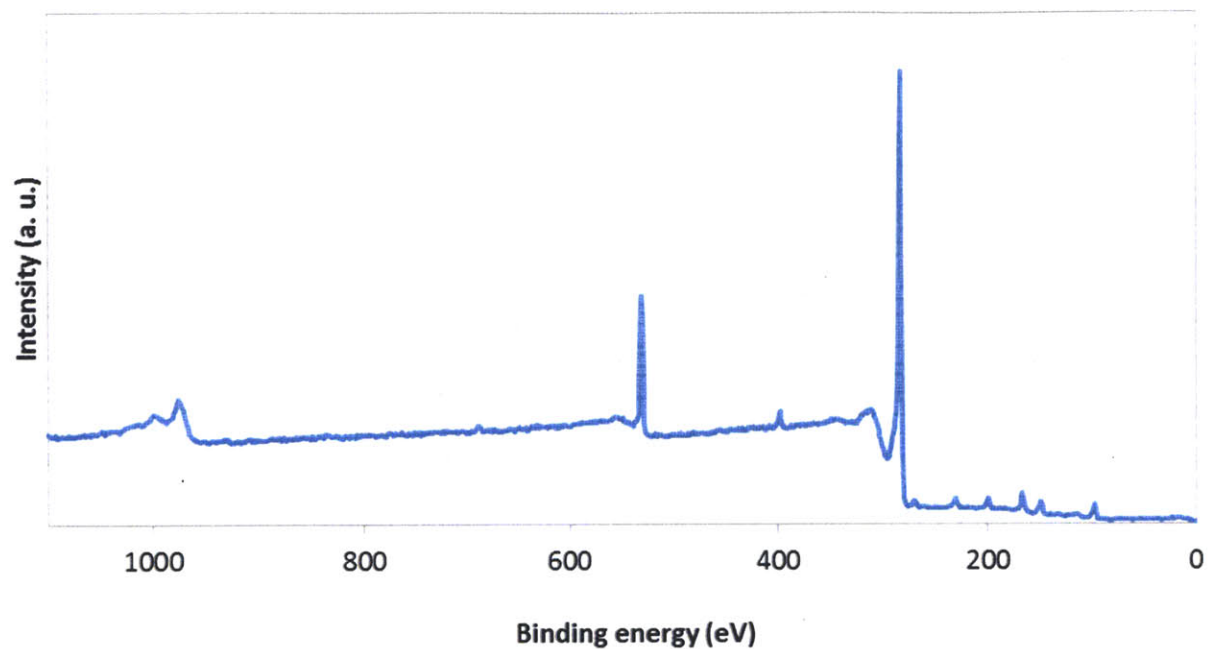


Figure 3.28. XPS analysis of Table 3.3, Entry 5

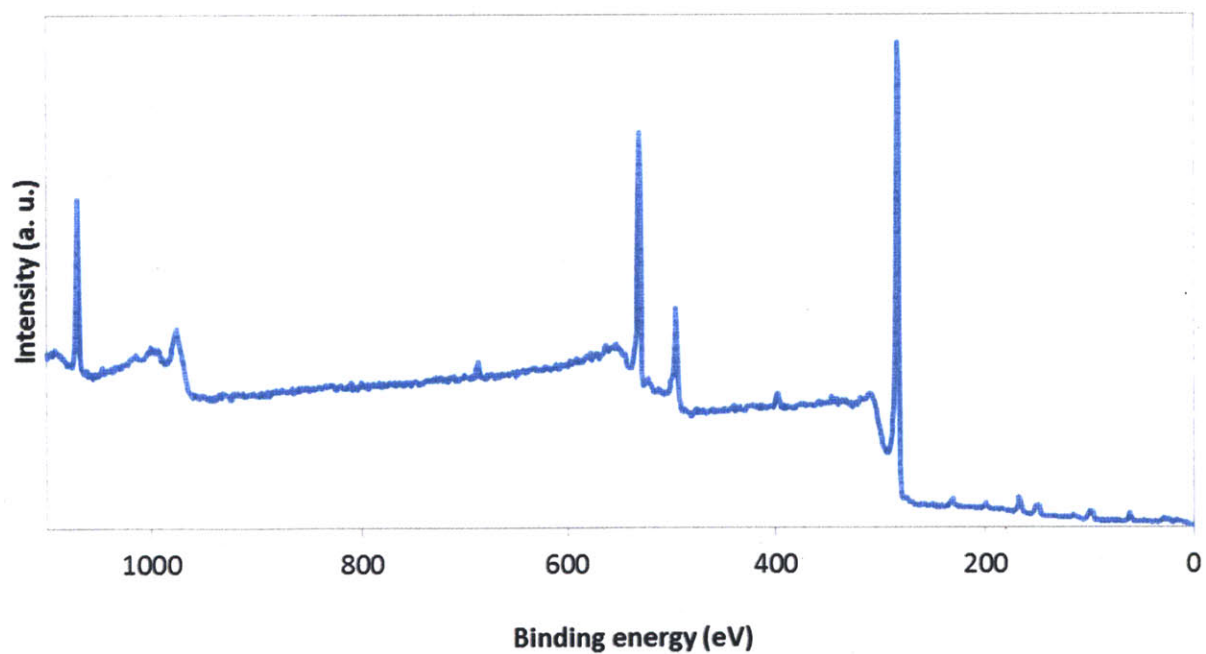


Figure 3.29. XPS analysis of Table 3.3, Entry 6

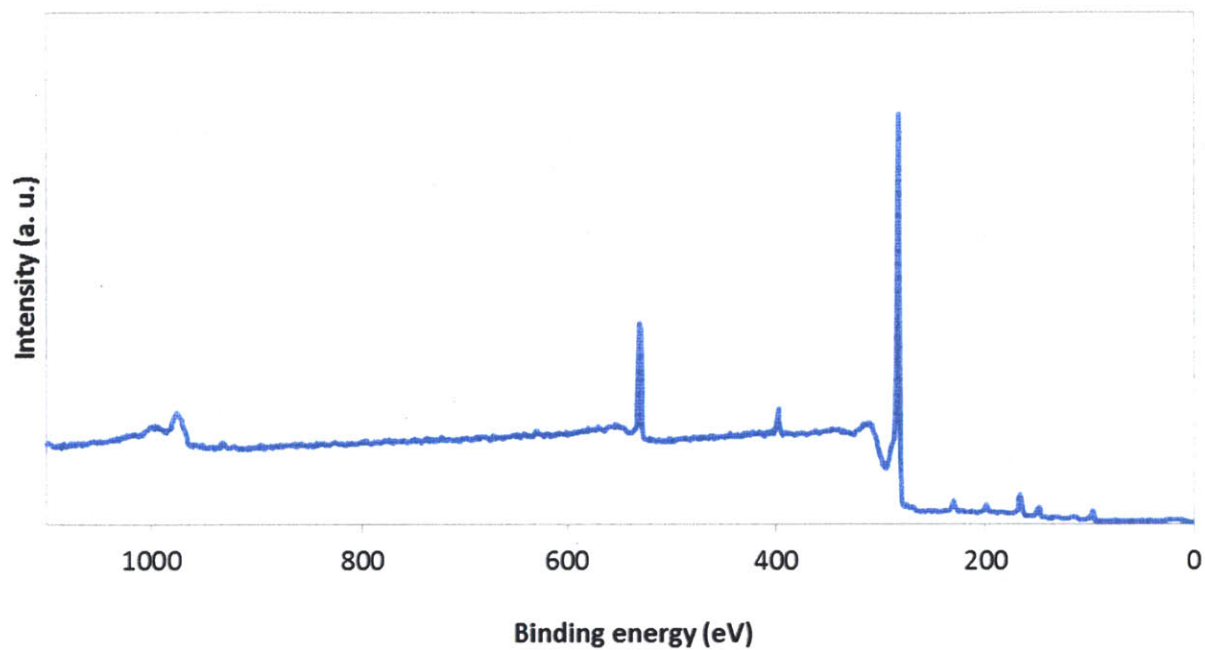


Figure 3.30. XPS analysis of Table 3.3, Entry 7

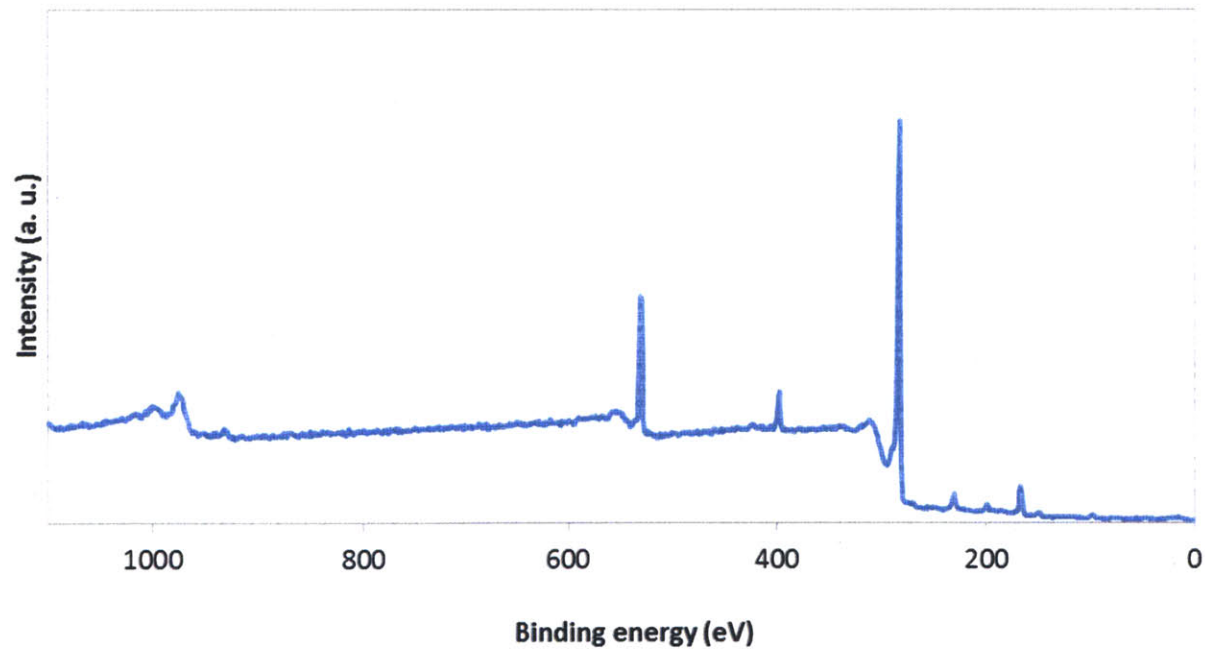


Figure 3.31. XPS analysis of Table 3.3, Entry 8

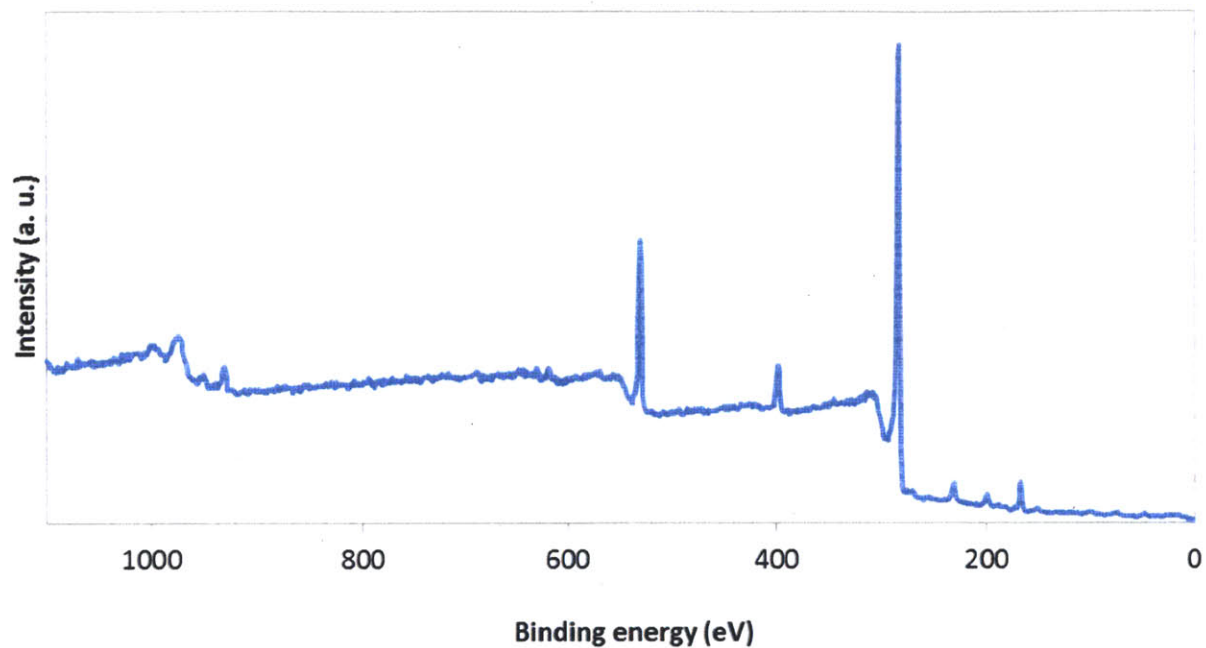


Figure 3.32. XPS analysis of *N*-tosyl aziridine functionalized SWCNTs

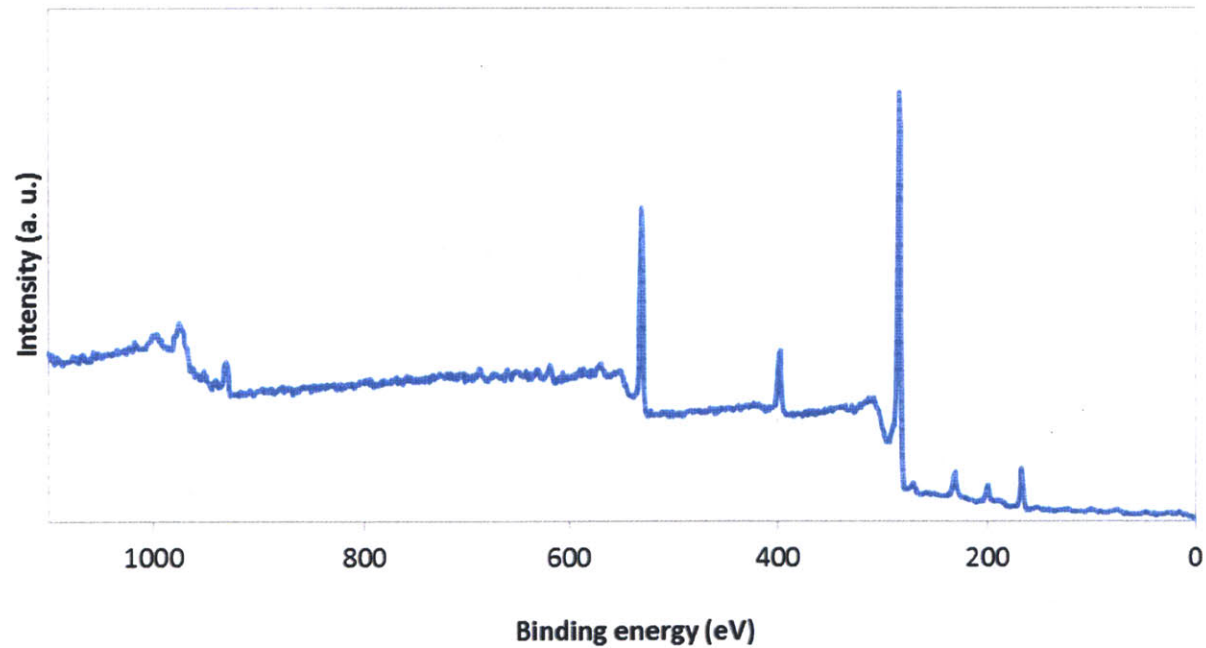


Figure 3.33. XPS analysis of *N*-tosyl aziridine functionalized graphite, procedure 1

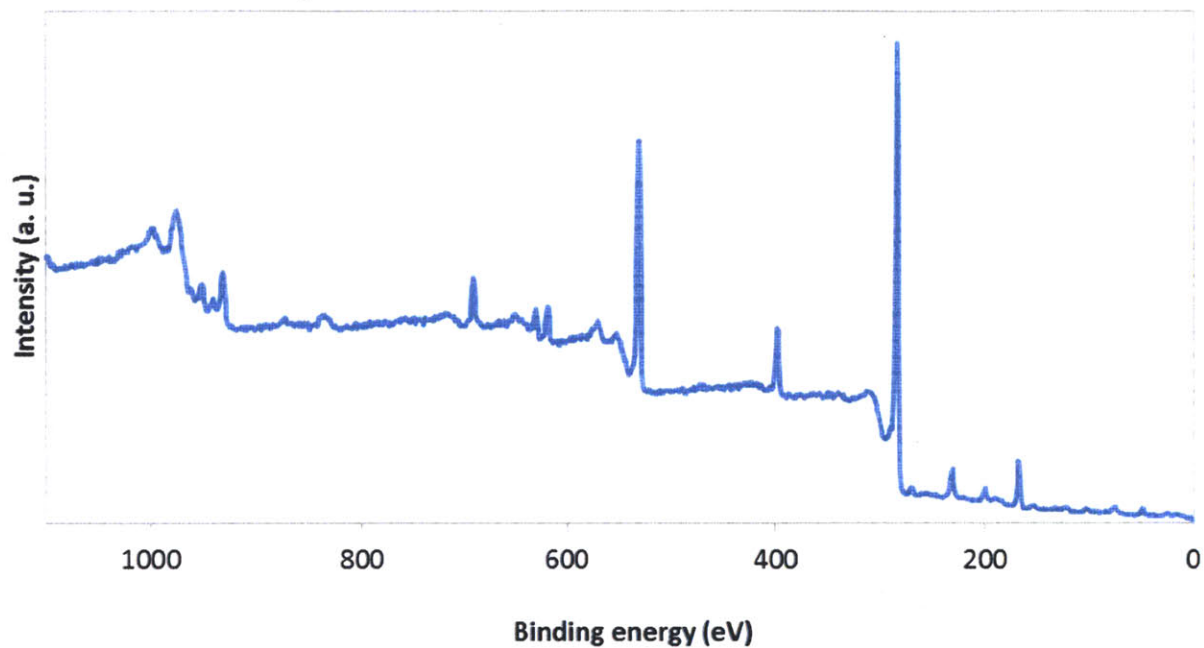


Figure 3.34. XPS analysis of *N*-tosyl aziridine functionalized graphite, procedure 2

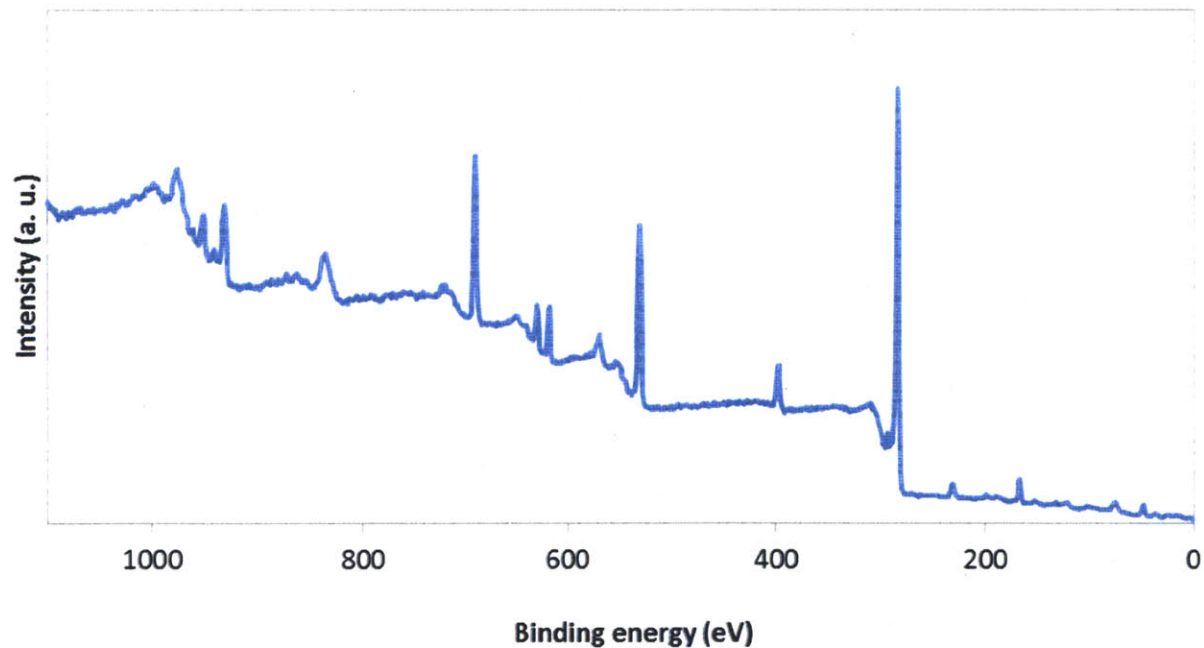


Figure 3.35. XPS analysis of *N*-tosyl aziridine functionalized graphite, procedure 3

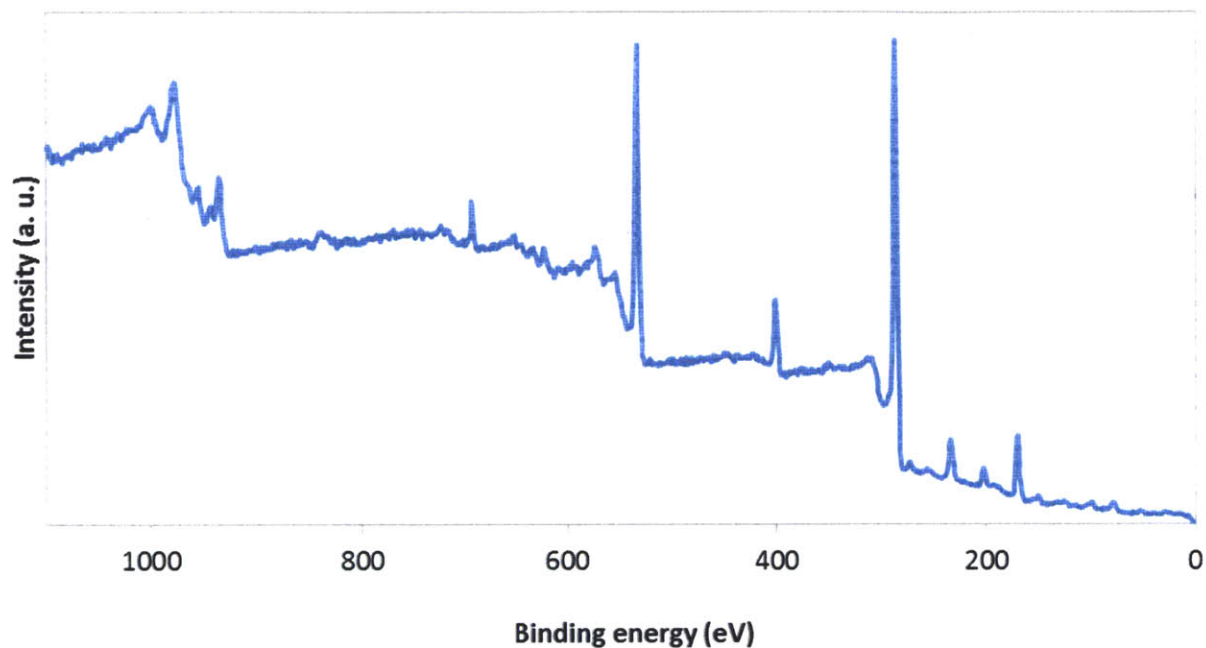


Figure 3.36. XPS analysis of *N*-tosyl aziridine functionalized graphite, procedure 4

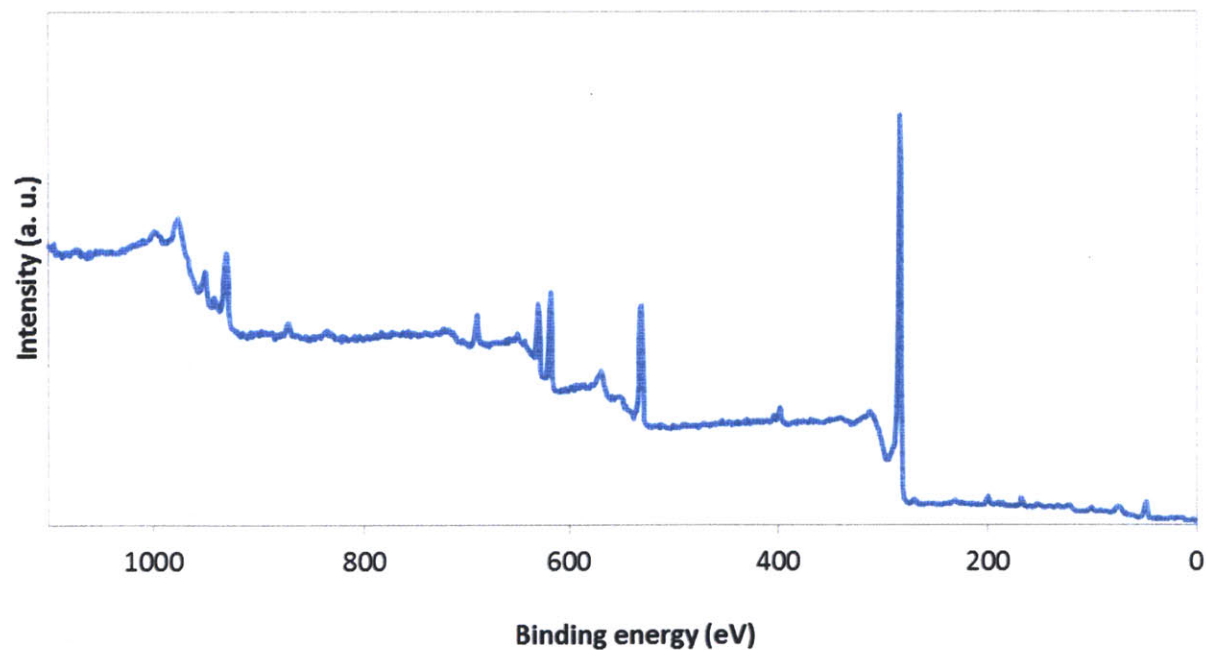


Figure 3.37. XPS analysis of *N*-nosyl aziridine functionalized graphite

3.5. References

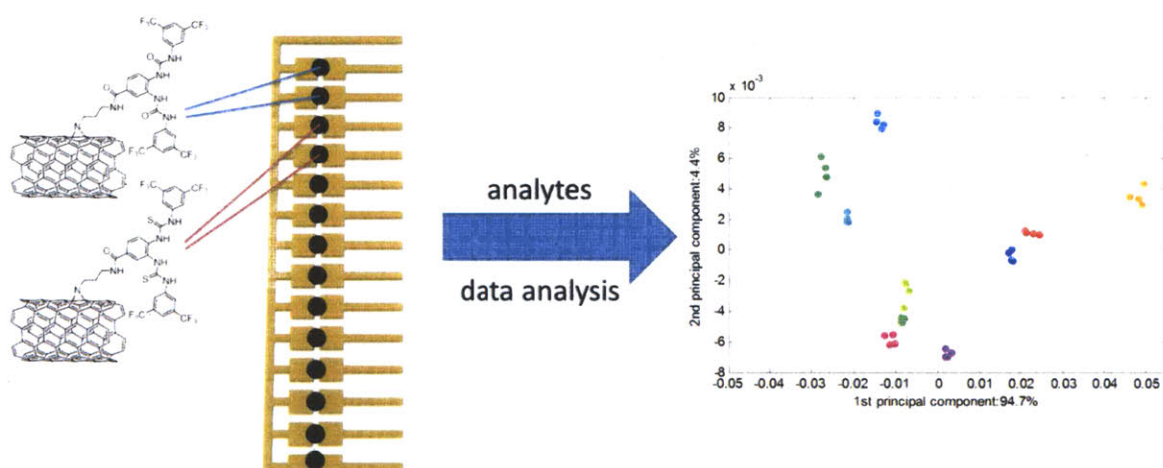
- (1) Iijima, S. *Nature*. **1991**, *354*, 56.
- (2) Tasis, D.; Tagmatarchis, N.; Bianco, A.; Prato, M. *Chem. Rev.* **2006**, *106*, 1105-36.
- (3) Balasubramanian, K.; Burghard, M. *Small*. **2005**, *1*, 180.
- (4) Weizmann, Y.; Lim, J.; Chenoweth, D. M.; Swager, T. M. *Nano Lett.* **2010**, *10*, 2466.
- (5) Lee, S. W.; Kim, B.-S.; Chen, S.; Shao-Horn, Y.; Hammond, P. T. *J. Am. Chem. Soc.* **2009**, *131*, 671.
- (6) Li, H.; Cheng, F.; Duft, A. M.; Adronov, A. *J. Am. Chem. Soc.* **2005**, *127*, 14518.
- (7) Zhang, W.; Swager, T. M. *J. Am. Chem. Soc.* **2007**, *129*, 7714.
- (8) Zhang, W.; Sprafke, J. K.; Ma, M.; Tsui, E. Y.; Sydlik, S. A.; Rutledge, G. C.; Swager, T. M. *J. Am. Chem. Soc.* **2009**, *131*, 8446.
- (9) Gao, C.; He, H.; Zhou, L.; Zheng, X.; Zhang, Y. *Chem. Mater.* **2009**, *21*, 360.
- (10) Schnorr, J. M.; Swager, T. M. *J. Mater. Chem.* **2011**, *21*, 4768.
- (11) Müller, P.; Fruit, C. *Chem. Rev.* **2003**, *103*, 2905.
- (12) Dias, H. V. R.; Lu, H.-L.; Kim, H.-J.; Polach, S. A.; Goh, T. K. H. H.; Browning, R. G.; Lovely, C. J. *Organometallics*. **2002**, *21*, 1466.
- (13) Knight, J. G.; Muldowney, M. P. *Synlett*. **1995**, *1995*, 949.
- (14) Dauban, P.; Sanière, L.; Tarrade, A.; Dodd, R. H. *J. Am. Chem. Soc.* **2001**, *123*, 7707.
- (15) Ando, T.; Minakata, S.; Ryu, I.; Komatsu, M. *Tetrahedron Lett.* **1998**, *39*, 309.
- (16) Vyas, R.; Gao, G.-Y.; Harden, J. D.; Zhang, X. P. *Org. Lett.* **2004**, *6*, 1907.
- (17) Averdung, J.; Luftmann, H.; Mattay, J. *Tetrahedron Lett.* **1995**, *36*, 2957.
- (18) Ulmer, L.; Mattay, J. *Eur.* **2003**, *2003*, 2933.
- (19) Mattay, J.; Averdung, J.; Luftmann, H.; Schlachter, I. *DE 19506230A1*. **1996**.
- (20) Nambo, M.; Segawa, Y.; Itami, K. *J. Am. Chem. Soc.* **2011**, *133*, 2402.

- (21) Bodnar, B. S.; Miller, M. J. *J. Org. Chem.* **2007**, *72*, 3929.
- (22) Minakata, S.; Tsuruoka, R.; Nagamachi, T.; Komatsu, M. *Chem. Commun.* **2008**, 323.
- (23) Dias, H. V. R.; Kim, H.-juhn; Lu, H.-ling; Rajeshwar, K.; Tacconi, N. R. D.; Derecskei-Kovacs, A.; Marynick, D. S. *Organometallics*. **1996**, *15*, 2994.
- (24) Dauban, P.; Dodd, R. H. *Synlett.* **2003**, 1571.
- (25) Kolb, H. C.; Finn, M. G.; Sharpless, K. B. *Angew. Chem. Int. Ed.* **2001**, *40*, 2004.
- (26) Bräse, S.; Gil, C.; Knepper, K.; Zimmermann, V. *Angew. Chem. Int. Ed.* **2005**, *44*, 5188-240.
- (27) Yamada, Y.; Yamamoto, T.; Okawara, M. *Chem. Lett.* **1975**, 361.
- (28) Vyas, R.; Chanda, B. M.; Bedekar, A. V. *Tetrahedron Lett.* **1998**, *39*, 4715.
- (29) Hu, X.; Sun, J.; Wang, H.-G.; Manetsch, R. *J. Am. Chem. Soc.* **2008**, *130*, 13820.
- (30) Knapp, S.; Yu, Y. *Organic letters.* **2007**, *9*, 1359.

Chapter 4

CHAPTER 4

Detecting Explosives with Sensory Arrays of Covalently Functionalized Single-Walled Carbon Nanotubes



Studies in this chapter are in collaboration with Daan van der Zwaag

4.1. Introduction

Carbon Nanotubes (CNTs) are well-suited for amperometric sensing applications as their conductivity can be influenced by their chemical environment.¹ Furthermore, their quasi-one-dimensional structure allows signal amplification based on a molecular wire approach similar to conjugated polymer sensors.² When utilizing networks of CNTs instead of single CNTs in a sensor, changes to the morphology of the network, caused, for example, by swelling with an analyte, can be an additional source of a sensing response. Depending on the electrical resistance of the individual CNTs compared to the CNT-CNT junctions either effect can dominate.³

One important group of targets for sensors are explosive compounds. Due to the simple manufacturing and potentially large damage caused by explosive-based weapons, terrorism using this type of weapons has been increasing in recent years.⁴ It would, therefore, be desirable to improve the sensing capabilities in this area in order to detect low volatility explosives such as 2,4,6-trinitrotoluene (TNT), tetranitro-triazacyclohexane (RDX), or pentaerythritol tetranitrate (PETN) (Figure 4.1). Several instrumental systems are aiming at this goal including ion mobility spectrometry (IMS), mass spectrometry (MS), and gas chromatography (GC), as well as the Fido system (FLIR systems) that is based on research previously conducted in our laboratory.⁵

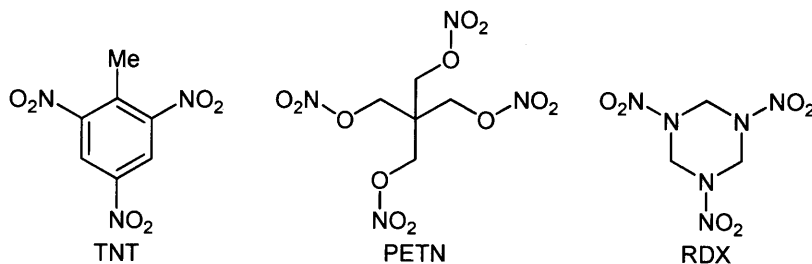


Figure 4.1. Common explosives TNT, PETN, RDX.

In addition to these platforms, it is desirable to develop amperometric sensors based on CNTs for the detection of explosive compounds. In contrast to the aforementioned established systems, this type of sensor benefits from its great simplicity. In principal, a sensor prototype can consist only of a power source and an ammeter connected to a network of functionalized CNTs *via* electrodes (Figure 4.2). This setup potentially facilitates manufacturing and miniaturization and reduces manufacturing costs all of which are advantageous for applications. As initial sensing targets, we chose nitromethane, which has been used in the 1995 Oklahoma City bombing,⁶ and cyclohexanone (Figure 4.3).

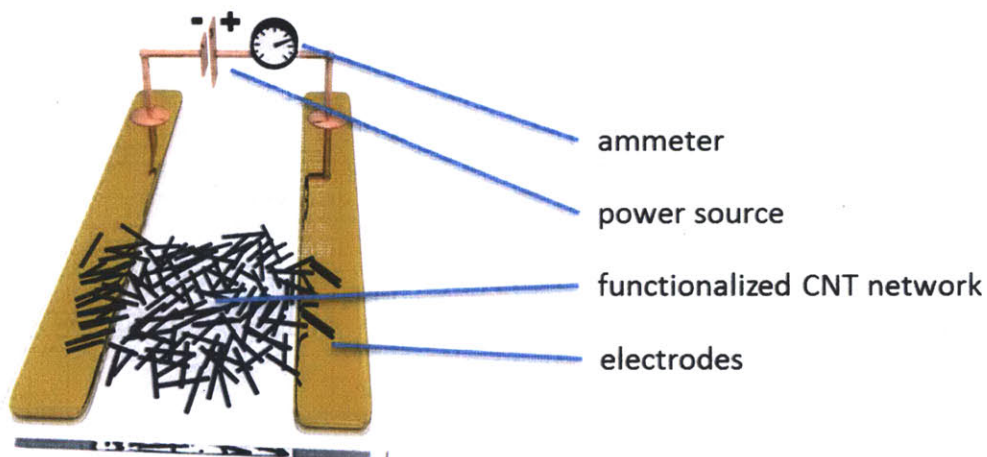


Figure 4.2. Schematic representation of an amperometric CNT-based sensor



Figure 4.3. Sensing targets nitromethane (1) and cyclohexanone (2).

While cyclohexanone itself is not explosive, it is commonly used in the purification of RDX and is therefore found in the headspace of RDX-based explosives.⁷ With a vapor pressure of 4470 ppm at room temperature, cyclohexanone is approximately nine orders of magnitude more volatile than RDX itself, rendering it an attractive substitute for the actual explosive as a sensing target.^{4,8}

When developing a sensor, several parameters are of interest.⁴ Among these are the sensitivity (i.e., the slope of a calibration curve), the limit of detection, and the selectivity of the sensor (i.e., the response to the desired analyte compared to the response to interferents). Furthermore, a high reproducibility of the sensing response to a certain analyte concentration is desired, for repeated measurements using the same device and across different devices. Lastly, a good stability of the sensor over time is an advantage for practical applications.

These parameters can be influenced by varying different aspects of the sensor. The choice of receptor or selector that interacts with the analyte can affect the sensitivity and selectivity. Furthermore, the material to which the receptor is attached, as well as the type of attachment, influences the performance of the sensor. Among CNT-based sensors, single- or multi-walled CNTs (SWCNTs and MWCNTs, respectively) can be chosen for this purpose and covalent or non-covalent attachment methods can be utilized. Lastly, the fabrication of a sensor can influence the sensing performance from sensitivity to reproducibility between devices.

For this project, we chose to use covalently functionalized SWCNTs as the sensing platform. Covalent functionalization reduces the conductivity of SWCNTs. Therefore, non-covalent functionalization of SWCNTs or covalent functionalization of MWCNTs are more common strategies employed for the fabrication of selective sensors⁹⁻¹¹ than covalent functionalization of

SWCNTs.^{12,13} Nevertheless, we hypothesized that covalent functionalization of SWCNTs could be advantageous for several reasons. First, covalent attachment of the receptor excludes the possibility of phase separation between receptor and CNTs and should thus lead to a higher stability of the devices compared to sensors based on non-covalently modified CNTs. Second, the decrease in the conductivity of the CNTs is not necessarily a disadvantage. In general, the response of an amperometric sensor is dominated by changes of the component with the highest resistance. A sensing mechanisms where the analyte alters the resistance of individual CNTs benefits from a high initial resistance of the CNTs, while a sensing mechanisms where the analyte affects resistance of the sensor at CNT-CNT junctions (or CNT-electrode junctions) benefits from highly conductive CNTs.³ As it is not trivial to predict the sensing mechanism, we based our decision for covalently functionalized SWCNTs on the expected higher stability of the sensors compared to non-covalently functionalized CNTs.

We chose thiourea and squaramide units as receptors (Figure 4.4). Both types of structures have been used in anion sensing (e.g., detection of phosphates, carboxylates, or nitrates) and we expected them to interact with the nitro and carbonyl groups of our target analytes.^{14,15}

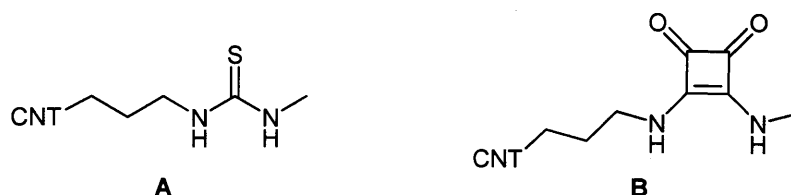


Figure 4.4. Thiourea (A) and Squaramide (B) based receptors attached to CNTs

Due to the different geometry of the two structures we expected them to show different sensitivities and selectivities in a sensor. Besides the geometry of the receptor, the receptor-analyte affinity is influenced by the acidity of the -NH protons where a higher acidity typically

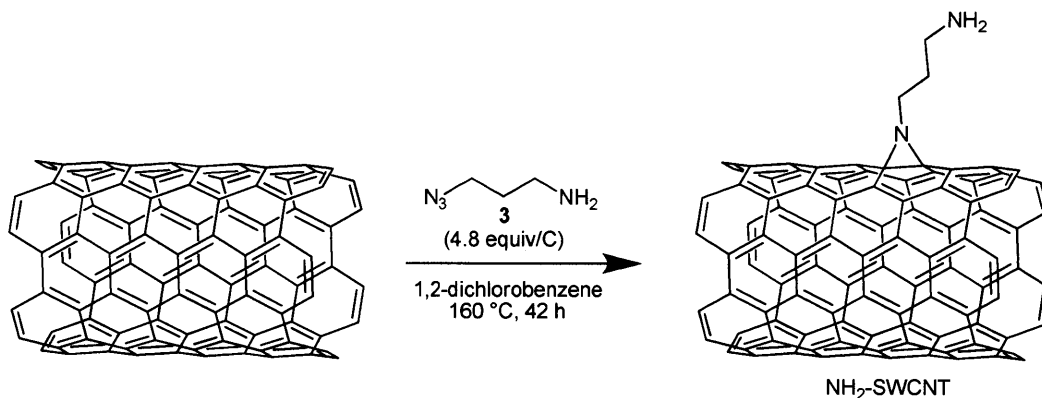
leads to stronger binding.¹⁶ We, therefore, tested different substituents on the squaramide and thiourea units to determine their influence on the sensing response.

4.2. Results and Discussion

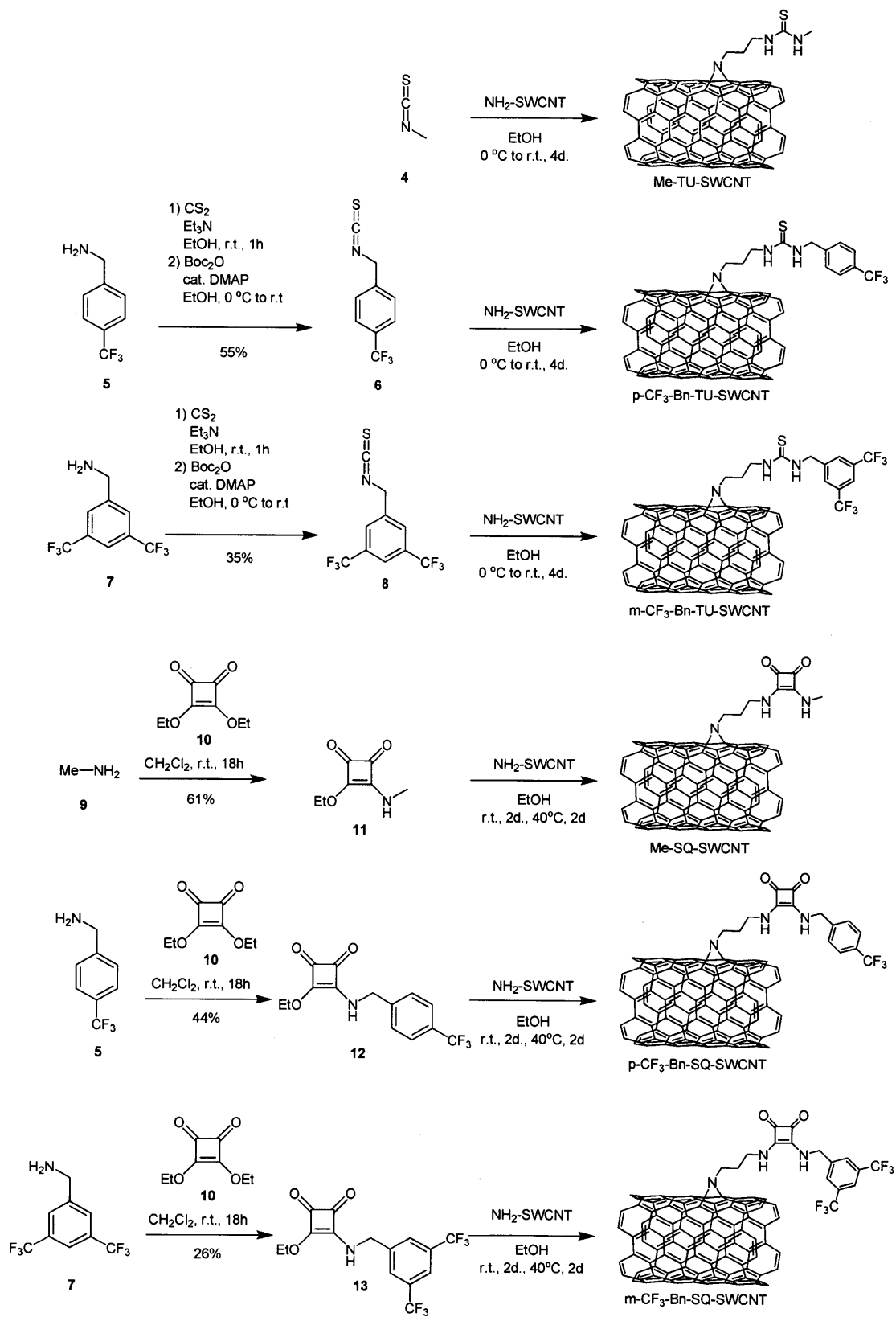
4.2.1. Functionalization of SWCNT with Thiourea and Squaramide Receptors

We installed thiourea and squaramide receptors on SWCNTs using a two-step approach. Initially, SWCNTs were functionalized with amine groups by reaction with 3-azidopropan-1-amine **3** (Scheme 4.1).¹⁷ The product was analyzed by X-ray photoelectron spectroscopy (XPS), showing a functional group density of 1 per 12 CNT carbon atoms (based on N 1s vs. C 1s signal).

Scheme 4.1. Installation of amino groups on SWCNTs.



In the second step, the obtained NH₂-SWCNTs were reacted with either an isothiocyanate reagent to obtain thiourea-functionalized SWCNTs or with the mono-ester of a squaramide for squaramide-functionalized SWCNTs (Scheme 4.2). The respective amines **5** and **7** gave the required isothiocyanates **6** and **8** *via* the dithiocarbamates in 55% and 35% yield, respectively.¹⁸ Squaramide reagents **11-13** were obtained in 26-61% yield by reacting amines **5**, **7**, and **9** with diethyl squarate **10**.¹⁹

Scheme 4.2. Functionalization of SWCNTs with thiourea and squaramide receptors.

Analysis of modified SWCNTs by XPS showed an increase in the O 1s signal in all samples (due to defect sites, pristine CNTs contain small amounts of oxygen by XPS as well), as well as presence of the expected F 1s signal for samples containing trifluoromethyl groups, and the presence of the sulfur signals for SWCNTs containing thiourea moieties (Figure 4.5).

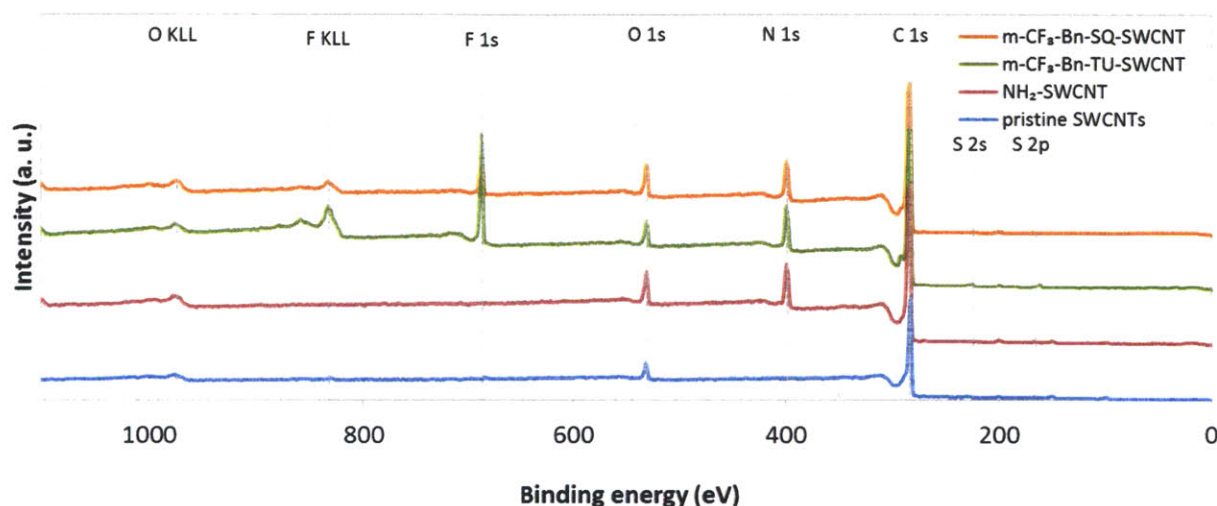


Figure 4.5. XPS analysis of pristine SWCNTs (blue trace), NH₂-SWCNT (red trace), m-CF₃-Bn-TU-SWCNT (green trace), and m-CF₃-Bn-SQ-SWCNT (orange trace).

We calculated functional group densities based on the F 1s and C 1s signals (for fluorine containing samples) or the O 1s and C 1s signals (for fluorine free samples). The functionalization of NH₂-SWCNT with thioureas yielded higher receptor densities of ca. 1 per 50 CNT carbon atoms compared to 1 per 100-150 CNT carbon atoms for the squaramides (Table 4.1). We attribute this difference in the degree of functionalization to the higher reactivity of isothiocyanates (**4**, **6**, **8**) compared to the squaramide monoesters (**11-13**).

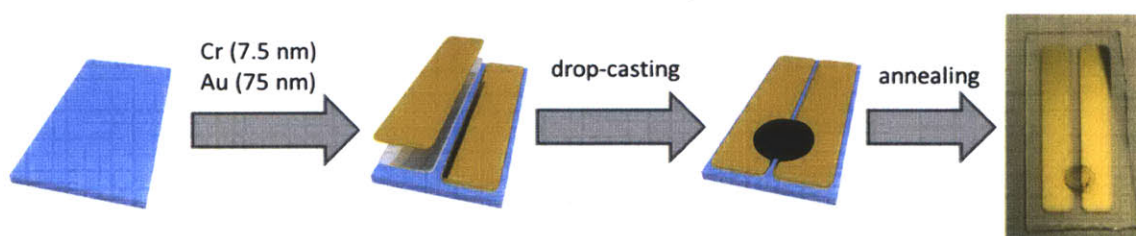
Table 4.1. Functional group densities for receptor-carrying SWCNTs

Functionalizes SWCNT	Functional group density ^a
NH ₂ -SWCNT	12 ^b
Me-TU-SWCNT	58 ^c
p-CF ₃ -Bn-TU-SWCNT	45 ^c
m-CF ₃ -Bn-TU-SWCNT	45 ^c
Me-SQ-SWCNT	108 ^b
p-CF ₃ -Bn-SQ-SWCNT	152 ^c
m-CF ₃ -Bn-SQ-SWCNT	131 ^c

^aSWCNT carbon atoms per functional group ^bbased on O 1s and C 1s signals in the product compared to NH₂-SWCNT; ^cbased on F 1s and C 1s signals

4.2.2. Sensor Fabrication and Evaluation

After functionalizing SWCNTs with thiourea and squaramide receptors, we tested the performance of the samples as sensors. We prepared devices by: (i) drop-casting a suspension of SWCNTs between gold electrodes on the surface of a glass slide, and (ii) annealing for 3 minutes at 100 °C under vacuum (Figure 4.6).

**Figure 4.6.** Fabrication of sensors.

Devices were analyzed by optical microscopy and scanning electron microscopy (SEM). Optical microscopy showed an inhomogeneous structure of the SWCNT film containing large aggregates

of CNTs (Figure 4.7a). SEM confirmed this film structure at low magnification (Figure 4.7b) and showed SWCNT bundles at higher magnification (Figure 4.7c-f).

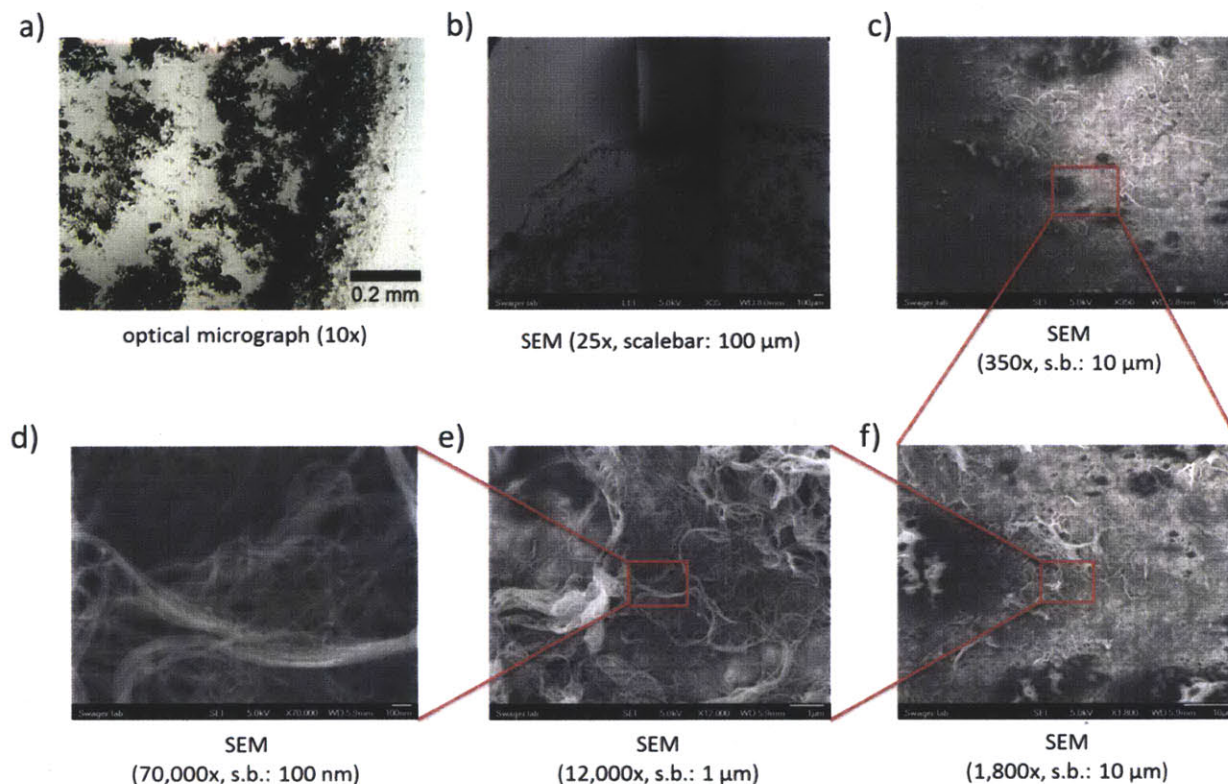


Figure 4.7. Micrographs of SWCNT devices. (a) Optical micrograph; (b)-(f) scanning electron micrographs at different magnifications.

During a measurement, a potential of 0.1 V was applied to the electrodes and the current through the SWCNT network was recorded. Before being able to evaluate the different devices, we had to establish a sensing setup that limited environmental effects and allowed reproducible measurements. Initially, we performed test measurements in a simple glovebox in the absence of an analyte, however, a significant baseline drift was observed (Figure 4.8).

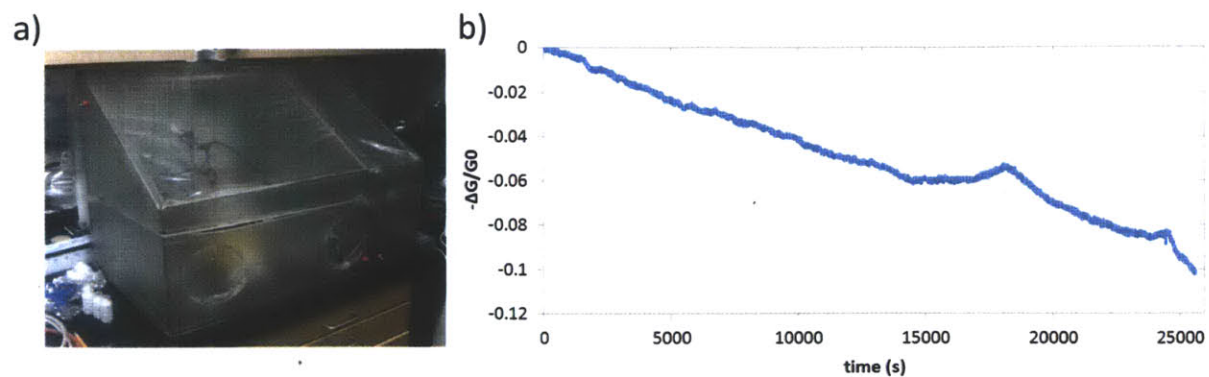


Figure 4.8. Glovebox for initial sensing measurements (a) photograph, (b) baseline drift over 7 h.

In order to improve the baseline stability during the measurements, we developed a Teflon enclosure for the sensing devices in collaboration with Joseph J. Walsh. The enclosure was equipped with electrodes to contact the devices as well as a gas inlet and outlet that could be connected to a nitrogen supply or gas generation system (Figure 4.9). When the enclosure was connected to a nitrogen supply, baseline drift was reduced from 1.6% to 0.3% over 1 h (Figure 4.10). Furthermore, the level of noise was reduced.

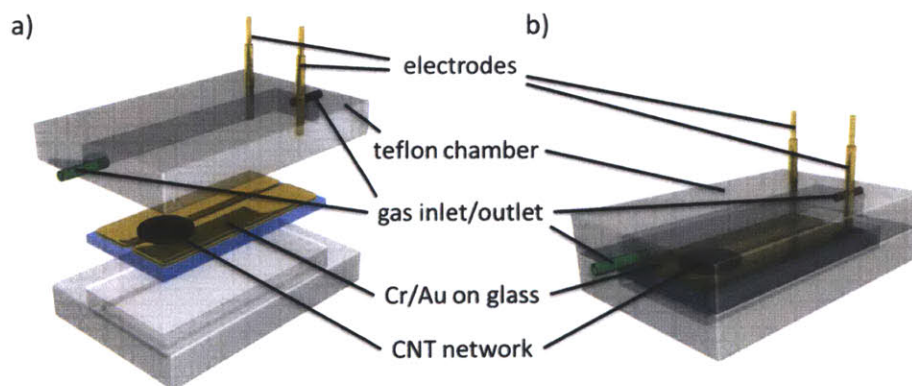


Figure 4.9. Gas flow chamber for sensing measurements.

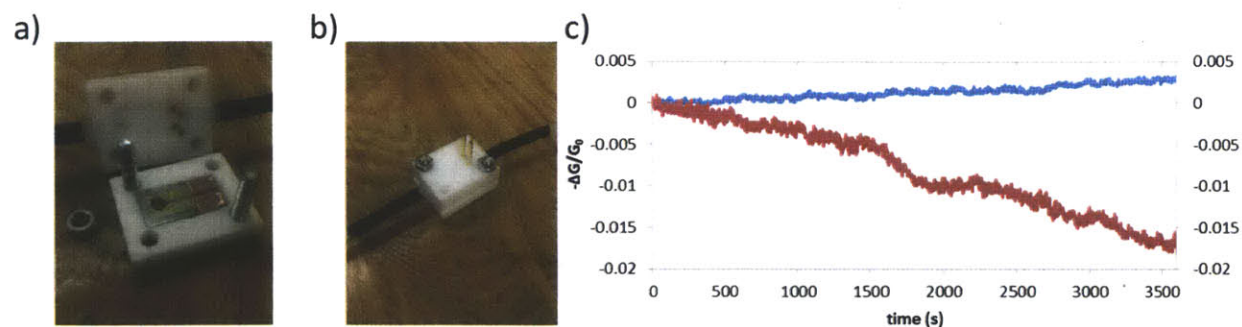


Figure 4.10. Baseline drift using a Teflon device enclosure. Photograph of (a) open and (b) closed enclosure; (c) baseline drift with enclosure connected to a nitrogen supply (blue trace) compared to baseline drift with glovebox depicted in Figure 4.8 (red trace).

After establishing a reliable sensing setup, we tested the response to cyclohexanone (**2**) of four types of sensing materials: thiourea, squaramide, and amine-modified SWCNT, and pristine SWCNTs. We exposed devices three times for 30 s to 57 ppm **2** (1.3% of room temperature equilibrium vapor concentration - supplied to devices using a gas generation system, see Experimental Section) and monitored the corresponding change in current ($-\Delta G/G_0$) using a potentiostat (Figure 4.11).

Pristine and amine-functionalized SWCNTs both showed a weak, albeit noticeable response, of 0.05-0.1% change in current to **2** (Figure 4.11a-b). The response of Me-TU-SWCNT and p-CF₃-Bn-TU-SWCNT was slightly higher (0.1-0.15%) with a lower level of noise (Figure 4.11c-d). Devices containing m-CF₃-Bn-TU-SWCNT showed the best response of 0.9% change in current (Figure 4.11e). Squaramide-functionalized SWCNTs on the other hand did not lead to a large change in current upon exposure to 57 ppm **2** (Figure 4.11f-h).

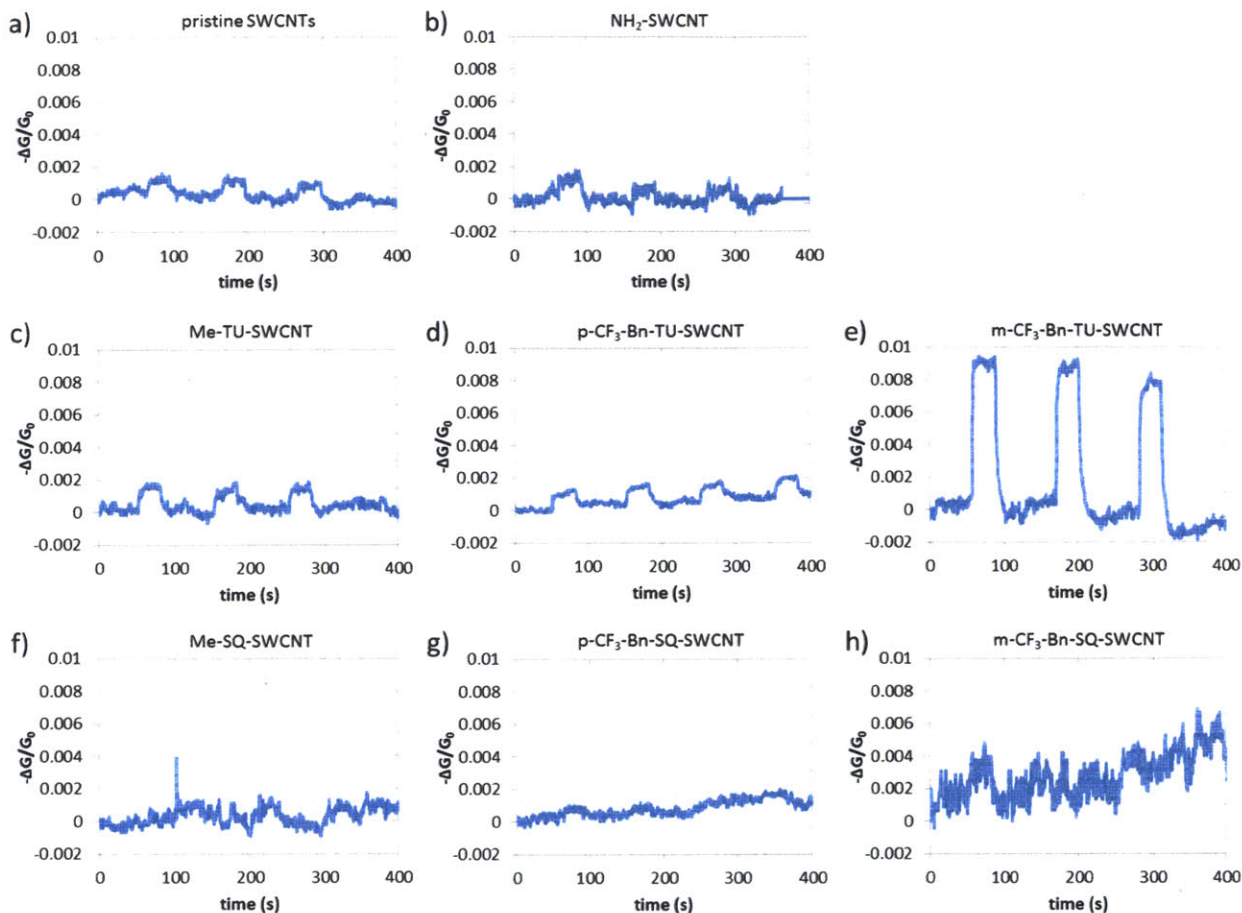


Figure 4.11. Sensing responses of devices with different types of SWCNTs to 57 ppm **2**, applied for 30 s starting at 50, 150, and 250 s.

Encouraged by the initial results with m-CF₃-Bn-TU-SWCNT, we investigated the reproducibility of the sensing response between devices containing this type of functionalized SWCNTs, their tolerance for repeated measurements, and their stability over time. We fabricated three devices and measured their response to 57 ppm and 283 ppm cyclohexanone. The devices showed good reproducibility for repeated measurements and across devices (Figure 4.12a). To test the device stability over time, the measurement with one device was repeated after storing it for 16 and 236 days under ambient conditions without any precautions (Figure 4.12b-d). After 16 days, the device still showed a reproducible response to **2**, albeit with a slightly reduced

sensitivity. The sensitivity was further reduced after 236 days, but a good response to 57 ppm and 283 ppm **2** could still be obtained with a very good reproducibility between subsequent measurements.

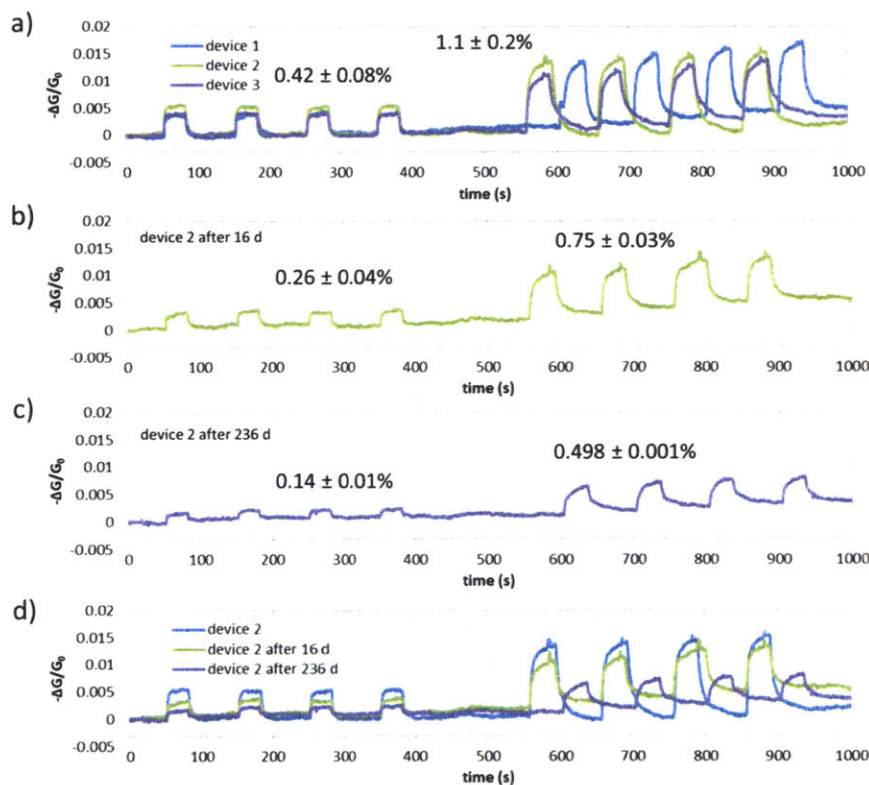


Figure 4.12. Sensing responses of devices fabricated using m-CF₃-Bn-TU-SWCNT. (a) response of three different devices exposed to 57 ppm cyclohexanone for 30 s every 100 s starting at 50 s as well as 283 ppm cyclohexanone for 30 s every 100 s starting at 600 s (device 1) or 550 s (devices 2 and 3); averages and errors are based on the four measurements at each concentration and across all devices; (b) response of device 2 after 16 days under ambient conditions upon exposure to 57 ppm cyclohexanone for 30 s every 100 s starting at 50 s as well as 283 ppm cyclohexanone for 30 s every 100 s starting at 550 s; (c) response of device 2 after 236 days under ambient conditions upon exposure to 57 ppm cyclohexanone for 30 s every 100 s starting at 50 s as well as 283 ppm cyclohexanone for 30 s every 100 s starting at 600 s; (d) overlay of sensing traces for freshly prepared device 2, device 2 after 16 days, and after 236 days under ambient conditions.

4.2.3. Optimization of Receptors

To optimize the performance of sensors in this study, we determined the association constant of several chemical analogs of m-CF₃-Bn-TU-SWCNT and p-CF₃-Bn-TU-SWCNT with **2** (Figure 4.13). The methyl substituted analogues of the receptors on p-CF₃-Bn-TU-SWCNT and m-CF₃-Bn-TU-SWCNT, **14** and **15**, were synthesized in 91% and 84% yield, respectively, by reacting amines **5** and **7** with methylisothiocyanate **4** (see Experimental Section). Additionally, the phenyl analogues of the receptors (**16** and **17**) were synthesized in 83% and 65% yield, respectively, from the commercially available isothiocyanate precursors and methylamine.

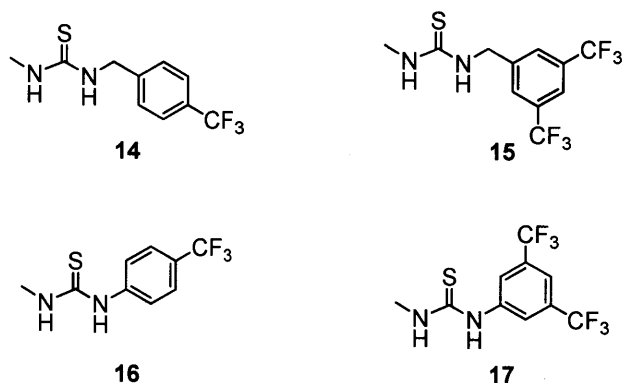
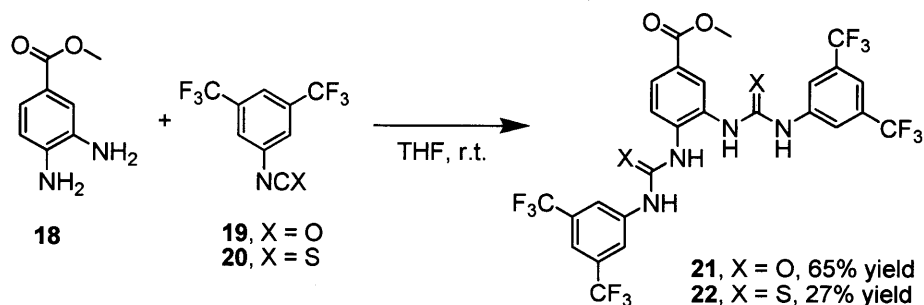


Figure 4.13. Model receptors for binding studies with substituted benzyl (**14**, **15**) and phenyl groups (**16**, **17**).

In addition to testing receptors with one thiourea unit, we anticipated that introduction of a second thiourea unit into the receptor may lead to enhanced binding to the analyte. Based on computational²⁰ and experimental²¹ studies that had been conducted with urea receptors for anion sensing and considering facile synthetic access to compounds that could be easily attached to amine SWCNTs, we decided to synthesize urea receptor **21** and its thiourea counterpart **22** (Scheme 4.3). We expected better interactions of the thiourea units with the analyte compared to urea units based on previous studies.¹⁵ On the other hand, it was not clear if the steric demand of

the thiourea groups allowed an optimal conformation for analyte binding. Therefore, we decided to investigate both, urea (**21**) and thiourea receptor (**22**). Starting from diamine **18** and isocyanate **19** or isothiocyanate **20**, the receptors were obtained in 65% and 27% yield, respectively.

Scheme 4.3. Synthesis of receptors with two urea (**21**) or thiourea units (**22**).



We chose to analyze titration experiments using nuclear magnetic resonance (NMR) to investigate analyte-receptor interactions.²² Association constants were determined based on the NMR data using the software WinEQNMR2.²³

Based on the shifts of the aromatic as well as -NH protons, K_a values between $1.1 \pm 0.7 \text{ M}^{-1}$ and $3.9 \pm 2.2 \text{ M}^{-1}$ were obtained for receptors **14-17** at 0.01 M receptor concentration in CDCl₃ (Table 4.2, Entries 1-4). Even though the observed errors are high, the measurements suggest that **17** could be a potential candidate for attachment to SWCNTs.

Table 4.2. Association constants for cyclohexanone and model receptors in CDCl₃

Entry	Model receptor	K_a (CDCl ₃)
1	14	$1.5 \pm 1.3 \text{ M}^{-1}$ ^a
2	15	$1.1 \pm 0.7 \text{ M}^{-1}$ ^a
3	16	$1.1 \pm 0.7 \text{ M}^{-1}$ ^a
4	17	$3.9 \pm 2.2 \text{ M}^{-1}$ ^a
5	22	$43 \pm 5 \text{ M}^{-1}$ ^b

^aaverage and error based on shifts of two aromatic and two NH protons; ^bbased on shift of proton at 4-position of CF₃ substituted aromatic rings of **22**.

21 was not sufficiently soluble in CDCl_3 to perform a binding study, presumably due to strong intermolecular hydrogen bonding interactions and **22** was only soluble in CDCl_3 up to 2.5 mM. At this concentration, an association constant of $42 \pm 5 \text{ M}^{-1}$ was determined (Table 4.2, Entry 5). The change in chemical shift of the protons in **22** suggests that cyclohexanone interacts with one -NH proton of each of the thiourea units (Figure 4.14). While a significant change is observed for protons *c* and *d*, protons *a* and *b* are barely affected by changes in cyclohexanone concentration.

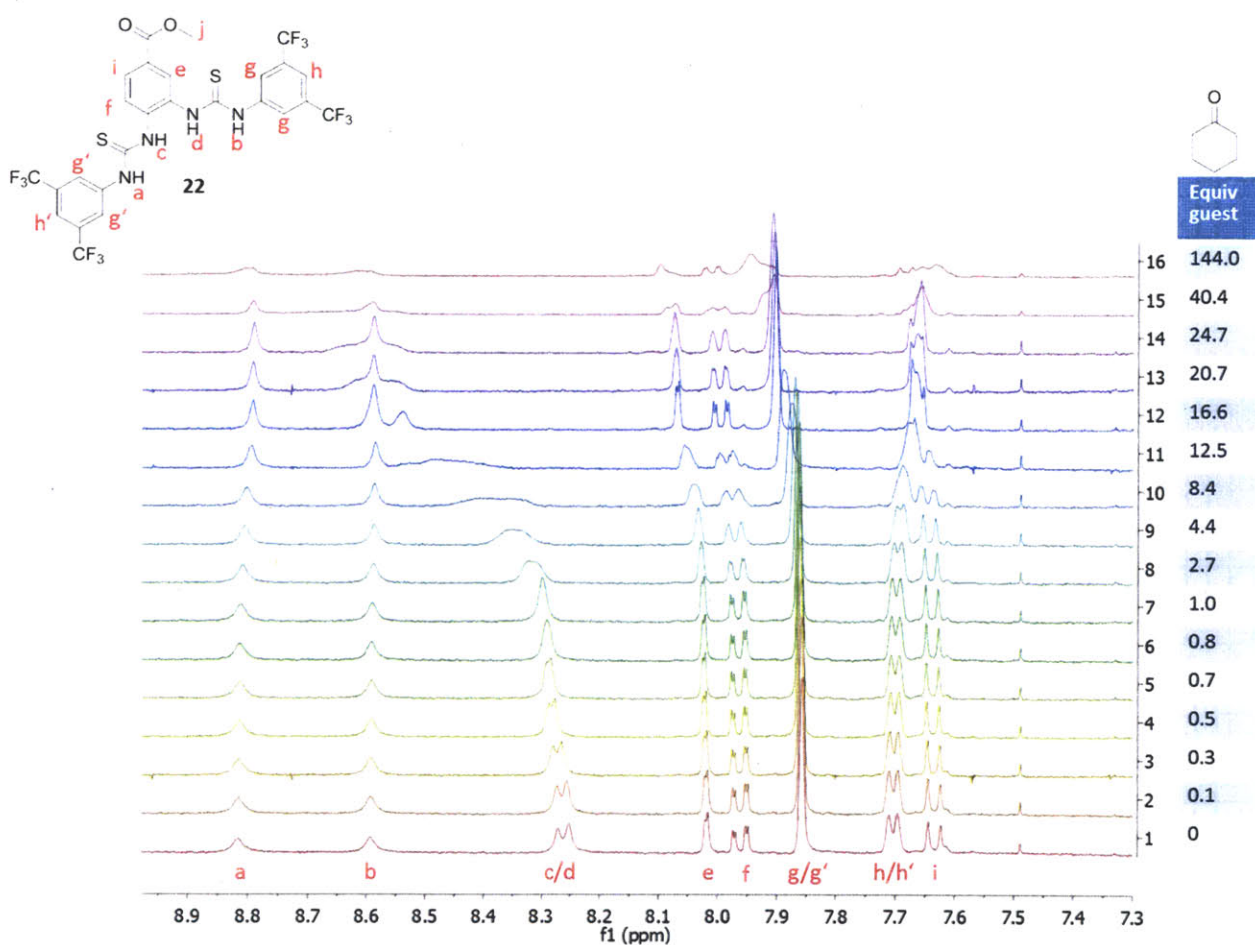
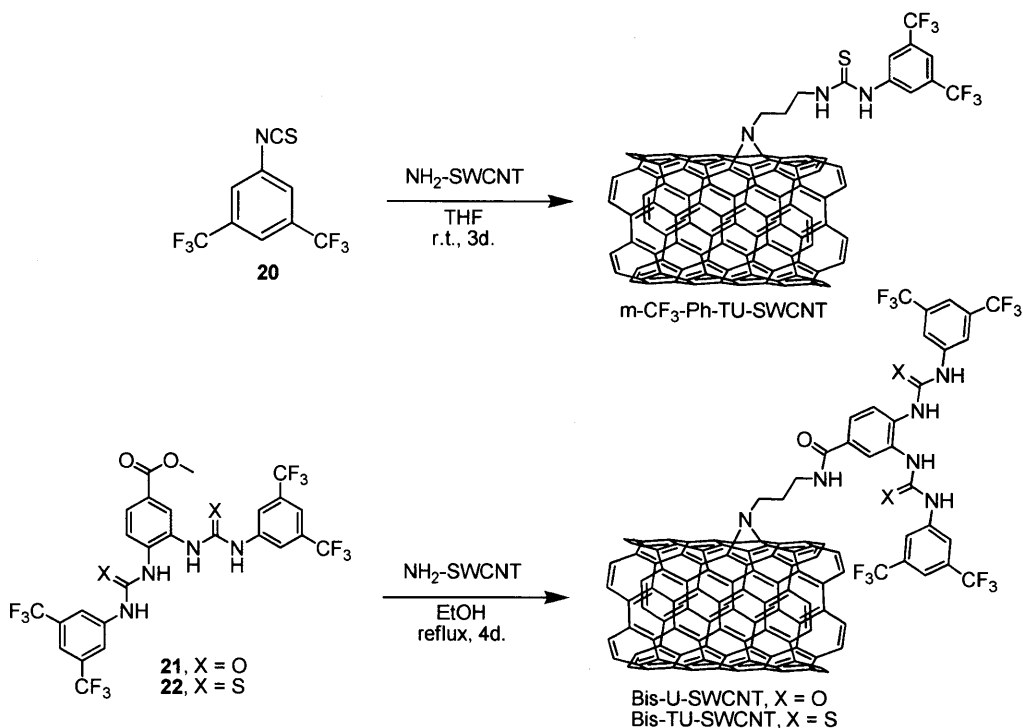


Figure 4.14. NMR binding study of **22** and cyclohexanone **2** in CDCl_3 .

Based on the results of the performed binding studies, we decided to functionalize SWCNTs with receptors analogous to **17**, **21**, and **22** (Scheme 4.4). Based on F 1s and C 1s signals by

XPS, functional group densities of 1 per 180 CNT carbon atoms (m-CF₃-Ph-TU-SWCNT), 1 per 130 CNT carbon atoms (Bis-U-SWCNT), and 1 per 100 CNT carbon atoms (Bis-TU-SWCNT) were obtained.

Scheme 4.4. Synthesis of m-CF₃-Ph-TU-SWCNT, Bis-U-SWCNT, and Bis-TU-SWCNT.



4.2.4. Sensor Array Measurements

After identifying m-CF₃-Ph-TU-SWCNT, Bis-U-SWCNT, and Bis-TU-SWCNT as potential candidates for a sensor, we decided to test them together with the other functionalized SWCNTs containing 3,5-CF₃-substituted phenyl groups, m-CF₃-Bn-TU-SWCNT and m-CF₃-Bn-SQ-SWCNT, as well as NH₂-SWCNT and pristine SWCNTs. While it would have been possible to perform these measurements one device at a time, we decided to develop a platform that allowed the simultaneous testing of an array of sensors. Besides being more time-efficient, this approach ensured that all sensors were exposed to exactly the same analyte concentration, gas flow rate,

and temperature during the measurements, as well as the same environmental factors during storage of the device between measurements.

We designed shadow masks that allowed the deposition of gold electrodes for 14 devices onto one glass slide (25 x 75 mm). The devices had separate working electrodes and a shared counter electrode with a gap size of 1 mm between electrodes (Figure 4.15). The distance between devices was set to 5.08 mm so that the glass slide could be contacted *via* a standard edge connector (0.1 inch spacing, every other contact was used). The edge connector was then connected to a potentiostat capable of simultaneous amperometric measurements.

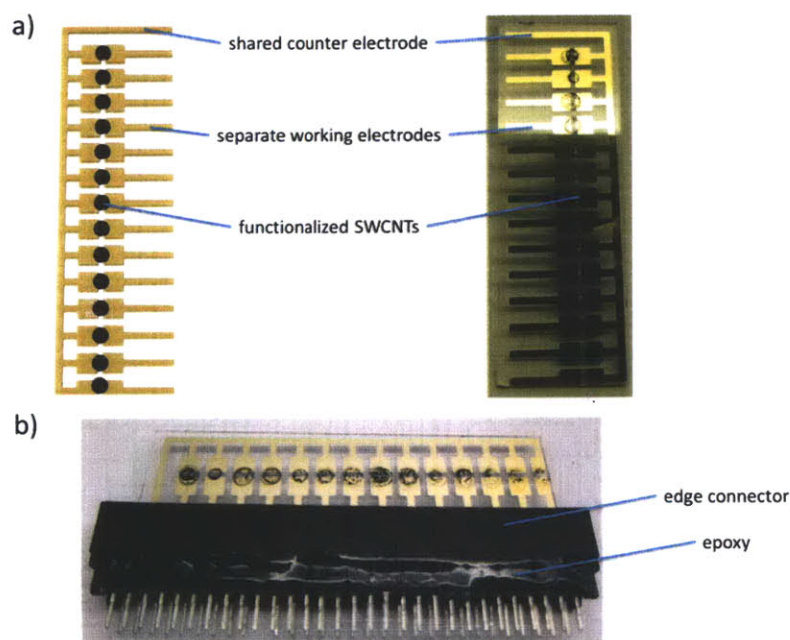


Figure 4.15. Devices for array measurements. (a) Schematic drawing and photograph of 14 devices on a glass slide; (b) photograph of glass slide with 14 devices contacted *via* an edge connector. Openings in the edge connector were covered with epoxy to provide a gas tight seal.

Functionalized and pristine SWCNTs were drop-cast between working and counter electrodes until the resistance across each inter-electrode gap was between 5 and 20 k Ω . Maintaining a

resistance within this range across devices ensured currents in the same range during the sensing measurement and, based on previous measurements, improved reproducibility across devices.

For the measurement, two devices each were prepared with the seven aforementioned types of SWCNTs (pristine SWCNTs, NH_2 -SWCNT, $m\text{-CF}_3\text{-Ph-TU-SWCNT}$, Bis-U-SWCNT, Bis-TU-SWCNT, $m\text{-CF}_3\text{-Bn-SQ-SWCNT}$, and $m\text{-CF}_3\text{-Bn-TU-SWCNT}$) on a 14-device glass slide. Testing two devices of each type of SWCNTs allowed a qualitative assessment of device to device reproducibility, while using seven different types of SWCNTs simultaneously provided an overview of differences between receptors.

The edge connector was enclosed in a custom-built Teflon enclosure that contained a gas flow channel and could be connected to a gas generation system analogous to the setup for single device measurements (Figure 4.9). Using the gas generation system, the devices were exposed to MeNO_2 and cyclohexanone as well as a range of common interferents at two different concentrations each (three for MeNO_2). For the interferents, concentrations of 1% and 0.5% of the equilibrium vapor concentration at 25 °C were chosen (Table 4.3). It would have also been possible to use the same concentration for each analyte. Using a similar fraction of the equilibrium vapor concentration, however, appeared to better reflect typical concentrations that would be encountered in real-life applications. For a better comparison of MeNO_2 and cyclohexanone, MeNO_2 was tested at the same concentrations as cyclohexanone in addition to 1% of its equilibrium vapor concentration.

Table 4.3. Analyte concentrations for array measurements.

Entry	Analyte	Concentration (ppm)	Relative Concentration ^a
1l	MeNO ₂	57	0.1%
1m	MeNO ₂	283	0.6%
1h	MeNO ₂	469	1%
2h	MeOH	1668	1%
2l	MeOH	834	0.5%
3h	THF	1905	1%
3l	THF	953	0.5%
4h	EtOAc	1244	1%
4l	EtOAc	622	0.5%
5h	hexanes	1994	1%
5l	hexanes	997	0.5%
6h	toluene	375	1%
6l	toluene	188	0.5%
7h	H ₂ O	313	1%
7l	H ₂ O	157	0.5%
8h	MeCN	1165	1%
8l	MeCN	583	0.5%
9h	acetone	3020	1%
9l	acetone	1510	0.5%
10l	cyclohexanone	57	1.3%
10h	cyclohexanone	283	6.3%

^aFraction of equilibrium vapor concentration at 25 °C.

The devices were exposed five times to each analyte and concentration for 30 s each, followed by 70 s of nitrogen stream at the same gas flow rate. A potential of 0.1 V was applied between working and counter electrodes and the current was recorded (Figure 4.16a).

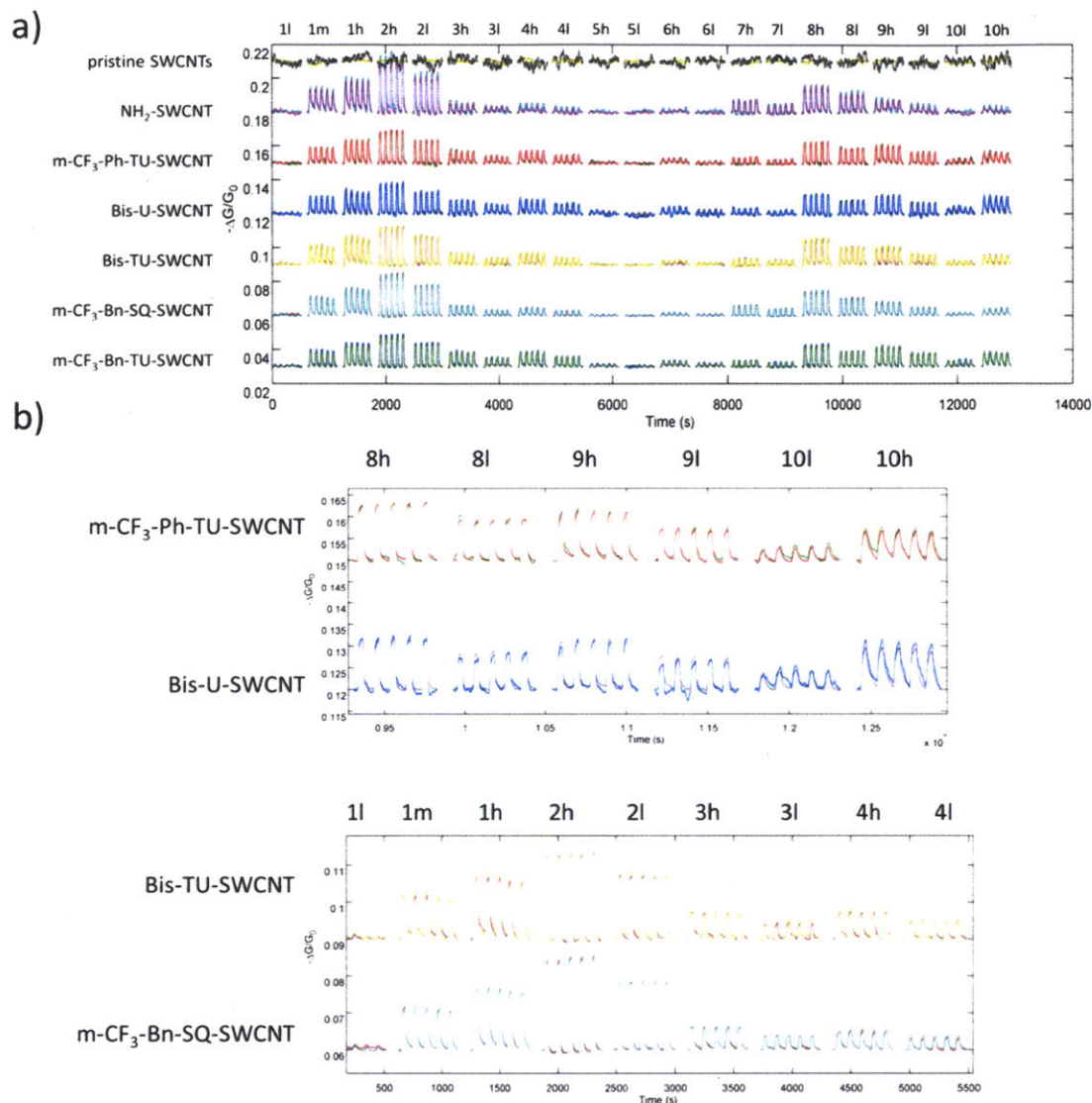


Figure 4.16. Sensing response of an array of SWCNT devices. Each line contains the overlaid response of two different devices of the same type of SWCNTs. Analytes and concentrations are listed in Table 4.3. Equilibration times when switching analytes or concentrations have been omitted for clarity. A 20 point floating average filter and baseline correction has been applied to the plotted data. (a) Overview of sensing response of all tested devices; (b) examples for reproducibility of consecutive measurements and across devices with the same type of SWCNTs.

A very good device to device reproducibility was observed and exposures to the same analyte and concentrations led to similar responses for consecutive measurements (Figure 4.16b). Figure 4.17 gives the peak heights of the sensing responses compared across analytes and devices.

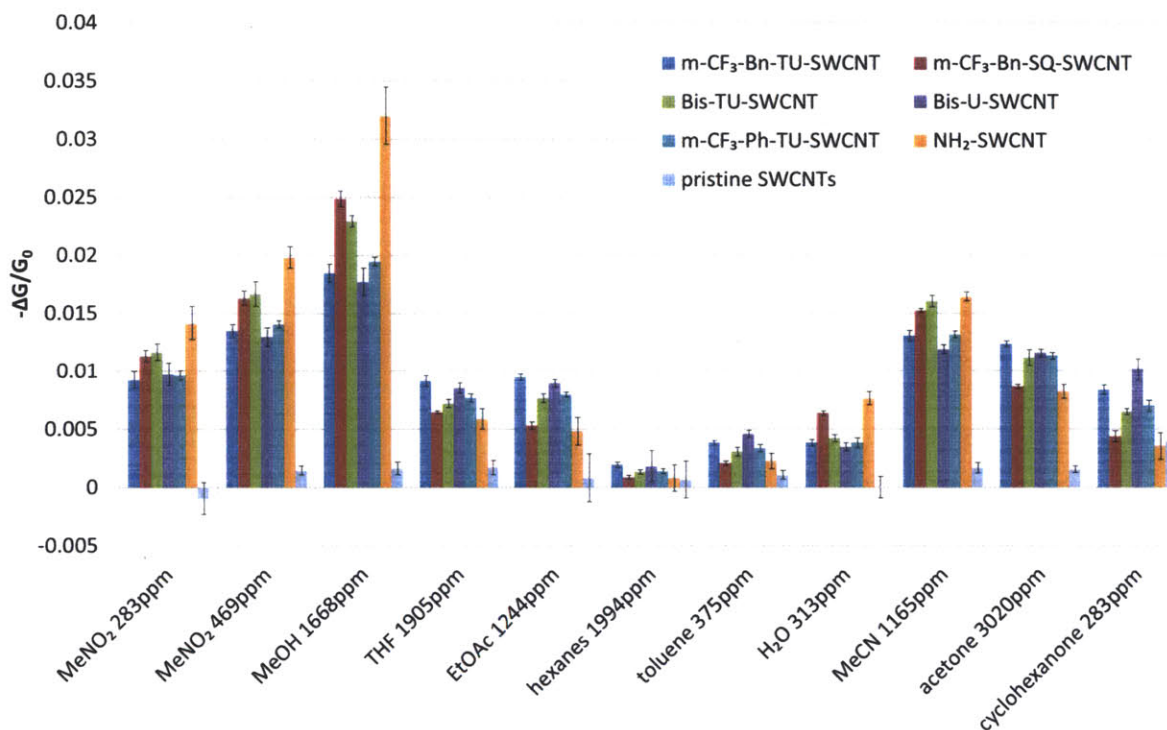


Figure 4.17. Sensing response of an array of SWCNT devices. Averages and errors shown are based on 4 peaks and 2 devices for each type of analyte and SWCNT.

Errors based on 4 consecutive measurements and 2 devices each were low except for pristine SWCNTs and NH₂-SWCNT, confirming good reproducibility. The devices carrying the developed receptors show good responses to MeNO₂ and cyclohexanone. However, they also exhibit responses to interferents that are polar and/or capable of hydrogen bonding with the receptors such as methanol, THF, acetonitrile or acetone. The response to hexanes and toluene on the other hand was weak. For the target analytes MeNO₂ and cyclohexanone, SWCNTs equipped with receptors containing two thiourea or urea units perform better than SWCNTs with

one thiourea or squaramide per functional group. In the case of MeNO₂, Bis-TU-SWCNT led to the highest response (besides NH₂-SWCNT). Bis-U-SWCNT exhibited the highest change in current when exposed to cyclohexanone among the tested SWCNTs, confirming the trend observed in NMR binding studies. When exposed to the same analyte concentration of MeNO₂ and cyclohexanone (283 ppm), m-CF₃-Bn-TU-SWCNT and Bis-U-SWCNT show similar responses of ca. 1% change in current. Pristine SWCNTs react more strongly to cyclohexanone, although they do not appear to be a reliable sensing material for the analytes at hand based on large errors and noise levels. All other functionalized SWCNTs show a more pronounced response to MeNO₂ than to cyclohexanone.

While the results with the target analytes were promising, the responses to potential interferents could potentially be problematic. At the observed selectivity, a single-device sensor would not be able to distinguish between the selected analytes. As the combined response pattern of all devices was, however, different for each analyte, combining the results of the array could lead to the desired selectivity.¹⁰ In order to explore this option, we performed principal component analysis (PCA) using the commercial MATLAB software (Figure 4.18). For PCA, the current change upon four exposures to each analyte at the respective higher concentration was used across 13 devices (seven different types of SWCNTs and two devices each, one device for pristine SWCNTs).

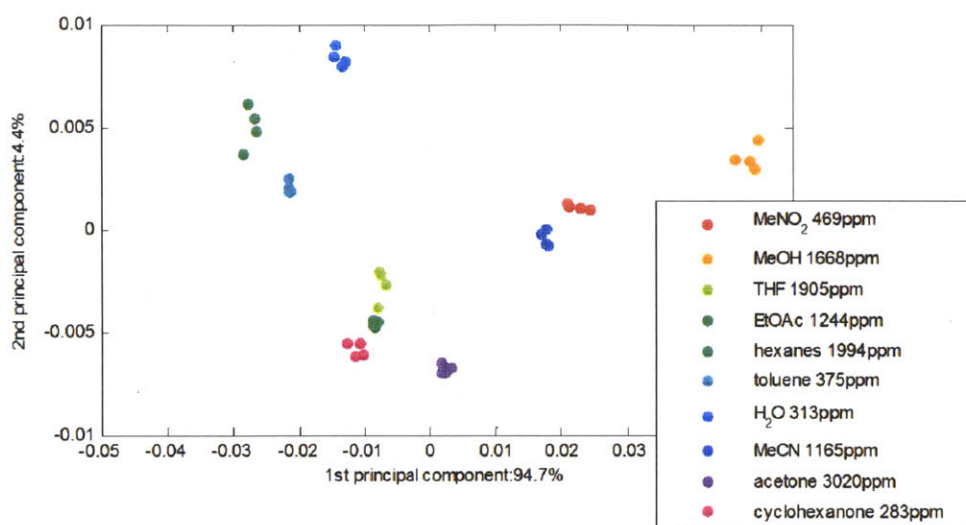


Figure 4.18. Principal component analysis of the array sensing responses. First and second principal component shown.

The scatter plot of the first two principal components collectively contributing to 99.1% of the variance showed good clustering of the four responses to each analyte. This further underlined the reproducibility of the measurements. Compared to the distance of points for the same analyte, clusters were well-separated showing some level of selectivity. Nevertheless, not all clusters were sufficiently separated to provide good selectivity in sensing applications. Points corresponding to cyclohexanone, ethyl acetate and THF for example all appeared in the same area. In order to achieve a higher level of selectivity, a wider array of chemically diverse receptors would have to be utilized in the sensing experiments. On the other hand, observing any separation in a PCA scatter plot for receptors as similar as the ones employed in this study shows that even small modifications can be reflected in the sensing response and optimizing receptors can thus be a valuable step in sensor development.

4.3. Conclusions

In summary, we have developed sensors based on SWCNTs covalently functionalized with urea, thiourea and squaramide-based receptors. Initially fabricated sensors showed a good response to 1.3% equilibrium vapor concentration of cyclohexanone, a compound commonly found as an impurity in RDX explosives. Based on solution NMR binding studies with model systems, additional candidates for receptors were identified and attached to SWCNTs. The new receptors were tested together with best performing candidates from the initial studies and a further improvement of the sensing response to cyclohexanone was observed.

Furthermore, the sensors were tested in an array with a variety of analytes including cyclohexanone and nitromethane, as well as common interferents. Receptors containing two thiourea or urea units in combination with electron poor 3,5-CF₃-substituted phenyl groups showed very good responses to the target analytes nitromethane and cyclohexanone. A very good device to device reproducibility and good stability over time was observed. The selectivity of the system can potentially be improved further by including a more diverse group of receptor-functionalized SWCNTs in the array measurements.

4.4. Experimental Section

Materials and Synthetic Manipulations

Synthetic manipulations were carried out under an argon atmosphere using standard Schlenk techniques. Single-walled carbon nanotubes were purchased from SouthWest Nano Technologies (SWeNT® CG100). All other chemicals were purchased from Sigma Aldrich and used as received. NMR spectra were recorded on Bruker Avance-400 spectrometers.

XPS Measurements

XPS spectra were recorded on a Kratos AXIS Ultra X-ray Photoelectron Spectrometer. The samples were drop-cast onto SiO₂/Si substrates for the measurements.

Scanning Electron Microscope Measurements

Scanning electron microscope (SEM) images were obtained on a JEOL 6700 scanning electron microscope.

3-azidopropan-1-amine 3. 3 was synthesized following a literature procedure.¹⁷ Note: Molecules with a high density of azide groups are potentially explosive and particular caution has thus to be used, especially when isolating azides.^{24,25} Before synthesizing the compound on the described scale the molecule was prepared on small scale and the explosive hazard has been evaluated (shock, heat). 65.6 g (0.3 mol) 3-bromopropylamine hydrobromide were dissolved in 200 mL H₂O and added to 39.0 g (2 equiv) sodium azide in 160 mL H₂O. The mixture was refluxed for 15 h and subsequently cooled in an ice bath. Afterward, it was poured into 400 mL diethyl ether containing 24 g NaOH (2 equiv). The organic phase was separated and the aqueous phase was extracted twice with 100 mL Et₂O. The combined organic phases were dried over MgSO₄, filtered and stored in solution. A small aliquot was concentrated for characterization by NMR. The concentration in solution was determined by ¹H-NMR to be 0.3 M using toluene as an internal standard. Yield: 470 mL of 0.3 M solution (47%). ¹H-NMR (CDCl₃, 400 MHz): δ = 3.33 (t, 2H, *J* = 6.6 Hz); 2.76 (t, 2H, *J* = 7.0 Hz); 1.68 (quin, 2H, *J* = 6.8 Hz); 1.17 (s, broad, 2H). ¹³C-NMR (CDCl₃, 100 MHz): δ = 49.2, 39.4, 32.6.

1-(isothiocyanatomethyl)-4-(trifluoromethyl)benzene 6. 5 (0.81 g, 4.60 mmol) was dissolved in 5 mL absolute EtOH. While stirring, CS₂ (3.50 g, 46.0 mmol) and Et₃N (0.47 g, 4.60 mmol)

were added. After stirring for 60 min., the solution was cooled on an ice bath, precipitating dithiocarbamate. Once cooled, a solution of Boc_2O (0.98 g, 4.50 mmol) in 1 mL absolute EtOH and a solution of DMAP (17 mg, 0.14 mmol) in 1 mL absolute EtOH were added. After stirring at 0 °C for 5 minutes, the reaction mixture was warmed to r.t. The mixture was stirred until evolution of gas had completed and was then concentrated. The product was purified by flash silica chromatography (DCM, gradient to 2% MeOH) elutes product first. Yield: 0.544 g (2.51 mmol, 55%). $^1\text{H-NMR}$ (400 MHz, CDCl_3): δ 7.63 (d, 2H, $J = 8.0$ Hz), 7.42 (d, 2H, $J = 8.4$ Hz), 4.77 (s, 2H). $^{13}\text{C-NMR}$ (100 MHz, CDCl_3): δ 138.4 (s), 134.0 (s broad), 130.9 (q, $J = 32.5$ Hz), 127.3 (s), 126.2 (q, $J = 3.8$ Hz), 124.0 (q, $J = 270.5$ Hz), 48.4 (s).

1-(isothiocyanatomethyl)-3,5-bis(trifluoromethyl)benzene 8. **8** was prepared from **7** following the same procedure as described for **6**.: 0.461 g (1.62 mmol, 35%). $^1\text{H-NMR}$ (400 MHz, CDCl_3): δ 7.84 (s, 1H), 7.76 (s, 2H), 4.87 (s, 2H). $^{13}\text{C-NMR}$ (100 MHz, CDCl_3): δ 137.2 (s), 136.1 (s broad), 132.7 (q, $J = 33.5$ Hz), 127.2 (q, $J = 3.7$ Hz), 123.1 (q, $J = 271.2$ Hz), 122.6 (m), 48.1 (s).

3-ethoxy-4-(methylamino)cyclobut-3-ene-1,2-dione 11. **10** (0.57 g, 3.34 mmol) was dissolved in 15 mL DCM in water-free conditions. A solution of **9** in THF (1.78 mL, 2.0 M) was added while stirring under Ar atmosphere. After stirring for 18, the mixture was filtered, and the filtrate was washed with 35 mL 1N HCl (aq). The organic layer was dried with Na_2SO_4 , filtered and concentrated. The product was isolated by flash silica chromatography (DCM to elute diethylsquarate, then DCM/MeOH 98:2). Yield: 0.315 g (2.03 mmol, 61%). The $^1\text{H-NMR}$ spectrum shows 2 full sets of peaks, due to a high rotation barrier around the C-N bond (ratio isomer 1 to isomer 2: 3.8). $^1\text{H-NMR}$ (400 MHz, CDCl_3): Isomer 1: δ 7.31 (s broad, 1H), 4.65 (q, 2H, $J = 6.8$ Hz), 3.06 (d, 3H, $J = 4.8$ Hz), 1.35 (t, 3H, $J = 6.8$ Hz). Isomer 2: δ 6.66 (s broad, 1H), 4.57 (q broad, 2H, $J = 6.8$ Hz), 3.19 (s broad, 3H), 1.30 (t broad, 3H). $^{13}\text{C-NMR}$ (100 MHz,

CDCl₃): δ 189.8, 182.8, 177.8, 173.4, 69.8, 31.4, 16.0. HRMS calc. for C₇H₁₀NO₃ [M+H]⁺: 156.0655, found: 156.0669. [M+H]⁺

3-ethoxy-4-((4-(trifluoromethyl)benzyl)amino)cyclobut-3-ene-1,2-dione 12. 10 (0.57 g, 3.34 mmol) was dissolved in 15 mL DCM in water-free conditions, and a solution of **5** (0.61 g, 3.51 mmol) in 3.5 mL DCM was added while stirring. After stirring for 18 h, the mixture was filtered, and the filtrate was washed with 35 mL 1N HCl (aq). The organic layer was dried with Na₂SO₄, filtered and concentrated. The product was isolated by flash silica chromatography (DCM to elute diethylsquarate, then DCM/MeOH 98:2). Yield: 0.506 g (1.48 mmol, 44%). Two isomers were obtained (ratio isomer 1 to isomer 2: 3.3). ¹H-NMR (400 MHz, CDCl₃): Isomer 1: δ 7.94 (s broad, 1H), 7.54 (d, 2H, *J* = 7.6 Hz), 7.39 (d, 2H, *J* = 7.6 Hz), 4.69 (d, 1H, *J* = 6.4 Hz), 4.65 (s broad, 2H), 4.61 (d, 1H, *J* = 5.2 Hz), 1.36 (t, 3H, *J* = 6.4 Hz). Isomer 2: 7.54 (d, 2H, *J* = 7.6 Hz), 7.39 (d, 2H, *J* = 7.6 Hz), 6.93 (s broad, 1H), 4.82 (s broad, 2H), 4.69 (d, 1H, *J* = 6.4 Hz), 4.61 (d, 1H, *J* = 5.2 Hz), 1.36 (t, 3H, *J* = 6.4 Hz). ¹³C-NMR (100 MHz, CDCl₃): δ 189.7 (s), 183.0 (s), 178.1 (s), 172.7 (s), 141.4 (s), 130.4 (q, *J* = 32.3 Hz), 128.1 (s), 126.0 (q, *J* = 3.7 Hz), 124.1 (q, *J* = 270.5 Hz), 70.2 (s), 48.1 (s), 15.9 (s). HRMS calc. for C₁₄H₁₂F₃NO₃ [M+H]⁺: 300.0842, found: 300.0853. [M+H]⁺

3-((3,5-bis(trifluoromethyl)benzyl)amino)-4-ethoxycyclobut-3-ene-1,2-dione 13. 13 was prepared from **10** and **7** as described for **12**. Yield: 0.320 g (0.87 mmol, 26%). Two isomers were obtained (ratio isomer 1 to isomer 2: 2.3). ¹H-NMR (400 MHz, CDCl₃): Isomer 1: δ 7.81 (s, 1H), 7.76 (s, 2H), 7.53 (s broad, 1H), 4.75 (q, 2H, *J* = 7.2 Hz), 4.73 (s broad, 2H), 1.41 (t, 3H, *J* = 7.2 Hz). Isomer 2: δ 7.81 (s, 1H), 7.76 (s, 2H), 5.91 (s broad, 1H), 4.92 (s broad, 2H), 4.75 (q, 2H, *J* = 7.2 Hz), 1.41 (t, 3H, *J* = 7.2 Hz). ¹³C-NMR (100 MHz, CDCl₃): δ 189.7 (s), 182.9 (s), 178.5 (s), 172.5 (s), 140.0 (s), 132.5 (q, *J* = 33.3 Hz), 128.3 (q, *J* = 2.8 Hz), 123.2 (q, *J* = 271.1 Hz), 122.3

(m), 70.5 (s), 47.6 (s), 15.8 (s). HRMS calc. for $C_{15}H_{11}F_6NO_3$ $[M+H]^+$: 368.0716, found: 368.0729. $[M+H]^+$

1-methyl-3-(4-(trifluoromethyl)benzyl)thiourea 14. **5** (175.2 mg, 1.0 mmol) and **4** (73.1 mg, 1.0 mmol) were each dissolved in 10 mL DCM. The solutions were combined and stirred at r.t. for 48 h. The product was isolated by flash silica chromatography in DCM:MeOH 97:3. Yield: 226.2 mg (0.91 mmol, 91%). 1H -NMR (400 MHz, $CDCl_3$): δ 7.53 (d, 2H, $J = 8.4$ Hz), 7.36 (d, 2H, $J = 8.0$ Hz), 6.57 (s broad, 2H), 4.72 (s, 2H), 2.89 (d, 3H, $J = 4.0$ Hz). ^{13}C -NMR (100 MHz, $CDCl_3$): δ 182.9 (s broad), 141.9 (s), 130.0 (q, $J = 32.3$ Hz), 127.8 (s), 125.8 (q, $J = 3.8$ Hz), 124.2 (q, $J = 270.4$ Hz), 47.9 (s), 30.9 (s broad). HRMS calc. for $C_{10}H_{11}F_3N_2S$ $[M+H]^+$: 249.0668, found: 249.0689. $[M+H]^+$

1-(3,5-bis(trifluoromethyl)benzyl)-3-methylthiourea 15. **7** (243.2 mg, 1.0 mmol) and **5** (73.1 mg, 1.0 mmol) were each dissolved in 10 mL DCM. The solutions were combined and stirred at r.t. for 48 h. The product was isolated by flash silica chromatography in DCM:MeOH 97:3. Yield: 266.4 mg (0.84 mmol, 84%). 1H -NMR (400 MHz, $CDCl_3$): δ 7.71 (s, 1H), 7.71 (s, 2H), 6.72 (s broad, 2H), 4.83 (d, 2H, $J = 1.2$ Hz), 2.88 (d, 3H, $J = 1.2$ Hz). ^{13}C -NMR (100 MHz, $CDCl_3$): δ 183.2 (s broad), 140.9 (s), 132.0 (q, $J = 33.2$ Hz), 127.8 (s), 123.3 (q, $J = 271.1$ Hz), 121.6 (m), 47.6 (s), 30.8 (s broad). HRMS calc. for $C_{11}H_{10}F_6N_2S$ $[M+H]^+$: 317.0542, found: 317.0543. $[M+H]^+$

1-methyl-3-(4-(trifluoromethyl)phenyl)thiourea 16. *p*-Trifluoromethylphenylisothiocyanate (203.2 mg, 1.0 mmol) was dissolved in 10 mL dry THF. **9** was added as a solution (1 mL 2.0 M, 2.0 mmol) *via* syringe. The solution was stirred at r.t. for 24 h and the product was isolated by flash silica chromatography in DCM:MeOH 98:2. Yield: 195.3 mg (0.83 mmol, 83%). 1H -NMR

(400 MHz, CDCl₃): δ 8.20 (s broad, 1H), 7.68 (d, 2H, $J = 8.4$ Hz), 7.35 (d, 2H, $J = 8.0$ Hz), 6.20 (s broad, 1H), 3.16 (d, 3H, $J = 4.8$ Hz). ¹³C-NMR (100 MHz, CDCl₃): δ 181.7 (s broad), 139.9 (s), 128.8 (q, $J = 32.8$ Hz), 127.5 (q, $J = 3.8$ Hz), 124.5 (s), 123.8 (q, $J = 270.6$ Hz), 32.4 (s). HRMS calc. for C₉H₉F₃N₂S [M+H]⁺: 235.0511, found: 235.0527. [M+H]⁺

1-(3,5-bis(trifluoromethyl)phenyl)-3-methylthiourea **17**. *p*-Trifluoromethylphenyl-isothiocyanate (271.2 mg, 1.0 mmol) was dissolved in 10 mL dry THF. **9** was added as a solution (1 mL 2.0 M, 2.0 mmol) *via* syringe. The solution was stirred at r.t. for 24 h and the product was isolated by flash chromatography in DCM:MeOH 98:2. Yield: 196.1 mg (0.65 mmol, 65%). ¹H-NMR (400 MHz, CDCl₃): δ 8.44 (s broad, 1H), 7.76 (s, 2H), 7.69 (s, 1H), 6.24 (s broad, 1H), 3.12 (d, 3H, $J = 4.8$ Hz). ¹³C-NMR (100 MHz, CDCl₃): δ 181.8 (s broad), 138.9 (s), 133.3 (q, $J = 34.0$ Hz), 124.6 (s), 122.9 (q, $J = 271.4$ Hz), 120.0 (m), 32.2 (s). HRMS calc. for C₁₀H₈F₆N₂S [M+H]⁺: 303.0385, found: 303.0370. [M+H]⁺

Methyl 3,4-bis(3-(3,5-bis(trifluoromethyl)phenyl)ureido)benzoate **21**. **19** (2.81 g, 11.0 mmol) was added to **18** (831 mg, 5.0 mmol) in 30 mL THF. The mixture was stirred at r.t. for 24 h after which the solvent was removed *in vacuo*. The crude product was recrystallized from 100 mL DCM and dried *in vacuo*. Yield: 2.17 g (3.2 mmol, 64%). ¹H-NMR (400 MHz, DMSO-*d*₆): δ 9.95 (s, 1H), 9.78 (s, 1H), 8.55 (s, 1H), 8.39 (s, 1H), 8.09 (d, 4H, $J = 18.4$ Hz), 8.03 (d, 1H, $J = 1.2$ Hz), 7.93 (d, 1H, $J = 8.8$ Hz), 7.76 (dd, 1H, $J = 8.4$ Hz, 2.0 Hz), 7.61 (d, 2H, $J = 8.4$ Hz), 3.81 (s, 3H). ¹³C-NMR (100 MHz, DMSO-*d*₆): δ 166.3 (s), 154.0 (s), 153.1 (s), 142.5 (s), 142.1 (s), 138.0 (s), 131.4 (q, $J = 32.5$ Hz), 131.3 (q, $J = 32.5$ Hz), 129.9 (s), 127.6 (s), 127.3 (s), 125.4 (s), 123.9 (q, $J = 271.1$ Hz), 123.9 (q, $J = 270.9$ Hz), 123.1 (s), 119.8 (s), 118.7 (s), 115.2 (s), 52.7 (s). HRMS calc. for C₂₆H₁₆F₁₂N₄O₄ [M+H]⁺: 677.1053, found: 677.1073. [M+H]⁺

Methyl 3,4-bis(3-(3,5-bis(trifluoromethyl)phenyl)thioureido)benzoate 22. 20 (2.98 g, 11.0 mmol) was added to **18** (831 mg, 5.0 mmol) in 30 mL THF. The mixture was stirred at r.t. for 22 h after which 1 g (3.7 mmol) **20** were added. After stirring for two additional hours, the solvent was removed *in vacuo*. The crude product was washed with hexanes and DCM. Yield: 941 mg (27%). ¹H-NMR (400 MHz, DMSO-*d*₆): δ 10.39 (s, 1H), 10.32 (s br, 1H), 10.02 (s, 1H), 9.91 (s br, 1H), 8.17 (d, 2H, *J* = 4.4 Hz), 8.06 (d, 1 H, *J* = 1.6 Hz), 7.91 (dd, 1 H, *J* = 8.4 Hz, 2.0 Hz), 7.76 (s br, 2H), 7.74 (d, 1H, *J* = 8.4 Hz), 3.88 (s, 3H). HRMS calc. for C₂₆H₁₆F₁₂N₄O₂S₂ [M+H]⁺: 709.0596, found: 709.0611. [M+H]⁺

NH₂-SWCNT. 150 mg (12.5 mmol C) SWCNTs were added to a flame dried Schlenk flask. 6 g (60 mmol) **3** and 30 mL 1,2-dichlorobenzene were added. The mixture was sonicated for 15 min and then equipped with a reflux condenser and stirred at 160 °C for 42 h. The solvent was distilled off and the residue was washed on a 0.2 μm fluoropore filter membrane with CH₂Cl₂, methanol, ethanol, water, methanol, and hexanes. The product was dried *in vacuo*. N/C ratio by XPS (based on N 1s vs. C 1s): 16.7% (functional group density: 8.3%).

Me-TU-SWCNT. 10 mg NH₂-SWCNT were sonicated for 15 min in 8 mL ethanol. 36.7 mg (0.5 mmol) **4** in 3 mL ethanol were added dropwise at 0 °C. The mixture was stirred for 48 h. The solid was collected by filtration and the product was washed on a filter with ethanol, CH₂Cl₂, methanol, water, methanol, and hexanes and subsequently dried *in vacuo*. Functional group density based on O 1s and C 1s signals by XPS: 58 CNT carbon atoms per functional group.

p-CF₃-Bn-TU-SWCNT. 20 mg NH₂-SWCNT were sonicated for 15 min in 15 mL ethanol. 217 mg (1.0 mmol) **6** in 5 mL ethanol were added dropwise at 0 °C. The mixture was stirred for 48 h. The solid was collected by filtration and the product was washed on a filter with ethanol,

CH₂Cl₂, methanol, water, methanol, and hexanes and subsequently dried *in vacuo*. Functional group density based on F 1s and C 1s signals by XPS: 45 CNT carbon atoms per functional group.

m-CF₃-Bn-TU-SWCNT. 20 mg NH₂-SWCNT were sonicated for 15 min in 15 mL ethanol. 256 mg (1.0 mmol) **8** in 5 mL ethanol were added dropwise at 0 °C. The mixture was stirred for 48 h. The solid was collected by filtration and the product was washed on a filter with ethanol, CH₂Cl₂, methanol, water, methanol, and hexanes and subsequently dried *in vacuo*. Functional group density based on F 1s and C 1s signals by XPS: 45 CNT carbon atoms per functional group.

Me-SQ-SWCNT. 20 mg NH₂-SWCNT were sonicated for 15 min in 15 mL ethanol. 155 mg (1.0 mmol) **11** in 15 mL ethanol were added. The mixture was stirred for 48 h at r.t. and subsequently for 48 h at 40 °C. The solid was collected by filtration and the product was washed on a filter with ethanol, CH₂Cl₂, methanol, water, methanol, and hexanes and subsequently dried *in vacuo*. Functional group density based on O 1s and C 1s signals by XPS: 108 CNT carbon atoms per functional group.

p-CF₃-Bn-SQ-SWCNT. 20 mg NH₂-SWCNT were sonicated for 15 min in 15 mL ethanol. 299 mg (1.0 mmol) **12** in 15 mL ethanol were added. The mixture was stirred for 48 h at r.t. and subsequently for 48 h at 40 °C. The solid was collected by filtration and the product was washed on a filter with ethanol, CH₂Cl₂, methanol, water, methanol, and hexanes and subsequently dried *in vacuo*. Functional group density based on F 1s and C 1s signals by XPS: 152 CNT carbon atoms per functional group.

m-CF₃-Bn-SQ-SWCNT. 17.5 mg NH₂-SWCNT were sonicated for 15 min in 15 mL ethanol. 319 mg (0.87 mmol) **13** in 15 mL ethanol were added. The mixture was stirred for 48 h at r.t. and subsequently for 48 h at 40 °C. The solid was collected by filtration and the product was washed on a filter with ethanol, CH₂Cl₂, methanol, water, methanol, and hexanes and subsequently dried *in vacuo*. Functional group density based on F 1s and C 1s signals by XPS: 131 CNT carbon atoms per functional group.

m-CF₃-Ph-TU-SWCNT. 20 mg NH₂-SWCNT were sonicated for 2 min in 15 mL THF. 271 mg (1.0 mmol) 1-isothiocyanato-3,5-bis(trifluoromethyl)benzene were added and the mixture was stirred at r.t. for 3 days. The solid was collected by filtration and the product was washed on a filter with ethanol, CH₂Cl₂, methanol, water, methanol, and hexanes and subsequently dried *in vacuo*. Functional group density based on F 1s and C 1s signals by XPS: 180 CNT carbon atoms per functional group.

Bis-U-SWCNT. 20 mg NH₂-SWCNT were sonicated for 5 min in 15 mL ethanol. 709 mg (1.0 mmol) **22** were added and the mixture was refluxed for 4 days. The solid was collected by filtration and the product was washed on a filter with ethanol, water, ethanol, CH₂Cl₂, and hexanes and subsequently dried *in vacuo*. Functional group density based on F 1s and C 1s signals by XPS: 130 CNT carbon atoms per functional group.

Bis-TU-SWCNT. 20 mg NH₂-SWCNT were sonicated for 5 min in 15 mL ethanol. 676 mg (1.0 mmol) **21** were added and the mixture was refluxed for 4 days. The solid was collected by filtration and the product was washed on a filter with ethanol, water, ethanol, CH₂Cl₂, and hexanes and subsequently dried *in vacuo*. Functional group density based on F 1s and C 1s signals by XPS: 100 CNT carbon atoms per functional group.

Device preparation

Glass slides (VWR Microscope Slides) were cleaned by ultrasonication in acetone for 10 min, and after drying they were subjected to UV radiation in a UVO cleaner (Jelight Company Inc.) for 3 min. Using an aluminum mask, layers of chromium (10 nm) and gold (75 nm) were deposited leaving a 1 mm gap using a metal evaporator purchased from Angstrom Engineering with home built aluminum shadow masks.

Pristine SWCNTs were added to CH_2Cl_2 at a concentration of 1 mg per 5 mL, NH_2 -SWCNTs were added to ethanol and all other functionalized SWCNTs were added to 1:1 mixtures of CH_2Cl_2 /*iso*-propanol at the same concentration. The samples were sonicated for 2 min (bath sonicator). Volumes of 1 μL of the respective SWCNT dispersion were drop-cast between the gold electrodes until a resistance of 5-20 $\text{k}\Omega$ was achieved.

Sensing measurements

The devices were enclosed in a homemade Teflon gas flow chamber for sensing measurement. The low concentration gas mixtures were produced using a KIN-TEK gas generator system. A trace amount of analyte emitted from a permeation tube is mixed with a nitrogen stream (oven flow), which can be further diluted with nitrogen (dilution flow) (Figure 6.6). We performed calibration measurements by placing the analyte in the oven flow for set amounts of time and determined its weight loss.

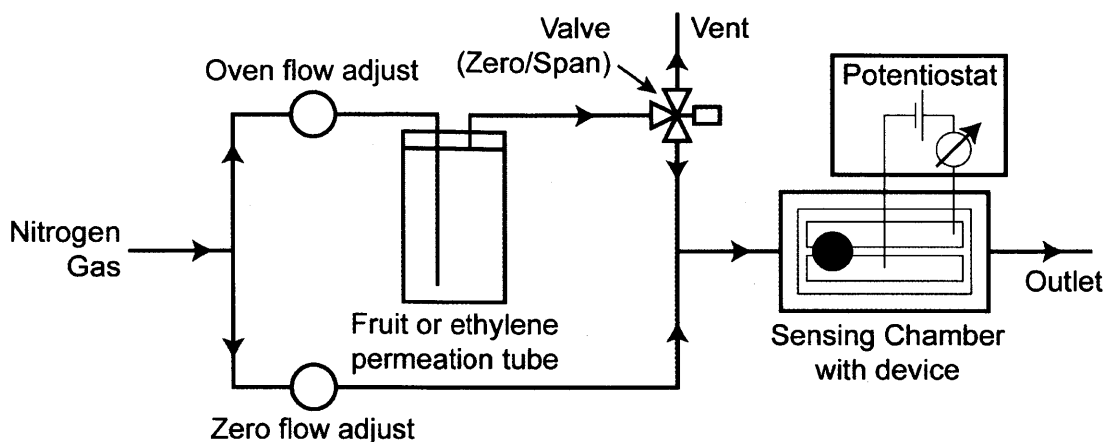


Figure 4.19. Experimental setup for sensing measurements: A continuous gas flow is directed through the device chamber. The gas stream can be switched between nitrogen gas (“Zero” mode) or the nitrogen gas analyte mixture (“Span” mode), in which the gas stream runs through the flow chamber containing the analyte.

Electrochemical measurements were performed using a PalmSens handheld potentiostat (PalmSens Instruments) for single device measurements or a EmStat-MUX handheld potentiostat (PalmSens Instruments) for array measurements. A constant bias voltage of 0.1 V was applied across the device, while current vs. time was measured. During the measurement the volume of gas flow over the device was held constant and switched between nitrogen and analyte/nitrogen.

NMR binding studies

The receptor was dissolved in CDCl_3 at a concentration of 0.01 M (for **14-17**) or 2.5 mM (for **22**) and a ^1H NMR spectrum was measured. Subsequently, **2** was added to achieve a ratio of **2** to the receptor of 0.1, 0.3, 0.5, 0.7, 0.9, 1.0, 3.0, 5.0, 10.0, 15.0, 20.0, 25.0, and 50.0 (for **14-17**) and 0.1, 0.3, 0.5, 0.7, 0.8, 1.0, 2.7, 4.4, 8.4, 12.5, 16.6, 20.7, 24.7, 40.4, and 144 (for **22**). A ^1H NMR spectrum was recorded after every addition and the chemical shifts of the protons were recorded. Using the software package WinEQNMR2 with the chemical shifts of the NH and aromatic

protons (for **14-17**) or proton at the 4-position of the CF₃-substituted phenyl group in **22** (labeled h' in **Figure 4.14**), association constants were determined.

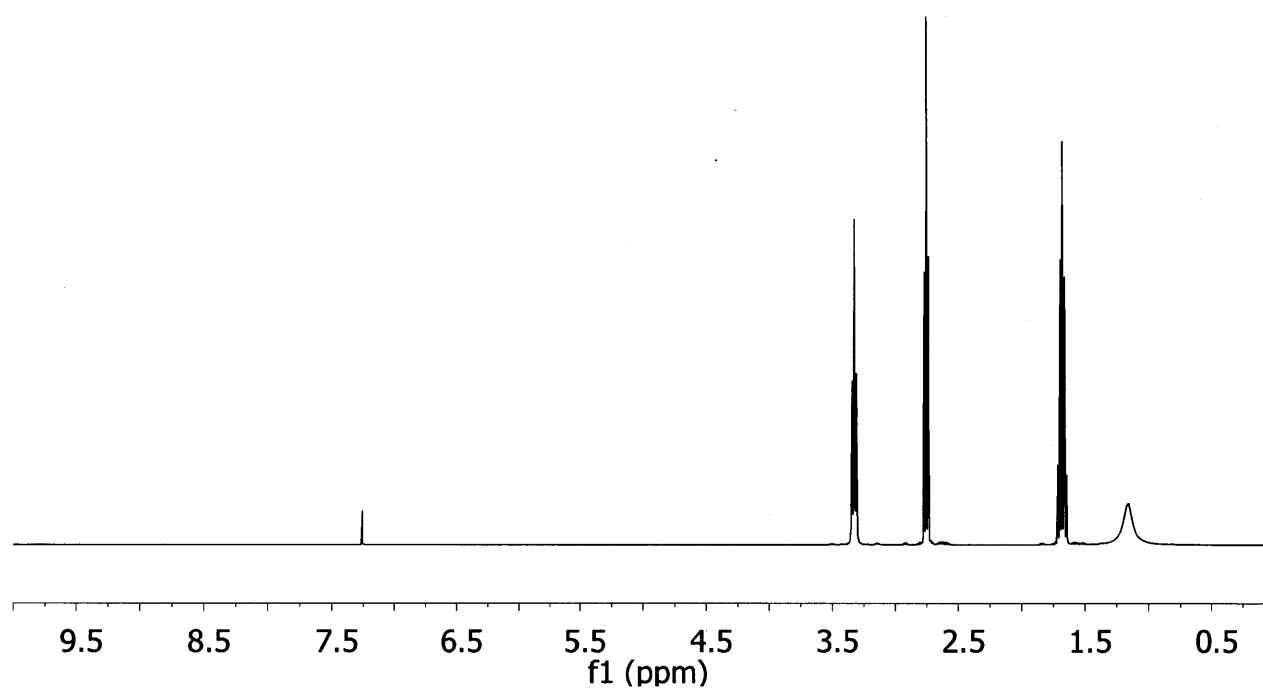


Figure 4.20. ^1H NMR Spectrum of 3 (CDCl_3)

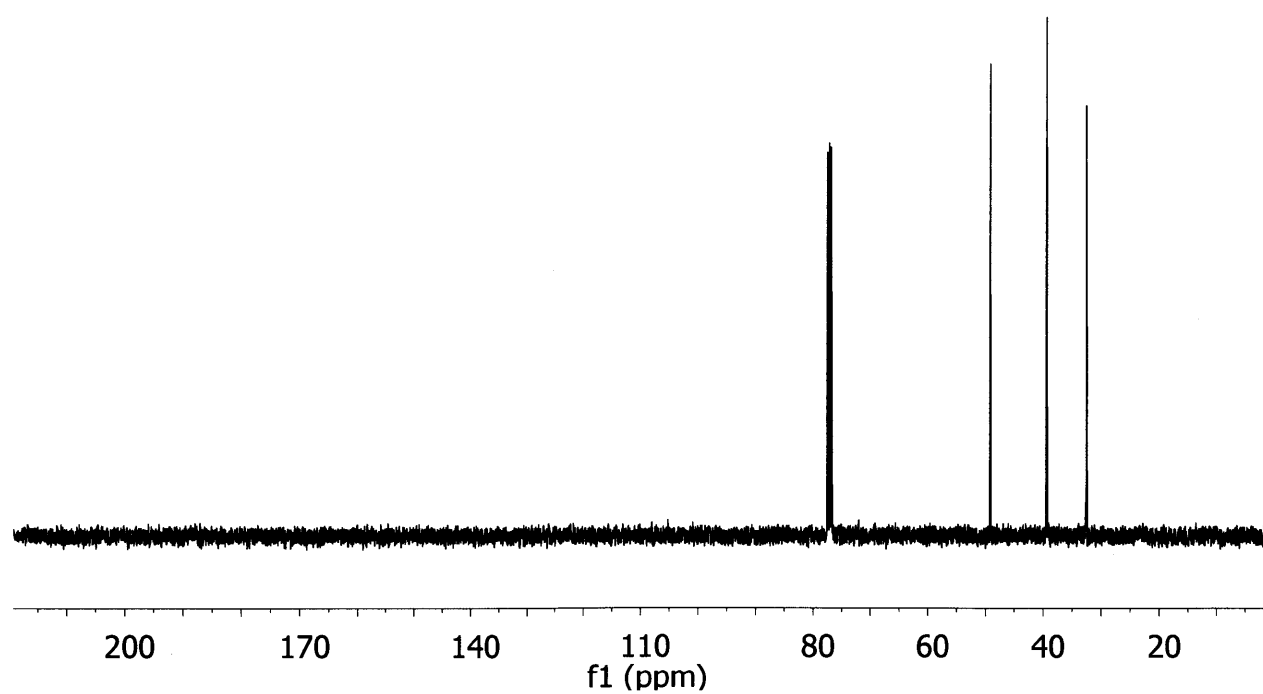


Figure 4.21. ^{13}C NMR Spectrum of 3 (CDCl_3)

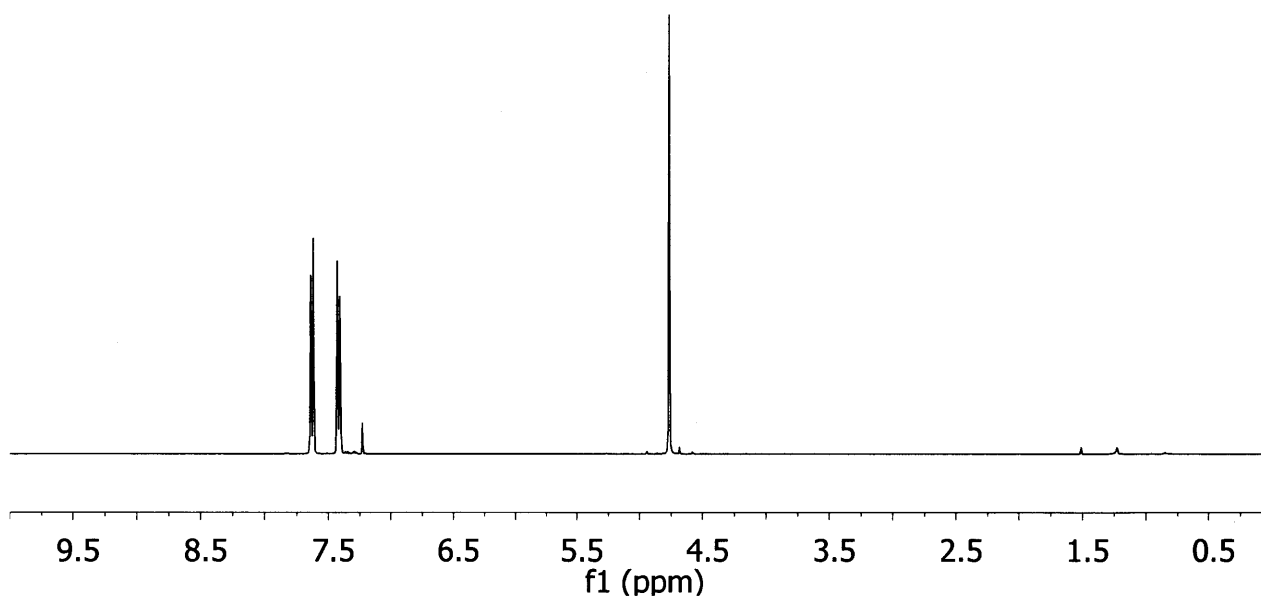


Figure 4.22. ^1H NMR Spectrum of 6 (CDCl_3)

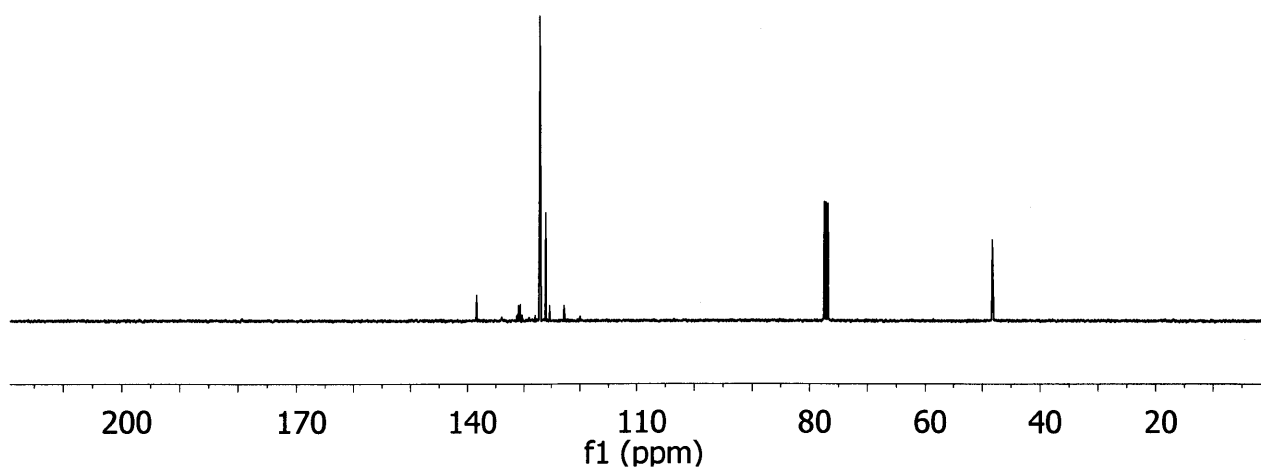


Figure 4.23. ^{13}C NMR Spectrum of 6 (CDCl_3)

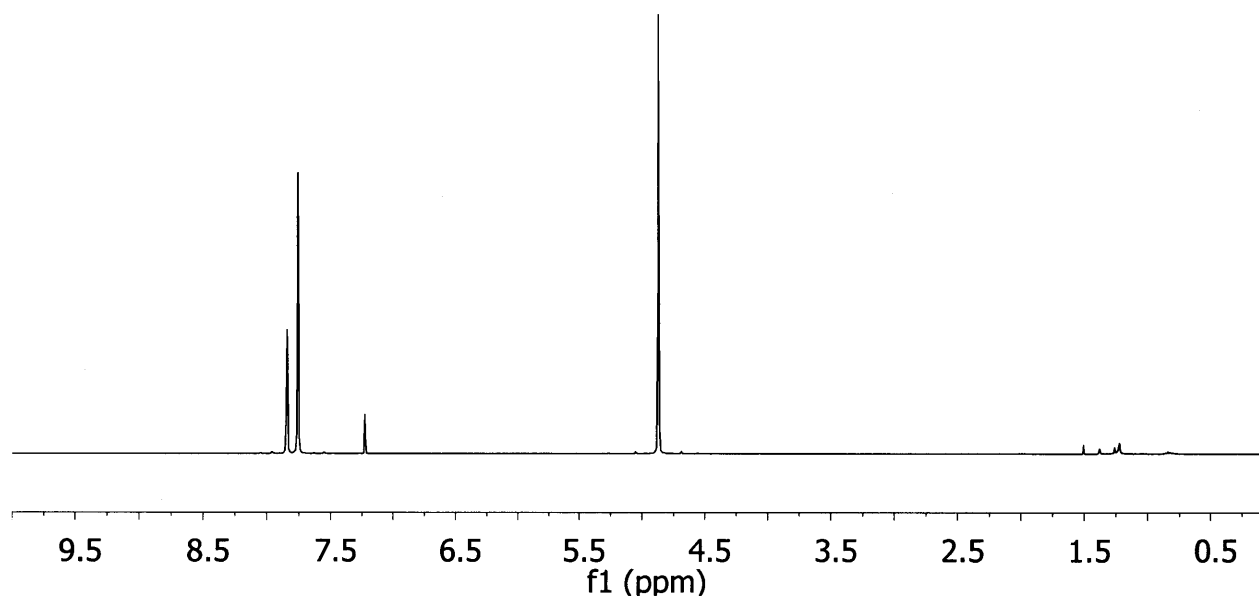


Figure 4.24. ¹H NMR Spectrum of **8** (CDCl₃)

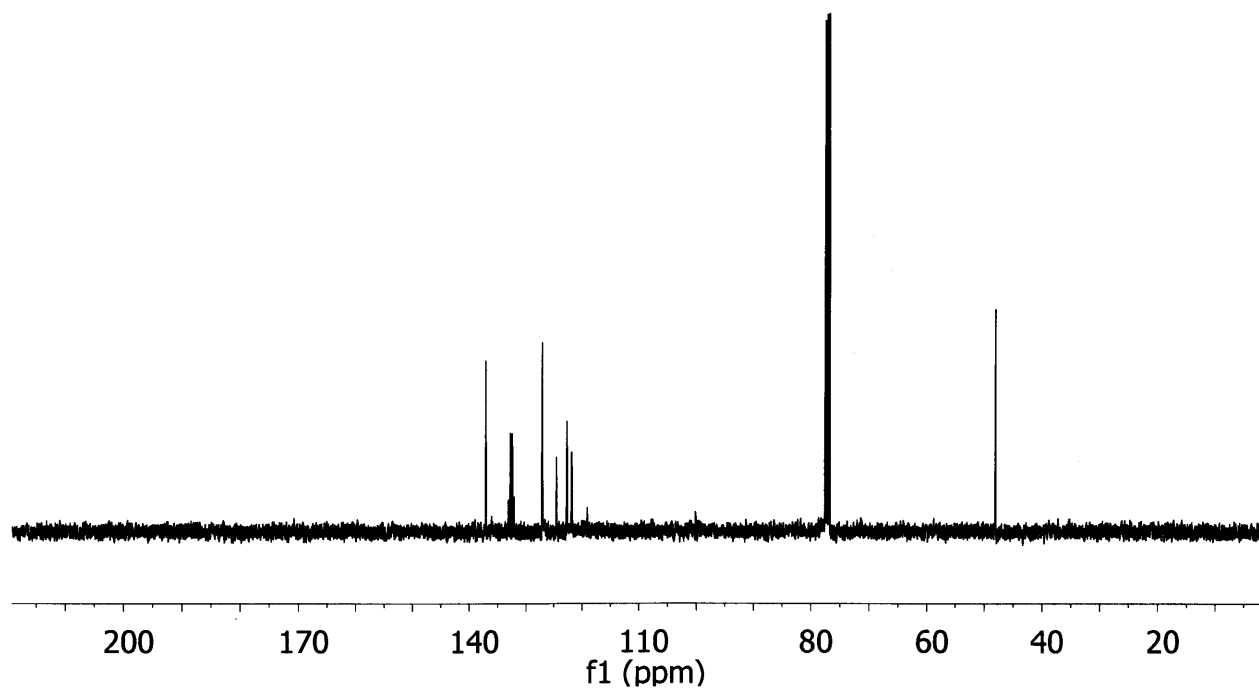


Figure 4.25. ¹³C NMR Spectrum of **8** (CDCl₃)

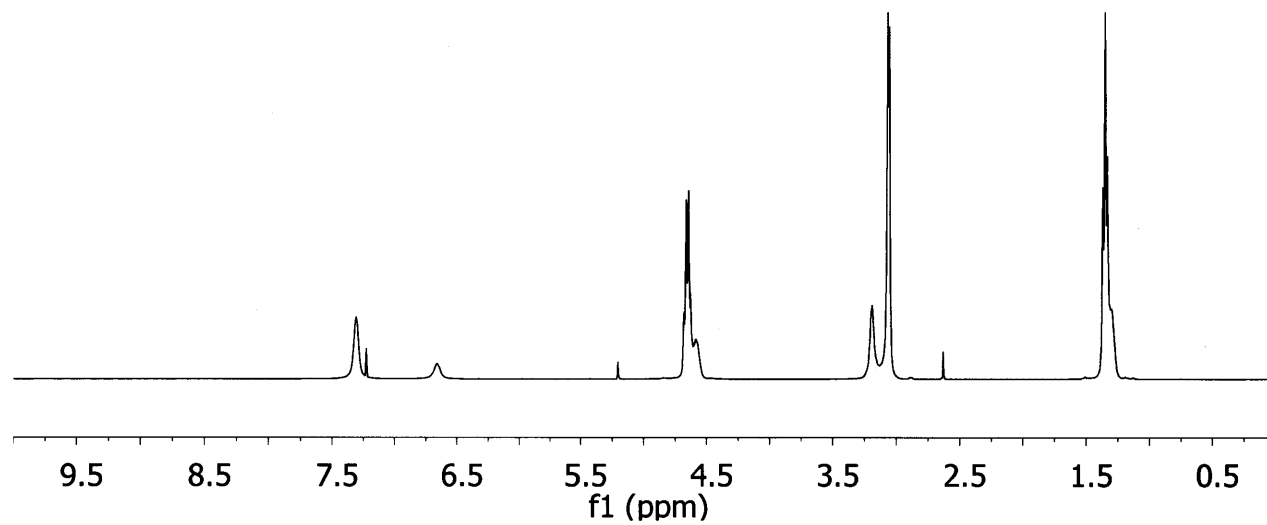


Figure 4.26. ^1H NMR Spectrum of **11** (CDCl_3)

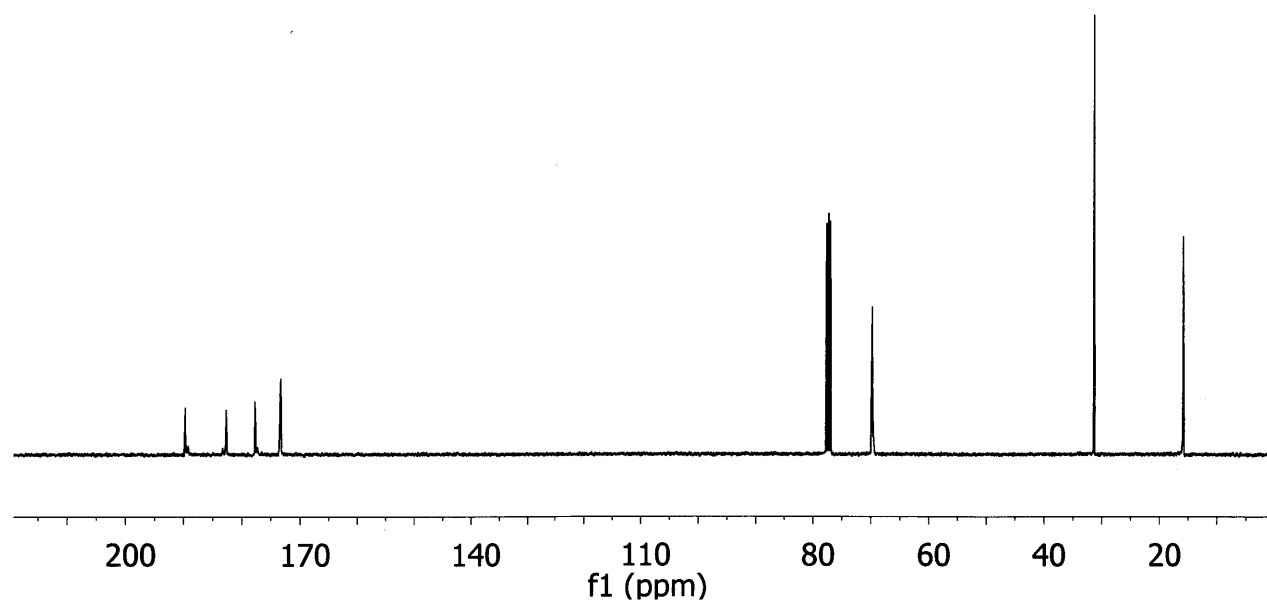


Figure 4.27. ^{13}C NMR Spectrum of **11** (CDCl_3)

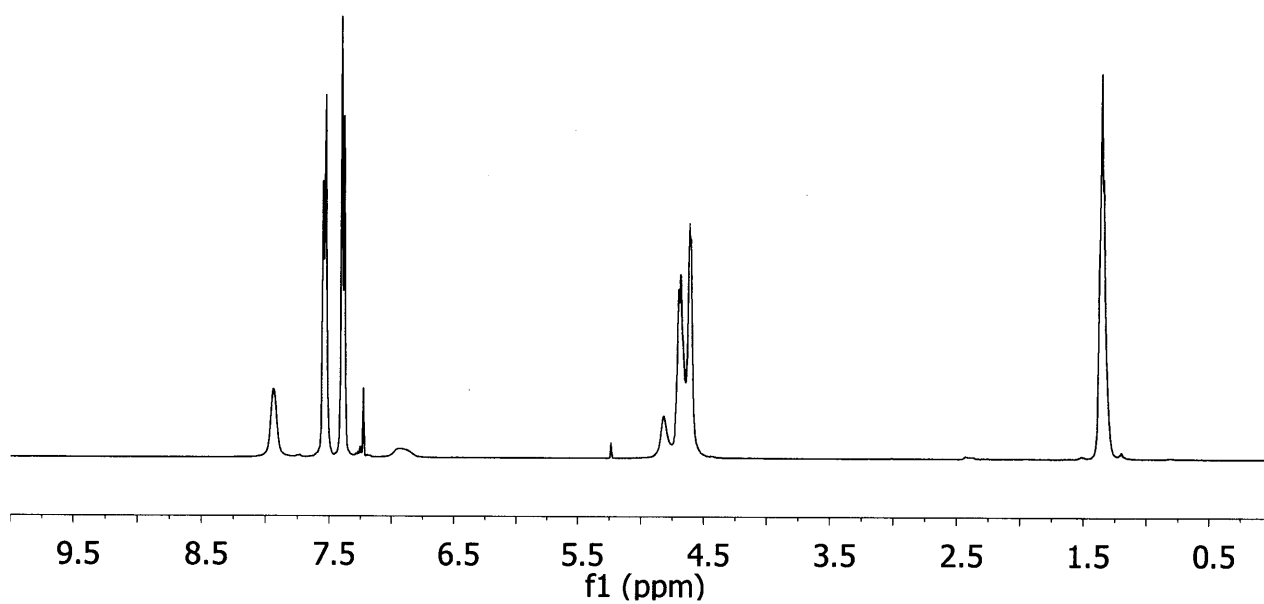


Figure 4.28. ^1H NMR Spectrum of 12 (CDCl_3)

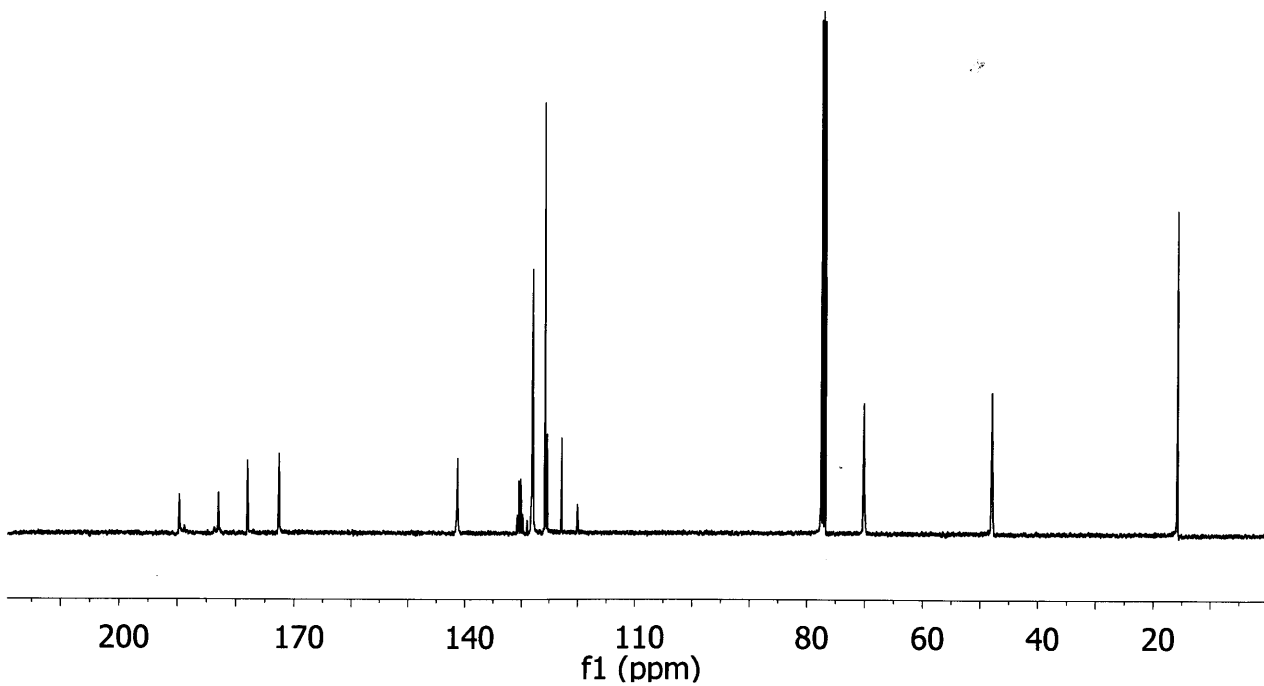


Figure 4.29. ^{13}C NMR Spectrum of 12 (CDCl_3)

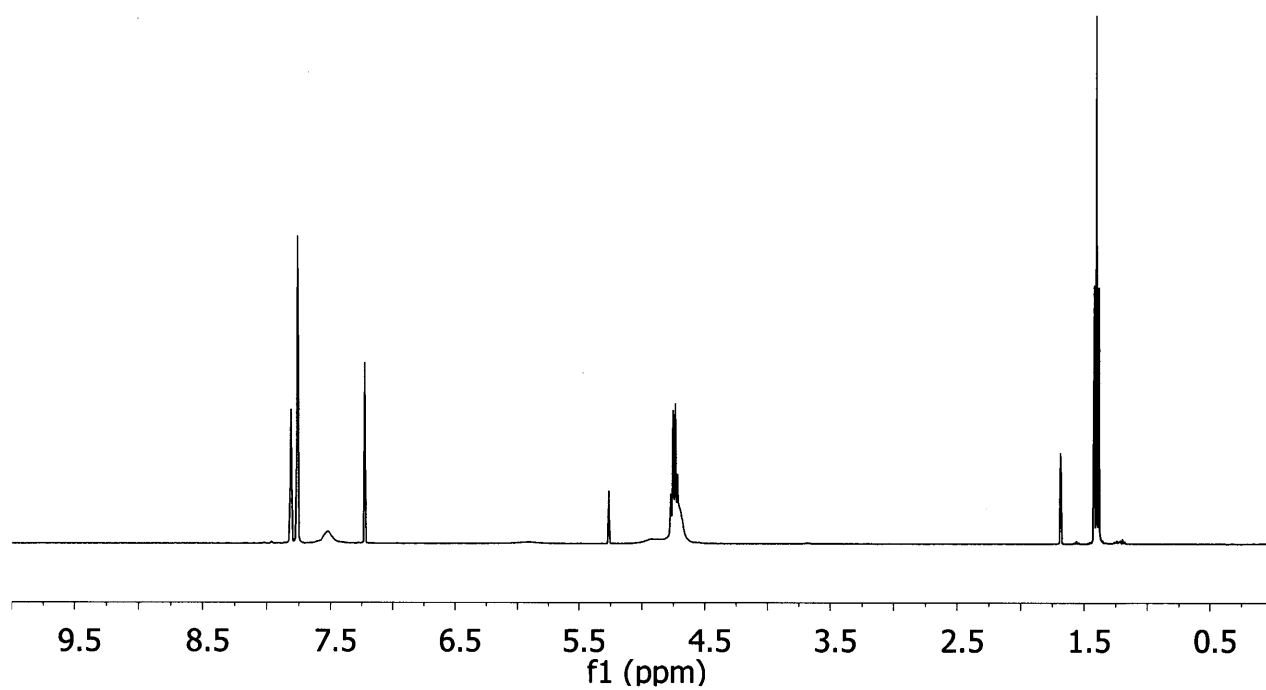


Figure 4.30. ^1H NMR Spectrum of **13** (CDCl_3)

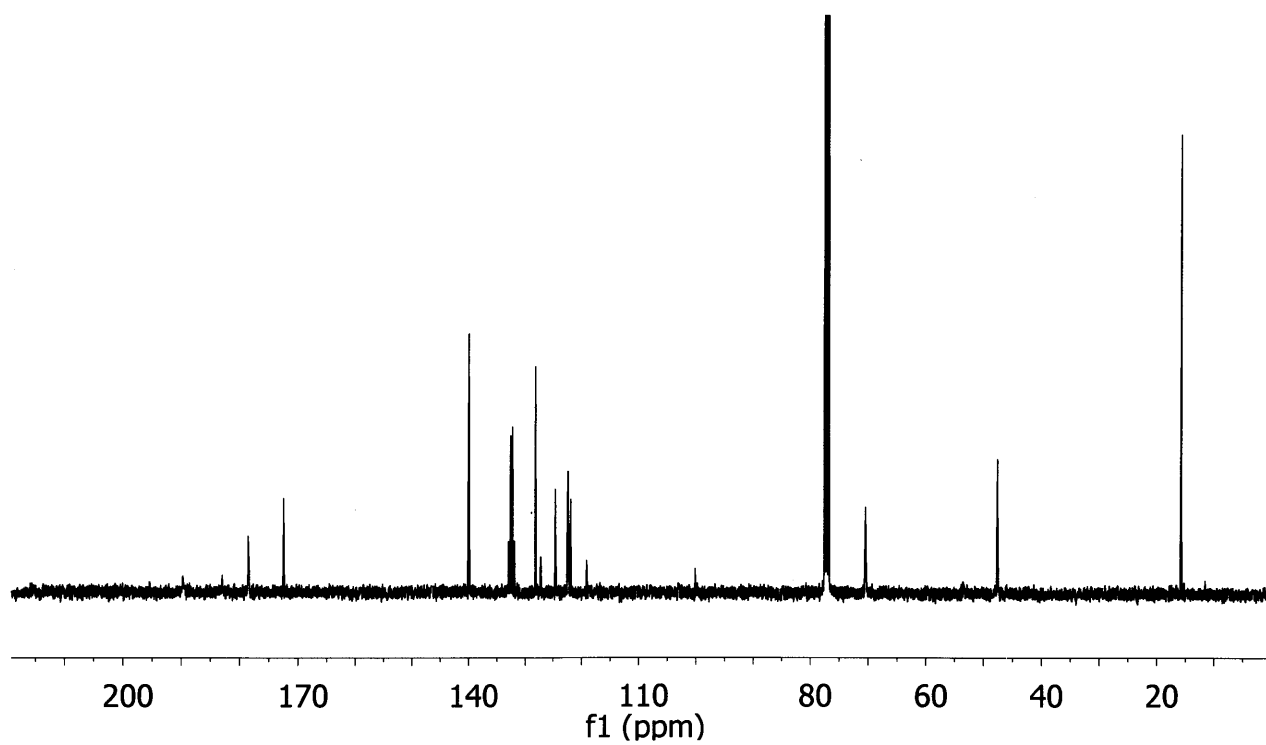


Figure 4.31. ^{13}C NMR Spectrum of **13** (CDCl_3)

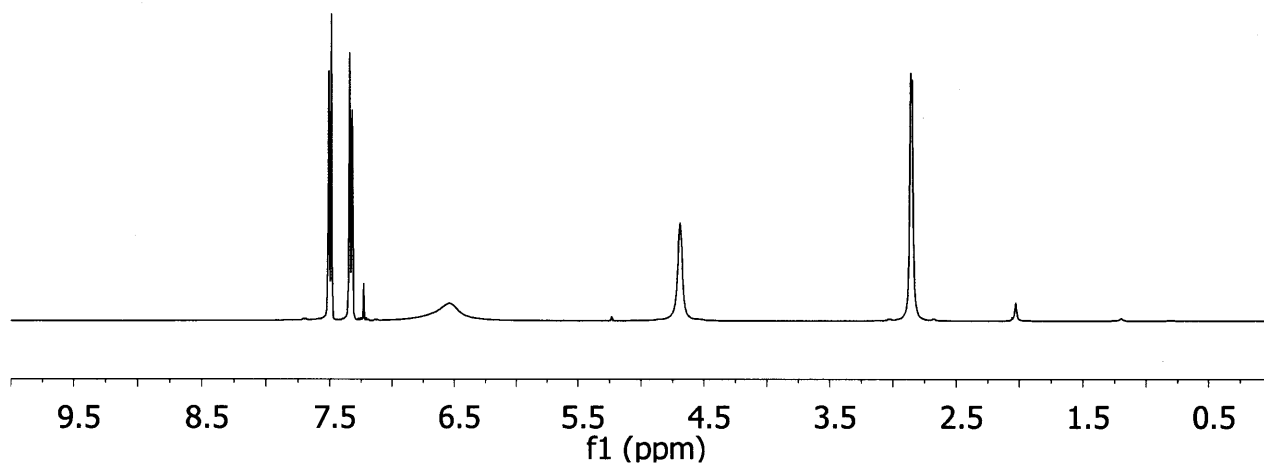


Figure 4.32. ^1H NMR Spectrum of **14** (CDCl_3)

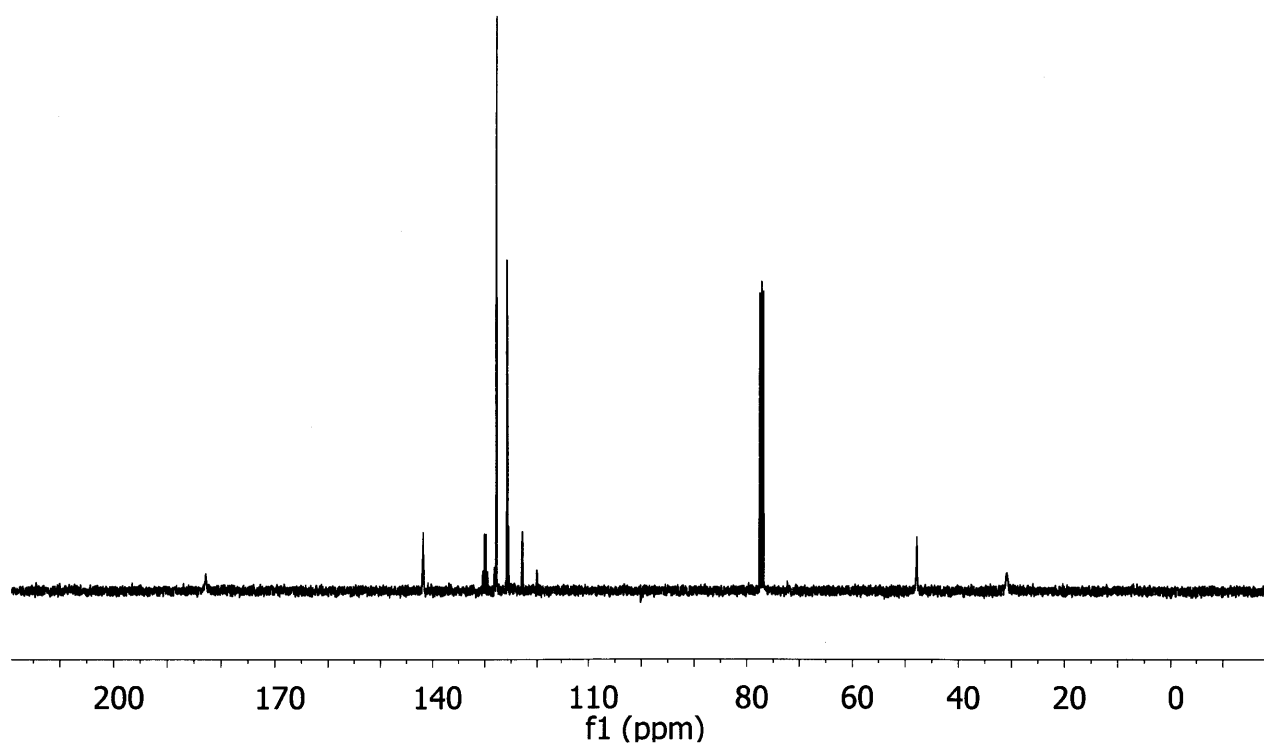


Figure 4.33. ^{13}C NMR Spectrum of **14** (CDCl_3)

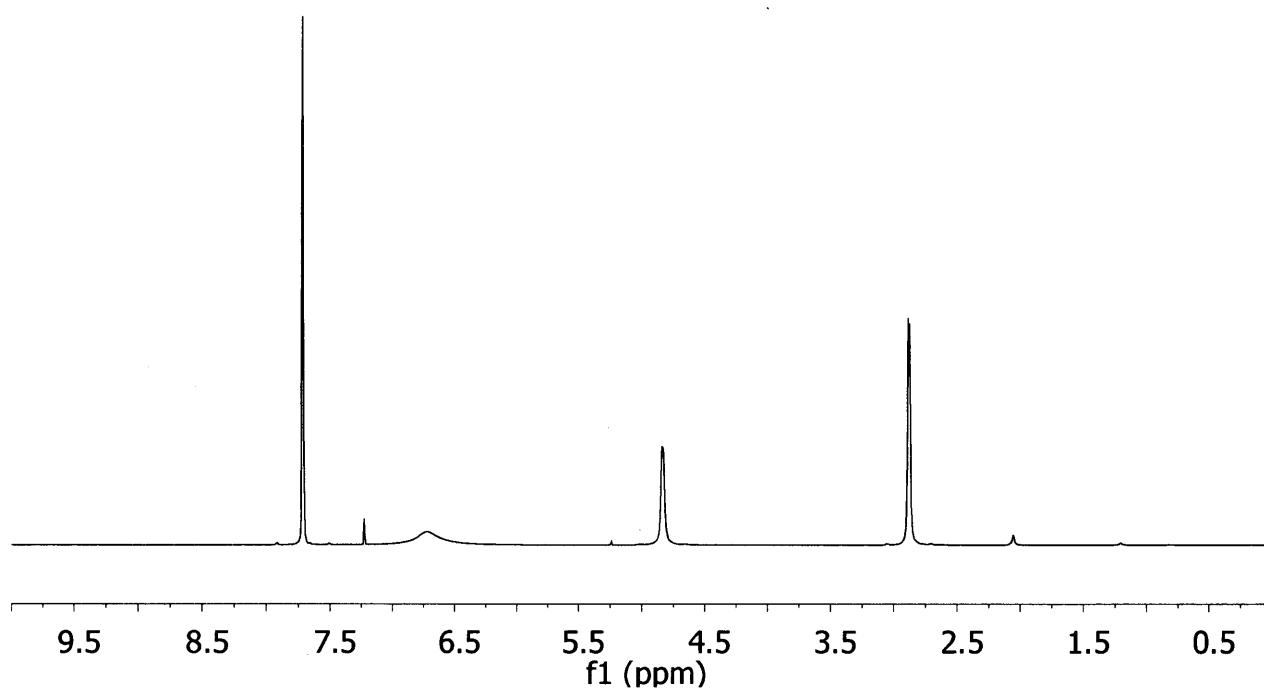


Figure 4.34. ^1H NMR Spectrum of **15** (CDCl_3)

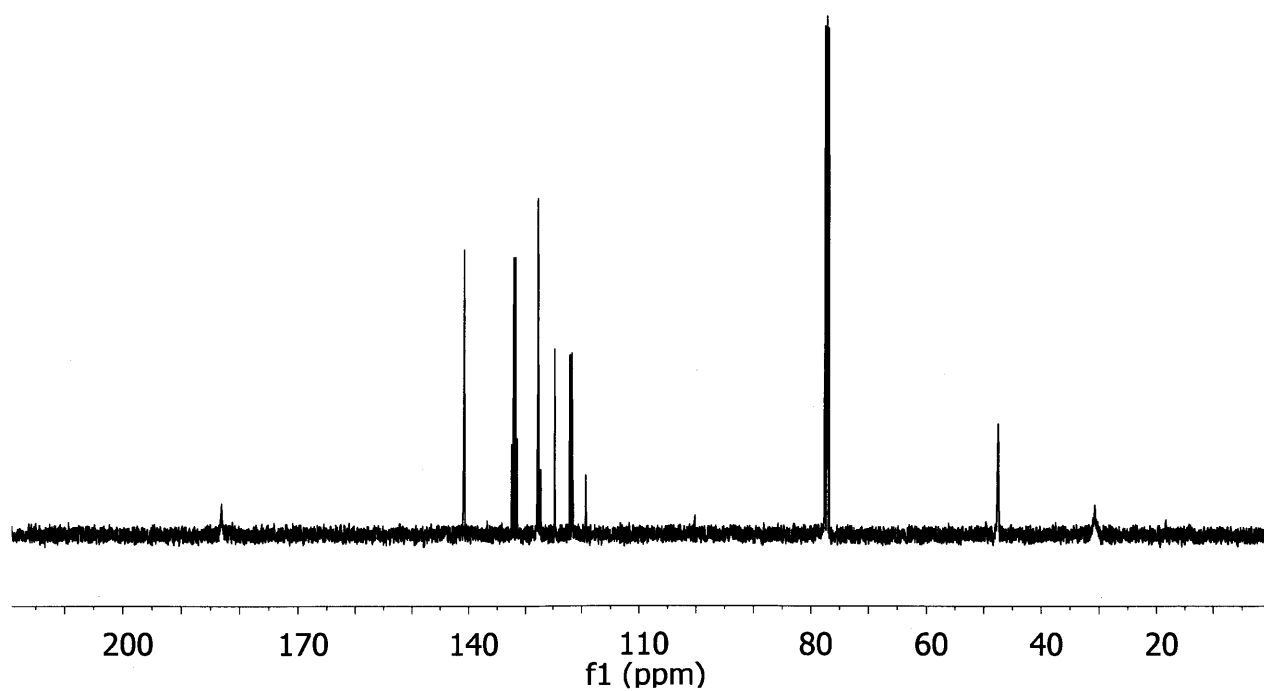


Figure 4.35. ^{13}C NMR Spectrum of **15** (CDCl_3)

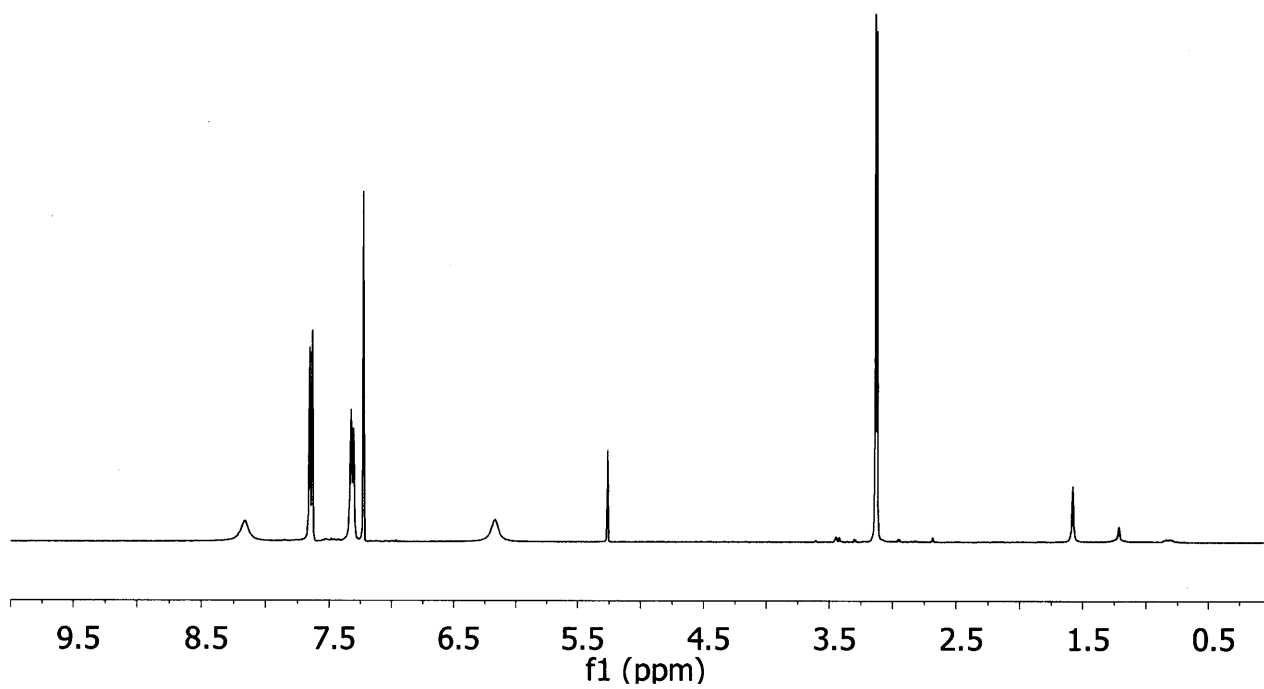


Figure 4.36. ^1H NMR Spectrum of 16 (CDCl_3)

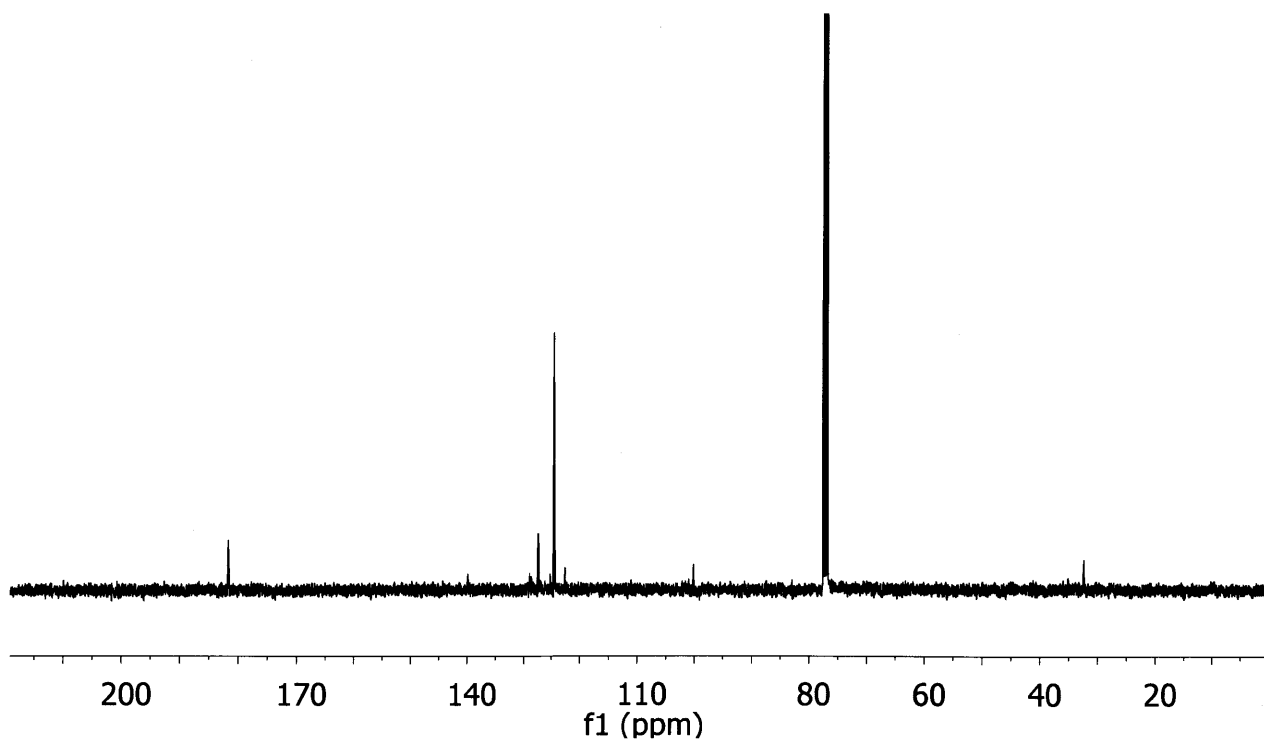


Figure 4.37. ^{13}C NMR Spectrum of 16 (CDCl_3)

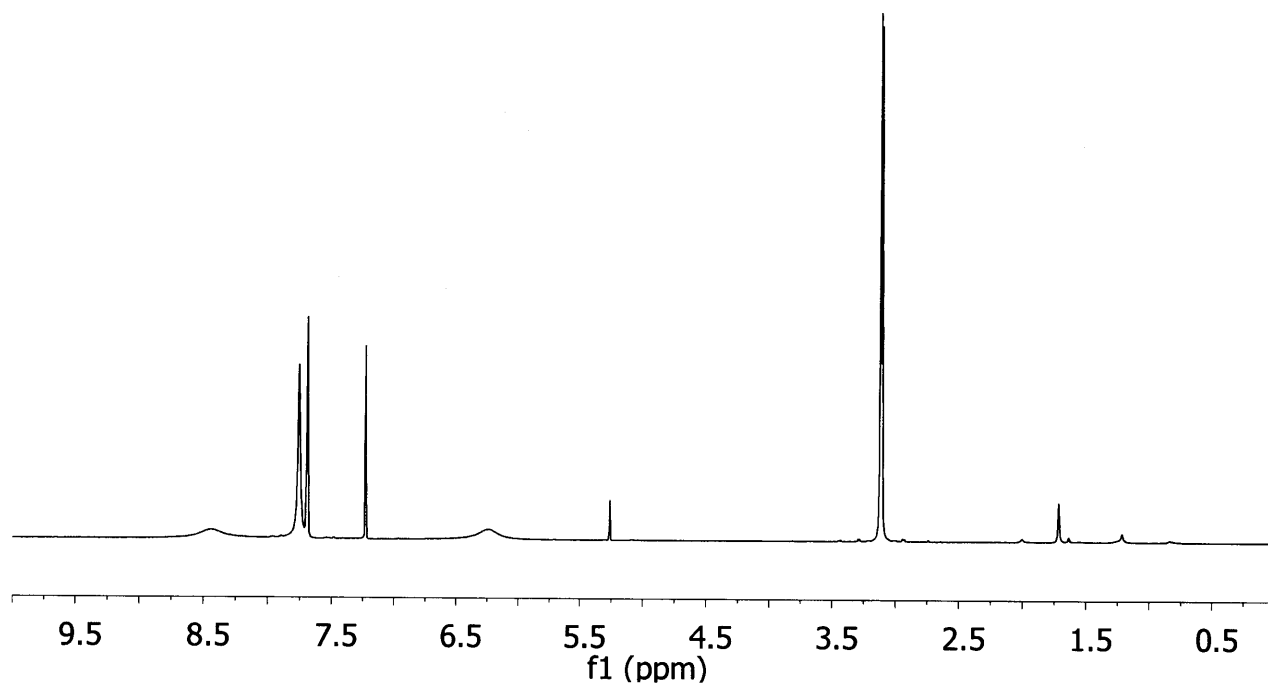


Figure 4.38. ^1H NMR Spectrum of **17** (CDCl_3)

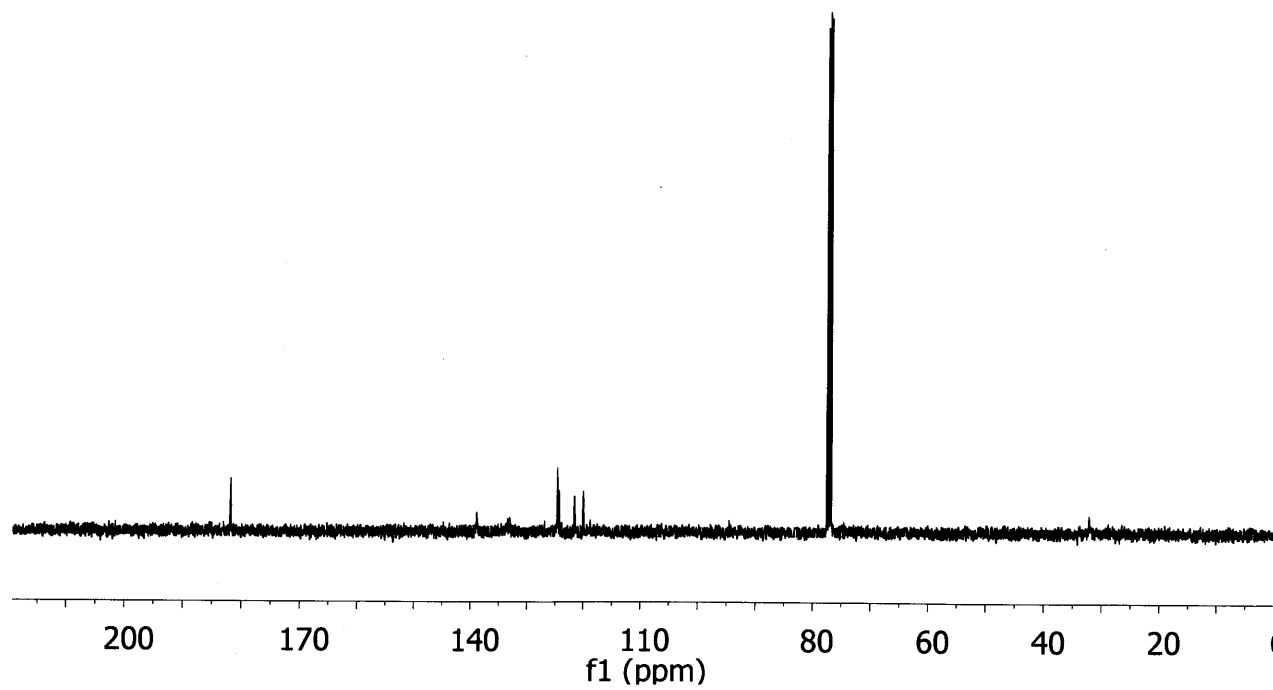


Figure 4.39. ^{13}C NMR Spectrum of **17** (CDCl_3)

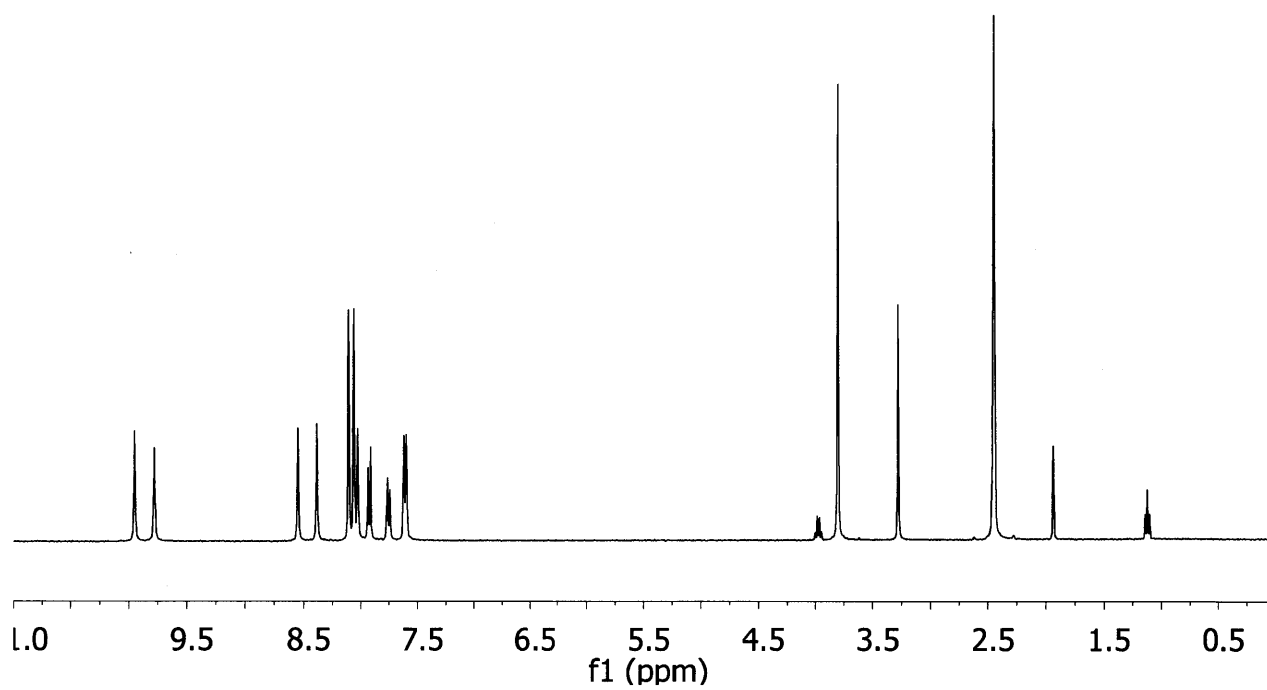


Figure 4.40. ^1H NMR Spectrum of **21** ($\text{DMSO-}d_6$)

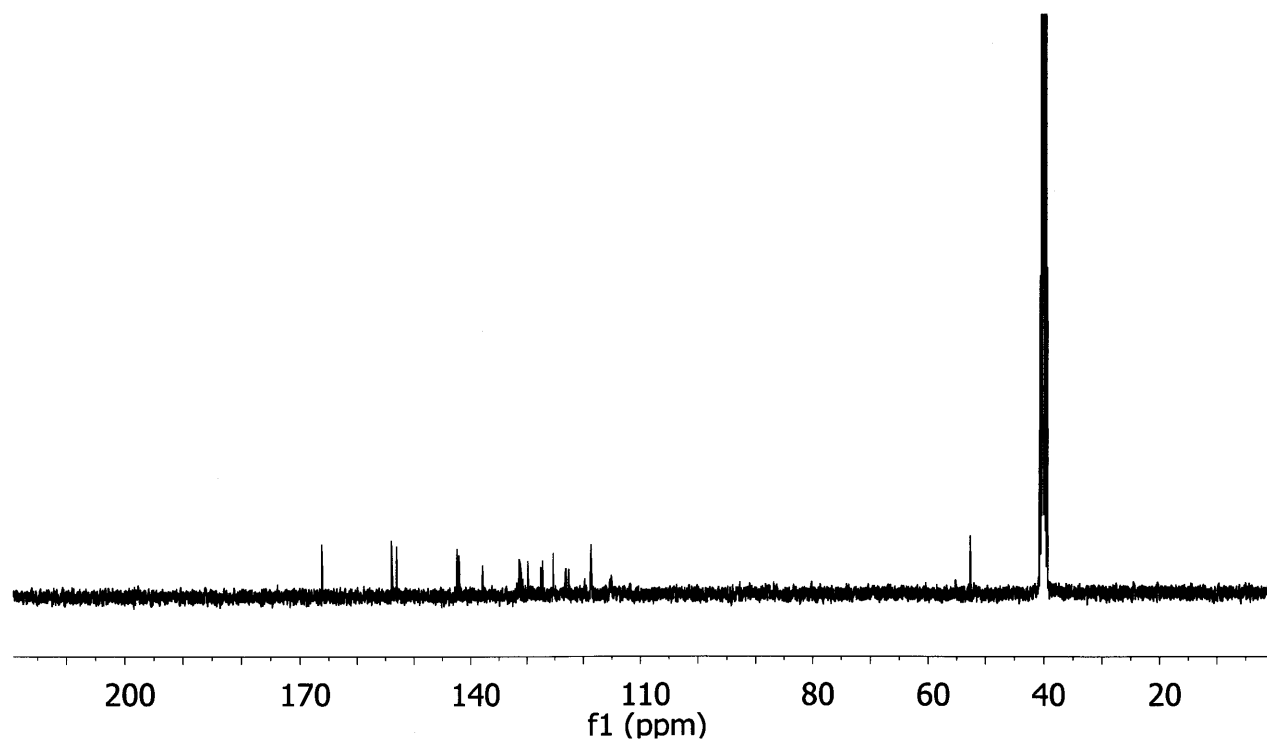


Figure 4.41. ^{13}C NMR Spectrum of **21** ($\text{DMSO-}d_6$)

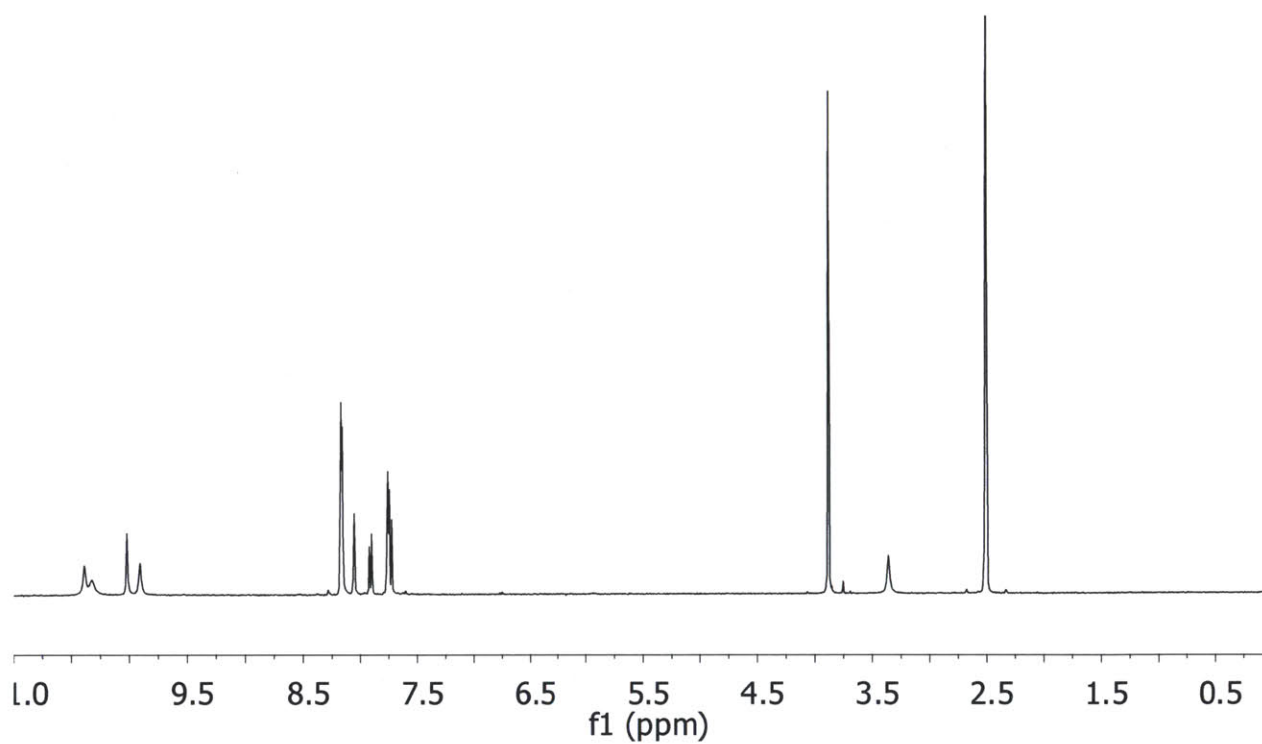


Figure 4.42. ^1H NMR Spectrum of **22** ($\text{DMSO-}d_6$)

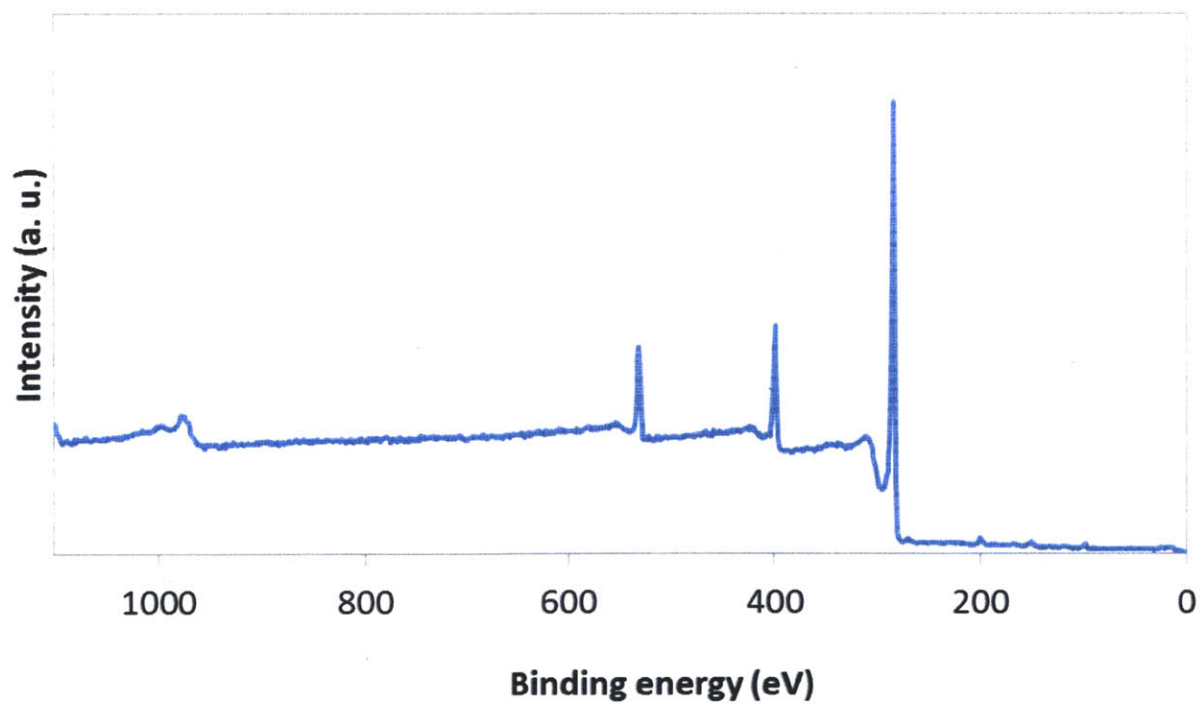


Figure 4.43. XPS analysis of NH_2 -SWCNT

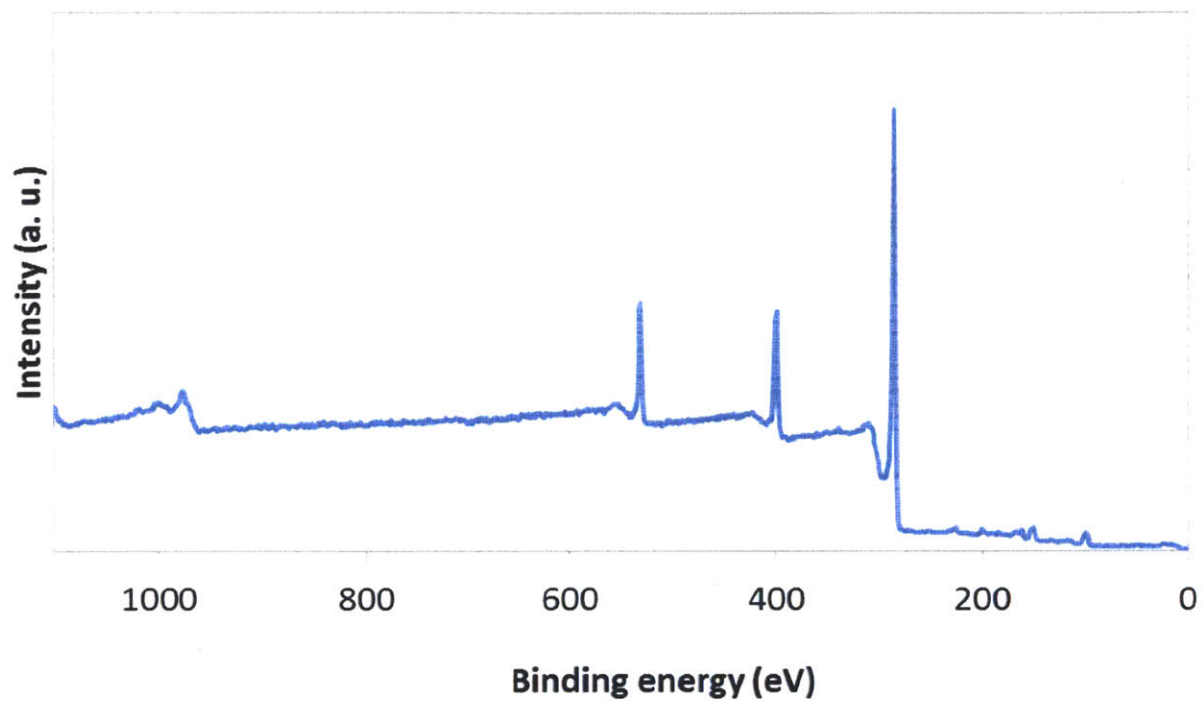


Figure 4.44. XPS analysis of Me-TU-SWCNT

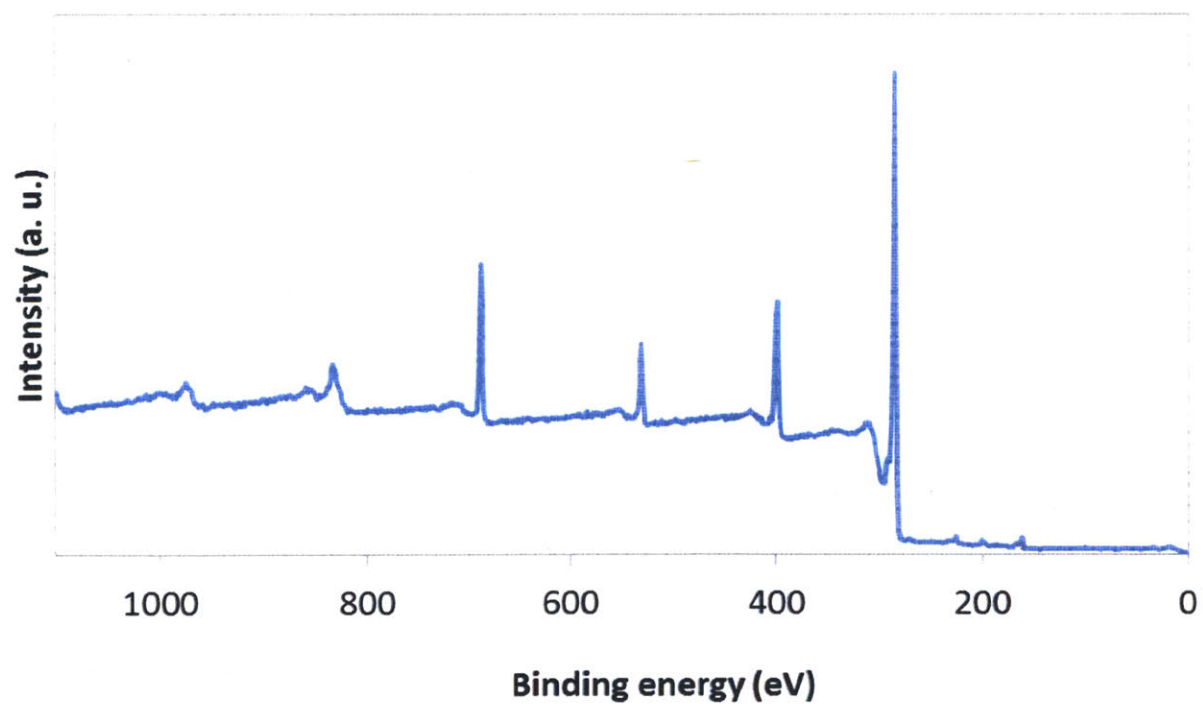


Figure 4.45. XPS analysis of p-CF₃-Bn-TU-SWCNT

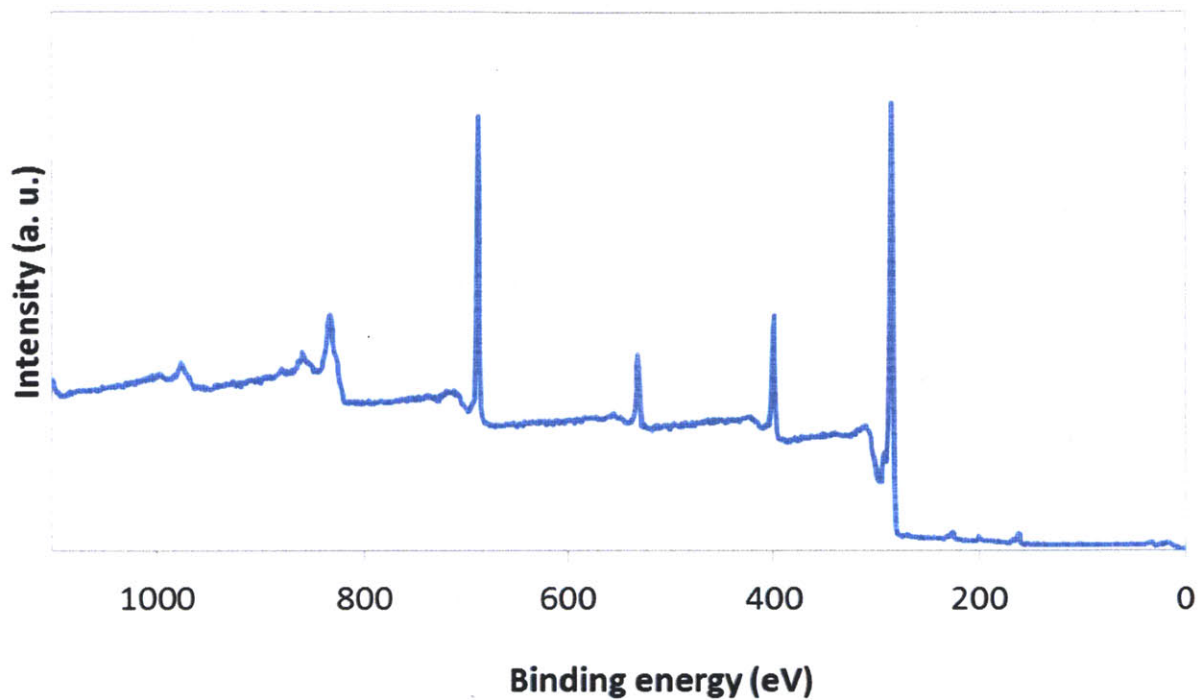


Figure 4.46. XPS analysis of m-CF₃-Bn-TU-SWCNT

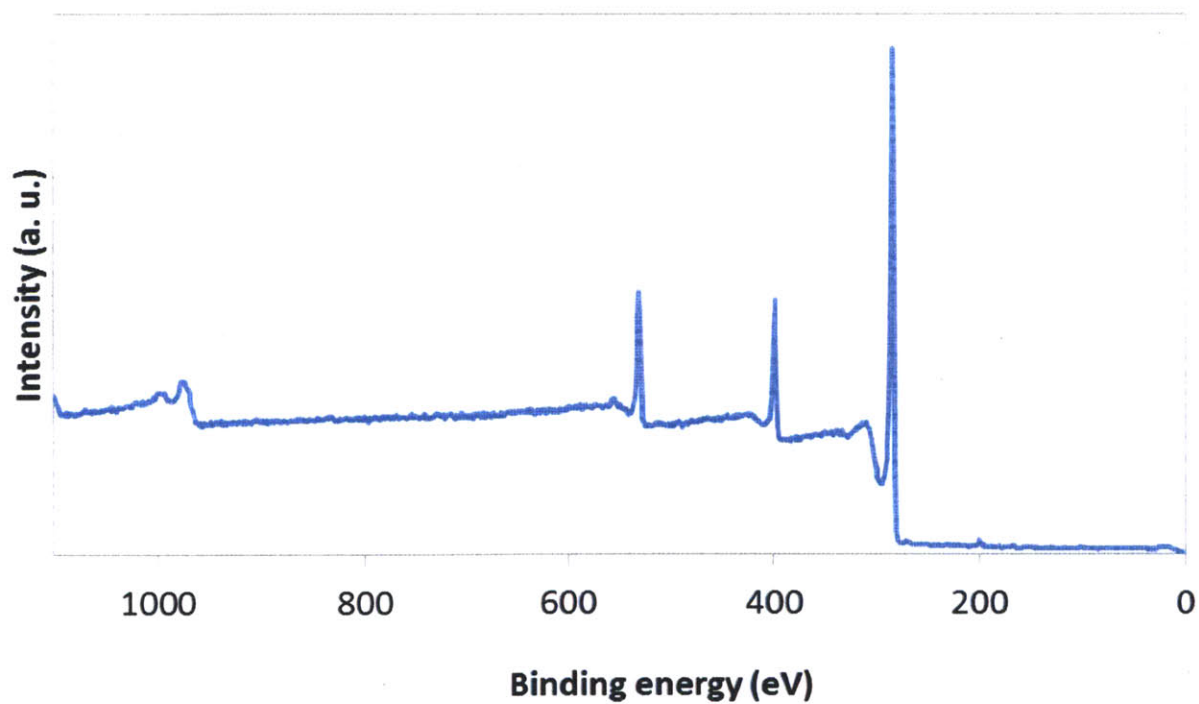


Figure 4.47. XPS analysis of Me-SQ-SWCNT

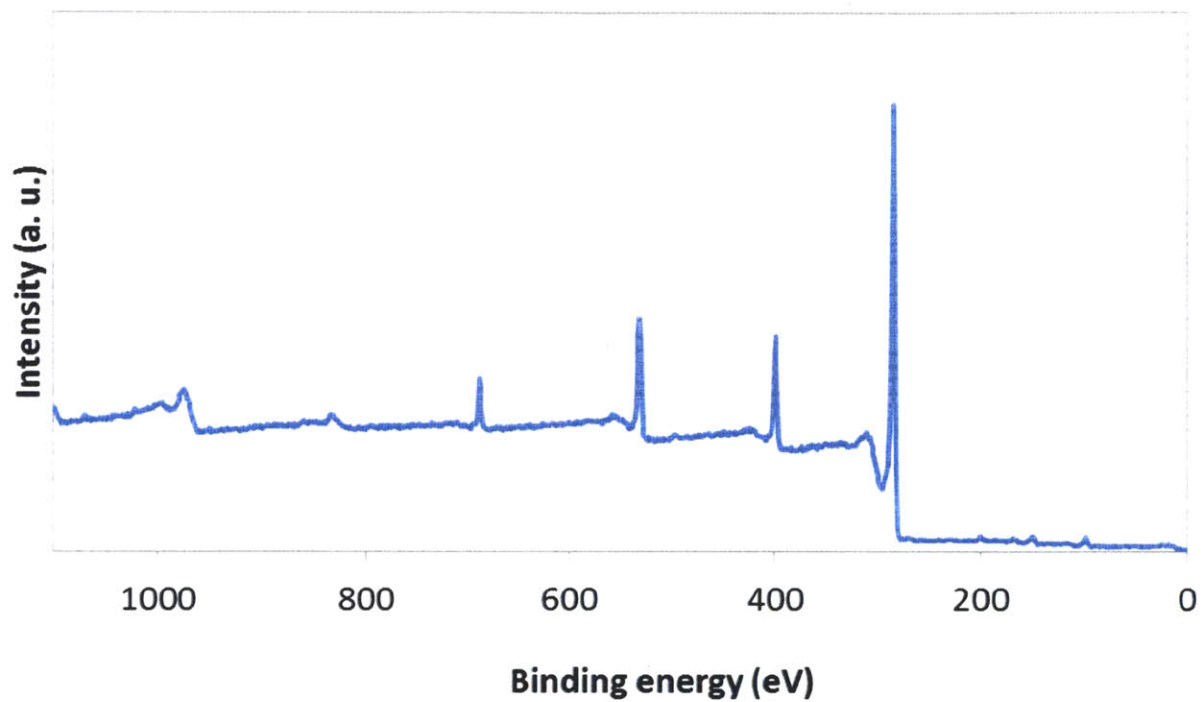


Figure 4.48. XPS analysis of p-CF₃-Bn-SQ-SWCNT

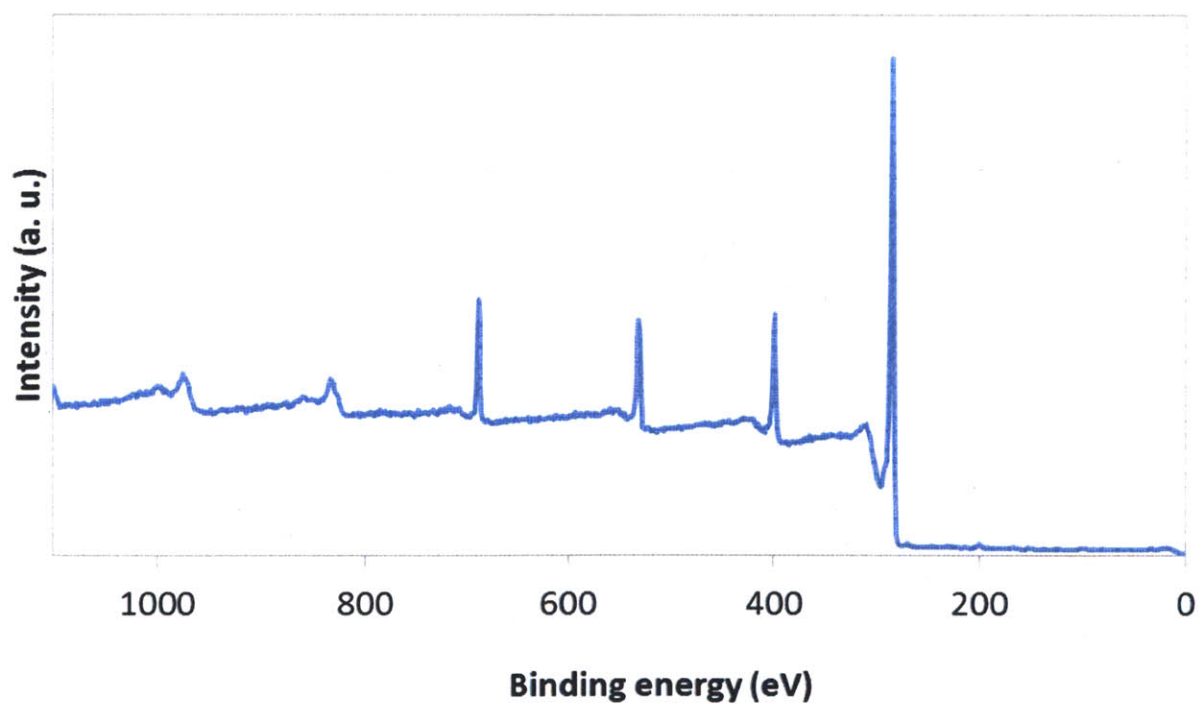


Figure 4.49. XPS analysis of m-CF₃-Bn-SQ-SWCNT

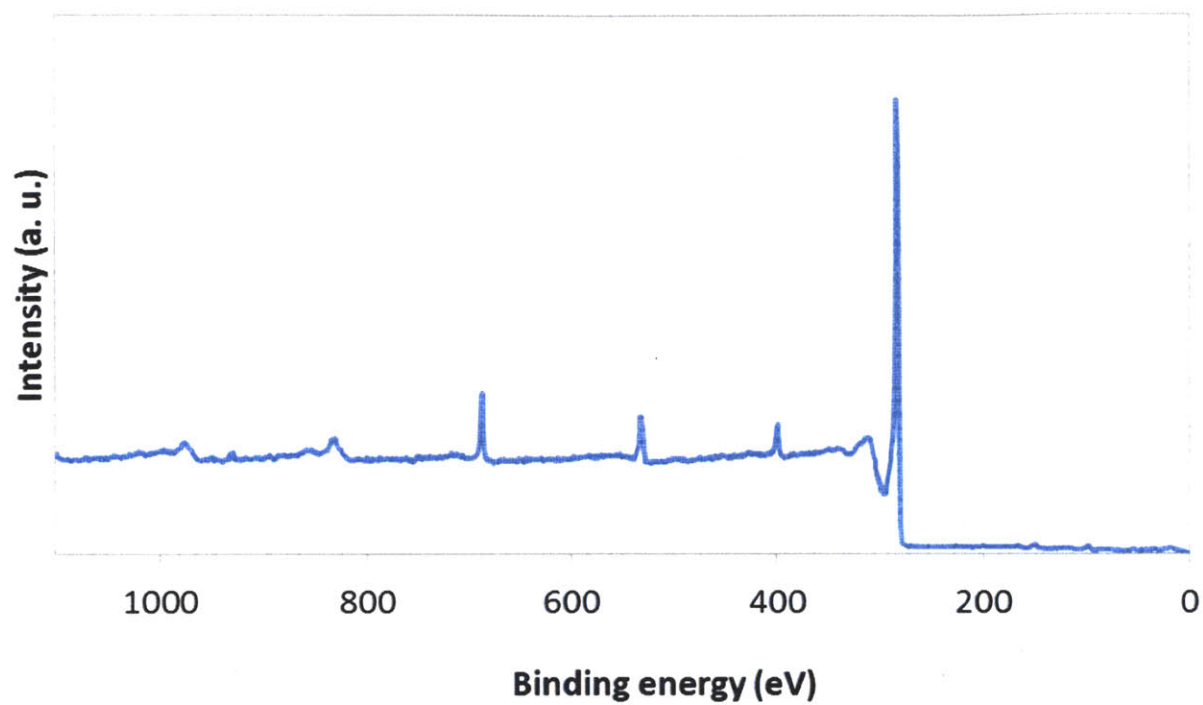


Figure 4.50. XPS analysis of m-CF₃-Ph-TU-SWCNT

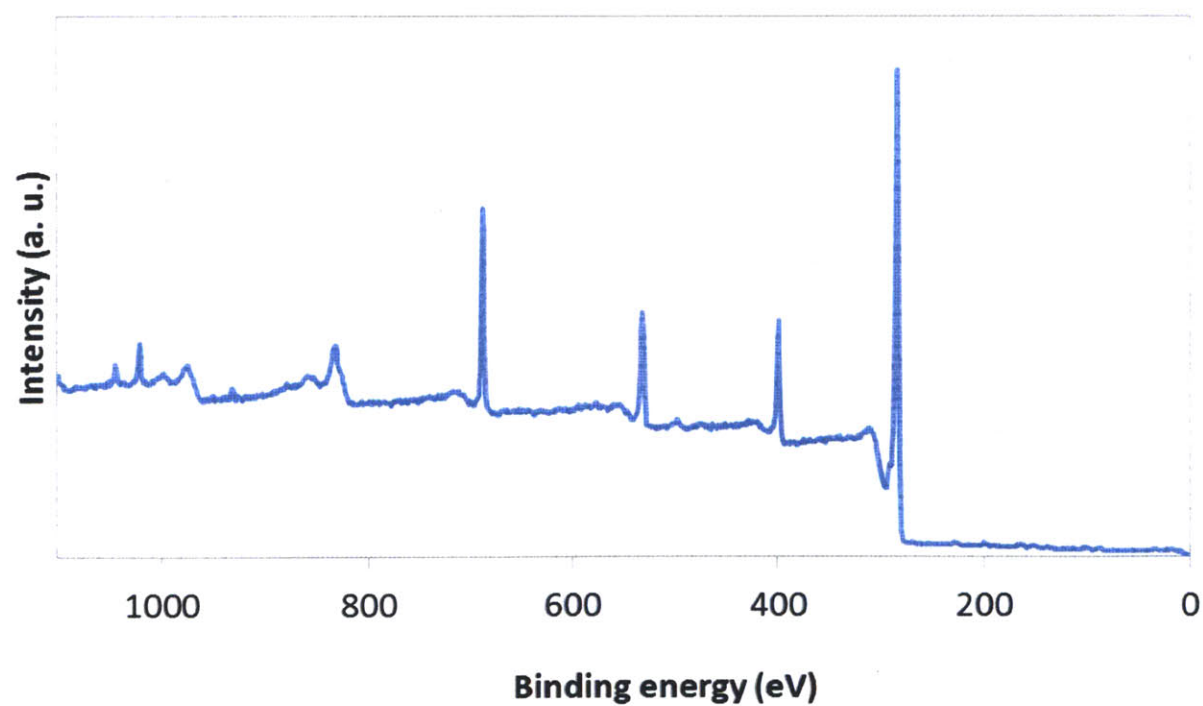


Figure 4.51. XPS analysis of Bis-U-SWCNT

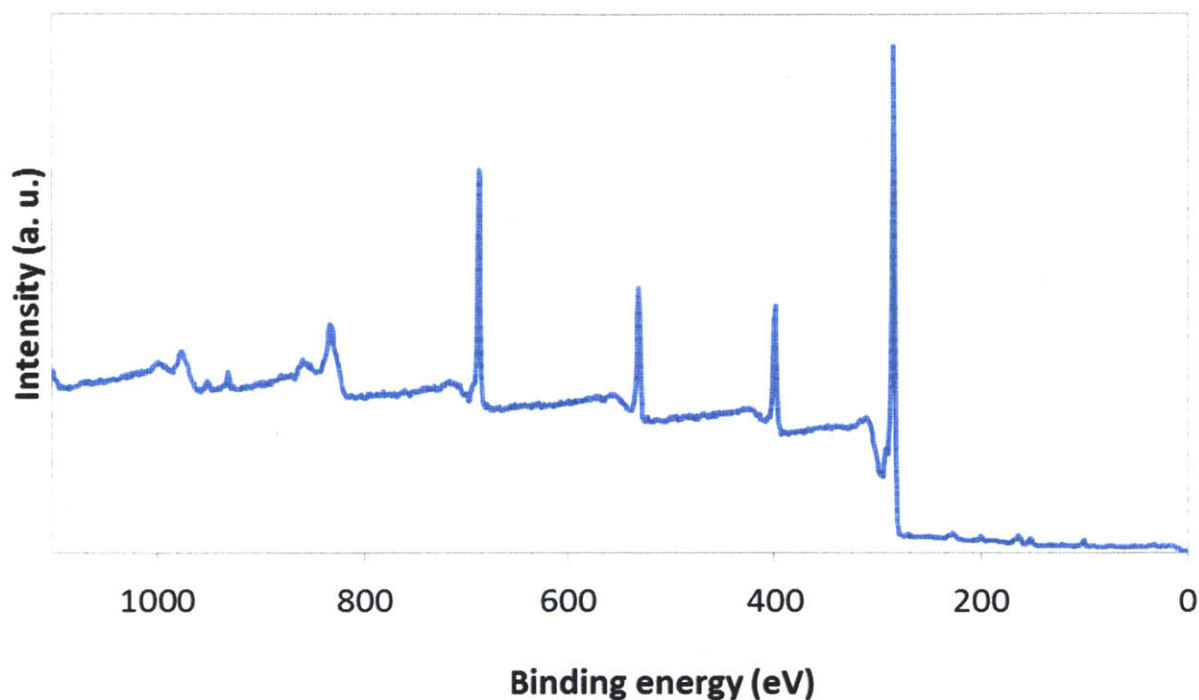


Figure 4.52. XPS analysis of Bis-TU-SWCNT

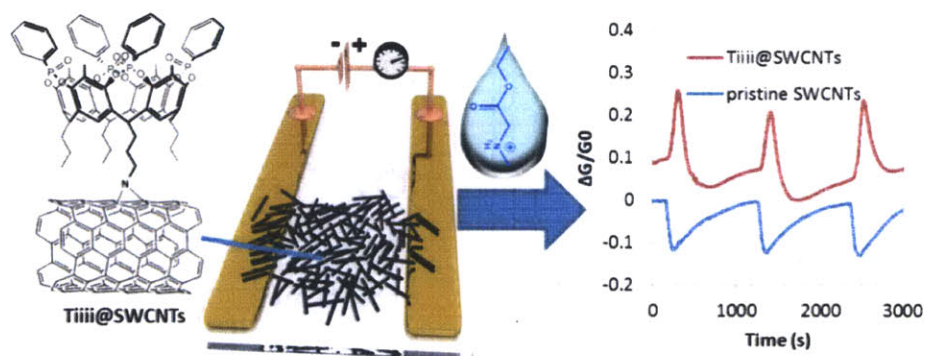
4.5. References

- (1) Schnorr, J. M.; Swager, T. M. *Chem. Mater.* **2011**, *23*, 646.
- (2) Swager, T. M. *Accounts Chem. Res.* **1998**, *31*, 201.
- (3) Salehi-Khojin, A.; Khalili-Araghi, F.; Kuroda, M. a; Lin, K. Y.; Leburton, J.-P.; Masel, R. I. *ACS nano.* **2011**, *5*, 153-8.
- (4) Senesac, L.; Thundat, T. G. *Materials Today.* **2008**, *11*, 28.
- (5) Yang, J.-shane; Swager, T. M. *J. Am. Chem. Soc.* **1998**, *7863*, 5321.
- (6) Pumera, M. *Electrophoresis.* **2006**, *27*, 244.
- (7) Lai, H.; Leung, A.; Magee, M.; Almirall, J. R. *Anal. Bioanal. Chem.* **2010**, *396*, 2997.
- (8) Cox, J. R.; Müller, P.; Swager, T. M. *J. Am. Chem. Soc.* **2011**, *133*, 12910.
- (9) Wang, F.; Yang, Y.; Swager, T. M. *Angew. Chem. Int. Ed.* **2008**, *47*, 8394.

- (10) Wang, F.; Swager, T. M. *J. Am. Chem. Soc.* **2011**, *133*, 11181.
- (11) Chen, R. J.; Zhang, Y.; Wang, D.; Dai, H. *J. Am. Chem. Soc.* **2001**, *123*, 3838.
- (12) Bekyarova, E.; Davis, M.; Burch, T.; Itkis, M. E.; Zhao, B.; Sunshine, S.; Haddon, R. C. *J. Phys. Chem. B.* **2004**, *108*, 19717.
- (13) Bekyarova, E.; Kalinina, I.; Sun, X.; Shastry, T.; Worsley, K.; Chi, X.; Itkis, M. E.; Haddon, R. C. *Adv. Mater.* **2010**, *22*, 848.
- (14) Amendola, V.; Fabbrizzi, L.; Mosca, L. *Chem. Soc. Rev.* **2010**, *39*, 3889.
- (15) Nishizawa, S.; Bühlmann, P.; Iwao, M.; Umezawa, Y. *Tetrahedron Lett.* **1995**, *36*, 6483.
- (16) Wilcox, C.; Kim, E.-il; Romano, D.; Kuo, L. H.; Burt, A. L. *Tetrahedron.* **1995**, *51*, 621.
- (17) Gao, C.; He, H.; Zhou, L.; Zheng, X.; Zhang, Y. *Chem. Mater.* **2009**, *21*, 360.
- (18) Munch, H.; Hansen, J. S.; Pittelkow, M.; Christensen, J. B.; Boas, U. *Tetrahedron Lett.* **2008**, *49*, 3117.
- (19) Rotger, M. C.; Piña, M. N.; Frontera, A.; Martorell, G.; Ballester, P.; Deyà, P. M.; Costa, A. *J. Org. Chem.* **2004**, *69*, 2302.
- (20) Hay, B. P. *Chem. Soc. Rev.* **2010**, *39*, 3700.
- (21) Brooks, S. J.; Gale, P. a; Light, M. E. *Chem. Commun.* **2005**, 4696.
- (22) Thordarson, P. *Chem. Soc. Rev.* **2011**, *40*, 1305.
- (23) Hynes, M. J. *J. Chem. Soc., Dalton Trans.* **1993**, 311.
- (24) Kolb, H. C.; Finn, M. G.; Sharpless, K. B. *Angew. Chem. Int. Ed.* **2001**, *40*, 2004.
- (25) Dauban, P.; Dodd, R. H. *Synlett.* **2003**, 1571.

CHAPTER 5

Highly Selective Detection of *N*-methylammonium Species with Cavitand-Functionalized SWCNTs



Studies in this chapter are in collaboration with Marco Dionisio and Vladimir K. Michaelis

Adapted and reprinted in part with permission from:

Dionisio, M; **Schnorr, J. M.**; Michaelis, V. K.; Griffin, R. G.; Swager, T. M.; Dalcanale, E.

“Cavitand-Functionalized SWCNTs for *N*-methylammonium Detection”

J. Am. Chem. Soc. **2012**, *134*, 6540-6543

Copyright 2012 American Chemical Society

5.1. Introduction

Carbon nanotubes (CNTs) are a promising sensing platform, because their conductivity can be influenced by their environment. Combined with their quasi-one-dimensional structure and high aspect ratio, they are ideal candidates for molecular wire type sensing systems.^{1,2} While pristine CNTs react to a variety of sensing targets, they lack selectivity^{3,4} and several functionalization strategies have been employed in order to render the CNTs selective toward certain analytes. These approaches include functionalization with polymers,⁵⁻⁸ metal nanoparticles,⁹⁻¹¹ and biomolecules.¹²⁻¹⁷ Some of these approaches are attractive due to the facile functionalization procedure, the readily available functionalization reagents or the potential variety of detectable analytes. When on the other hand a very high selectivity for a specific analyte is the main focus in developing a sensor, the use of molecular recognition units seems particularly promising.^{18,19} Such host-guest systems have been shown to provide a high level of selectivity and the functionalization of CNTs with cyclodextrins or calixarenes has led to the selective recognition of small molecules.²⁰⁻²⁴

To further explore the scope of CNT sensing with host-guest systems, we decided to focus on tetraphosphonate cavitands such as **Tiiii[C₃H₇, CH₃, Ph]** which have been explored in different contexts in the Dalcanale group where they have shown remarkable complexation capabilities toward charged *N*-methylammonium species.^{25,26} The high affinity of tetraphosphonate cavitands for these species is reflected in a high K_a value of approximately $4 \times 10^5 \text{ M}^{-1}$ in methanol for the complex of **Tiiii[C₃H₇, CH₃, Ph]** and *N*-methylbutyl ammonium chloride.²⁷ Even more importantly for a high selectivity, this value is two orders of magnitude higher than K_a for the closely related compounds butylammonium chloride and *N,N*-dimethylbutyl ammonium chloride (Figure 5.1).

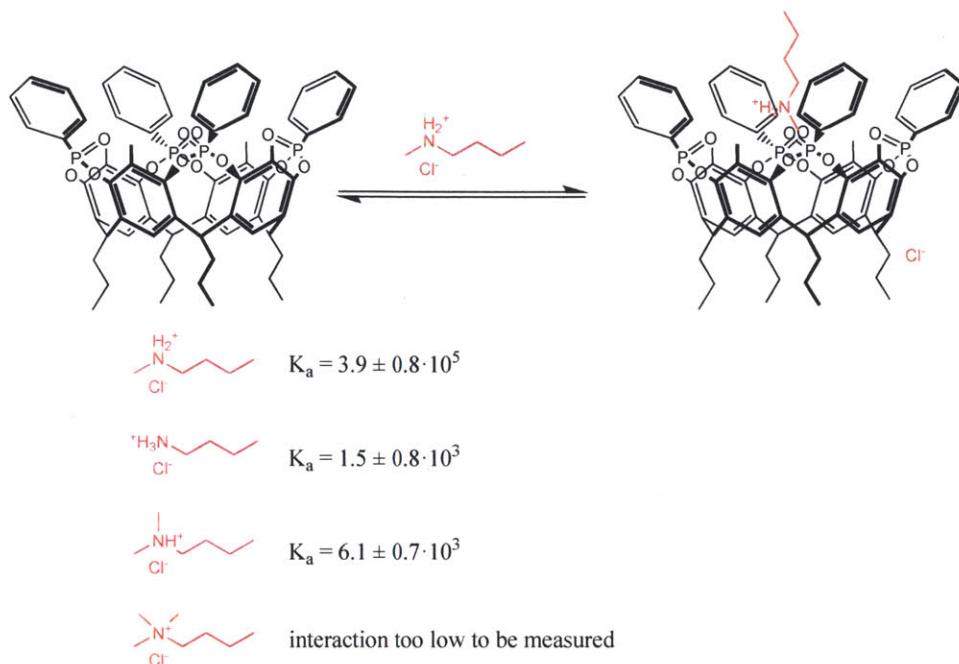


Figure 5.1. Interaction of tetraphosphonate cavitand Tiiii[C₃H₇, CH₃, Ph] with *N*-methylbutyl ammonium chloride in comparison to closely related compounds. Association constants are based on ref. 27 and have been obtained by isothermal titration calorimetry (ITC) in methanol

The association constants are influenced by the steric bulk of the guest and the favorable interactions between guest and cavitand. *N*-methylated secondary ammonium ions exhibit the best combination of sufficiently low steric repulsion with dipolar interactions of the positively charged nitrogen atom and the P=O groups together with C-H••• π interactions between methyl and aromatic rings of the cavity.²⁸

We envisioned that this difference in association constants could translate to a very high level of selectivity of an amperometric CNT-based sensor when the CNTs would be functionalized with tetraphosphonate cavitands.

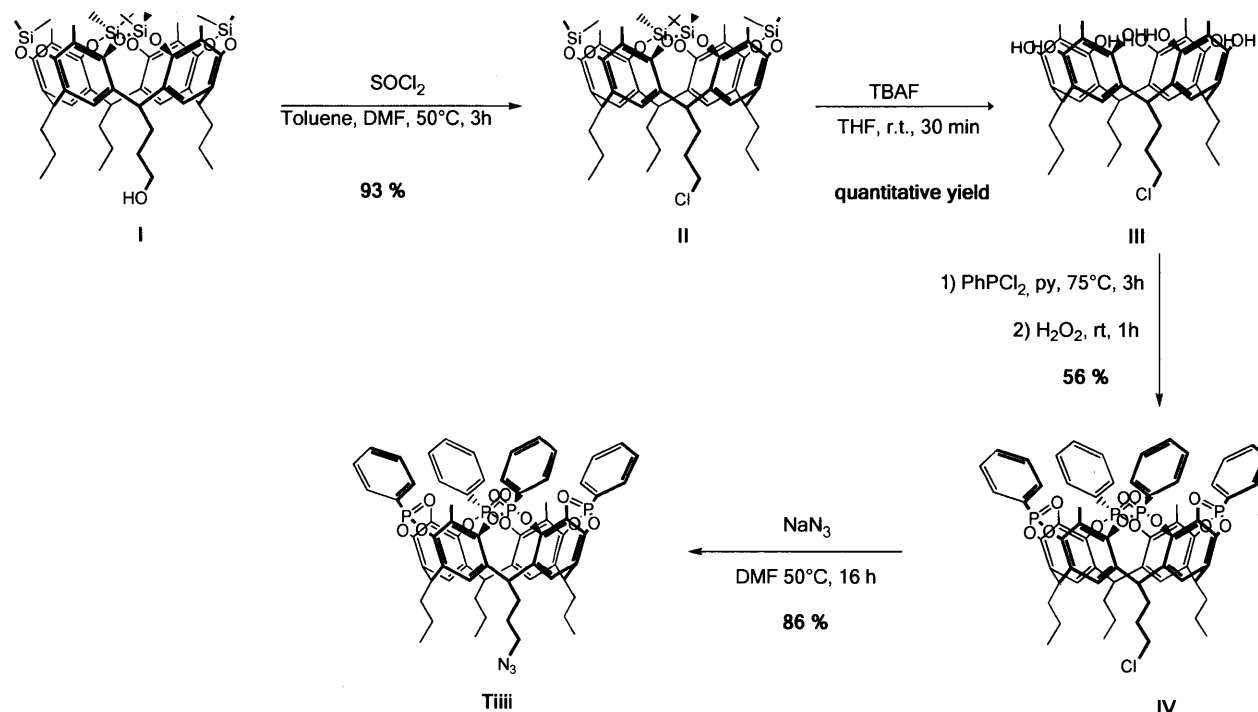
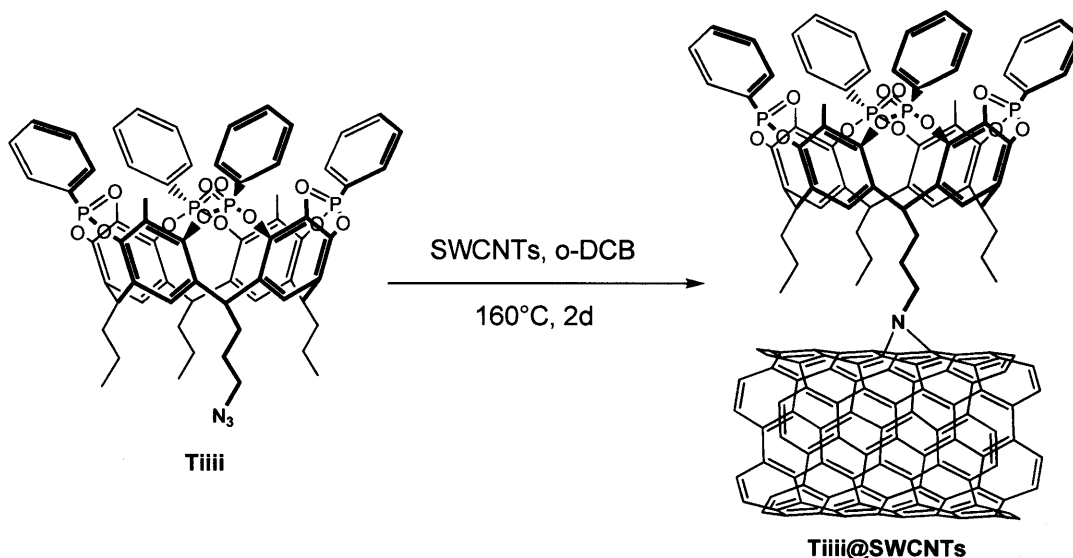
While non-covalent attachment of receptors to CNTs has been shown to provide good sensing results in other systems,^{23,24} we chose a covalent attachment strategy to potentially improve the

long-term stability under liquid sensing conditions. Furthermore, previous attempts in collaboration of the Swager and Dalcanale group using cavitands with pyrene units at the lower rim for non-covalent CNT functionalization resulted in a very limited degree of functionalization. We were hoping to overcome this limitation by introducing an azide group in the lower rim of the cavitand to utilize it for covalent attachment to the CNTs. As the CNT platform, we chose single-walled CNTs (SWCNTs).

5.2. Results and Discussion

5.2.1. Functionalization of Carbon Nanotubes with Cavitands

In order to attach the tetraphosphonate cavitand host to the SWCNTs, an azide moiety was installed on one of the alkyl chains of the lower rim. This synthesis of **Tiiii**[N₃, CH₃, Ph] was performed by Marco Dionisio starting from previously reported monohydroxy footed silyl cavitand **I**^{25,29} in four steps and 45% overall yield (Scheme 5.1). Initially, we attempted to perform a 1,3-dipolar cycloaddition reaction between **Tiiii**[N₃, CH₃, Ph] (from now onward referred to as **Tiiii**) and propargyl-functionalized SWCNTs similar to the synthesis of sulfonate CNTs described in chapter 2,³⁰ however, these attempts did not lead to the desired product. We therefore chose thermal aziridination as a direct way of functionalizing pristine SWCNTs, instead.³¹ This method had previously proved to be a reliable way of CNT functionalization (see chapter 4). Furthermore, we were hoping that the shorter distance between cavitand and CNTs compared to the previously explored “click”-chemistry approach would be beneficial for sensing. The functionalization reaction was performed at 160 °C in *ortho*-dichlorobenzene for 2 days (Scheme 5.2).

Scheme 5.1. Synthesis of monoazide footed tetraphosphonate cavitand **Tiiii**[N₃, CH₃, Ph]**Scheme 5.2.** SWCNT functionalization with **Tiiii**[N₃, CH₃, Ph]

The covalently functionalized **Tiiii@SWCNTs** were characterized by attenuated total reflectance Fourier transform infrared spectroscopy (ATR FTIR), X-ray photoelectron spectroscopy (XPS), and ³¹P magic-angle spinning nuclear magnetic resonance spectroscopy (MAS NMR). The

infrared spectra (between 1000 and 1500 cm^{-1}) of **Tiii@SWCNTs** displayed a broad band arising from the stretching of the PO bonds, P-phenyl group, and the aromatic skeleton, which overlap with one another. Furthermore, the azide peak of **Tiii** was no longer present in the ATR FTIR spectra of the reaction product, suggesting that aziridination has taken place (see experimental section). XPS confirmed the presence of phosphorous and nitrogen (P 2p and N 1s peaks, respectively) at a density that suggests one cavitand for every 50 CNT carbon atoms based on the P 2p vs C 1s signal (Figure 5.2).

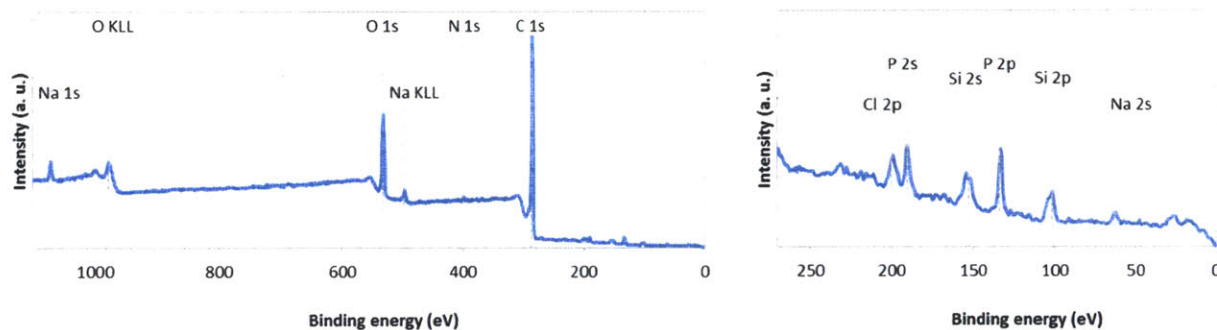


Figure 5.2. XPS spectrum of **Tiii@SWCNTs**. Si and F in the spectra originate from the silicon substrate used. Cl signals were attributed to trace amounts of residual *o*-DCB.

MAS NMR was performed by Vladimir K. Michaelis in the Griffin laboratory to further analyze the functionalized CNTs. The use of this technique is increasing for the characterization of modified CNTs based on the ^{13}C nucleus.^{32–34} However, obtaining high-resolution ^{13}C NMR spectra of CNTs remains a challenge due to the low isotopic abundance (1.1% ^{13}C) and great variability of carbon sites with different chemical shifts commonly seen in a CNT sample. In contrast to this, a very clear ^{31}P MAS NMR spectrum of **Tiii@SWCNTs** was obtained of the SWCNT bound cavitand, which benefited from high ^{31}P natural abundance (100%) and its high gyromagnetic ratio, both of which lead to greater sensitivity (Figure 5.3).

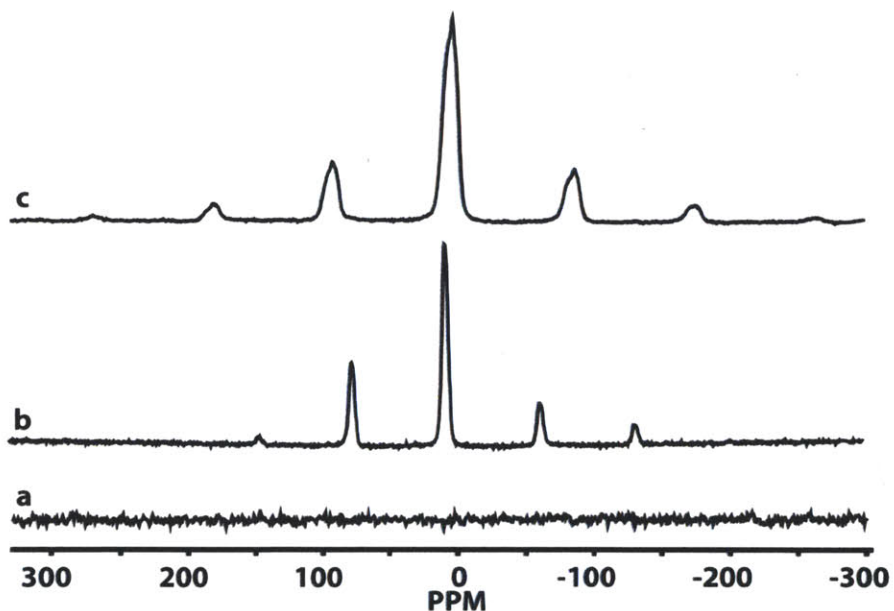


Figure 5.3. ^{31}P MAS NMR spectra of (a) pristine SWCNTs, (b) **TiIII**, and (c) **TiIII@SWCNTs**.

5.2.2. Binding Studies

After confirming the presence of the cavitand in the **TiIII@SWCNTs** sample we investigated the molecular recognition capabilities of the obtained material. Even though the Dalcanale group had previously shown that host-guest interactions are possible when the cavitand is immobilized on a surface (in this case silicon),³⁵ it was not clear what effect the attachment of the cavitand to SWCNTs would have on its binding ability. A potential challenge could be related to an unfavorable orientation of **TiIII** on the CNTs that hinders access to the binding site.

As solution binding studies (e.g. by NMR) are not possible with a CNT sample, we decided to utilize XPS to investigate the binding of a bromine labeled target analyte to **TiIII@SWCNTs** (Figure 5.4a).

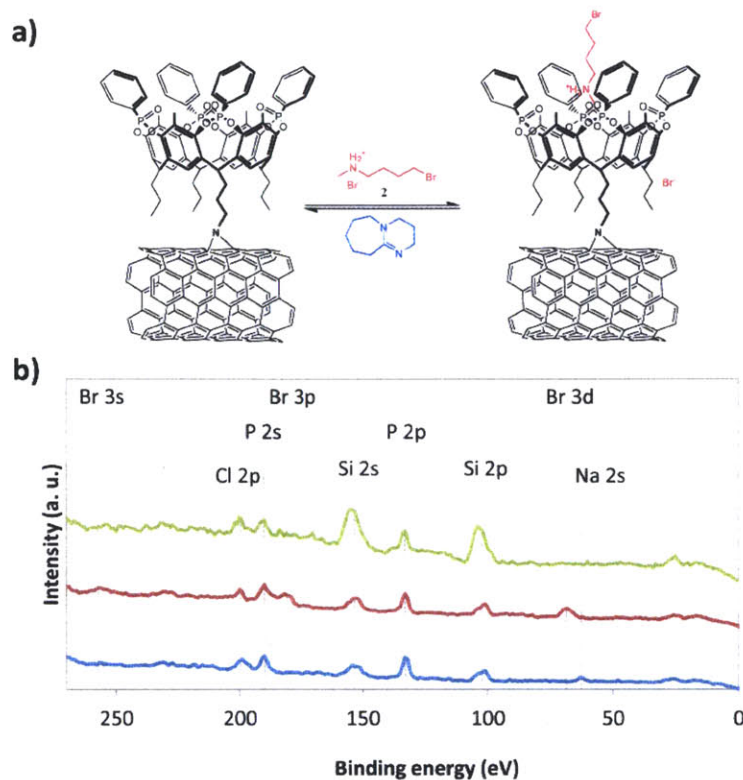


Figure 5.4. XPS binding study with **Ti^{III}@SWCNTs**. (a) Reversible binding of guest **2**; (b) XPS analysis of **Ti^{III}@SWCNTs** before exposure to **2** (blue), after exposure to **2** (red), and after subsequent washing with DBU (green). Si signals are due to the utilized Si substrate.

A suspension of **Ti^{III}@SWCNTs** in dichloromethane was treated with 4-bromo-*N*-methylbutylammonium bromide, which binds as a guest and has an XPS diagnostic bromide signal.²⁸ After washing to remove unbound analyte, the CNTs were analyzed by XPS showing signals for bromine including the main Br 3d peak, confirming successful binding of the analyte to **Ti^{III}@SWCNTs** (Figure 5.4b, red trace). Pristine SWCNT samples that were treated in a similar way, on the other hand, only contained trace amounts of bromine.

Subsequently, the sample was washed with 1,8-diazabicyclo[5.4.0]undec-7-ene (DBU). It had been shown previously that DBU can deprotonate the guest thus breaking the cavitand-guest complex.³⁶ Protonated DBU itself cannot bind to the cavity due to steric hindrance leading to a

guest-free host. Indeed, after washing with DBU, no bromine signals could be observed by XPS (Figure 5.4b, green trace).

While these results were promising, they only confirmed that 4-bromo-*N*-methylbutylammonium bromide preferably binds to **Tiii@SWCNTs** compared to pristine SWCNTs and can be removed by washing with base. They did not confirm in which fashion the binding takes place and if the analyte binds to the cavitand or to other features of the SWCNTs, e.g. defect sites that could have potentially been introduced during the functionalization reaction. This uncertainty is a general problem in binding studies that involve CNTs. Techniques that would be typically employed to further investigate binding such as solution NMR or UV-vis spectroscopy are very challenging due to the macroscopic and highly absorbing nature of the CNTs.

Encouraged by the initial success utilizing ^{31}P solid state NMR for the characterization of **Tiii@SWCNTs**, we decided to use the same technique to perform a binding study. **Tiii@SWCNTs** were treated with a solution of *N*-methylbutylammonium chloride and subsequently analyzed by ^{31}P MAS NMR. The ^{31}P signals are sensitive to the structural changes associated with the binding of an ammonium ion to the **Tiii@SWCNTs** and a downfield-shifted resonance is observed (Figure 5.5b). This shift was expected and is consistent with solution NMR studies of the base cavitand complex.²⁶

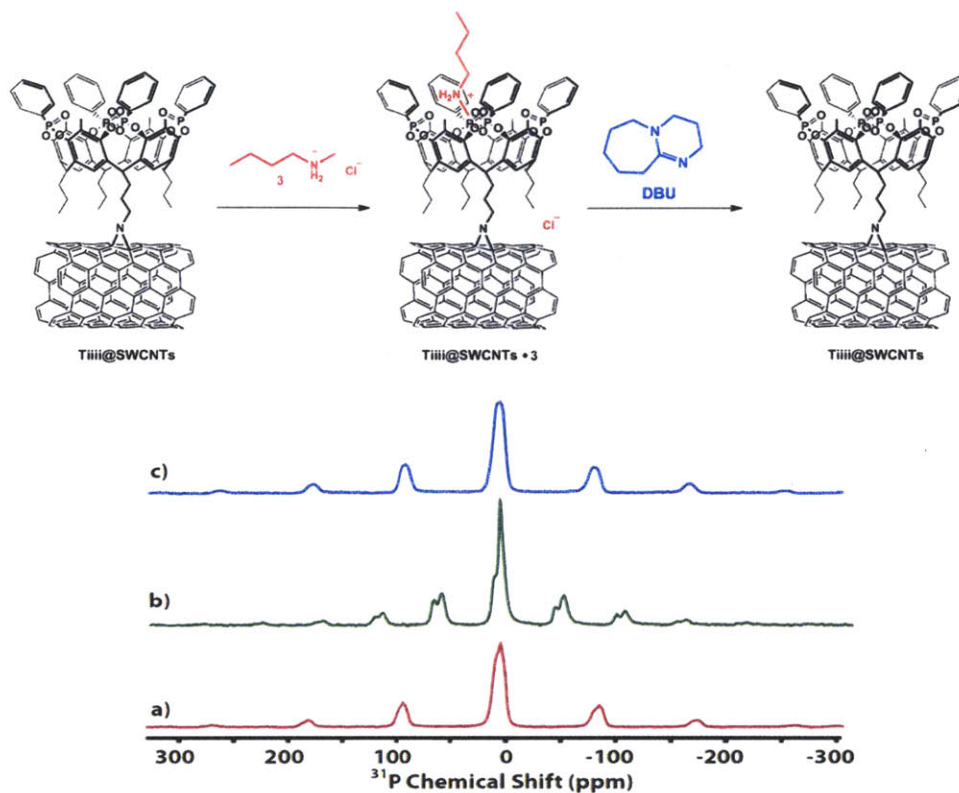


Figure 5.5. Host-guest binding studies using ^{31}P MAS NMR showing reversible binding of the host molecule. (a) Ti(III)@SWCNTs , red trace; (b) after treatment with the guest, green trace; (c) after subsequent washing with DBU, blue trace.

After subsequent washing with DBU, MAS NMR of the product yielded a spectrum similar to the one obtained before exposure of Ti(III)@SWCNTs to the guest (Figure 5.5c). This confirms the expected reversible binding of the guest and the previously observed pH dependence of the association constant.

5.2.3. Amperometric Sensing Measurements

Given that XPS and MAS NMR confirmed successful binding of secondary ammonium ions to the cavitand functionalized SWCNTs, we decided to test the practical utility of the material in a sensor prototype. As the target, we chose sarcosine, the *N*-methylated derivative of glycine.

Sarcosine is structurally related to the previously studied guests and is a potential biomarker for the progression of prostate cancer, although the discussion of its utility for this purpose is still ongoing.^{37,38} Binding studies with **Tiiii** immobilized on a silicon substrate had shown that the cavitand binds sarcosine over the potential interferent glycine with complete selectivity.³⁵

To prepare the sensor, an aliquot of the reaction solution of **Tiiii@SWCNTs** was directly drop-cast onto a glass slide decorated with two Au electrodes. The device was then washed by immersion in dichloromethane, methanol and hexanes to remove any excess of reagent before being dried in a nitrogen stream. This procedure allowed the use of smaller amounts of CNTs and thus **Tiiii** compared to traditional workup procedures and subsequent drop-casting. The latter is the better choice for the preparation of larger amounts of functionalized CNTs as it allows more thorough washing. In our case, on the other hand, limiting the amount of **Tiiii** which has to be used in 20-fold excess (by weight) in the reaction by reducing the overall reaction scale was the priority. After drying, the devices were analyzed by scanning electron microscopy (SEM) and atomic force microscopy (AFM), confirming the presence of SWCNT bundles (see experimental section).

The device was put into a Teflon enclosure that we had recently developed for the gas sensing project described in chapter 4 (Figure 5.6).

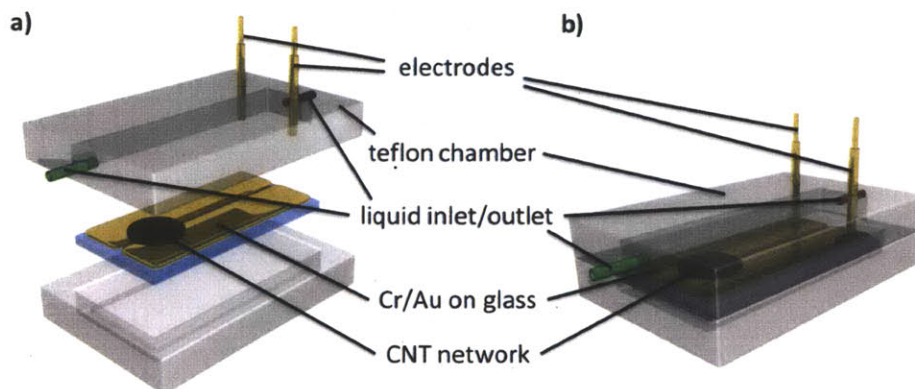


Figure 5.6. Liquid flow chamber for sensing measurements.

The gold electrodes of the device were contacted with connections to the outside of the chamber, and two ports on opposite sides of the chamber allowed directing a continuous flow of liquid through the chamber. The inlet port of the flow chamber was connected to a tubing system with two 3-way valves that allowed directing a liquid from one of two syringes through the chamber (Figure 5.7). By connecting both syringes to the same syringe pump, a constant flow rate of 0.5 mL/min was maintained for both syringes.

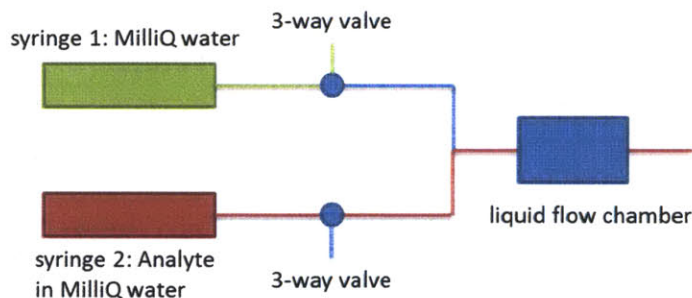


Figure 5.7. Setup for liquid flow sensing measurements. Using two 3-way valves, a liquid from one of two syringes could alternately be directed through the liquid flow chamber with the measurement device. Both syringes were connected to the same syringe pump ensuring the same flow rate for both liquids.

Initial measurements with sarcosine showed an increase in current when a device with **Tiiii@SWCNTs** was exposed to the analyte at pH 7 (Figure 5.8a). The magnitude of the change in current was however strongly dependent on the pH of the solution, and at pH 5, no change in current was observed upon exposure of the device to sarcosine (Figure 5.8b).

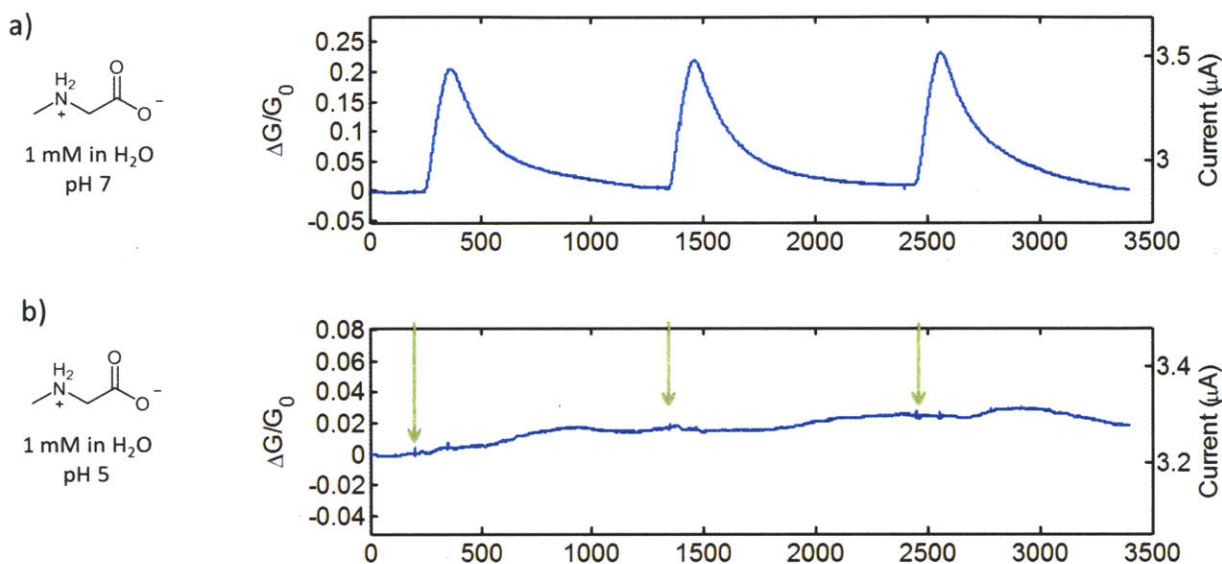


Figure 5.8. Sensing of sarcosine with **Tiiii@SWCNTs** at (a) pH 7 and (b) pH 5, green arrows indicate exposure to analyte.

We attribute this strong pH dependence to the zwitterionic nature of the analyte. Our data may suggest that the protonation of the carboxylate can affect its nonspecific interaction with the SWCNT surface.

In order to eliminate the effect of the carboxylate, we investigated the hydrochloride salt of sarcosine ethyl ester (**4**). The measurements were performed at pH 5 to ensure protonation of the amine. As controls, the weaker binding glycine ethyl ester hydrochloride (**5**) and tetraethylammonium chloride (**6**) that is too bulky for binding²⁷ were chosen.

Exposing the device to **4** at pH 5 resulted in an increase in current similar to exposing it to sarcosine, while exposure to **5** or **6** led to a current decrease (Figure 5.9). In many chemoresistive sensing systems a current change in the same direction is observed for the desired analytes and controls, albeit usually stronger for the target molecule. Instead, a current switch in opposite directions for the target analyte and interferences is rare, especially for compounds as closely related as **4** and **5**. Observing a change with a different sign provides a powerful level of selectivity as it can potentially distinguish between analytes regardless of their concentration.

Although the magnitude of the response to **4** varied from device to device (see experimental section), an increase in current when exposed to **4** was observed in all cases. To avoid errors related to device to device differences, all measurements in Figure 5.9 were conducted with the same **Tiii@SWCNTs** device. In contrast to the response at pH 5, exposing the device to **4** at pH 7, resulted in a current decrease similar to the response to **5** and **6** at pH 5. Previous studies at the silicon-water interface³⁵ showed that surface complexation by **Tiii** is effective only at pH low enough to ensure complete guest protonation. This suggests that specific binding between **4** and the cavitand is reduced as a result of the change in pH and non-specific interactions of **4** and the SWCNTs predominate.

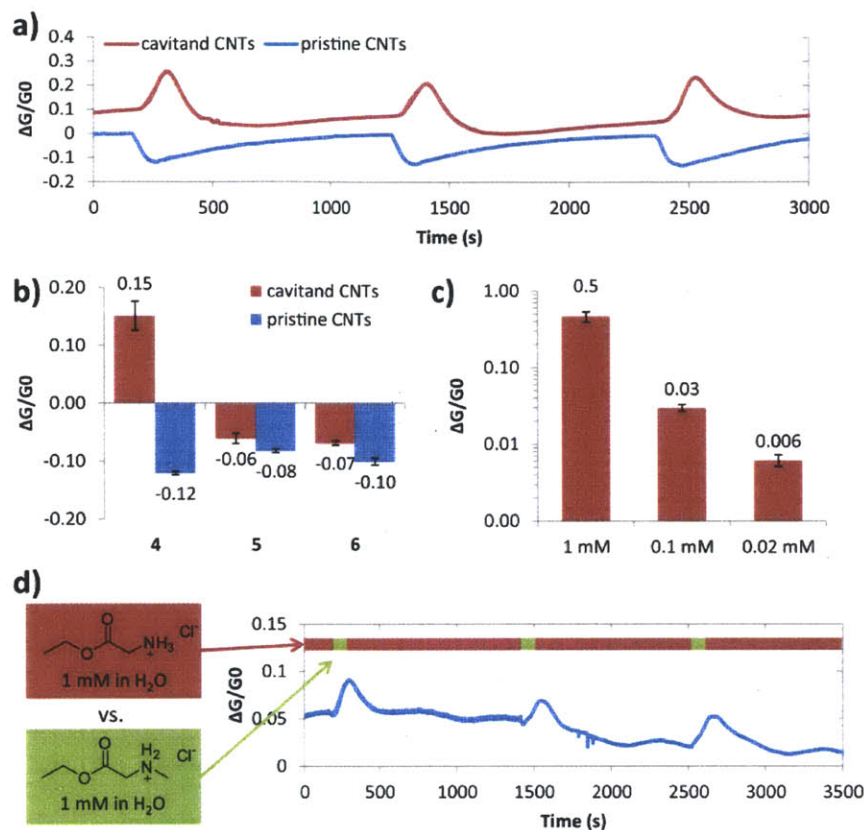


Figure 5.9. Liquid flow sensing experiments with **Tiii@SWCNT**-based devices at pH 5. a) **Tiii@SWCNTs** and pristine SWCNTs show opposite responses upon exposure to a 1 mM solution of **4** b) Comparison of the current change upon exposure of **Tiii@SWCNTs** and pristine SWCNTs devices to **4** (sarcosine ethyl ester hydrochloride), **5** (glycine ethyl ester hydrochloride) and **6** (tetraethylammonium chloride), error bars are based on three consecutive measurements c) Response of **Tiii@SWCNTs** devices to different concentrations of **4**, error bars are based on three consecutive measurements d) Response of **Tiii@SWCNTs** devices to alternating exposure to **4** and **5**

Controls with pristine SWCNTs showed a decrease in current for all investigated analytes (Figure 5.9b). In order to minimize the effect of a changing ionic strength of the solution on the sensing response, a device with **Tiii@SWCNTs** was alternately exposed to a 1 mM solution of **4** and **5** (instead of an analyte solution and water). An increasing current was observed in this

case as well when switching to **4** (Figure 5.9d). Finally, the detection limit for **4** was determined to be 0.02 mM (Figure 5.9c).

The utilized devices exhibited very good stability and no significant change in sensitivity was observed over several months of regular operation. When small variations in sensitivity were observed, the initial sensitivity could be restored by briefly immersing the device in methanol to remove residual analyte followed by drying in a nitrogen stream.

5.3. Conclusions

In summary, we have illustrated the use of covalently functionalized SWCNTs as a selective sensor in water. By introducing a tetraphosphonate cavitand as a specific molecular receptor, it was possible to selectively recognize *N*-methylammonium species. The covalent functionalization provided a high stability of **Tiiii@SWCNTs**-based devices and allowed for the formation of robust liquid sensing devices. As a proof of concept experiment, we demonstrated the selective detection of sarcosine ethyl ester hydrochloride, at concentrations as low as 0.02 mM. Interestingly, the sign of the current change upon exposure to the analyte is opposite for the controls, allowing selective detection of the analyte, regardless of its concentration.

5.4. Experimental Section

General Methods.

All reagents and chemicals were obtained from commercial sources and used without further purification.

Single-walled carbon nanotubes were purchased from SouthWest Nano Technologies (SWeNT® CG100). Dry pyridine was distilled from KOH before use. Column chromatography was performed using silica gel 60 (MERCK 70-230 mesh). Electrospray ionization ESI-MS experiments were performed on a Waters ZMD spectrometer equipped with an electrospray interface. Exact masses were determined using a LTQ ORBITRAP XL Thermo spectrometer equipped with an electrospray interface. ¹H NMR spectra were obtained using a Bruker AVANCE-300 (300 MHz) or a Bruker AVANCE 400 (400 MHz). All chemical shifts (δ) are reported in ppm relative to the proton resonances resulting from incomplete deuteration of the NMR solvents. ³¹P solution NMR spectra were obtained using a Bruker AVANCE-400 (162 MHz) spectrometer. All chemical shifts (δ) were recorded in ppm relative to external 85% H₃PO₄ at 0.00 ppm.

XPS spectra were recorded using a Kratos AXIS Ultra X-ray Photoelectron Spectrometer.

³¹P MAS NMR: NMR experiments were conducted on a home-built 360 (B₀ = 8.4T) spectrometer (courtesy of Dr. David Ruben) with a 4 mm triple-channel chemagnetics MAS probe. Samples were ground using a mortar and pestle, and placed within ZrO₂ rotors (60 μ l volume). Spectral acquisition included Bloch and Hahn-echo experiments, using between 128 and 4096 co-added transients, spinning frequency (ω_r) between 0 and 12 kHz and high power ¹H decoupling (ν_{rf} = 83 kHz) when required. Recycle delays were optimized for each sample and were typically 35 seconds. All ³¹P data were referenced using 85% H₃PO₄ (0.0 ppm).

Synthesis

The synthesis of T_{iiii}[N₃, CH₃, Ph] was performed by Marco Dionisio (Scheme 5.1).

Monochloro silylcavitand (II). To a solution of monohydroxy footed silylcavitand^{25,29} (0.76 g, 0.80 mmol) in dry toluene (15 ml), 5 drops of DMF were added. The suspension was cooled to 0°C and thionyl chloride was slowly added (2.40 mmol, 175 μ l). The resulting suspension was stirred for 2h at 50°C. The solvent was evaporated. Then, the residue was dissolved in chloroform and washed with water before being dried over MgSO₄. The removal of the solvent gave II as a brownish solid (0.72g, 0.74 mmol, 93%). ¹H-NMR (CDCl₃, 400 MHz): δ = 7.21 (bs, 4H, ArH); 4.65 (t, 4H, ³J= 7.9 Hz, ArCH); 3.64 (t, 2H, ³J= 6.4 Hz, CH₂CH₂Cl); 2.39 (m, 2H, CH₂CH₂CH₂Cl); 2.21 (m, 6H, CH₂CH₂CH₃); 1.95 (s, 12H, ArCH₃); 1.82 (m, 2H, CH₂CH₂Cl); 1.35 (m, 6H, CH₂CH₂CH₃); 1.09 (t, 9H, ³J=7.3 Hz, CH₂CH₂CH₃); 0.55 (s, 12H, SiCH_{3,out}); -0.63 (s, 12H, SiCH_{3,in}). ESI-MS: *m/z* calcd. for C₅₂H₇₁ClO₈Si₄ (970.4), [M+Na]⁺: 993.4. Found: 993.5 [M-Na]⁺.

Monochloro resorcinarene (III). To a solution of II (0.59 g., 0.60 mmol) in THF (15ml), acetic acid (6 mmol, 350 μ l) and 80% w/w TBAF (6 mmol, 1.90 ml) were added at 0°C. The solution was stirred for 30 min at room temperature, then NH₄Cl_{aq} was added. The solution was diluted with ethyl acetate and the organic layer was separated, washed three times with NH₄Cl_{aq}, then NaCl_{aq} and dried over MgSO₄. The removal of the solvent afforded III as a brown solid (0.47 g, 0.60 mmol, quantitative yield). ¹H-NMR (Acetone-d₆, 300 MHz): δ = 8.37 (m, 8H, ArOH); 7.51 (s, 2H, ArH); 7.50 (s, 2H, ArH); 4.49 (t, 4H, ³J=7.9 Hz, ArCH); 3.71 (t, 2H, ³J= 6.7 Hz, CH₂CH₂Cl); 2.53 (m, 2H, CHCH₂CH₂CH₂Cl); 2.35 (m, 6H, CHCH₂CH₂CH₃); 2.13 (s, 12H, ArCH₃); 1.83 (m, 2H, CH₂CH₂CH₃); 1.38 (m, 6H, CH₂CH₂CH₃); 1.02 (t, 9H, ³J=7.3 Hz, CH₂CH₂CH₃). ESI-MS: *m/z* calcd. for C₄₄H₅₅ClO₈ (746.4), [M+Na]⁺ 769.6. Found: 769.50. [M+Na]⁺.

Monochloro footed tetraphosphonate cavitand Tiiii[Cl, CH₃, Ph] (IV). To a solution of III (0.47g, 0.63 mmol) in freshly distilled pyridine (12 mL), dichlorophenylphosphine (380 μ l, 2.84 mmol) was added slowly, at room temperature. After 3 hours of stirring under N₂ at 75 °C, the solution was cooled down to room temperature and 4.5 mL of aqueous 35% H₂O₂ were added. The resulting mixture was stirred for 1 h at room temperature. Then, the solvent was removed *in vacuo*. Addition of water resulted in the precipitation of a white powder. The crude product was purified by column chromatography (9:1 DCM:EtOH) affording IV as a brownish solid (0.44 g, 0.35 mmol, 56 %). ¹H-NMR (CDCl₃, 400 MHz): δ = 8.13 (m, 8H, P(O)ArH_O); 7.68 (m, 4H, P(O)ArH_P); 7.58 (m, 8H, P(O)ArH_M); 7.40 (bs, 4H, ArH); 4.84 (t, 4H, ³J= 7.8 Hz, ArCH); 3.74 (t, 2H, ³J= 7.2 Hz, CH₂CH₂Cl); 2.63 (m, 2H, CH₂CH₂CH₂Cl); 2.43 (m, 6H, CH₂CH₂CH₃); 2.20 (s, 12H, ArCH₃); 1.92 (m, 2H, CH₂CH₂CH₂Cl); 1.47 (m, 6H, CH₂CH₂CH₃); 1.09 (t, 9H, ³J= 7.3 Hz, CH₂CH₂CH₃). ³¹P{¹H} NMR (CDCl₃, 161.9 MHz): δ = 7.70 (bs, P(O)). ESI-MS: *m/z* calcd. for Tiiii[Cl, CH₃, Ph] C₆₈H₆₇ClO₁₂P₄ (1234.32); [M+Na]⁺ 1257.75. Found:1257.78 [M+Na]⁺.

Monoazide footed tetraphosphonate cavitand Tiiii[N₃, CH₃, Ph] (Tiiii) To a solution of Tiiii[Cl, CH₃, Ph] (IV) (0.44 g, 0.35 mmol) in DMF (15 ml), sodium azide was added (68 mg, 1.1 mmol). The solution was stirred overnight at 55°C. Then, the solvent was evaporated and the crude was suspended in water and filtered affording Tiiii as a brown solid (0.38 g., 0.31 mmol, 86%). ¹H-NMR (CDCl₃, 400 MHz): δ = 8.14 (m, 8H, P(O)ArH_O); 7.65 (m, 4H, P(O)ArH_P); 7.57 (m, 8H, P(O)ArH_M); 7.19 (s, 4H, ArH); 4.87 (m, 4H, ArCH); 3.48 (t, 2H, ³J= 6.2 Hz, CH₂CH₂N₃); 2.38 (m, 20H, CH₂CH₂CH₂N₃ + CH₂CH₂CH₃ + ArCH₃); 1.73 (m, 2H, CH₂CH₂CH₂N₃); 1.47 (m, 6H, CH₂CH₂CH₃); 1.09 (t, 9H, ³J= 7.2 Hz, CH₂CH₂CH₃). ³¹P{¹H} NMR (CDCl₃, 161.9 MHz): δ = 6.13 (bs P(O)). HR ESI-MS: calculated for the complex Tiiii[N₃, CH₃, Ph] C₆₈H₆₇N₃O₁₂P₄ (1241.36752) [M+Na]⁺: 1264.35729. Found:1264.35674.

General procedure for SWCNT functionalization

10 mg of SWCNTs were placed in a Schlenk flask and purged with argon for 10 minutes. $\text{Tiii}[\text{N}_3, \text{CH}_3, \text{Ph}]$ (200 mg, 0.16 mmol) was introduced with the addition of 1 ml of *o*-DCB. The suspension was sonicated for 10 minutes and subsequently stirred at 160°C for two days under argon. After evaporation of the solvent, the crude product was dispersed in dichloromethane and sonicated for 10 min. It was then filtered on 2 μm millipore filter and washed with hexane, dichloromethane, and acetone.

Attenuated total reflectance Fourier transform infrared spectroscopy (ATR FTIR)

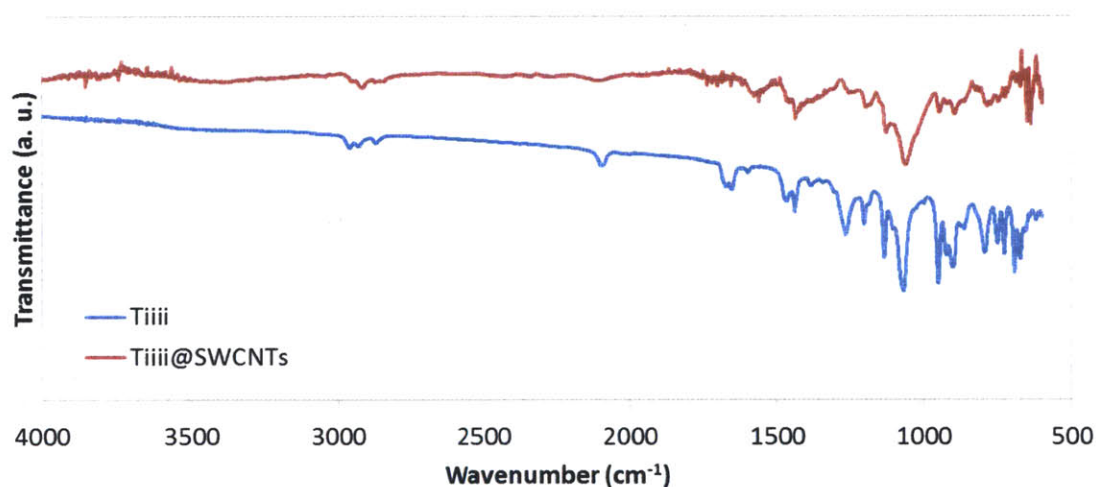


Figure 5.10. ATR-FTIR Tiii (blue trace) and Tiii@SWCNTs (red trace).

XPS complexation studies

To a dichloromethane (1 ml) suspension of **Tiiii@SWCNTs** (5 mg, 0.9 μM of cavitand) a guest solution (4-bromo-*N*-methylbutylammonium bromide, **2**) in dichloromethane was added (5 equivalent as a 4.3 μM dichloromethane solution). After 12 h the suspension was filtered and the solid washed with dichloromethane. The solid was collected, dried, redispersed in dichloromethane and drop-cast onto a silicon slide for the XPS measurement. After the XPS measurement, the material was sonicated with DBU (9.2 equivalents relative to initially used guest) in 5 mL dichloromethane for 10 min and then stirred overnight. Afterward, the **Tiiii@SWCNTs** were collected by filtration, washed with dichloromethane, dried and drop-cast for the following XPS measurement.

As a control experiment, pristine SWCNTs (5 mg) were treated with a similar guest solution for 12 h. The sample was washed and dried in a similar fashion and then analyzed by XPS as well.

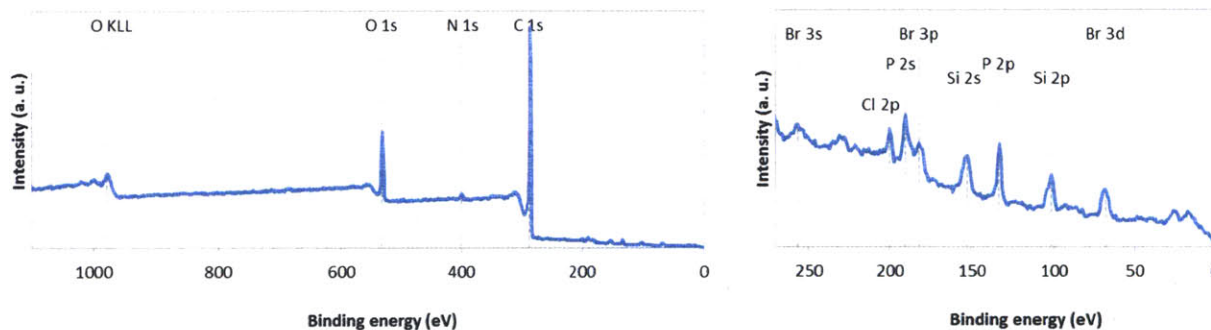


Figure 5.11. XPS spectrum of **Tiiii@SWCNTs** after treatment with guest **2**.

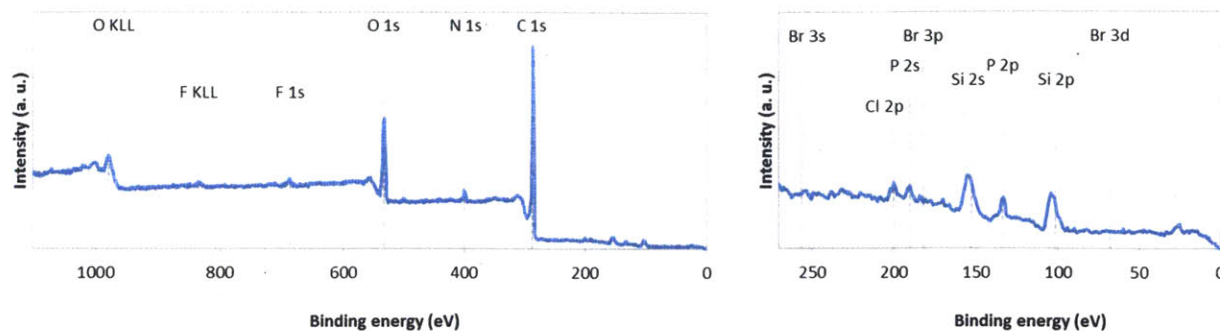


Figure 5.12. XPS spectrum of **Tiiii@SWCNTs•2** after washing with DBU. Positions of Br signals are labeled for better comparison to **Figure 5.11**.

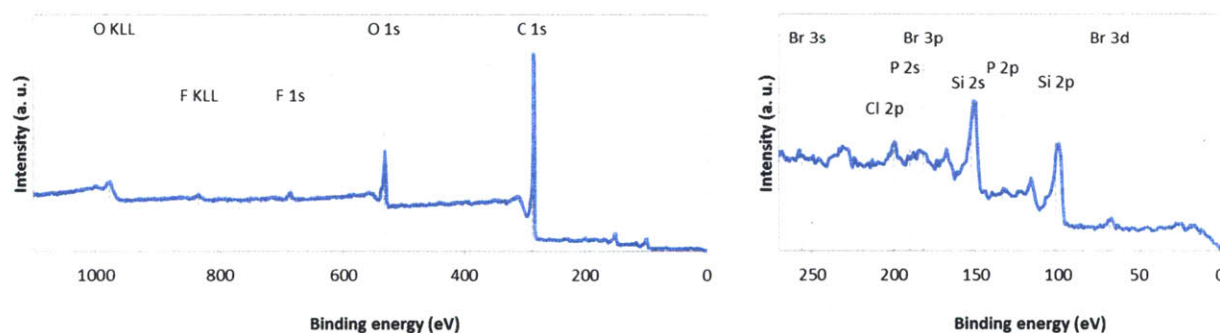


Figure 5.13. XPS spectrum of pristine SWCNTs after treatment with **2**. Positions of Br and P signals are labeled for better comparison to **Figure 5.11**.

Solid State-NMR complexation studies

Tiiii@SWCNTs (40 mg, 7.5 μ M) were treated with 5 equivalents of *N*-methylbutyl ammonium chloride (4.29 mM solution in dichloromethane). After 12h the suspension was filtered and the solid washed with dichloromethane. The powder was collected, dried and analyzed by MAS NMR.

The **Tiiii@SWCNTs•2** complex was redispersed in dichloromethane and treated with an excess of DBU solution (4.29 mM solution in dichloromethane). After 12 h the suspension was filtered

and the solid washed with dichloromethane. The powder was collected, dried and investigated by MAS NMR.

Tiii@SWCNT device preparation

1 mg of SWCNTs were placed in a 2 mL vial and purged with argon for 10 minutes. Tiii[N₃, CH₃, Ph] (13 mg, 10.5 μmol) was introduced with the addition of 0.1 ml 1,2-dichlorobenzene. The suspension was sonicated for 1 min and subsequently stirred at 160°C for 40 h. After cooling to room temperature, 1 mL of dichloromethane was added and 3 x 1 μL of the resulting suspension were drop-cast onto glass slides that had been decorated with Cr/Au electrodes (10 nm Cr, 75 nm Au, 0.3 mm gap between electrodes). The devices were immersed in three consecutive vials with dichloromethane, then three vials with methanol followed by three vials with hexanes. Afterward, the devices were dried in a nitrogen stream and then briefly heated (heat gun).

Pristine SWCNT device preparation

Pristine SWCNTs were suspended in dichloromethane (1 mg per mL), sonicated for 2 min. and drop-cast onto glass slides that had been decorated with Cr/Au electrodes. Subsequently, the devices were dried in a similar fashion as the Tiii@SWCNTs devices.

Scanning electron microscopy (SEM)

Devices of Tiii@SWCNTs were inspected by scanning electron microscopy (SEM) on a JEOL JSM 6700F SEM.

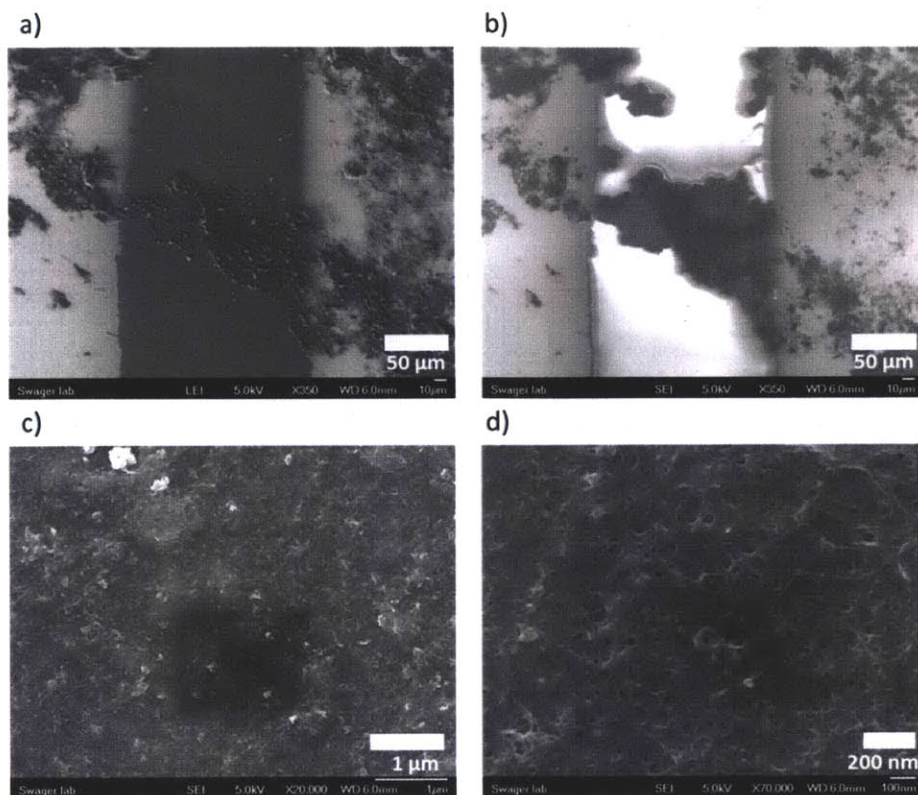


Figure 5.14. SEM images of **TiIII@SWCNT** film used in sensing measurements. a) 350x LEI b) 350x SEI c) 20,000x SEI d) 70,000x SEI

Low resolution SEM images (Figure 5.14 a-b) of the devices show a rough film that covers part of the glass surface between the gold electrodes. At higher magnification, CNT bundles are visible (Figure 5.14c-d).

Atomic force microscopy (AFM)

Devices of **TiIII@SWCNTs** were inspected by atomic force microscopy (AFM) using an Agilent 5100 AFM in tapping mode. AFM tips were obtained from App Nano (ACTA-20, <10 nm radius). A flattening procedure was applied to the data shown. AFM images of the devices confirm the morphology of the film as observed by SEM. Furthermore a high surface roughness

was observed (RMS surface roughness of 285 nm with feature heights above 1 μm in Figure 5.15).

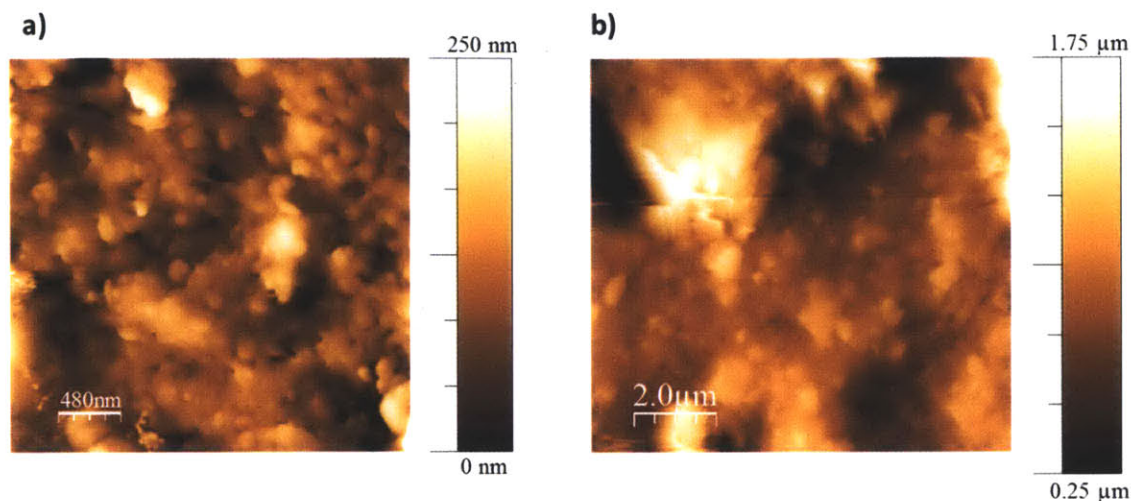


Figure 5.15. AFM images of Tiii@SWCNT film used in sensing measurements

Amperometric Sensing Measurements

Electrochemical measurements were performed using a PalmSens handheld potentiostat connected to a laptop computer. A constant bias voltage of 0.05 V was applied across the device, while current vs. time was measured.

In a typical measurement, the device was first exposed to MilliQ water. Subsequently, a 1 mM analyte solution in water was directed through the device for 100 s, followed by MilliQ water for 1000 s. In each measurement, the device was exposed to the analyte at least three times.

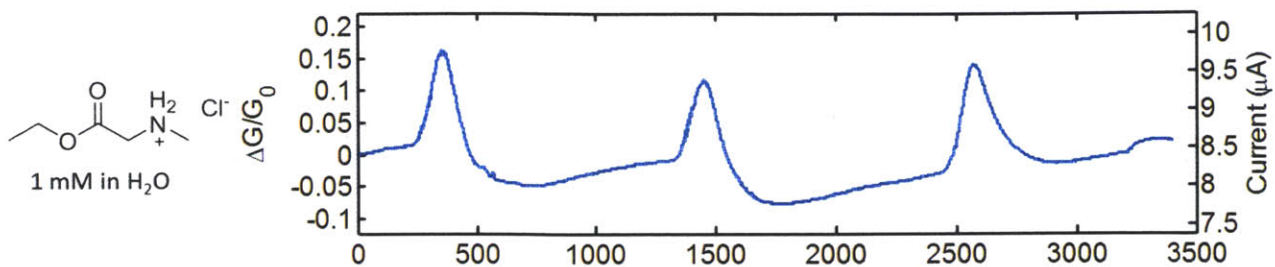


Figure 5.16. Sensing of **4** with **TiIII@SWCNTs** at pH 5.

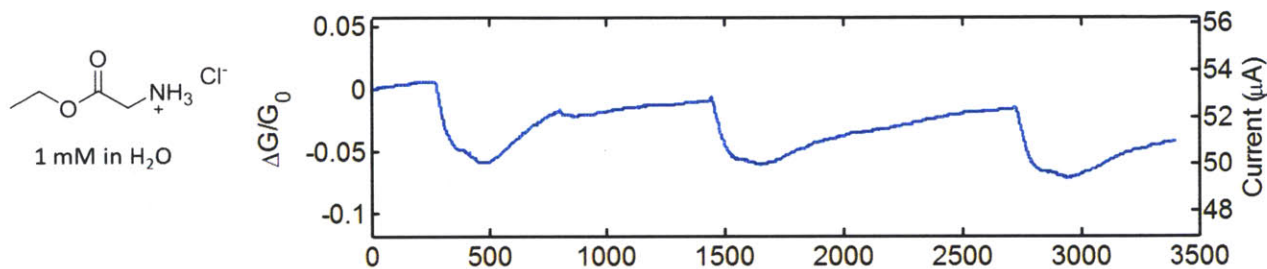


Figure 5.17. Sensing of **5** with **TiIII@SWCNTs** at pH 5.

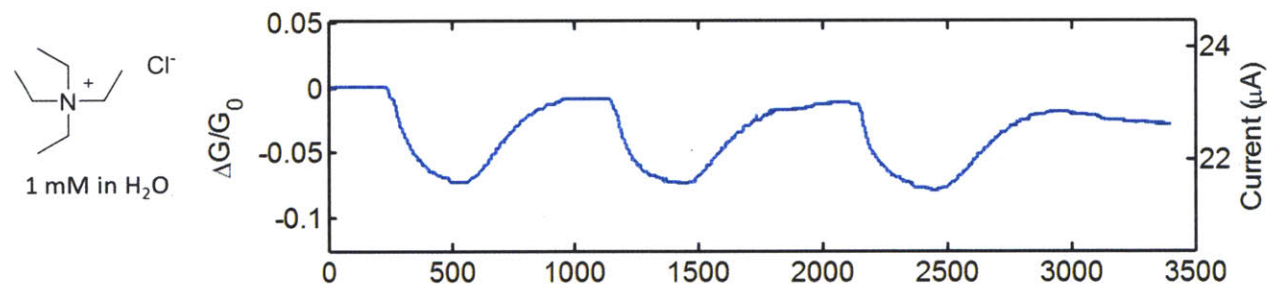


Figure 5.18. Sensing of **6** with **TiIII@SWCNTs** at pH 5.

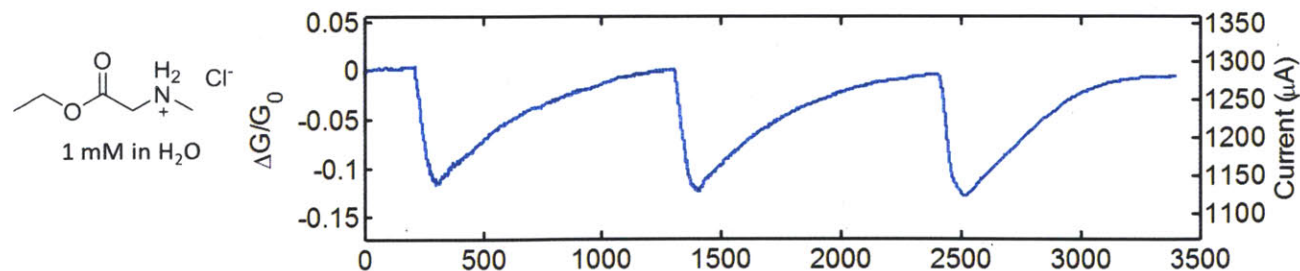


Figure 5.19. Sensing of **4** with pristine SWCNTs at pH 5.

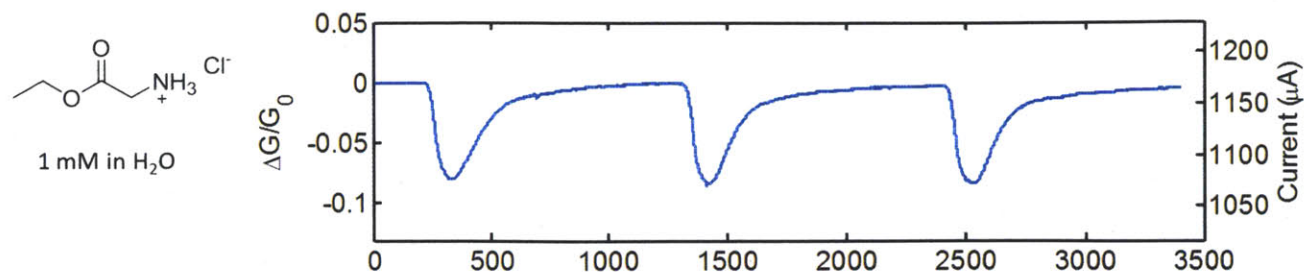


Figure 5.20. Sensing of **5** with pristine SWCNTs at pH 5.

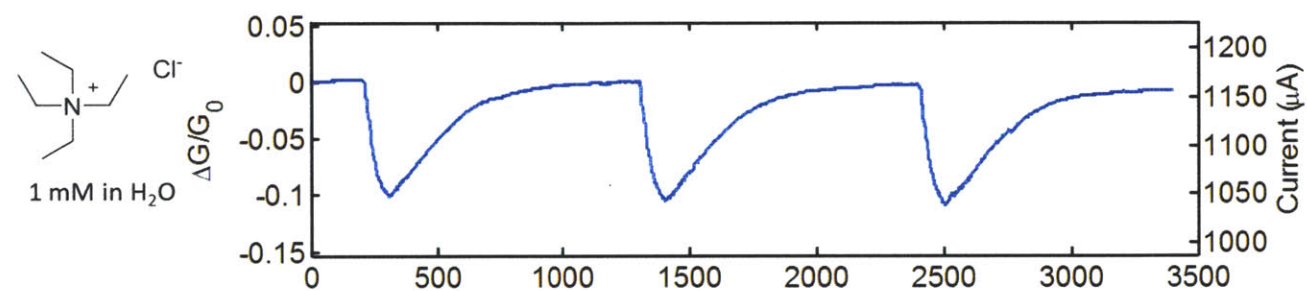


Figure 5.21. Sensing of **6** with pristine SWCNTs at pH 5.

To investigate the device to device reproducibility, the response of four different devices to **4** was compared (Figure 5.22-25). Due to the device fabrication technique, the structure of the CNT network varies from device to device which results in different responses to **4** (Figure 5.26), while the error for measurements with the same device, is small compared to the device to device differences.

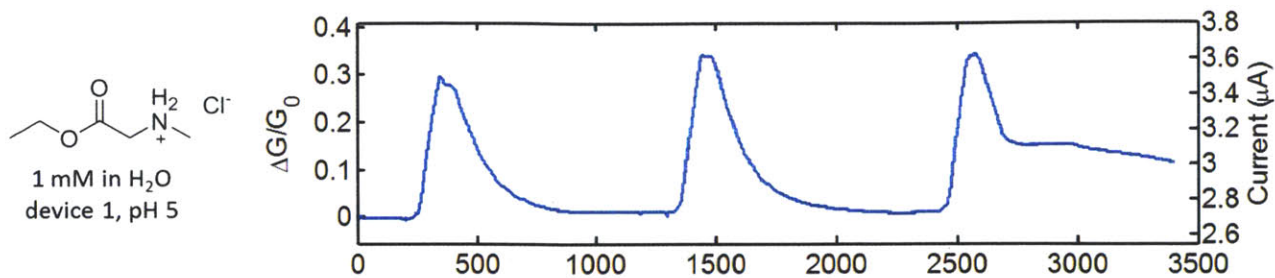


Figure 5.22. Sensing of **4** with **TiIII@SWCNTs** at pH 5 using device 1.

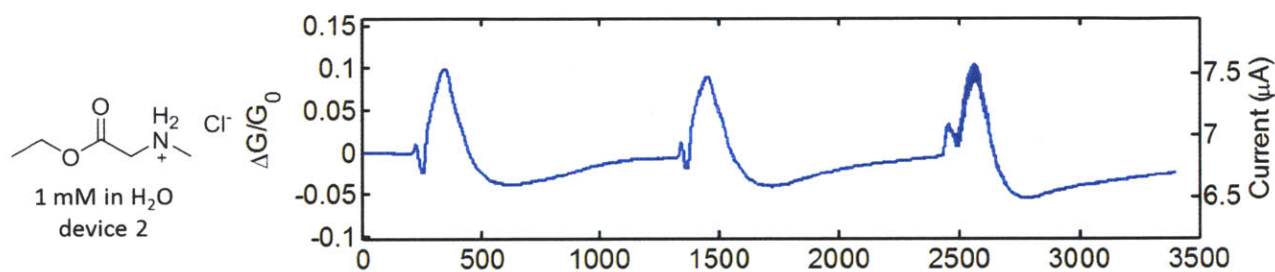


Figure 5.23. Sensing of **4** with **TiIII@SWCNTs** at pH 5 using device 2.

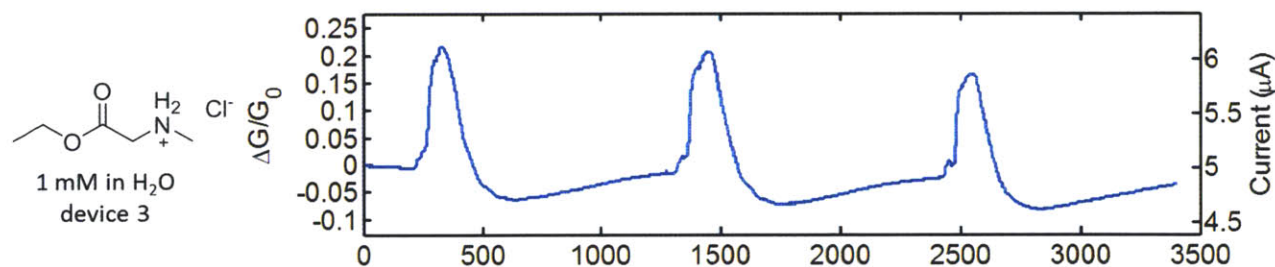


Figure 5.24. Sensing of **4** with **TiIII@SWCNTs** at pH 5 using device 3.

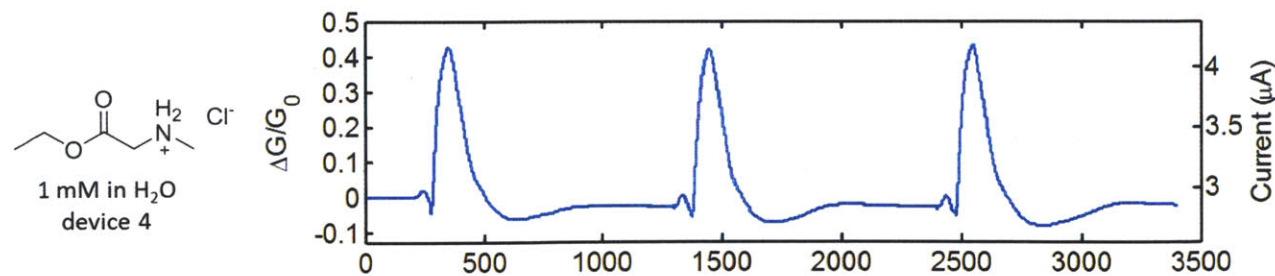


Figure 5.25. Sensing of **4** with **TiIII@SWCNTs** at pH 5 using device 4.

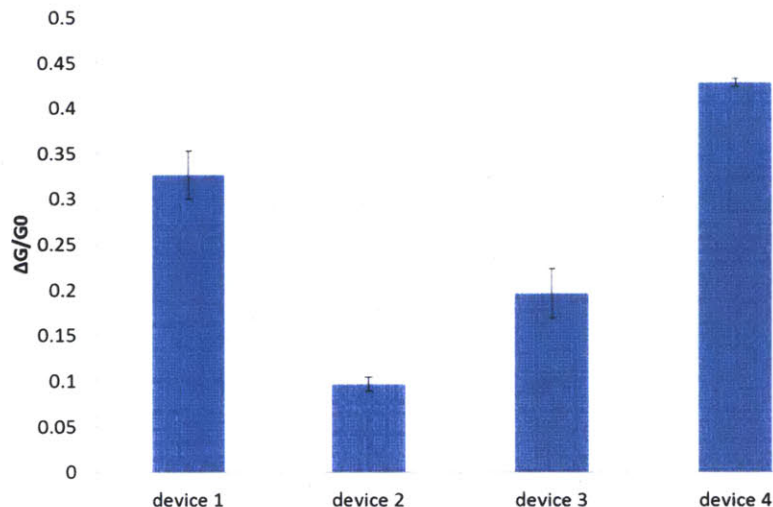


Figure 5.26. Sensing of **4** with $\text{Ti}^{\text{III}}@$ SWCNTs using different devices, error bars are based on three consecutive measurements with the same device.

To investigate the pH dependence of sensing of **4** with $\text{Ti}^{\text{III}}@$ SWCNTs, a measurement was performed at pH 7 showing a decrease in current when the device was exposed to the analyte. This can be attributed to the decreasing binding constant with increasing pH and as a result a response comparable to that of weaker binders (**5** or **6**) at pH 5.

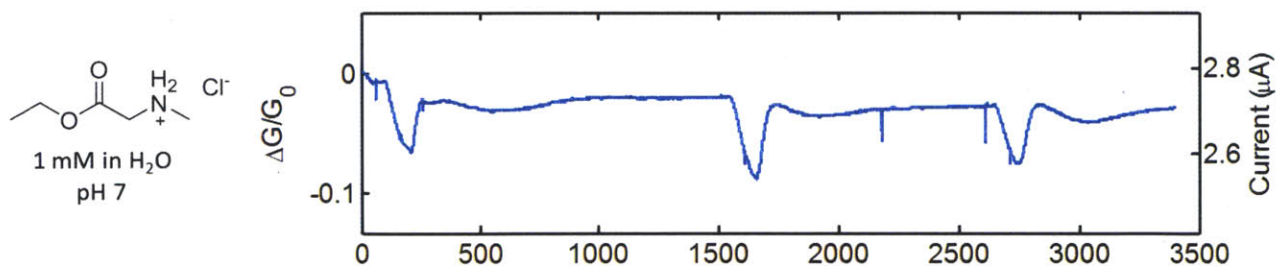


Figure 5.27. Sensing of **4** with $\text{Ti}^{\text{III}}@$ SWCNTs at pH 7 (using device 1).

5.5. References

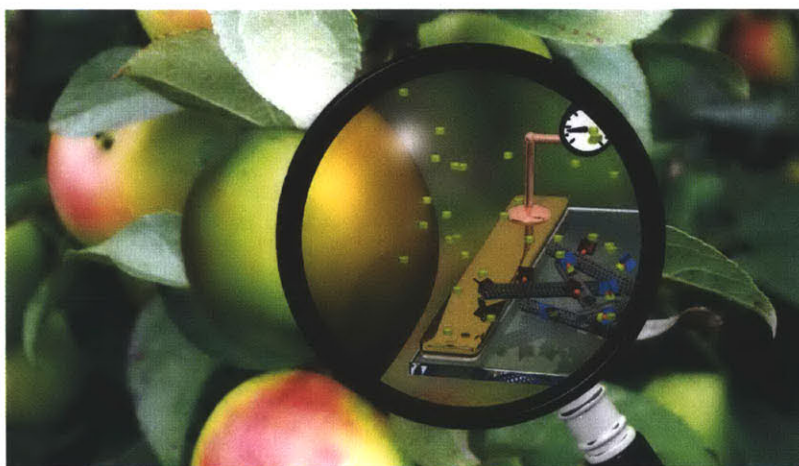
- (1) Swager, T. M. *Accounts Chem. Res.* **1998**, *31*, 201.
- (2) Schnorr, J. M.; Swager, T. M. *Chem. Mater.* **2011**, *23*, 646.
- (3) Potyrailo, R. A.; Surman, C.; Nagraj, N.; Burns, A. *Chem. Rev.* **2011**, *111*, 7315.
- (4) Liu, S.; Shen, Q.; Cao, Y.; Gan, L.; Wang, Z.; Steigerwald, M. L.; Guo, X. *Coord. Chem. Rev.* **2010**, *254*, 1101.
- (5) Li, L.; Yang, Z.; Gao, H.; Zhang, H.; Ren, J.; Sun, X.; Chen, T.; Kia, H. G.; Peng, H. *Adv. Mater.* **2011**, *23*, 3730.
- (6) Kim, T. H.; Lee, B. Y.; Jaworski, J.; Yokoyama, K.; Chung, W.-J.; Wang, E.; Hong, S.; Majumdar, A.; Lee, S.-W. *ACS nano.* **2011**, *5*, 2824.
- (7) Wei, B.; Zhang, L.; Chen, G. *New J. Chem.* **2010**, *34*, 453.
- (8) Wang, F.; Gu, H.; Swager, T. M. *J. Am. Chem. Soc.* **2008**, *130*, 5392.
- (9) Wei, G.; Xu, F.; Li, Z.; Jandt, K. D. *J. Phys. Chem. C.* **2011**, *115*, 11453.
- (10) Fang, Y.; Guo, S.; Zhu, C.; Dong, S.; Wang, E. *Chem. Asian J.* **2010**, *5*, 1838.
- (11) Lai, G.; Wu, J.; Ju, H.; Yan, F. *Adv. Funct. Mater.* **2011**, *21*, 2938.
- (12) Guo, X.; Gorodetsky, A. A.; Hone, J.; Barton, J. K.; Nuckolls, C. *Nat. Nanotechnol.* **2008**, *3*, 163.
- (13) Sorgenfrei, S.; Chiu, C.-yang; Gonzalez, R. L.; Yu, Y.-J.; Kim, P.; Nuckolls, C.; Shepard, K. L. *Nat. Nanotechnol.* **2011**, *6*, 126.
- (14) Chen, R. J.; Zhang, Y.; Wang, D.; Dai, H. *J. Am. Chem. Soc.* **2001**, *123*, 3838.
- (15) Lei, J.; Ju, H. *Nanomed. Nanobiotechnol.* **2010**, *2*, 496.
- (16) Tang, X.; Bansaruntip, S.; Nakayama, N.; Yenilmez, E.; Chang, Y.-L.; Wang, Q. *Nano Lett.* **2006**, *6*, 1632.
- (17) Wu, H.-C.; Chang, X.; Liu, L.; Zhao, F.; Zhao, Y. *J. Mater. Chem.* **2010**, *20*, 1036.
- (18) Descalzo, A. B.; Martínez-Máñez, R.; Sancenón, F.; Hoffmann, K.; Rurack, K. *Angew. Chem. Int. Ed.* **2006**, *45*, 5924.

- (19) Pirondini, L.; Dalcanale, E. *Chem. Soc. Rev.* **2007**, *36*, 695.
- (20) Ogoshi, T.; Ikeya, M.; Yamagishi, T.-aki; Nakamoto, Y.; Harada, A. *J. Phys. Chem. C.* **2008**, *112*, 13079.
- (21) Zhao, Y.-L.; Stoddart, J. F. *Accounts Chem. Res.* **2009**, *42*, 1161-71.
- (22) Wang, F.; Yang, Y.; Swager, T. M. *Angew. Chem. Int. Ed.* **2008**, *47*, 8394.
- (23) Wang, F.; Swager, T. M. *J. Am. Chem. Soc.* **2011**, *133*, 11181.
- (24) Kong, L.; Wang, J.; Meng, F.; Chen, X.; Jin, Z.; Li, M.; Liu, J.; Huang, X.-J. *J. Mater. Chem.* **2011**, *21*, 11109.
- (25) Yebeutchou, R. M.; Tancini, F.; Demitri, N.; Geremia, S.; Mendichi, R.; Dalcanale, E. *Angew. Chem. Int. Ed.* **2008**, *47*, 4504.
- (26) Yebeutchou, R. M.; Dalcanale, E. *J. Am. Chem. Soc.* **2009**, *131*, 2452.
- (27) Dionisio, M.; Oliviero, G.; Menozzi, D.; Federici, S.; Yebeutchou, R. M.; Schmidtchen, F. P.; Dalcanale, E.; Bergese, P. *J. Am. Chem. Soc.* **2012**, *134*, 2392.
- (28) Biavardi, E.; Favazza, M.; Motta, A.; Fragalà, I. L.; Massera, C.; Prodi, L.; Montalti, M.; Melegari, M.; Condorelli, G. G.; Dalcanale, E. *J. Am. Chem. Soc.* **2009**, *131*, 7447.
- (29) Hauke, F.; Myles, A. J.; Rebek, J. J. *Chem. Commun.* **2005**, 4164.
- (30) Schnorr, J. M.; Swager, T. M. *J. Mater. Chem.* **2011**, *21*, 4768.
- (31) Gao, C.; He, H.; Zhou, L.; Zheng, X.; Zhang, Y. *Chem. Mater.* **2009**, *21*, 360.
- (32) Singh, P.; Kumar, J.; Toma, F. M.; Raya, J.; Prato, M.; Fabre, B.; Verma, S.; Bianco, A. *J. Am. Chem. Soc.* **2009**, *131*, 13555.
- (33) Singh, P.; Toma, F. M.; Kumar, J.; Venkatesh, V.; Raya, J.; Prato, M.; Verma, S.; Bianco, A. *Chem. Eur. J.* **2011**, *17*, 6772.
- (34) Engtrakul, C.; Davis, M. F.; Mistry, K.; Larsen, B. a; Dillon, A. C.; Heben, M. J.; Blackburn, J. L. *J. Am. Chem. Soc.* **2010**, *132*, 9956.
- (35) Biavardi, E.; Tudisco, C.; Maffei, F.; Motta, A.; Massera, C.; Condorelli, G. G.; Dalcanale, E. *Proc. Natl. Acad. Sci. USA.* **2012**, *109*, 2263.
- (36) Biavardi, E.; Battistini, G.; Montalti, M.; Yebeutchou, R. M.; Prodi, L.; Dalcanale, E. *Chem. Commun.* **2008**, 1638.

- (37) Sreekumar, A.; Poisson, L. M.; Rajendiran, T. M.; Khan, A. P.; Cao, Q.; Yu, J.; Laxman, B.; Mehra, R.; Lonigro, R. J.; Li, Y.; Nyati, M. K.; Ahsan, A.; Kalyana-Sundaram, S.; Han, B.; Cao, X.; Byun, J.; Omenn, G. S.; Ghosh, D.; Pennathur, S.; Alexander, D. C.; Berger, A.; Shuster, J. R.; Wei, J. T.; Varambally, S.; Beecher, C.; Chinnaiyan, A. M. *Nature*. **2009**, *457*, 910.
- (38) Jentzmik, F.; Stephan, C.; Miller, K.; Schrader, M.; Erbersdobler, A.; Kristiansen, G.; Lein, M.; Jung, K. *Eur. Urol.* **2010**, *58*, 12.

CHAPTER 6

Determining Fruit Ripeness with SWCNT-based Sensors



Studies in this chapter are in collaboration with Birgit Esser

Adapted and reprinted in part with permission from:

Esser, B.; **Schnorr, J. M.**; Swager, T. M. “Selective Detection of Ethylene Gas Using Carbon Nanotube-based Devices: Utility in Determination of Fruit Ripeness”

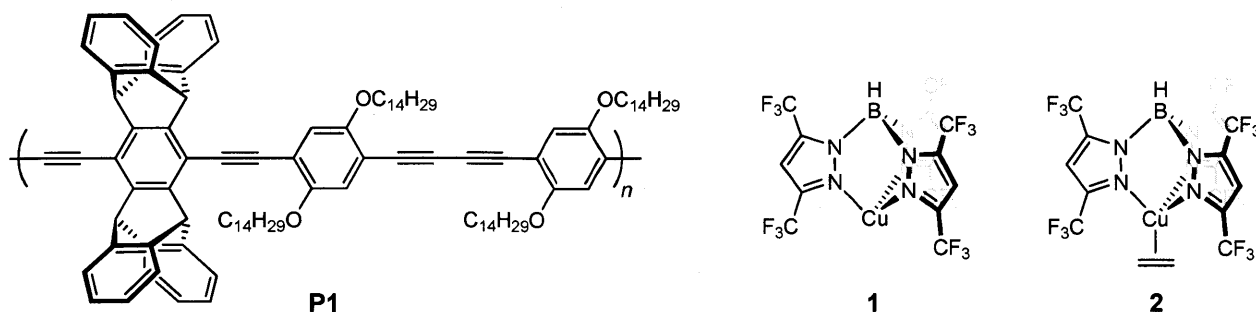
Angew. Chem. Int. Ed. **2012**, *Early View Article*

6.1. Introduction

Ethylene plays an important role in a variety of processes in plants. Among others, it initiates ripening of fruit, promotes flowering, and causes senescence of leaves and flowers.¹ Being able to accurately monitor ethylene concentrations is of high importance in the horticultural industries. The internal ethylene concentration in fruit can serve as an indicator for determining the ideal time of harvest, while monitoring of the atmospheric ethylene level in storage facilities and during transportation is crucial for avoiding overripening and eventually spoilage of fruit. Currently, a variety of systems are available, which rely on gas chromatography² or laser acoustic spectroscopy.³ Both of these methods however require relatively expensive instrumentation and are thus mostly suited for use in large storage facilities and not for monitoring small amounts, e.g. in storage rooms of grocery stores or during transport. Other ethylene sensing options include amperometric⁴ or electrochemical⁵ methods or take advantage of changes in luminescence properties.^{6,7} Additionally, colorimetric gas-sampling tubes are commercially available.¹

In our laboratory, Birgit Esser has previously demonstrated that thin films of poly(*p*-phenylene butadiynylene) **P1** and copper scorpionate **1** can be utilized to detect ethylene (Scheme 6.1).⁷ In a mixture of **P1** and **1**, the copper scorpionate quenches the fluorescence of the polymer. Exposing the system to ethylene leads to formation of ethylene complex **2**, reducing the interaction of the copper complex with the polymer and thus restoring the initial fluorescence. Complex **1** was chosen because its ethylene complex **2** is one of the most stable copper-ethylene complexes known.^{8,9} Furthermore, **1** is not easily oxidized under ambient conditions, which is important for its practical utility in a sensor. Using the commercially available Fido platform with the polymer/Cu(I) system, real time detection of 1000 ppm ethylene was possible.⁷

Scheme 6.1. Poly(*p*-phenylene butadiynylene) **P1**, copper scorpionate **1** and copper ethylene complex **2**



While these results were promising, a further improvement of the sensitivity of the system was necessary to monitor ethylene concentrations in typical applications. Desired concentrations in ripening rooms are held between 10 and 200 ppm, which is in the same range as the ethylene concentration in the vicinity of ripening fruit. In storage facilities, ethylene concentrations are kept below 1 ppm to suppress undesired ripening.¹ Besides improving the sensitivity, it was also desirable to switch from a fluorescence based sensing scheme to an amperometric system. The latter greatly simplifies the required instrumentation and in the simplest case only a power source and an ammeter is required in addition to the sensing unit. We were hoping to achieve both improvements by switching from a conjugated polymer to an SWCNT-based system. Similar to the sensors described in chapters four and five, the conductivity of a network of CNTs between two electrodes would be affected by exposure to an analyte. We envisioned that combining complex **1** with SWCNTs would lead to nanotube-copper interactions. Exposing the system to ethylene and the resulting binding of the molecule to the copper centers would likely affect the interactions between the copper and the CNTs or lead to a swelling of the CNT network. In both cases, ethylene binding would alter the electronic properties of the CNT network (Figure 6.1).

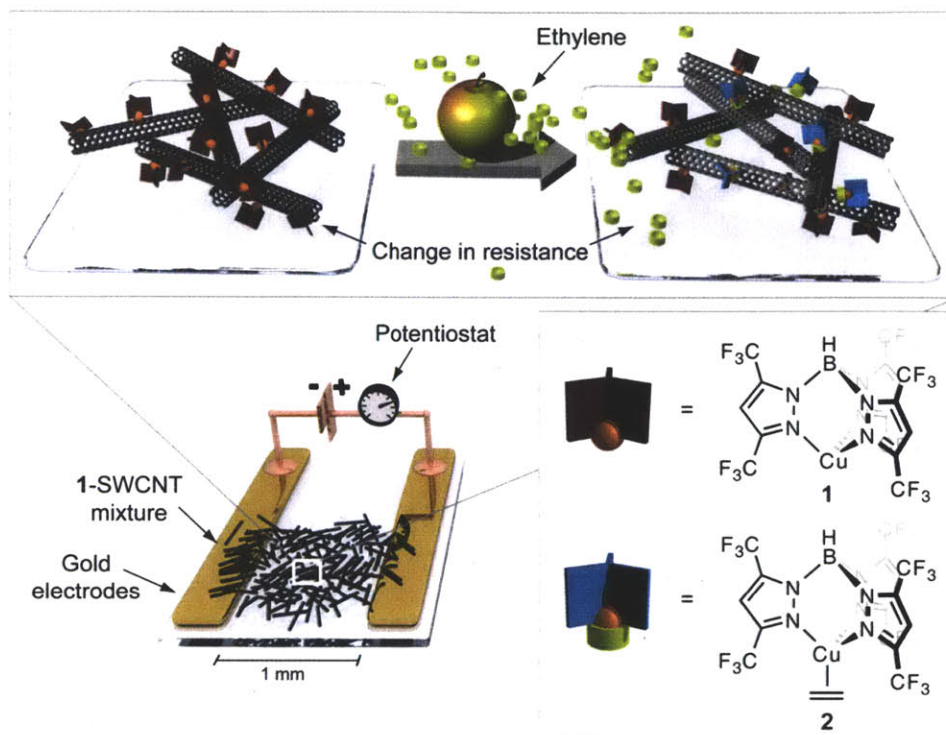


Figure 6.1. Schematic representation of ethylene detection by an amperometric sensor: A network of SWCNTs containing copper complex **1** is deposited between two electrodes. Exposure to ethylene leads to formation of **2** resulting in a resistance change of the network.

Initial attempts by Birgit Esser included the functionalization of SWCNTs with thioether moieties that we expected to promote the interaction of **1** and nanotubes. This was done both via non-covalent wrapping of SWCNTs with sulfide-carrying polythiophenes as well as through covalent functionalization with ethyl phenyl sulfide groups. However, control experiments showed that better results could be obtained by simple mixing of pristine SWCNTs with **1**. In this chapter, the development of a sensing system that can detect sub-ppm concentrations of ethylene based on this non-covalent SWCNT functionalization approach is described together with the test of its practical utility in monitoring ripening stages of different fruit.

6.2. Results and Discussion

6.2.1. Non-covalent SWCNT Functionalization and Sensor Fabrication

In order to prepare the sensing material, copper(I) complex **1** carrying a fluorinated tris(pyrazolyl)borate ligand in toluene was mixed with pristine SWCNTs in *o*-dichlorobenzene in a 6:1 molar ratio (**1** to CNT carbons). After subsequent sonication, the resulting suspension of **1**-SWCNT was drop-cast onto glass slides that were equipped with gold electrodes. For a 1 mm gap between the two electrodes, resistances of 1 – 5 k Ω were typically measured after drying *in vacuo*.

Initially, the devices were analyzed by Fourier-transform infrared spectroscopy (FT-IR) as well as Raman spectroscopy. IR spectroscopy of **1**-SWCNT shows C-F stretching modes of the ligand between 1080 and 1260 cm^{-1} . Furthermore, the ν_{BH} shift is observed at 2607 cm^{-1} (Figure 6.2).

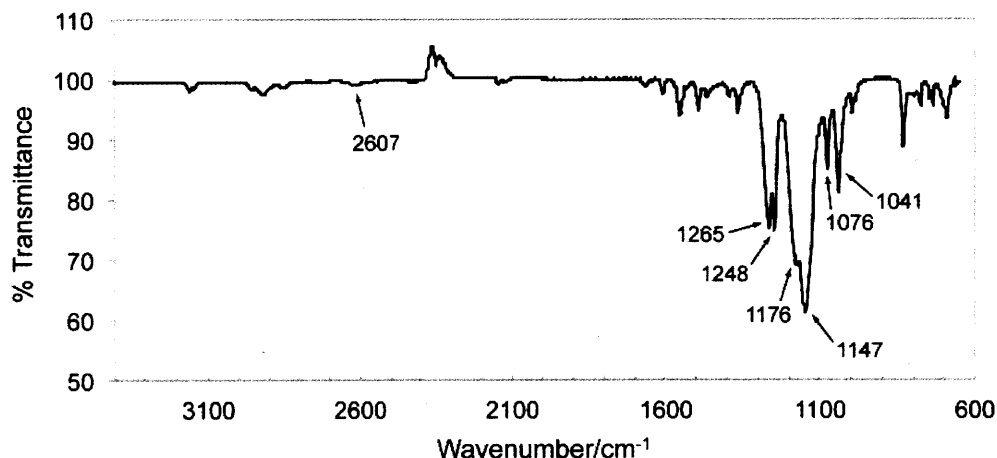


Figure 6.2. FT-IR spectrum of **1**-SWCNT.

Raman spectroscopy of **1**-SWCNT shows a slight shift of the G and G' bands to lower energies compared to pristine SWCNTs (Figure 6.3). This can indicate p-type doping and thus confirms the interaction of **1** with the CNTs.¹⁰

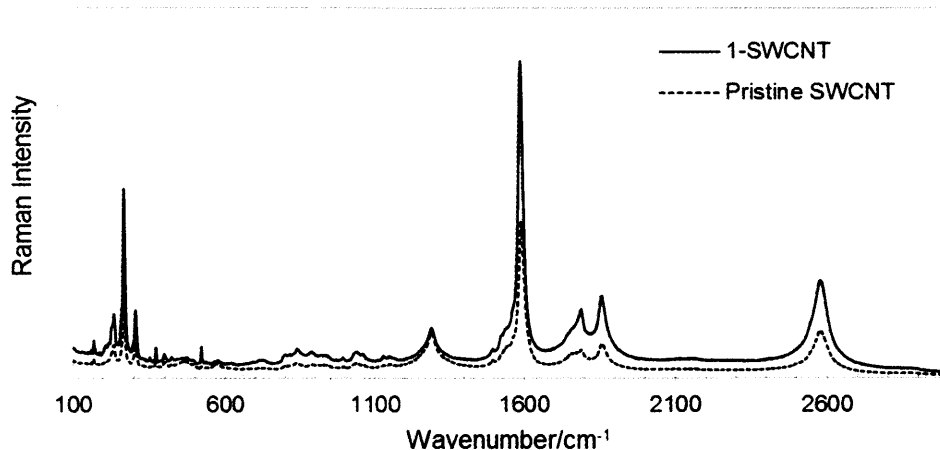


Figure 6.3. Raman spectrum of 1-SWCNT in comparison to pristine SWCNTs.

To further confirm the presence of complex **1** in 1-SWCNT, X-ray photoelectron spectroscopy (XPS) was performed (Figure 6.4). Signals were observed for the expected elements Cu, F, N and C, and the ratio of SWCNT carbons to **1** was determined to be 22:1 based on the Cu 2p signal. This ratio is different from the initial 6:1 ratio in the mixing process, which could be caused by an inhomogeneous drop-casting suspension or partial evaporation of **1** in the ultra-high vacuum system of the XPS instrument ($< 2 \cdot 10^{-8}$ Torr).

High resolution XPS scans of the Cu 2p region showed the characteristic pattern for copper(I) consisting of two peaks at 932 and 952 eV (Figure 6.4b). The binding energies for the Cu 2p electrons in 1-SWCNT are consistent with the energies observed for **1** and **2** (calibrated using the F 1s peak at 687 eV). Furthermore, no significant amounts of Cu(II) could be observed for 1-SWCNT, which would have resulted in an additional set of signals at 934 and 954 eV.

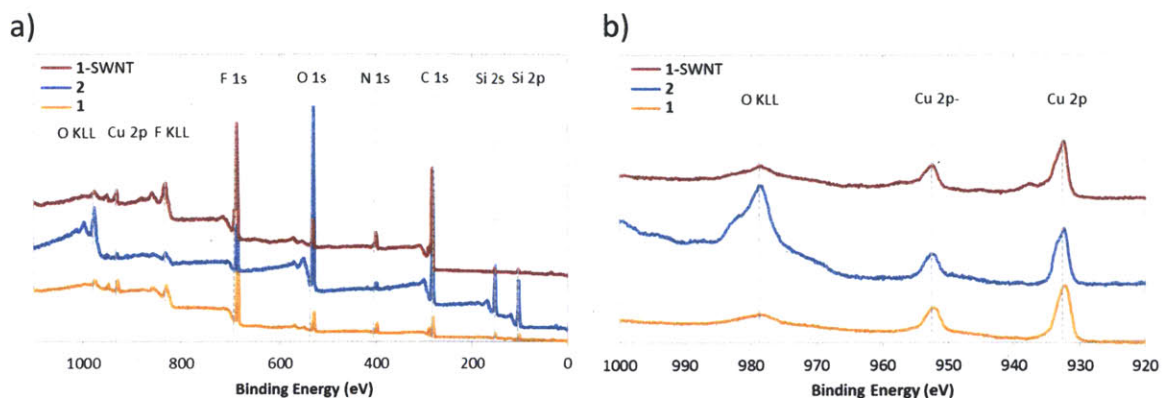


Figure 6.4. XPS measurements: (a) Survey scans of 1, 2, and 1-SWCNT and (b) high resolution scans of the Cu 2p region of 1, 2, and 1-SWCNT. Si and O signals are due to the utilized (partially oxidized) silicon substrate.

In order to investigate the structure of the obtained film after drop-casting, scanning electron microscopy (SEM) was employed. Images of 1-SWCNT at 3,300x magnification show a smooth film (Figure 6.5a), and at higher magnification SWCNT bundles are visible (Figure 6.5b).

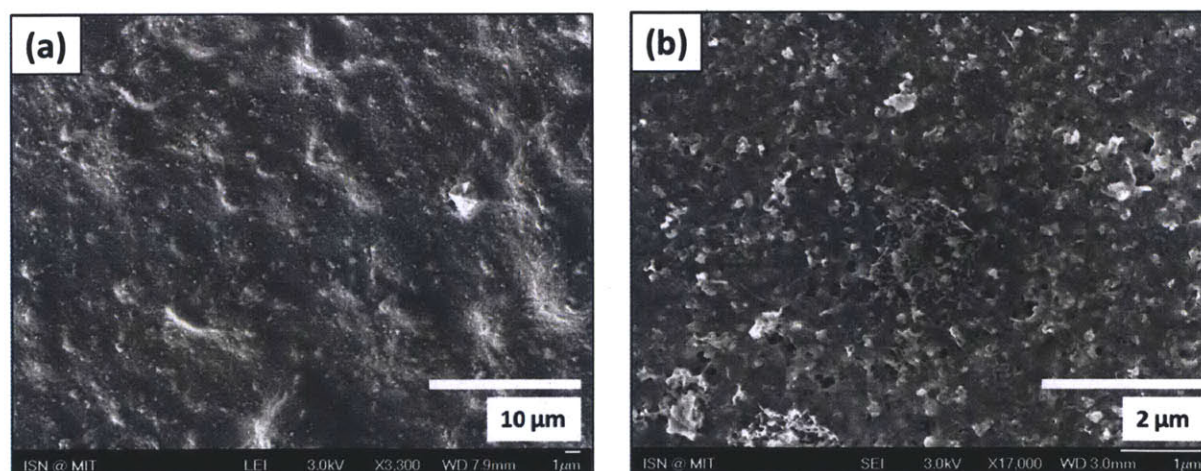


Figure 6.5. SEM images of 1-SWCNT devices: (a) 1-SWCNT drop-cast on glass at 3,300x magnification and (b) at 17,000x magnification

6.2.2. Ethylene Sensing: Sensitivity, Selectivity, and Stability

The ethylene sensing experiments were performed by connecting a Teflon enclosure containing the device (see chapters 4 and 5) to a gas generation system (Figure 6.6).

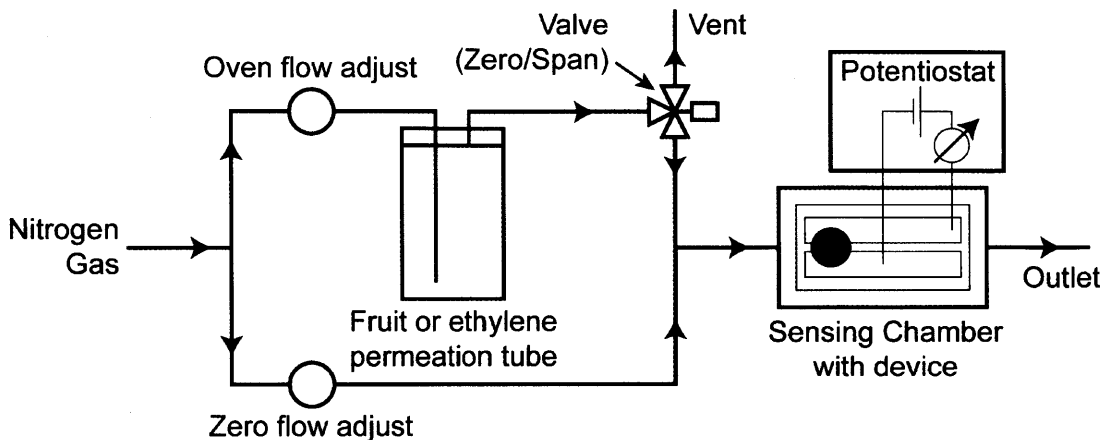


Figure 6.6. Experimental setup for sensing measurements: A continuous gas flow is directed through the device chamber. The gas stream can be switched between nitrogen gas (“Zero” mode) or the nitrogen gas analyte mixture (“Span” mode), in which the gas stream runs through the flow chamber containing the analyte (ethylene) or a piece of fruit.

In the gas generation system, a stream of nitrogen gas is split into two parts, one of which is directly led to the Teflon enclosure with the device (“zero flow”). The other part is passed over a permeation tube with ethylene, a vial with a potential interferent, or over a piece of fruit. During exposure (“span mode”) this stream is mixed with the zero flow stream before being passed over the device. Using this system, we were able to deliver between 0.5 and 50 ppm of ethylene as well as the desired concentrations of potential interferents or fruit vapor.

Using the described setup, we initially investigated how the type of utilized SWCNTs affects the sensing performance. As described in chapter 1, SWCNTs vary widely in length, diameter, and

chirality. We chose to prepare 1-SWCNT devices from five different types of commercially available SWCNTs:

- SG65 (SouthWest NanoTechnologies): tube diameter 0.8 ± 0.1 nm, 90% carbon content by weight, >50% (6,5)CNTs, >90% of tubes are semiconducting
- SG65-SRX (SouthWest NanoTechnologies): tube diameter 0.8 ± 0.1 nm, 99% carbon content by weight, >30% (6,5)CNTs, >95% of tubes are semiconducting
- SG76 (SouthWest NanoTechnologies): tube diameter 0.9 ± 0.2 nm, 90% carbon content by weight, >50% (7,6)CNTs, high conductivity
- CG100 (SouthWest NanoTechnologies): tube diameter 1.0 ± 0.3 nm, 90% carbon content by weight, good electrical conductivity
- Unidym (Unidym, Super Pure): tube diameter 1.0 ± 0.2 nm, Fe(IV) residue by TGA: <5 wt%

Upon exposure to 20 ppm ethylene, 1-SWCNT devices prepared from SG65 SWCNTs showed the highest current change (Figure 6.7).

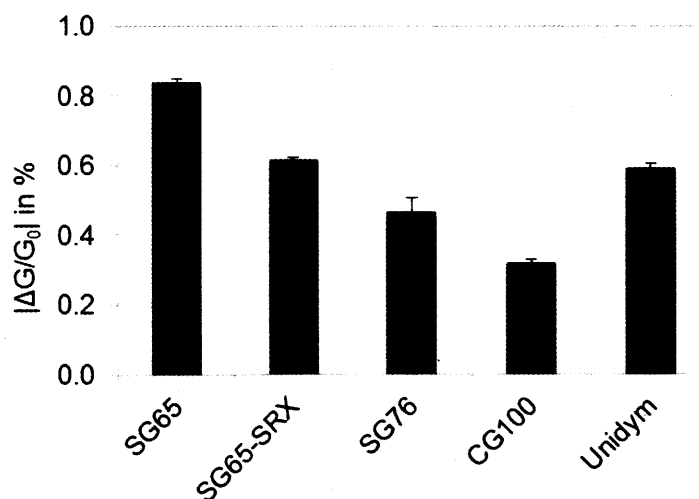


Figure 6.7. Response of 1-SWCNT devices prepared from different types of SWCNTs to 20 ppm ethylene.

The variance in performance of the different devices can be based on a variety of factors including the SWCNT purity, chirality, conductivity, aspect ratio, and radius. Based on the significant difference between SG65 and SG65-SRX, which both contain mostly semiconducting species, have a similar aspect ratio and are of comparable purity, we estimate that the higher content of small diameter (6,5)SWCNTs in SG65 is an important contributor to a good sensing response. Typically, a higher curvature of a graphitic carbon system leads to a higher reactivity, which could in turn lead to a better interaction of the CNT surface with 1.

After choosing SG65 SWCNTs for the sensor preparation, we measured the response of 1-SWCNT devices to ethylene exposures at concentrations between 0.5 and 50 ppm showing good signal to noise ratios for concentrations as low as 1 ppm (Figure 6.8).

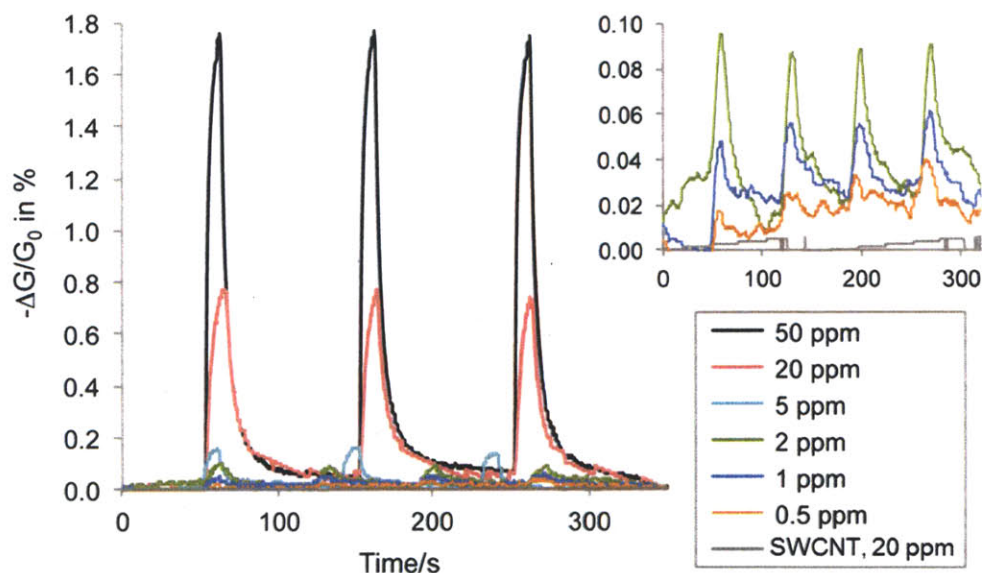


Figure 6.8. Relative response of 1-SWCNT devices to 0.5, 1, 2, 5, 20, and 50 ppm ethylene and of pristine SWCNT to 20 ppm ethylene (the inset shows the response of 1-SWCNT to 0.5, 1, and 2 ppm and of SWCNT to 20 ppm ethylene). Data plotted is the 5 s floating average of the measurement data.

In the range of 1 to 50 ppm a linear relationship between ethylene concentration and current change was observed (Figure 6.9) facilitating the determination of ethylene levels in potential applications.

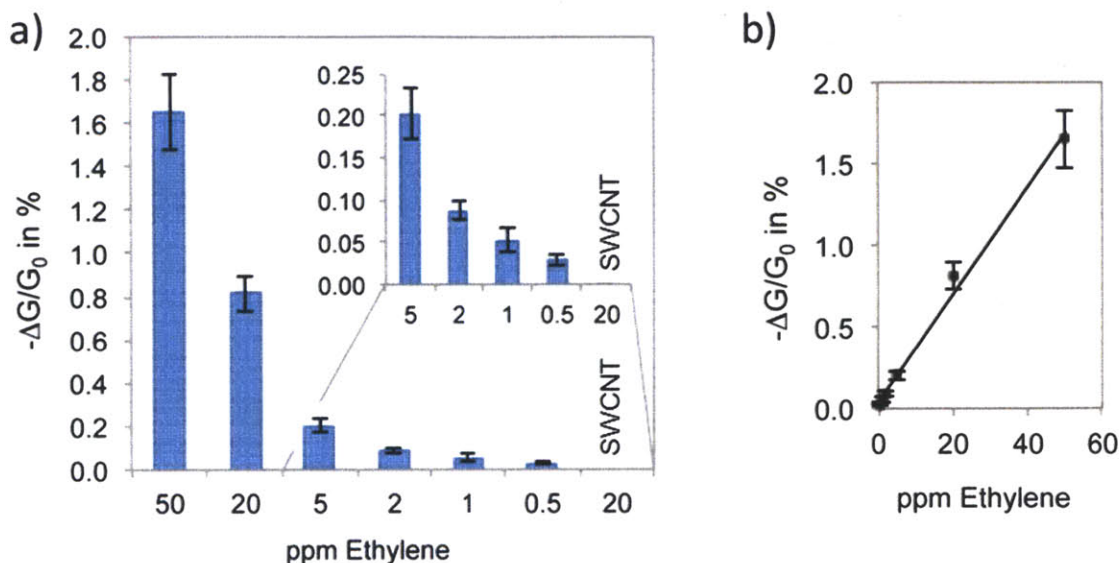


Figure 6.9. (a) Average responses from three different 1-SWCNT devices each to different ethylene concentrations as well as the response of pristine SWCNT devices to 20 ppm ethylene; (b) average response vs. ethylene concentration for 1-SWCNT devices.

While a good sensitivity was observed using 1-SWCNTs, pristine SWCNTs led to no response to 20 ppm ethylene. Further controls using devices prepared by mixing 2, $[\text{Cu}(\text{CH}_3\text{CN})_4]\text{PF}_6$ (3), or the sodium complex 4 with SWCNTs showed no response to ethylene in the latter two cases, and in the case of 2-SWCNT a current change was observed that was 75% lower than the change for 1-SWCNT (Figure 6.10).

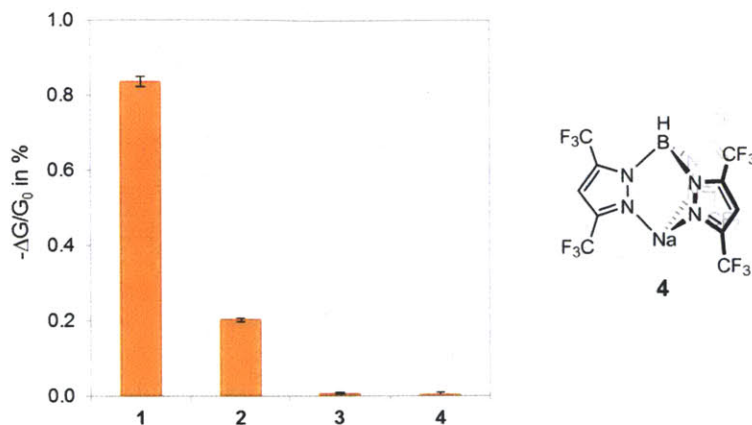


Figure 6.10. Responses of devices made from **1**-SWCNT, **2**-SWCNT, SWCNTs with **3**, and **4**-SWCNT to 20 ppm ethylene.

The selectivity of **1**-SWCNT devices was evaluated by measuring their response to a variety of solvents representing different functional groups as well as their response to the fruit metabolites ethanol and acetaldehyde. Concentrations of 75 to 200 ppm were chosen for these potential interferents, and the responses of the devices were compared to 50 ppm ethylene (Figure 6.11).

All responses to interferents were lower than the response to ethylene, even though the concentrations of the interferents were increased by factors between 1.5 and 4. High responses were observed for acetonitrile, THF and acetaldehyde, while the other analytes only caused small changes in current.

Depending on the type of fruit, ripening typically occurs at concentrations between 0.1 and 1 ppm.¹ The ethylene concentration in storage rooms is therefore kept below these thresholds. While the sensitivity of **1**-SWCNT devices was within the range of ethylene levels in ripening rooms, a further improvement of this parameter was desirable to expand the application scope of the devices to storage facilities.

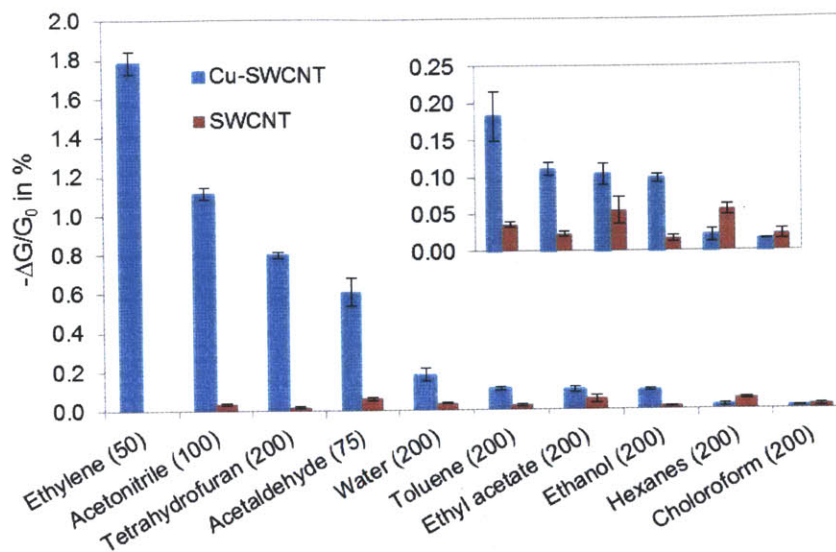


Figure 6.11. Response of **1**-SWCNT devices and pristine SWCNTs to 50 ppm ethylene and various potential interferents. Concentrations are given in ppm.

In order to improve the sensitivity of devices of **1**-SWCNT, 5 wt% cross-linked polystyrene beads (0.4-0.6 μm) were added to the mixture of **1** and SWCNTs before devices were prepared. We envisioned that introduction of polystyrene beads would lead to a higher surface area of the **1**-SWCNT network. Furthermore, we hoped that ethylene would diffuse into the polymer which could lead to a concentration effect of the analyte in the vicinity of the functionalized SWCNTs. SEM images of these **1**-PS-SWCNT devices confirmed additional surface features attributed to the polystyrene beads as well as the presence of SWCNT bundles at higher magnification (Figure 6.12).

Sensing tests with **1**-PS-SWCNT devices showed a 1.3-2.2-fold increase in current change when exposed to ethylene concentrations of 0.5, 1, and 2 ppm compared to **1**-SWCNT. In addition to the increase in current change, **1**-PS-SWCNT devices show a reduced error and noise level

(compare Figure 6.8 and Figure 6.13) at low ethylene concentrations allowing the detection of 0.5 ppm ethylene.

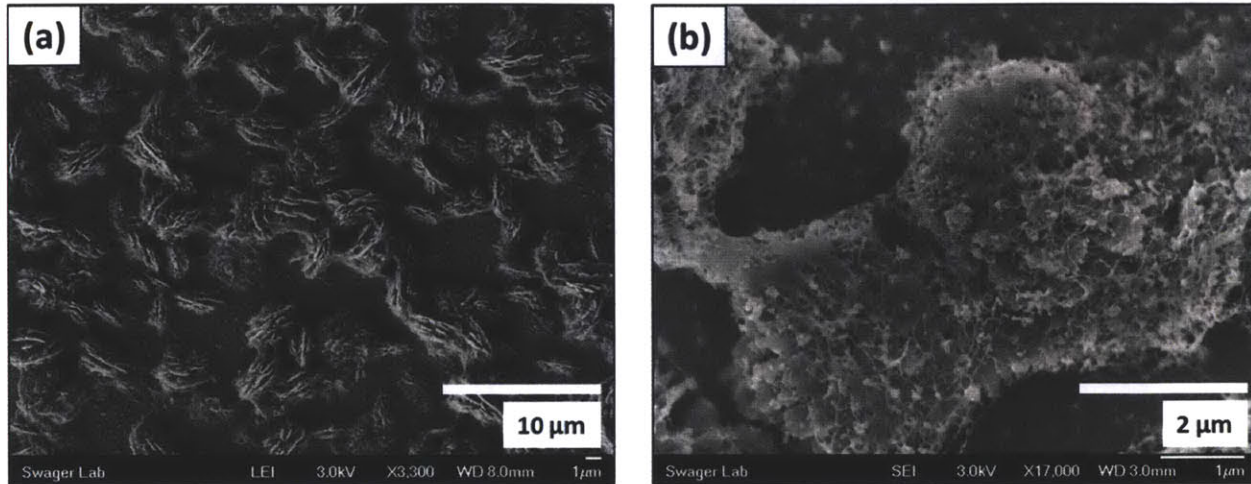


Figure 6.12. SEM images of 1-PS-SWCNT devices with 5 wt% cross-linked polystyrene beads drop-cast on glass (a) at 3,300x magnification and (b) at 17,000x magnification.

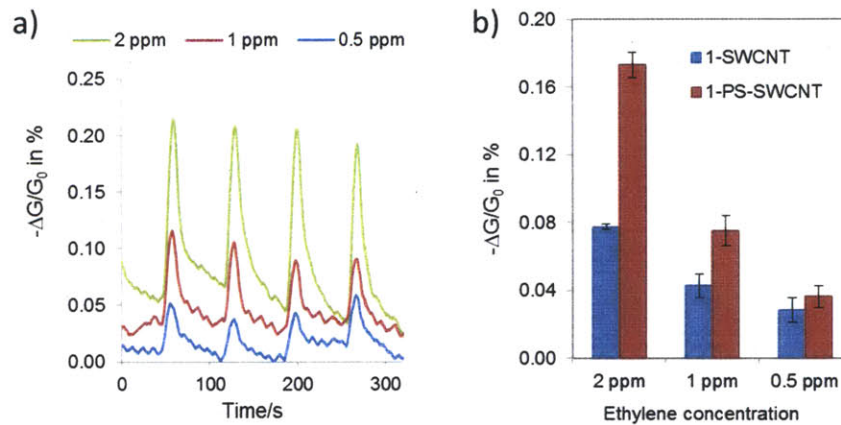


Figure 6.13. Response of 1-SWCNT and 1-PS-SWCNT devices to 0.5, 1, and 2 ppm ethylene. (a) Current traces of 1-PS-SWCNT devices exposed to ethylene; 5 s floating average; (b) Comparison between 1-SWCNT and 1-PS-SWCNT devices.

6.2.3. Monitoring of Fruit Ripening

After confirming a sensitivity of 1-SWCNT devices that was in the right range for practical applications, we were interested in exploring the response of the devices to ripening fruit. To perform measurements with fruit, we replaced the ethylene permeation tube in the gas generation system (see Figure 6.6) by a chamber containing a piece of fruit (Figure 6.14).

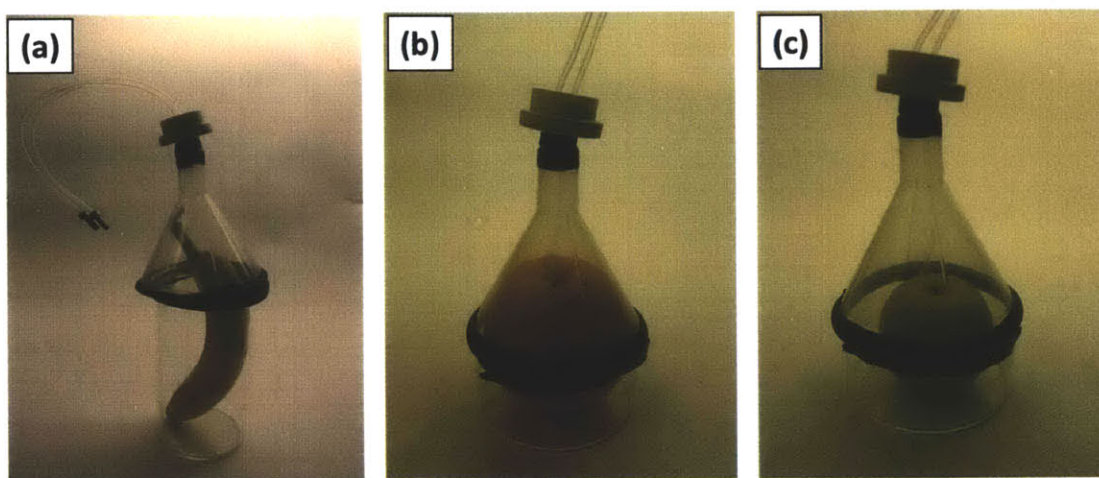


Figure 6.14. Examples for analyte chambers containing (a) banana, (b) orange, and (c) apple.

A continuous flow of nitrogen carrier gas was passed over the piece of fruit and subsequently through a Teflon enclosure containing the 1-SWCNT device (during exposure). Between exposures, the gas stream from the fruit was directed to a vent. This procedure avoided accumulation of fruit vapor in the analyte chamber between exposures and thus led to results more comparable to measurements in the field.

We tested different types of fruit: banana, avocado, apple, pear, and orange and compared the responses to these fruit to the response generated by 20 ppm ethylene (Figure 6.15). The largest response (normalized to 100 g fruit) was obtained for banana, followed by avocado, apple, pear, and orange.

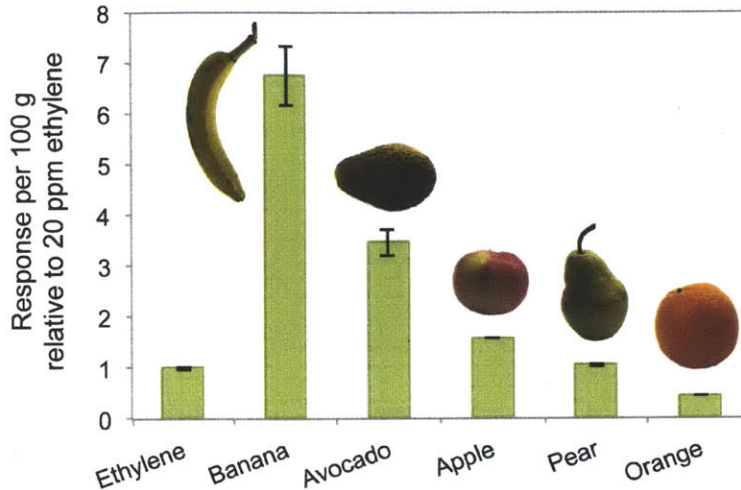


Figure 6.15. Response of 1-SWCNT devices to different fruit compared to the response to 20 ppm ethylene. Responses are normalized to 100 g fruit.

The response to all fruit was well within the sensitivity range of the sensor. Besides the orange, all responses were higher than the reference response to 20 ppm ethylene which corresponds to emission rates higher than 9600 nL min^{-1} per 100 g.

Based on respiration rate (release of CO_2) as well as ethylene production, fruit can be categorized into climacteric and non-climacteric fruit.¹ Among the tested fruit, banana, avocado, apple, and pear belong to the climacteric group, which shows a large increase of CO_2 and C_2H_4 production during ripening, while non-climacteric oranges show a low and more stable emission of these gases. After reaching ripeness, ethylene production decreases, allowing the determination of ripening levels by measuring the ethylene concentration in the vicinity of fruit.

Using 1-SWCNT sensors, we monitored the ethylene production of different fruit over time (Figure 6.16). A climacteric rise of ethylene production could be observed for the pear and avocado after the first week followed by a decrease in ethylene production of the pear indicating that the climax (ripeness) had been passed.

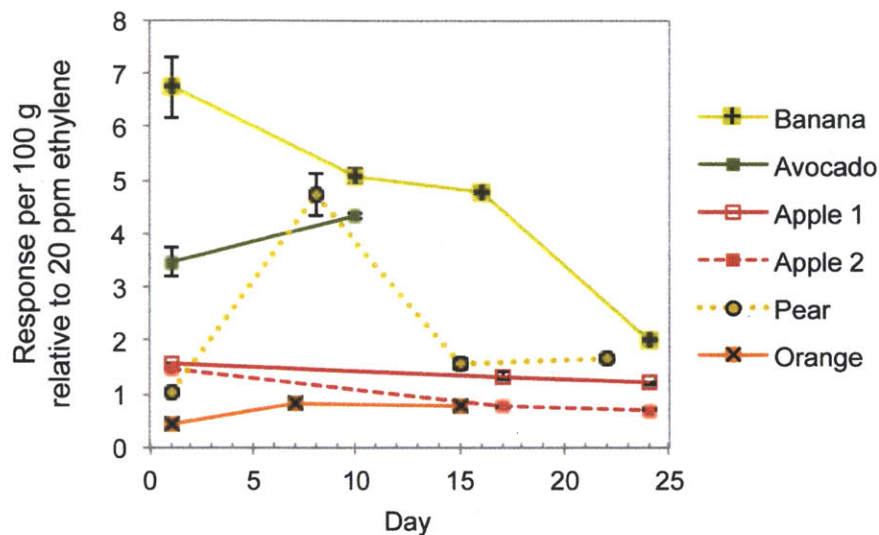


Figure 6.16. Response of 1-SWCNT devices to different fruit during ripening relative to 20 ppm ethylene and normalized to 100 g fruit. Apple 1 was stored in a refrigerator between measurements while apple 2 was kept at room temperature.

For all other climacteric fruits, declining ethylene levels were observed during the experiment, indicating that we had obtained them at or past the maximum level of ripeness. To investigate the effect of temperature on senescence, we stored one apple in a refrigerator between measurements while another one was kept at room temperature. As expected, a slower decline of ethylene levels was observed for the apple that had been stored below room temperature. In contrast to the other investigated fruit, the non-climacteric orange showed overall low ethylene levels without large variations over time.

6.3. Conclusions

In summary, we have developed an ethylene sensor by non-covalently functionalizing SWCNTs with a copper(I) complex (**1**). Sensor prototypes fabricated from 1-SWCNT exhibited a good sensitivity, which was further improved by adding cross-linked polystyrene beads to the mixture, so that ethylene concentrations as low as 0.5 ppm could be detected. This detection limit is

within the desired range for applications in the horticultural industries. The sensors showed good selectivity for ethylene over possible interferents.

We demonstrated the practical utility of the sensor by measuring ethylene emissions of a variety of fruit. Furthermore, it was possible to follow the ripening stages of fruit over time using the presented system.

6.4. Experimental Section

Materials and devices were prepared by Birgit Esser, who also performed most of the sensing measurements and control experiments. Jan M. Schnorr measured the IR, Raman, and XPS spectra and performed SEM measurements.

Materials and Synthetic Manipulations

Synthetic manipulations were carried out under an argon atmosphere using standard Schlenk techniques. $[\text{CF}_3\text{SO}_3\text{Cu}]_2\cdot\text{C}_6\text{H}_6$ was purchased from TCI America, hydrotris[3,5-bis(trifluoromethyl)pyrazol-1-yl]borato sodium ($\text{Na}[\text{HB}(3,5-(\text{CF}_3)_2\text{-pz})_3]$) was prepared following a literature procedure.⁸ Single-walled carbon nanotubes were purchased from SouthWest NanoTechnologies (SWeNT® SG65, SWeNT® SG65-SRX, SWeNT® SG76, and SWeNT® CG100) or from Unidym (HIPCO® Super Purified). Cross-linked polystyrene particles (0.4-0.6 μm diameter) were purchased from Spherotech and transferred from water into toluene. Dry toluene was purchased from J. T. Baker. All other chemicals were purchased from Sigma Aldrich and used as received. NMR spectra were recorded on Bruker Avance-400 spectrometers.

Synthesis of **1**

1 was prepared using the following procedure: 8 mg (15.9 μmol) $[\text{CF}_3\text{SO}_3\text{Cu}]_2\cdot\text{C}_6\text{H}_6$ were dissolved in 3 mL dry, degassed toluene. 17 mg (43.5 μmol) hydrotris[3,5-bis(trifluoromethyl)pyrazol-1-yl]borato sodium ($\text{Na}[\text{HB}(3,5\text{-(CF}_3)_2\text{-pz)}_3]$) were added, and the mixture was stirred for 14 h at r.t. The reaction mixture was filtrated through a syringe filter to receive a colorless solution of **1** with a concentration of $\sim 6 \mu\text{mol/mL}$ (6 mM).

The exact concentration of **1** was determined in the following way: A small amount of the solution was purged with ethylene for 20 min. The solvent was then evaporated, and the concentration of **1** determined by NMR spectroscopy using benzene as a reference for integration.

Preparation of **1**-SWCNT

0.50 mg (41.6 μmol carbon) of SWCNTs were suspended in 0.8 mL dry *o*-dichlorobenzene, and 1.16 mL (6.9 μmol) of a 6 mM solution of **1** in toluene were added. The mixture was sonicated at 30 °C for 30 min. The resulting black dispersion of **1**-SWCNT was used to prepare devices.

Preparation of **1**-PS-SWCNT

0.50 mg (41.6 μmol carbon) of SWCNTs were suspended in 0.8 mL dry *o*-dichlorobenzene, and 1.16 mL (6.9 μmol) of a 6 mM solution of **1** in toluene as well as 2.4 μL of a suspension of cross-linked polystyrene particles in toluene (5 $\mu\text{g/mL}$) were added. The mixture was sonicated at 30 °C for 30 min. The resulting black dispersion of **1**-PS-SWCNT was used to prepare devices.

Device preparation

Glass slides (VWR Microscope Slides) were cleaned by ultrasonication in acetone for 10 min, and after drying they were subjected to UV radiation in a UVO cleaner (Jelight Company Inc.) for 3 min. Using an aluminum mask, layers of chromium (10 nm) and gold (75 nm) were deposited leaving a 1 mm gap using a metal evaporator purchased from Angstrom Engineering with home built aluminum shadow masks.

Volumes of 1 μL of the dispersion of 1-SWCNT were drop-cast between the gold electrodes followed by drying in vacuum until a resistance of 1-5 $\text{k}\Omega$ was achieved.

Sensing Measurements

The devices were enclosed in a homemade Teflon gas flow chamber for sensing measurement (Figure 6.17). The gold electrodes of the device are contacted with connections to the outside of the gas flow chamber, and two ports on opposite sides of the chamber allow directing a continuous gas flow through the chamber.

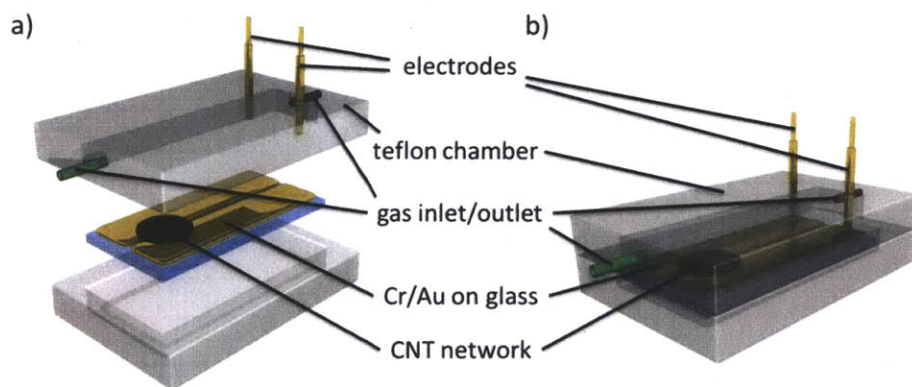


Figure 6.17. Gas flow chamber for sensing measurements.

The low concentration gas mixtures were produced using a KIN-TEK gas generator system. A trace amount of analyte emitted from a permeation tube is mixed with a nitrogen stream (oven flow), which can be further diluted with nitrogen (dilution flow) (Figure 6.6). For ethylene, refillable permeation tubes were used, while for the interferences we performed calibration measurements by placing the solvent in the oven flow for set amounts of time and determined the weight loss in analyte. For fruit measurements the fruit was placed in a flow chamber, through which the “oven flow” was directed, which was then further diluted with nitrogen.

Electrochemical measurements were performed using an AUTOLAB instrument from Eco Chemie B.V. A constant bias voltage of 0.1 V was applied across the device, while current vs. time was measured. During the measurement the volume of gas flow over the device was held constant and switched between nitrogen and analyte/nitrogen.

Testing of Different SWCNT Types and Control Experiments

While optimizing sensitivity of the devices to ethylene, we tested different types of SWCNTs. Devices made from different 1-SWCNT dispersions following the general procedure were compared with regard to their response to 20 ppm ethylene. Similar control experiments were performed using devices prepared from dispersions of 2-SWCNT, 4-SWCNT and SWCNTs with $[\text{Cu}(\text{CH}_3\text{CN})_4]\text{PF}_6$.

Fruit Information

Fruit of the following types and weight was purchased from a Farmer's market:

Banana (Cavendish) – 142.5 g

Avocado (Hass) – 170.7 g


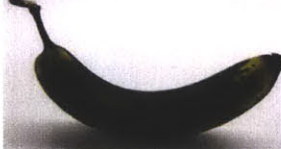








Apple 1 (Macintosh) – 119.1 g

Apple 2 (Macintosh) – 111.3 g

Pear (Comice) – 246.1 g

Orange (Navel) – 265.0 g

Table 6.1. Pictures of fruit on different days of measurement.

			
Banana, Day 1	Banana, Day 10	Banana, Day 16	Banana, Day 24
			
Avocado, Day 1	Apple 1, Day 24	Apple 2, Day 24	
			
Pear, Day 1	Pear, Day 15	Orange, Day 1	

IR Measurements

IR spectra were recorded on a SMART iTR purchased from Thermo Scientific. The sample was drop-cast onto a KBr card, and the spectrum was measured in transmission mode.

Raman Measurements

Raman spectra were measured on a Horiba LabRAM HR Raman Spectrometer using excitation wavelengths of 785 nm and 532 nm. The samples were drop-cast onto SiO₂/Si substrates for the measurement.

XPS Measurements

XPS spectra were recorded on a Kratos AXIS Ultra X-ray Photoelectron Spectrometer. The samples were drop-cast onto SiO₂/Si substrates for the measurements. As the copper complex **1** is air sensitive, it was drop-cast under argon and the exposure to air was kept minimal (< 2 min) during the transfer into the XPS instrument. In the case of **1** and **2** sample charging was observed and a charge neutralizer was used. The resulting shift in energy was compensated by calibrating using the F 1s peak at 687 eV.

Scanning Electron Microscope Measurements

Scanning electron microscope (SEM) images were obtained on a JEOL 6700 scanning electron microscope.

Devices (prepared as described in device preparation) were analyzed by SEM, showing a relatively smooth film of **1**-SWCNTs on the glass substrate (Figure 6.5). When 5 weight-% of cross-linked polystyrene beads (0.4-0.6 μm) were mixed with **1**-SWCNTs before drop-casting, an increase of the surface roughness and thus the surface area can be observed (Figure 6.12a). At

higher magnification, CNT bundles were observed on the surface of the polymer as well as on the glass substrate (Figure 6.12b).

6.5. References

- (1) Kader, A. A.; Reid, M. S.; Thompson, J. F. *Postharvest Technology of Horticultural Crops*; Kader, A. A., Ed.; University of California, Agricultural and Natural Resources, 2002; p. 39.
- (2) Pham-Tuan, H.; Vercaemmen, J.; Devos, C.; Sandra, P. *J. Chromatogr. A*. **2000**, *868*, 249.
- (3) Scotoni, M.; Rossi, A.; Bassi, D.; Buffa, R.; Iannotta, S.; Boschetti, A. *Appl. Phys. B*. **2005**, *82*, 495.
- (4) Jordan, L. R.; Hauser, P. C.; Dawson, G. A. *Analyst*. **1997**, *122*, 811.
- (5) Zevenbergen, M. A. G.; Wouters, D.; Dam, V.-A. T.; Brongersma, S. H.; Crego-Calama, M. *Anal. Chem*. **2011**, *83*, 6300.
- (6) Green, O.; Smith, N. A.; Ellis, A. B.; Burstyn, J. N. *J. Am. Chem. Soc.* **2004**, *126*, 5952.
- (7) Esser, B.; Swager, T. M. *Angew. Chem. Int. Ed.* **2010**, *49*, 8872.
- (8) Dias, H. V. R.; Jin, W.; Kim, H.-J.; Lu, H.-L. *Inorg. Chem.* **1996**, *35*, 2317.
- (9) Dias, H. V. R.; Wu, J. *Eur. J. Inorg. Chem.* **2008**, 509.
- (10) Jorio, A.; Dresselhaus, M.; Saito, R.; Dresselhaus, G. F. *Raman Spectroscopy in Graphene Related Systems*; Wiley-VCH: Weinheim, 2011; p. 327.

Curriculum Vitae – Jan M. Schnorr

Personal Information

Full name: Jan Markus Schnorr
Degree: Diplom Chemiker (equivalent to M. Sc. in Chemistry)
Date/Place of birth: September 19th, 1980, Frankfurt/Main, Germany
Nationality: German
E-mail: jschnorr@mit.edu

Work Experience

08/2007 **PhD Student, Massachusetts Institute of Technology (MIT), Cambridge MA, USA**

– 06/2012 Supervisor: Prof. Timothy Swager, Department of Chemistry

Thesis Title: Functionalization and applications of carbon nanotubes

- Developed new reaction conditions and gained extensive experience in functionalization of nano-carbon materials (including inert atmosphere and high pressure reactions) as well as synthesis of organic precursors
- Conducted study on functionalized carbon nanotubes as additives in catalysis
- Designed, fabricated and tested chemoresistive sensor prototypes using thermal evaporation of electrodes, drop-casting and spin-coating of materials and resistance measurements
- Characterized materials and devices by NMR, UV-vis, IR and Raman spectroscopy, XPS, TGA, SEM, optical microscopy, electrochemistry (CV, amperometry), MALDI-TOF, and GC-MS
- Worked on several multidisciplinary (chemistry and chemical, electrical, or mechanical engineering) and international projects
- Wrote one patent and authored two publications in international peer reviewed journals
- Wrote 60 contributions to *Synfacts*, a monthly journal with summaries of recent publications
- Supervised two MIT undergraduate students and one master student from Radboud University, Nijmegen, The Netherlands
- Led nano-carbon modification subgroup; initiated weekly meetings to strengthen research discussions and collaborations within group
- Lectured recitations in introductory organic chemistry and graded problem sets and exams as a teaching assistant for organic chemistry lecture and laboratory class

01/2007 **Research Assistant, Max Planck Institute for Polymer Research, Mainz, Germany**

– 07/2007 Supervisor: Prof. Klaus Müllen

Research: Synthesis of boron containing oligomers and dendrimers with ruthenium core

- Published results in *Angew. Chem. Int. Ed.* 2008

09/2000 **Mandatory military service** in Kulsheim, Germany

– 06/2001

- Maintained tank electronics and hydraulics, evaluated problems and performed repairs

Education

08/2007 **Massachusetts Institute of Technology (MIT), Cambridge MA, USA**

– 06/2012 Candidate for PhD in Chemistry, June 2012 (GPA: 4.2/5.0)

- Relevant coursework in organic chemistry, polymer chemistry and organic electronics

Education (continued)

- 10/2001 **J. W. Goethe University, Frankfurt/Main, Germany**
– 11/2006 Diplom in Chemistry (equivalent to M. Sc.)
- Final grade: 1.1 (scale: 1.0 very good to 5.0 insufficient)
 - Diploma thesis research on ferrocenyl boranes (title: “Ferrocenhaltige Hydroborierungsreagenzien”)

Leadership

- 08/2011 **Team Leader, European Career Fair 2012 at MIT, Cambridge MA, USA**
– present Leading the candidate interview scheduling team and hotel organizing team and responsible for contacting international companies
- 06/2008 **Co-Chair, ACS Graduate Student Symposium Planning Committee, Boston MA, USA**
– 08/2010 Organized graduate student symposium ‘Chemistry and Policy: Solving Problems at the Interface’ at fall 2010 ACS meeting ; Led team of 10 student volunteers; 9 speakers presented (including Harvard Professor George Whitesides and former CIA director Prof. John Deutch); Raised budget: \$23,800
- 03/2003 **Head of Cub Scout program, Hessen, Germany**
– 12/2006 BdP Scout Youth Organization in state of Hessen, Germany
Led team of 8 volunteers in charge of training ca. 100 group leaders; planned programs and organized events for 500 members of the scout organization

Awards and Scholarships

- 05/2010 Vivian A. and E. Emerson **Morse travel grant** for attendance of the 9th International Symposium on Functional π -Electron Systems (F-Pi-9) in Atlanta, Georgia (USA)
- 10/2003 **Scholarship of German National Academic Foundation** (Studienstiftung des Deutschen Volkes) during final 3 years of chemistry studies
– 11/2006
- 11/2004 **Dr. Albert Hloch-Award** for excellent preliminary diploma in chemistry
- 10/2001 **Scholarship of German Chemical Industry Association** (Verband der Chemischen Industrie) during first 2 years of chemistry studies
– 10/2003
- 06/2000 **Award of German Physical Society** (Deutsche Physikalische Gesellschaft) for excellent performance in physics

Patents

- (1) Swager, T. M.; **Schnorr, J. M.** High Charge Density Structures, Including Carbon-based Nanostructures and applications thereof. **2010**, U.S. Pat. Apl. Serial No.: 61/122,256 (12/12/2008).
- (2) Esser, B., **Schnorr, J. M.**, Swager, T. M.; Ethylene Sensor. **2012**, Provisional Patent Apl. Serial No.: 61/614,834 (03/23/2012).

Publications

- (1) Esser, B.; **Schnorr, J. M.**; Swager, T. M. Selective Detection of Ethylene Gas Using Carbon Nanotube-based Devices: Utility in Determination of Fruit Ripeness. *Angew. Chem. Int. Ed.* **2012**, *accepted*.
- (2) Dionisio, M; **Schnorr, J. M.**; Michaelis, V. K.; Griffin, R. G.; Swager, T. M.; Dalcanale, E. Cavitand-Functionalized SWCNTs for *N*-methylammonium Detection *J. Am. Chem. Soc.* **2012**, *134*, 6540.
- (3) **Schnorr, J. M.**; Swager, T. M. Wiring-up catalytically active metals in solution with sulfonated carbon nanotubes. *J. Mater. Chem.* **2011**, *21*, 4768.

- (4) **Schnorr, J. M.**; Swager, T. M. Emerging Applications of Carbon Nanotubes. *Chem. Mater.* **2011**, *23*, 646.
- (5) Scheibitz, M.; Li, H.; **Schnorr, J.**; Sánchez Perucha, A.; Bolte, M.; Lerner, H.-W.; Jäkle, F.; Wagner, M. Ferrocenylhydridoborates: synthesis, structural characterization, and application to the preparation of ferrocenylborane polymers. *J. Am. Chem. Soc.* **2009**, *131*, 16319-29.
- (6) Haberecht, M. C.; **Schnorr, J. M.**; Andreitchenko, E. V.; Clark, C. G.; Wagner, M.; Müllen, K. Tris(2,2'-bipyridyl)ruthenium(II) with branched polyphenylene shells: a family of charged shape-persistent nanoparticles. *Angew. Chem. Int. Ed.* **2008**, *47*, 1662-7.
- (7) Schmidt, M. U.; Buchsbaum, C.; **Schnorr, J. M.**; Hofmann, D. W. M.; Ernrich, M. Pigment Orange 5: crystal structure determination from a non-indexed X-ray powder diagram. *Z. Kristallogr.* **2007**, *222*, 30-33.
- (8) Nozonovic, S.; Nachtsheim, B.; Scheuermann, S.; **Schnorr, J.**; Silvers, R.; Wagner, M.; Schwalbe, H. Problemlösendes Denken in Gruppenarbeit lernen. *Nachr. Chem.* **2005**, *53*, 978-980.

Presentations

- (1) **Schnorr, J. M.**; Han, G. D.; Ramirez-Monroy, A.; Swager, T. M. Functionalized Carbon Nanotubes as Soluble Molecular Wires. *Challenges in Renewable Energy, International Symposium on Advancing the Chemical Sciences (ISACS 4)*. **2011**, Cambridge, MA (USA), poster
- (2) Collins, W. R.; **Schnorr, J. M.**; Schmois, E.; Lewandowski, W.; Swager, T. M. Methods for the Covalent Surface Functionalization of Graphene. *Nature Materials Symposium: Graphene: The Road to Applications*. **2011**, Cambridge, MA (USA), poster
- (3) **Schnorr, J. M.**; Swager, T. M. Highly Water Soluble Ionic Carbon Nanotubes and Their Use as Electronic Conductors in Polar Solvents. *Material Research Society Fall Meeting 2010*. **2010**, Boston, MA (USA), oral presentation
- (4) **Schnorr, J. M.**; Swager, T. M. Connecting metal centers in solution with water soluble multi-walled carbon nanotubes. *American Chemical Society National Meeting Fall 2010*. **2010**, Boston, MA (USA), oral presentation
- (5) **Schnorr, J. M.**; Swager, T. M. Highly Ionic, Water Soluble Multi-Walled Carbon Nanotubes. *9th International Symposium on Functional Pi-Electron Systems (F-Pi 9)*. **2010**, Atlanta, GA (USA), poster

Acknowledgements

First and foremost, I would like to thank my research advisor, Prof. Tim Swager, for his support, guidance and inspiration. He has been a great mentor whose creativity and passion for science has always encouraged me to expand my boundaries and face new challenges. His style of leadership with respect for each team member and the right way to motivate each individual is a great example how to run a group. I would like to thank Tim for the freedom he gave me and for making my time at MIT a fun experience. It has been a great pleasure to be part of the team and I am very grateful for the last five years.

I would like to thank Prof. Greg Fu, the chair of my thesis committee, for his guidance and advice over the last years. I highly respect him for his immense knowledge and great ability to teach. I would like to thank the members of my thesis committee, Prof. Tim Jamison and Prof. Sarah O'Connor, for their advice and feedback regarding the 4th year proposal and during the 2nd year oral exam, respectively. Profs. Harald Schwalbe, Thomas Prisner, and Matthias Wagner were my undergraduate mentors at University of Frankfurt and I am grateful for their advice and support on the way to my Diplom and when applying at MIT. I would also like to thank Prof. Klaus Müllen who gave me the opportunity to work in his research group for six months before I moved to Boston.

I gratefully acknowledge the Institute for Soldier Nanotechnologies (ISN) for providing funding over the last years. In addition to the funding, the ISN provided a good place to meet and interact with colleagues across disciplines.

I am proud and consider myself very fortunate to be part of the Swager team and I would like to thank the past and present group members for contributing to this great experience. It is a good feeling to be surrounded by a group of people who combine intelligence, skill and expertise in their field with the belief that being friendly and supportive is not a distraction but a way to be successful. In particular, I would like to thank my fellow subgroup captains, Jon, Becca, Jolene, Grace, and Joe for putting a lot of effort into making the group an even better place to be. Kelvin, Joel, John and Jon as our past and present volleyball captains together with our teams including Jeewoo, Brett, Jolene, Barney, Hitoshi, Yu, Yi, Scott, and Wiktor have made sure we get our required dose of sun in the summer. Even during colder weather, the Chang lunch club always provided an additional reason to leave the basement at least once per day thanks to the efforts of Duncan, Birgit, Carlos (1.0 and 2.0), Sébastien, Jisun, Markrete, Jens, David, and multiple Andreases. I would also like to thank pub Meister Markus and his successor Tamara for getting

great people together every week who make the non-scientific part of life much more enjoyable. Among many others, it was great spending some of my time in Cambridge with Christin, Niki, Steffi, Silvia, Jacky, Luis, Heather, Bettina, Nils, Holger, Nicole and Christoph.

From the first days in Boston, my class mates at MIT were great friends, provided support and advice or had good ideas for fun activities and I am very happy that I met Becca, Olesya, Jose, Shuang, Jason, Stef, Nicole, Julia, Charlene and our other colleagues and that I could spend time with them in the last years.

During my time in the Swager group, there were many opportunities for collaborations and it has been a great pleasure to work together with Birgit, Daan, Yossi, Joe, Marco, Vlad, Kittipong, Priam, Kerri, Benjamin, Clarissa, and Zeke as well as Andrea and Raj with their respective teams. It has also been a lot of fun to be part of our nanoC and sensing team and I would like to thank Kat, Ellen, Birgit, Grace, Joe, Kelvin, Jason, Brendan, Eilaf, Stef, John, Carlos, Yulin, Duncan and Jisun for lots of helpful advice and suggestions.

Many other people have helped me over the years, including Caitlin and Kathy who are making sure everything works perfectly in our lab, Libby who is a true expert on XPS, the DCIF team, Jeff, Anne, Deborah and Li Li, Bill with SEM questions, and last but not least, the team at the ChemEd office (Melinda, Susan, Jennifer, Mary, and Lynn). Without them, many parts of this thesis would not have been possible.

One thing that makes MIT and Boston a special place are the many opportunities to take initiative and organize events together with friends and colleagues. I am grateful that I could be part of the Graduate Student Symposium Planning Committee that organized a symposium at the fall 2010 ACS meeting as well as the European Career Fair team 2012. I am happy about the many new friends I met in both teams and impressed by how much a group of motivated volunteers can achieve.

Finally, I would like to thank my family. It is sometimes hard to believe how lucky I am that they are part of my life. We have spent many funny and serious moments together that I do not want to miss. Knowing that they will always support me whatever will happen makes me very happy and gives me strength and confidence. I cannot thank them enough.